NASA-CR-196296

CALSPAN UB RESEARCH CENTER

# FINAL REPORT FOR NASA GRANT NAG3-581-- EXPERIMENTAL MEASUREMENTS AND ANALYTICAL ANALYSIS RELATED TO GAS TURBINE HEAT TRANSFER : PART I : TIME-AVERAGED HEAT-FLUX AND SURFACE-PRESSURE MEASUREMENTS ON THE VANES AND BLADES OF THE SSME FUEL-SIDE TURBINE AND COMPARISON WITH PREDICTION

# AND

# PART II : PHASE-RESOLVED SURFACE-PRESSURE AND HEAT-FLUX MEASUREMENTS ON THE FIRST BLADE OF THE SSME FUEL-SIDE TURBINE

N94-36969

Unclas

G3/34 0018313

(NASA-CR-196296) EXPERIMENTAL MEASUREMENTS AND ANALYTICAL ANALYSIS RELATED TO GAS TURBINE HEAT TRANSFER. PART 1: TIME-AVERAGED HEAT-FLUX AND SURFACE-PRESSURE MEASUREMENTS ON THE VANES AND BLADES OF THE SSME FUEL-SIDE TURBINE AND COMPARISON WITH PREDICTION.(Calspan-Buffalo Univ. Research Center) 173 p

CUBRC FINAL REPORT NO. 640II
MAY 1994

PREPARED FOR:
NASA LEWIS RESEARCH CENTER
21000 BROOKPARK RD.
CLEVELAND, OH 44135

CALSPAN-UB RESEARCH CENTER P.O. BOX 400, BUFFALO, NEW YORK 14225 TEL. (716) 631-6900 FAX (716) 631-4166

# PART I: TIME-AVERAGED HEAT-FLUX AND SURFACE-PRESSURE MEASUREMENTS ON THE VANES AND BLADES OF THE SSME FUEL SIDE TURBINE AND COMPARISON WITH PREDICTION

by


M.G. Dunn and J. Kim

Calspan-UB Research Center

Buffalo, NY 14225



CUBRC Report No. 6401

Prepared for the

NASA Lewis Research Center

21000 Brookpark Rd.

Cleveland, OH 44135

March, 1992

## ABSTRACT

Time averaged Stanton number and surface-pressure distributions are reported for the first-stage vane row, the first stage blade row, and the second stage vane row of the Rocketdyne Space Shuttle Main Engine two-stage fuel-side turbine. Unsteady pressure envelope measurements for the first blade are also reported. These measurements were made at 10%, 50%, and 90% span on both the pressure and suction surfaces of the first stage components. Additional Stanton number measurements were made on the first stage blade platform, blade tip, and shroud, and at 50% span on the second vane. A shock tube was used as a short duration source of heated and pressurized air to which the turbine was subjected. Platinum thin-film heat flux gages were used to obtain the heat-flux measurements, while miniature silicon-diaphragm flush-mounted pressure transducers were used to obtain the pressure measurements. The first stage vane Stanton number distributions are compared with predictions obtained using a version of STAN5 and a quasi-3D Navier-Stokes solution. This same quasi-3D N-S code was also used to obtain predictions for the first blade and the second vane.

## ACKNOWLEDGEMENTS

This research was performed by the Calspan UB Research Center under support of the NASA Lewis Research Center, Cleveland, OH, Grant No. NAG3-581. The authors gratefully acknowledge the contributions made to the success of this program by the contract monitors K.C. Civinskas and Dr. R. Gaugler of the NASA Lewis Research Center. Thanks are also extended to R. J. Boyle and K.C. Civinskas for performing the predictions to the data upon which we heavily depended. This work would have not been possible without the contributions of the many Calspan engineers and technicians, especially John R. Moselle, Robert M. Meyer, Shirley J. Sweet, Jeffrey L. Barton, and Robert M. Field.

# TABLE OF CONTENTS

## LIST OF FIGURES

## LIST OF TABLES

# SECTION 1

# INTRODUCTION

The results described in this document are a summary of the work performed under support of NASA Lewis Research Center Grant No. NAG3-581. This program was initiated in 1986 with the purpose of providing fundamental data that could be used to validate predictive codes that would be used to predict the heat transfer distributions and pressure loadings for the SSME fuel-side turbopump. Prior to the time that a full scale pump became available, the Garrett TFE 731-2HP turbine was used to develop techniques for obtaining the basic data of interest and for investigating the applicability of various predictive techniques. The results of this effort have been reported in Dunn, 1986, Dunn et al., 1986, Rae et al., 1988, Taulbee, Tran, and Dunn, 1988, Dunn, et al., 1989, Dunn, 1990, Tran and Taulbee, 1991, and George, Rae and Woodward, 1991. Once the SSME turbine stage became available, all attention focused on that machine with the purpose of: (a) providing experimental information for code validation to the turbopump consortium, and (b) to provide comparison data for a blowdown test rig at Marshall Space Flight Center which uses the same multi-stage turbine. The program was structured so that time-averaged, time-resolved, and phase-averaged data were to be obtained.

The results of several previous measurement programs that utilized many of the same diagnostic techniques as used here, but for different turbine stages, have been reported in Dunn and Stoddard, 1979 (Garrett TFE 731-2); Dunn and Hause, 1982 (Garrett TFE 731-2); Dunn, Rae, and Holt, 1984 (Garrett TFE 731-2); Dunn, Martin, and Stanek (Air Force LART), 1986; Dunn and Chupp, 1988 (Teledyne 702); Dunn and Chupp, 1989 (Teledyne 702); and Dunn, Bennett, Delaney, and Rao, 1990 (Allison Test Turbine). The short-duration facility used for the experiments reported here is the same one used to obtain the results reported in Dunn, Bennett, Delaney, and Rao, 1990.

The flow and heat transfer that occur in a turbine stage (or stages) represent one of the most complicated environments seen in any practical machine: the flow is unsteady (especially in the rotor), can be transonic, is generally three-dimensional, and is subjected to strong body forces. Despite these problems, satisfactory designs and expansions of operating envelopes have been achieved over the years due to the development of a sound analytical understanding of the flow and heat-transfer mechanics that define performance and to advances in materials and manufacturing processes. The analytical developments were made possible by a series of approximations, in which the level of detail retained in the modeling was sufficient to reveal important physical effects, while still allowing solutions to be found by available analytical/numerical methods.

The major milestones in the development of these methods have been the approximations that flow through each blade row is steady in coordinates fixed to the blades, that three-dimensionality can be handled by treating a series of two-dimensional flows in hub-to-shroud and blade-to-blade surfaces, and that the effects of viscosity can be estimated by non-interacting boundary-layer calculations and by loss models to account for secondary flow.

This technology base is surrounded by many analyses and numerical codes which can treat the flow on higher levels of approximation, and which are used from time to time to provide refined estimates of the flowfield and heat transfer, typically near a design point. Three-dimensional and unsteady flow effects are two areas where recently developed computational tools can provide useful information on the flow conditions, at least for the first stage of a multistage turbine. However, in the second and subsequent stages, these effects become more pronounced. The current state-of-the-art analyses can predict reasonably well the second stage vane pressure distribution but the predicted heat-flux levels on the second vane are not as good as desired as illustrated by Blair, Dring, and Joslyn, 1988. These analyses are probably not adequate for the second rotor row, but experimental data have not been generally available for comparison with the prediction.

The results presented in this report contribute heat-flux data for the midspan region of the second stage vane.

Unsteadiness and three-dimensionality are direct consequences of the interaction of blades moving through vane wakes and the impact of multiple blade rows. The environment associated with the SSME fuel side turbine lends itself to a multistage analysis. Until very recently, such an analysis would have been envisioned as a complete, time-accurate, fully three-dimensional description of the flowfield. Some first steps toward the calculation of such flows can be seen in the work of Rai, 1987 and Rai and Madavan, 1988, but it is clear that the computational costs of this approach could very quickly become prohibitive. An alternative to the Rai approach is that described by Hah, 1984. Metzger, Dunn, and Hah, 1990(a), used a flowfield defined using the calculated technique described in Hah, 1984 to perform turbine tip and shroud heat-transfer predictions for a Garrett TFE 731 HP turbine stage. These predictions were shown to compare favorable with experimental results. Another approach to the problem is the one proposed by Giles, 1988, which has also been applied to turbine data obtained in a short-duration facility for a Rolls-Royce turbine by Abhari, Guenette, Epstein, and Giles, 1991.

Another approach to the problem is that described by Rao and Delaney, 1990, which until the present time, has only been applied to a single stage. The method proposed by these authors solves the quasi-three-dimensional Euler/Navier-Stokes equations using the explicit hopscotch scheme. The full stage computation is performed by coupling vane and blade solutions on overlapping O-type grids. In Dunn, Bennett, Delaney, and Rao, 1990, comparisons are given between the predictions of Rao and Delaney, 1990, and experimental data that were obtained for a full-stage turbine using the same experimental techniques described in this paper. Comparisons are presented for the time-averaged surface pressure, the unsteady envelope of the surface pressure, and the phase-resolved surface pressure near the trailing edge of the vane and on the blade. The agreement between the predictions and the measurements was found to be very good.

Detailed heat-flux data of the same type mentioned above were also obtained and will be presented in the open literature in the near future.

An alternate approach that is receiving current attention is based on a formulation of the passage-averaged equations of Adamczyk, 1985 and 1986, which until now have been used only as an analysis tool. It is apparent that this technique holds promise as the basis of a design method whose physical basis is considerably advanced beyond the current state of the art, and whose numerical implementation is simple enough to achieve without the need for excessive hours of supercomputer time. The formulation of closure models necessary to exploit Adamczyk's formulation relies on the availability of time-resolved flowfield data. Some of this information can be obtained from the work of Dring and Joslyn, 1986, who have probed the flow field within and around a one-and-one-half stage rotating turbine.

Civinskas, Boyle, and McConnaughey, 1988, have previously presented an analysis of the first stage blade of the turbine used here. The predictions presented here are a continuation of that work. The Navier-Stokes analysis of heat transfer was done using a modified version of the quasi-3D thin layer code developed by Chima, 1986. The modifications are explained in Boyle, 1991. An additional change for the purposes of this paper has been to incorporate the transition model of Mayle, 1991 for the first vane and the intermittency model of Mayle and Dullenkopf, 1989, 1990, for the first blade and the second vane. In addition to the quasi-3D Navier-Stokes analysis, the STAN5 (Crawford and Kays, 1976) boundary layer analysis, as modified by Gaugler, 1981 was used. Both the Navier-Stokes and boundary analyses used the MERIDL hub-to-shroud analysis of Katsanis and McNally, 1977 to determine the stream tube variation at appropriate spanwise locations. The edge conditions for the STAN5 boundary layer analysis were obtained using the TSONIC analysis of Katsanis, 1969.

The rotor blade tip of a gas turbine engine moves in close proximity to the outer stationary shroud. Typically, the gap between blade tip and shroud is kept as small as possible in order to reduce losses. Active control of the gap is difficult and, even under the best of conditions, does not reduce the gap to zero. It would not be desirable to reduce this tip gap too much because during transient engine excursions a rotor rub might occur which may be more detrimental to the engine than the tip losses are to the performance. It is common practice for the turbine tip gap to be on the order of 1% to 1.5% of the blade height. The leakage flow is driven by the higher pressure on the blade pressure surface forcing fluid through the gap towards the suction surface and can result in relatively large heat transfer levels on the blade tip and on the blade suction surface in the vicinity of 90% to 100% span near the trailing edge. Heat transfer levels on the stationary shroud are also relatively large by comparison to blade midspan levels, but not as large as on the tip.

Many authors have studied the flow in the tip gap region: e.g., Allen and Kofskey, 1955; Booth, Dodge and Hepworth, 1982; Mayle and Metzger, 1982; Wadia and Booth, 1982; Bindon, 1986; Moore and Tilson, 1988; and Metzger and Rued, 1989. Heat-transfer measurements on the moving blades and the stationary shroud have been made by Dunn, Rae and Holt, 1984(a) and 1984(b), Dunn, Martin and Stanek, 1986, Dunn, 1989 and by Epstein, 1985 on the stationary shroud. Metzger, Dunn and Hah, 1990 applied the results of a three-dimensional Navier-Stokes solution (technique described in Hah, 1984) obtained for the actual experimental conditions and turbine (Garrett TFE 731-2-HP) to exercise a simple model of the tip flow and estimate the local heat flux levels for comparison with the experimental results.

In the remainder of this report, Section 2 provides a description of the experimental technique, the turbine flow path, and the instrumentation. Section 3 presents the experimental results and a comparison with predictions. Section 4 presents an estimate of the turbine efficiency based on the measured heat-flux distributions and the flowpath measurements. The appendicies provide information regarding the airfoil coordinates, the instrumentation locations, along with a tabular listing of the data.

# SECTION 2

# DESCRIPTION OF THE EXPERIMENTAL TECHNIQUE, THE TURBINE FLOW PATH, AND THE INSTRUMENTATION

## 2.1 The Experimental Technique

The measurements are performed utilizing a shock-tunnel to produce a short-duration source of heated and pressurized gas that passes through the turbine. Air has been selected as the test gas for these experiments. A schematic of the experimental apparatus illustrating the shock tube, an expansion nozzle, a large dump tank and a device that houses the turbine stage and provides the flow path geometry is shown in Figure 2.1.1. The shock tube has a 0.47-m (18.5-inch) diameter by 12.2-m (40-feet) long driver tube and 0.47-m (18.5-inch) diameter by 18.3-m (60-feet) long driven tube. The driver tube was designed to be sufficiently long so that the wave system reflected from the endwall (at the left-hand end of the sketch) would not terminate the test time prematurely. At the flow conditions to be run for these measurements, the test time is very long for a shock tunnel facility being on the order of 40 milliseconds.

In order to initiate an experiment, the test section is evacuated while the driver, the double diaphragm section, and the driven tube are pressurized to predetermined values. Pressure values are selected to duplicate the design flow conditions. The flow function $\dot{w}\sqrt{\theta}/\delta$, wall-to-total temperature ratio ($T_w/T_0$), stage pressure ratios, and corrected speed are duplicated. The shock-tunnel facility has the advantage that the value of $T_0$ can be set at almost any desired value in the range of 800 °R to 3500 °R (Shock tubes obviously can operate at higher $T_0$ values than 3500 °R, but at the expense of test time. Test time is a parameter that one does not sacrifice easily), and the test gas can be selected to duplicate the desired specific heat ratio. The pressure ratio across the turbine is established by the throat area of the flow control nozzle located at the exit end of the device housing the turbine. It is desirable to locate this throat as close to the turbine exit

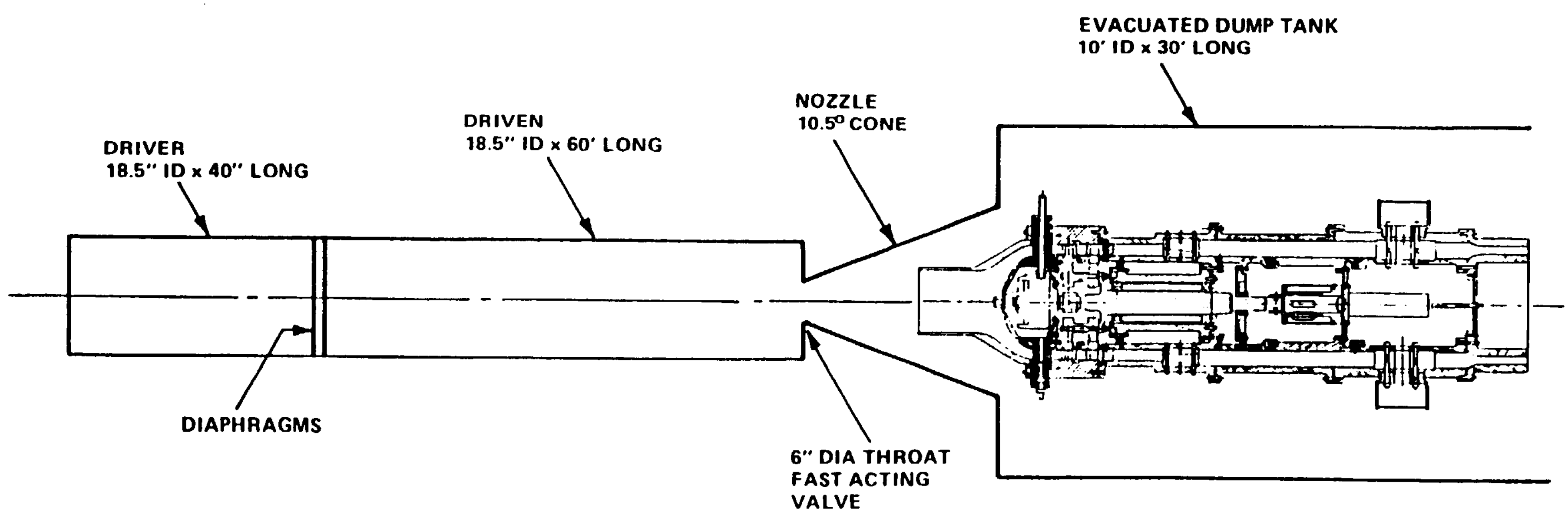


Figure 2.1.1 SKETCH OF THE SSME TURBINE STAGE LOCATED IN THE SHOCK-TUNNEL

as is practical to reduce the time required to fill the cavity between the rotor exit and the choke. The model (shown later in Figure 2.3.1) is currently being redesigned to move the throat closer to the turbine exit. Simple one-dimensional calculations provide a good first estimate of the necessary exit area. Another characteristic of this facility is that the total pressure (or the Reynolds number) at the entrance to the vane row can be changed by moving the inlet to the device housing the turbine axially in the expanding nozzle flow so as to intercept the flow at a different freestream Mach number. If this doesn't provide sufficient range, then the reflected-shock pressure can be increased or the total temperature can be decreased in order to increase the Reynolds number, which was the approach taken in these tests.

Figure 2.1.2 is a photograph of the facility illustrating many of the components described in the preceding paragraph. Figure 2.1.3 is a wave diagram for the shock tube. The gas that subsequently passes through the turbine has been processed by both the incident and the reflected shock shown in Figure 2.1.3. The reflected-shock reservoir gas is expanded in the primary nozzle which has the effect of increasing the flow velocity, decreasing the total pressure and maintaining the total temperature at the reservoir value. The device housing the turbine will not pass all of the weight flow available in the primary nozzle, so the inlet must be carefully located in order to avoid a hammer shock. That is, there must be sufficient flow area for a normal shock to establish outside the inlet and for the remainder of the flow not passed through the turbine to pass between the lip of the inlet and the nozzle wall. If the inlet is placed too far into the nozzle, the nozzle flow will be blocked and very large short-duration forces will be exerted on the device with potentially disastrous effects. The flow downstream of the inlet normal shock is subsonic at a pressure determined by the shock strength at the particular pick-off location in the expansion.

## 2.2 The SSME Turbine

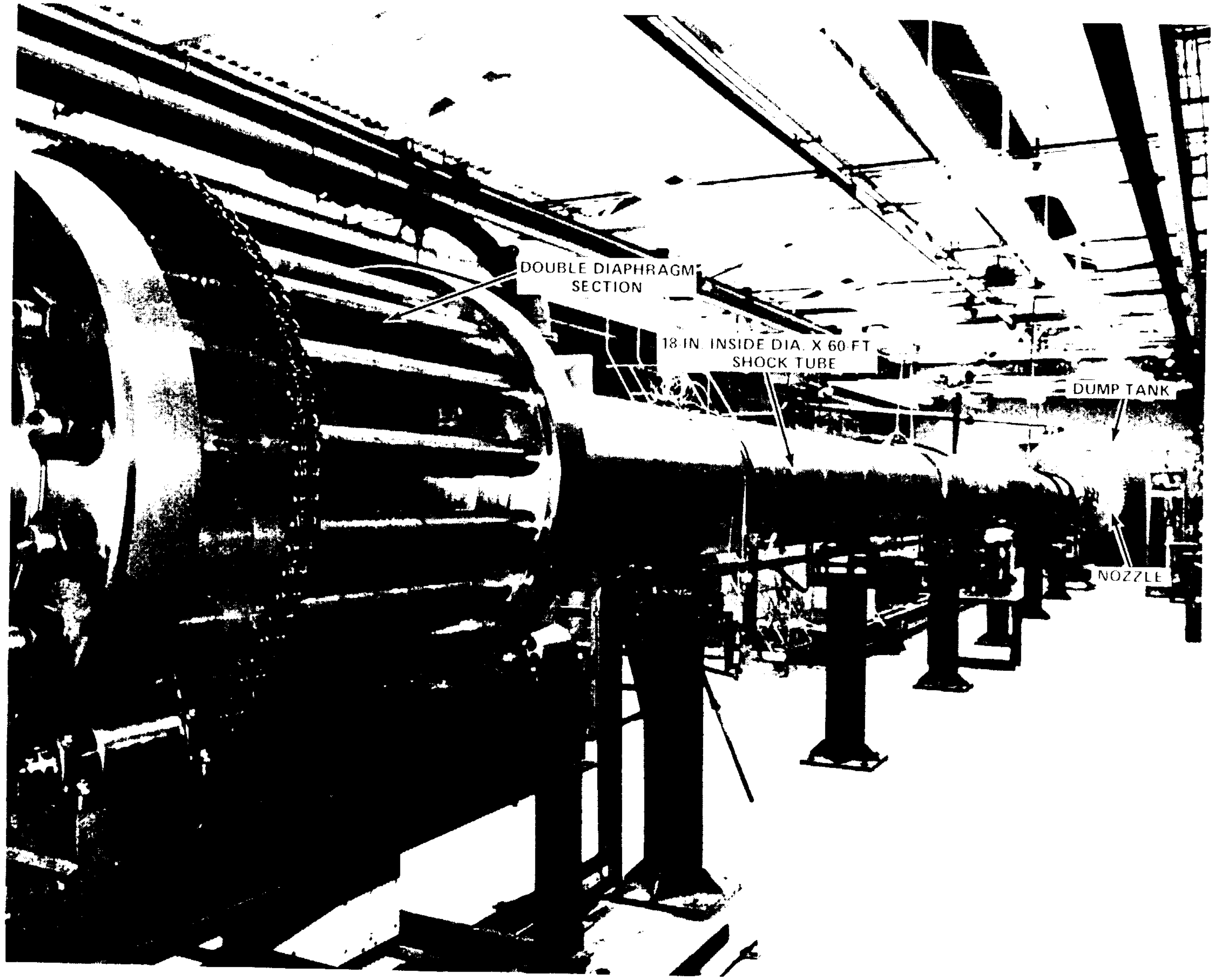


Figure 2.1.2 PHOTOGRAPH OF CALSPAN'S SHOCK-TUNNEL FACILITY FOR TURBINE RESEARCH

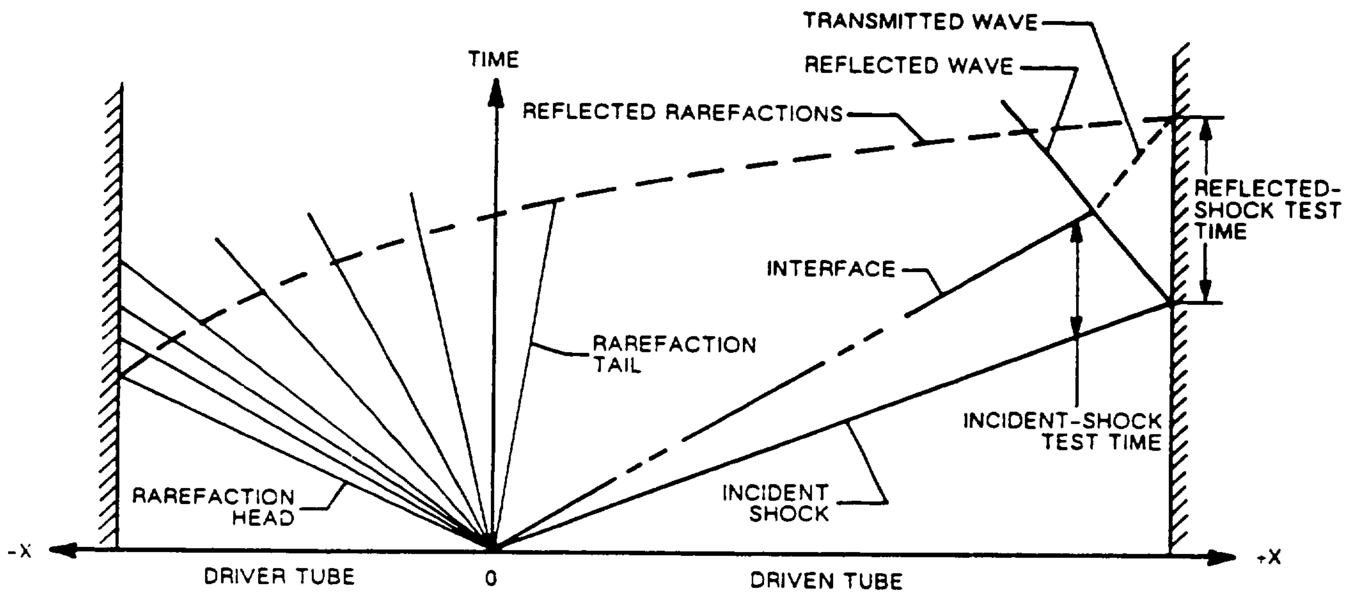


Figure 2.1.3 SKETCH OF A TYPICAL SHOCK-TUBE WAVE DIAGRAM

Photographs of the first stage vane row (41 vanes), the first stage rotor row (63 blades), and the second stage vane row (39 vanes) are shown on Figures 2.2.1-2.2.5. The second stage rotor (not shown) has 59 blades. The tip/shroud clearance for the first stage rotor at the design speed condition is ~0.015 inches or 1.6% of blade height. Figures 2.2.1 and 2.2.2 show photographs of the front and rear view of the first-stage vane row illustrating a cut-back (which was accounted for in the analysis to be described later) of the vane near the hub endwall trailing edge. It can be seen that the surface finish of the vane row is much smoother than it is for the blades. An enlarged photograph of the blade surface qualitatively illustrating the surface roughness on the blade is shown on Figure 2.2.6. The surface roughness for this blade has been measured* and a typical profilometer scan of the blade surface is given in Figure 2.2.7. The results shown in this figure suggest an rms roughness of about 150,000 Å which was used in the analysis of the heat-transfer data. Figures 2.2.4 and 2.2.5 are photographs of the second vane illustrating a surface finish comparable to the first vane and the absence of a cut-back at the trailing edge. The vane and blade coordinates are listed in the Appendix in section A.1.

## 2.3 The Turbine Flow Path

Figure 2.3.1 is a drawing of the turbine stage illustrating the extent to which the flowpath of the SSME hardware has been reproduced. The preburner dome and bolt, the 13 struts upstream of the first-stage vane, the 12 flow straighteners, and 6 struts downstream of the second rotor have been included. At the exit of the model is a flow choke which is used to control both the mass flow through the turbine as well as the turbine exit pressure. The choke area computed using a one-dimensional approximation to the flow yielded exit areas very close to those required.

---

* Roughness measurements were performed at the United Technologies Research Center and supplied to CUBRC courtesy of M. Blair. Figure 4(b) has been reproduced here with permission of M. Blair.

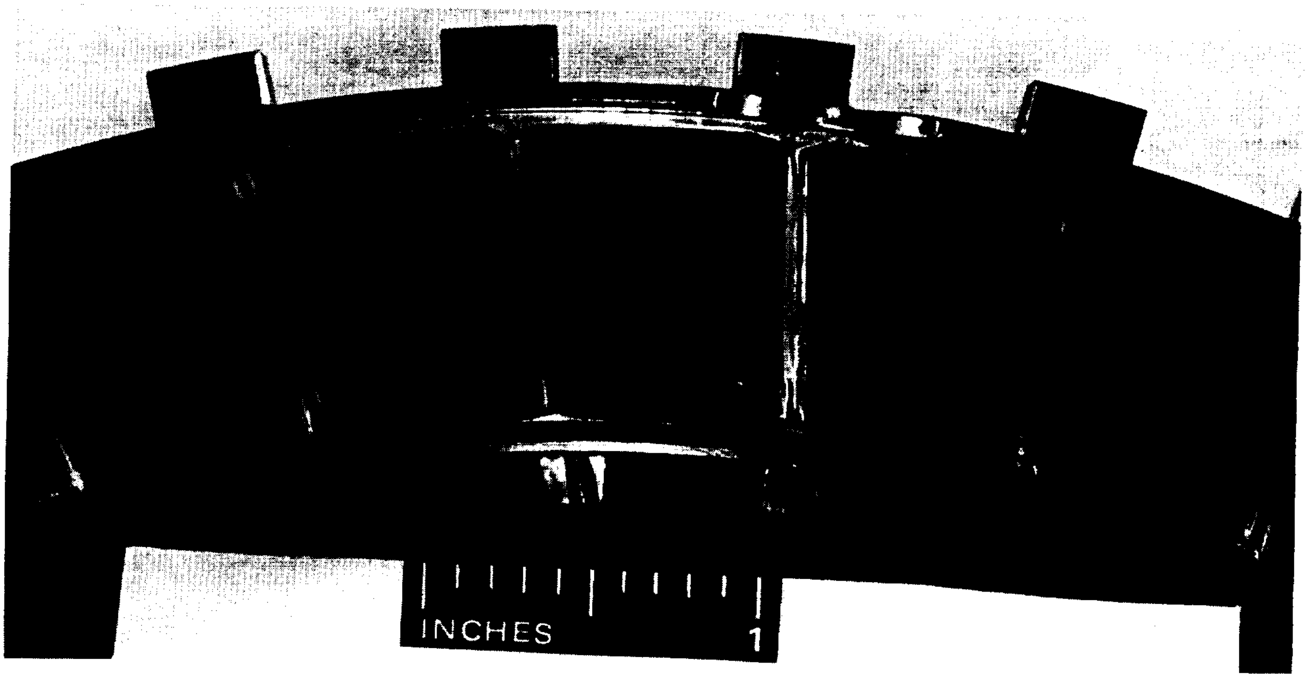


Figure 2.2.1 PHOTOGRAPH OF SSME FUEL-SIDE TURBINE FIRST STAGE VANE, FRONT VIEW

CUT BACK OF VANE

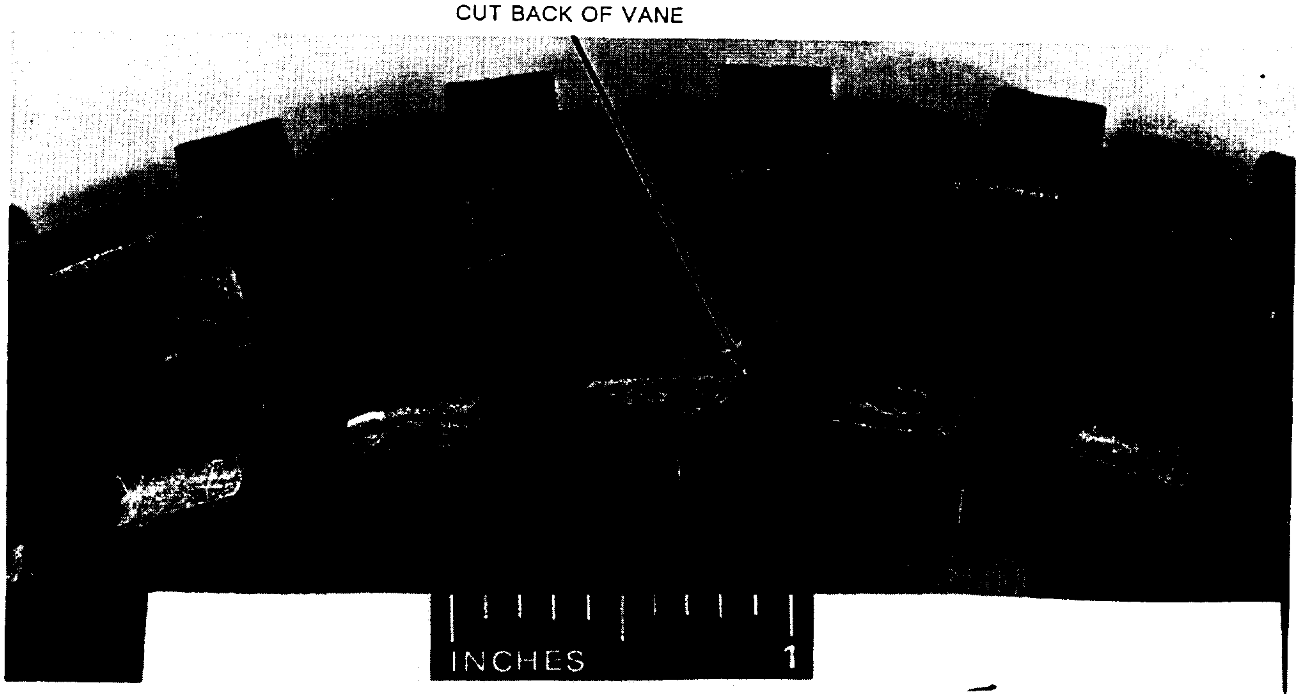


Figure 2.2.2 PHOTOGRAPH OF SSME FUEL-SIDE TURBINE FIRST STAGE VANE, REAR VIEW

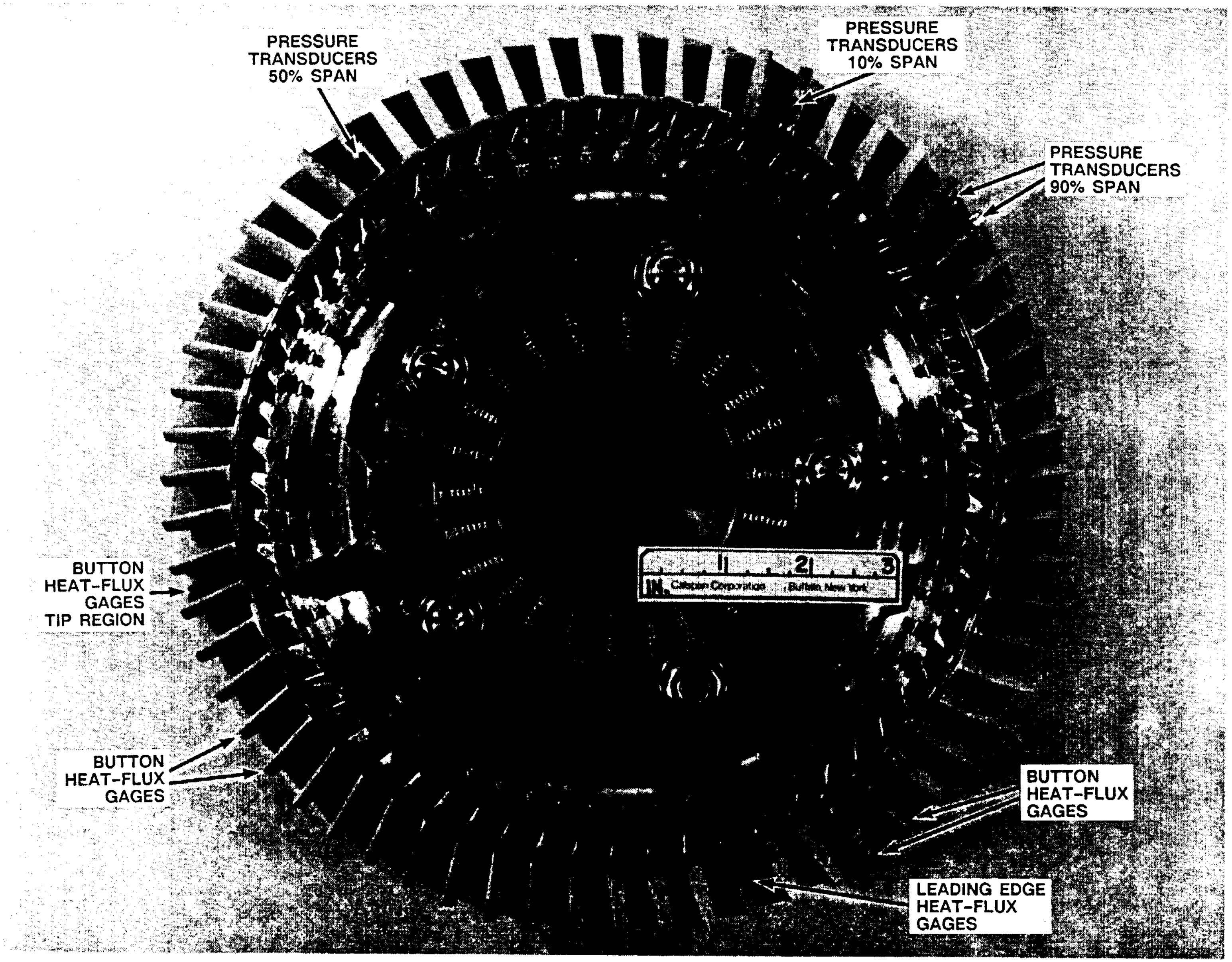


Figure 2.2.3 PHOTOGRAPH OF SSME FUEL-SIDE TURBINE FIRST STAGE ROTOR, FRONT VIEW

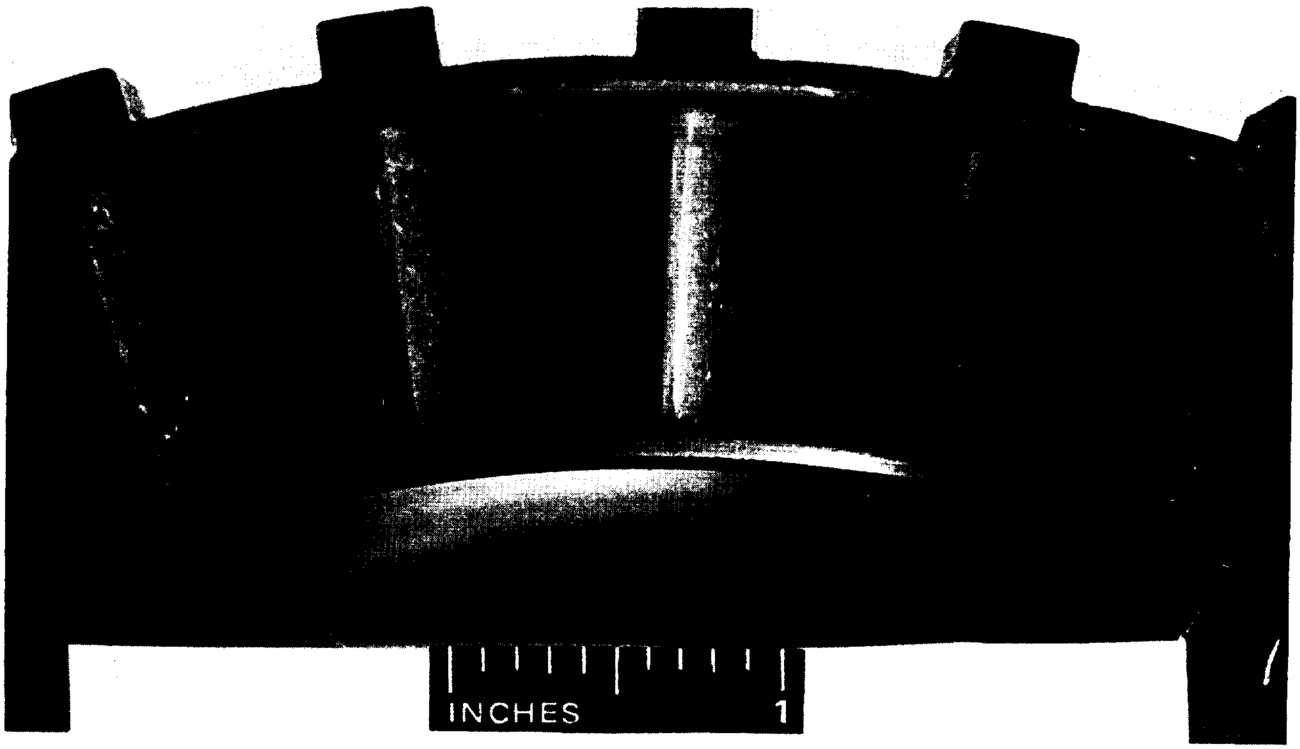


Figure 2.2.4 PHOTOGRAPH OF SSME FUEL-SIDE TURBINE SECOND STAGE VANE, FRONT VIEW

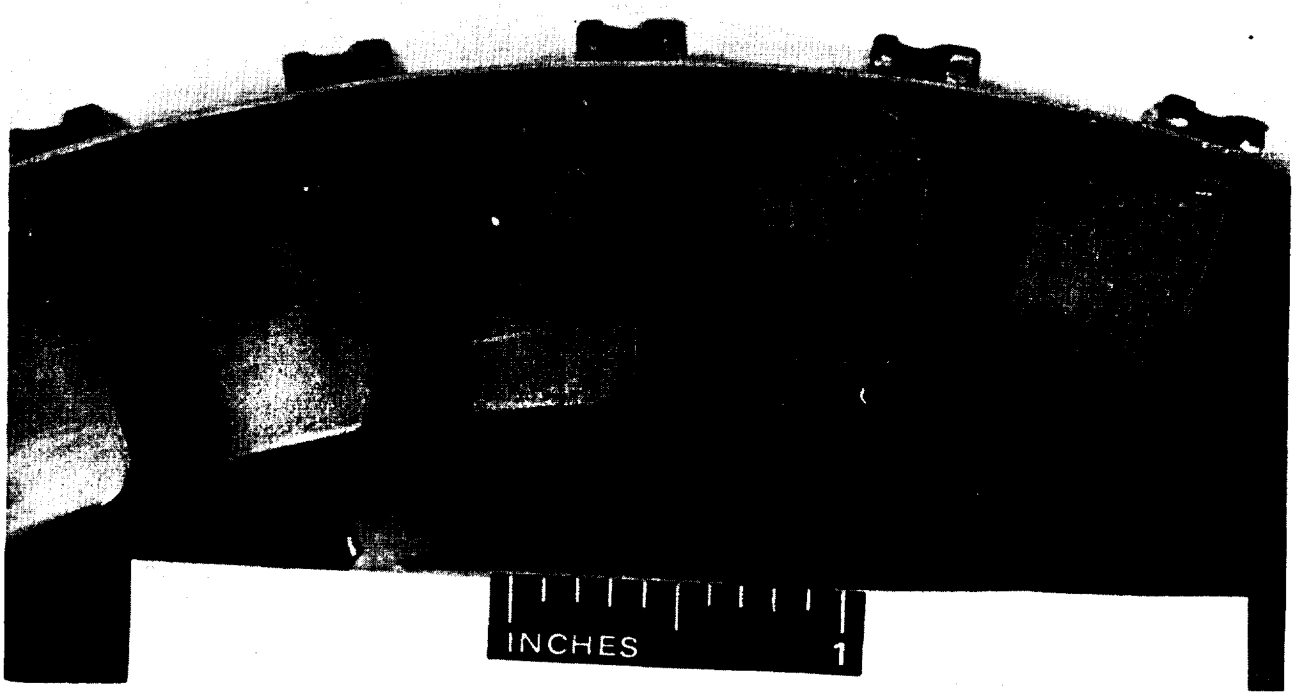


Figure 2.2.5 PHOTOGRAPH OF SSME FUEL-SIDE TURBINE SECOND STAGE VANE, REAR VIEW


Figure 2.2.6 ENLARGED PHOTOGRAPH OF FIRST BLADE SURFACE ROUGHNESS

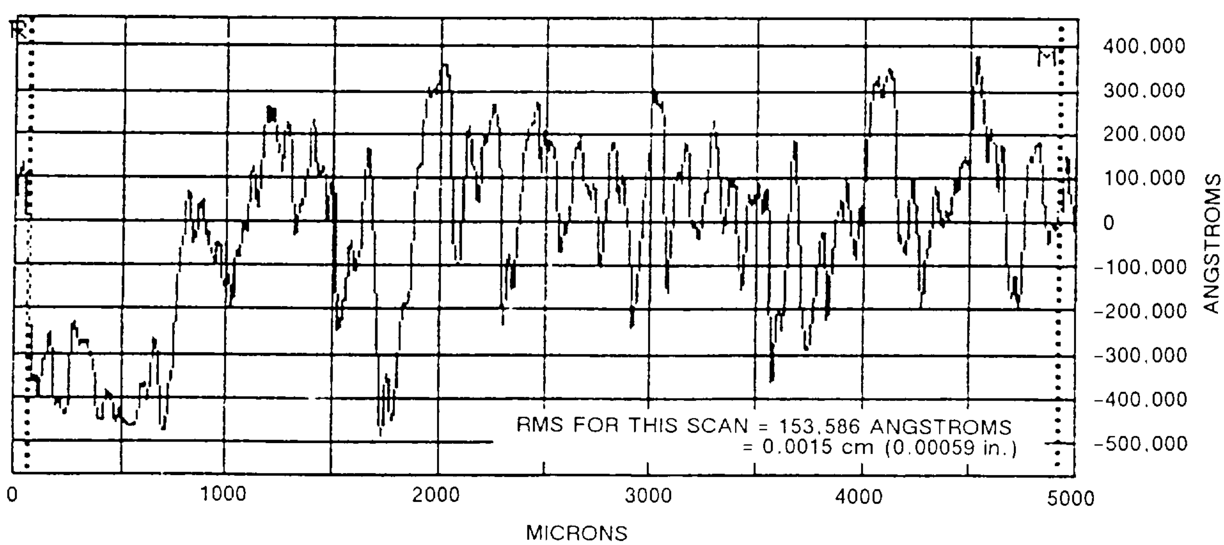


Figure 2.2.7 PROFILOMETER SCAN OF BLADE SURFACE

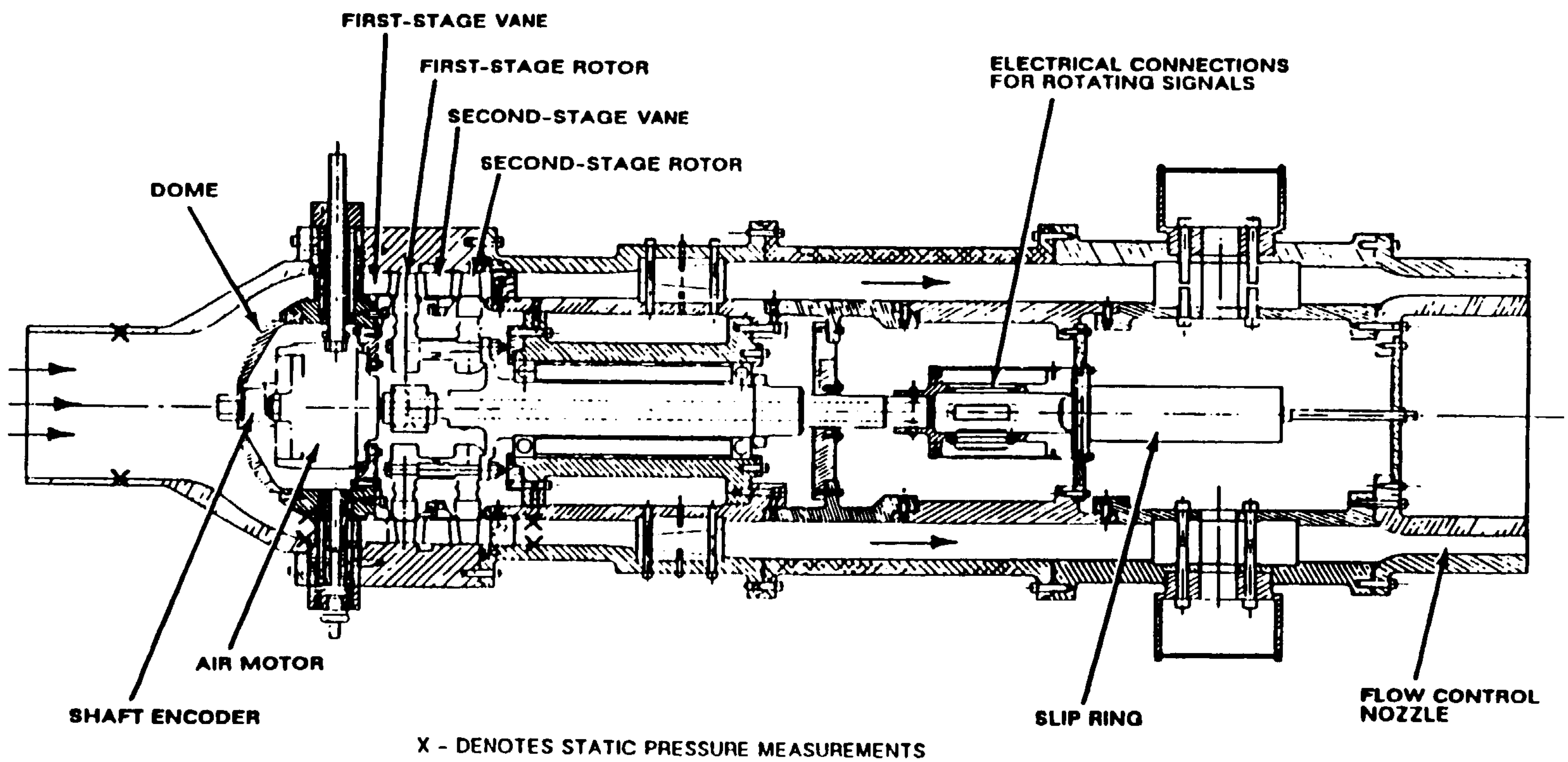


Figure 2.3.1 SKETCH OF DEVICE HOUSING SSME TURBINE STAGE

Mounted onto the forward end of the drive motor shaft is a 1000 pulse/revolution Hewlett Packard HEDS 5000 shaft encoder from which turbine speed and angular position is determined. This unit outputs a TTL pulse every 360°/1000=0.36° and a second TTL pulse once every revolution (the zero-crossing pulse). The shaft encoder was initially aligned such that the zero-crossing pulse occurred when the stagnation point of the first stage rotor blade containing the leading edge insert (heat-transfer) gage described in the next section was 12.2° CCW from TDC of the first stage vane. The pulses from the shaft encoder are used to trigger the data recording system. Since the turbine speed is not kept constant during the run, a 25 MHz timing pulse in the form of a ramp signal is fed into one channel of the high frequency data recorder to determine the arrival time of each encoder pulse. Mounted on the downstream end of the shaft is a 200 channel, freon/oil cooled, slip ring unit.

## 2.4 Heat-Flux Instrumentation

The heat-flux measurements were performed using thin-film resistance thermometers. These devices represent an old and very well established technology that was developed as part of the early hypersonics flow research work in the late 1950's for measurement of heat-flux distributions in short-duration facilities. The thin-film gages are made of platinum (~100 Å thick) and are hand painted on an insulating Pyrex (7740) substrate in the form of a strip that is approximately $1.02 \times 10^{-4}$-m (0.004-in) wide by about $5.08 \times 10^{-4}$-m (0.020-in) long. The response time of the elements is on the order of $10^{-8}$ s. The substrates containing the heat-flux gages are Epoxied within the base metal throughout the turbine stage. The substrate onto which the gage is painted can be made in many sizes and shapes.

Both button-type gages and the contoured leading-edge inserts were used for this work. The first stage vane and blade row were instrumented using both types of instrumentation along the 10%, 50%, and 90% span locations. Some gages were installed in the first stage blade shroud, blade platform, and blade tip. The second stage vane had button gages only along the 50% span. The locations of the heat transfer instrumentation are summarized in the Appendix in section A.2. Figure 2.4.1 is a photograph of a rotor blade that has been instrumented with button-types gages and Figure 2.4.2 is a photograph of a blade containing a contoured leading-edge insert. Each of the gages has two lead wires. The wires from the gages on the rotor are routed through the hollow shaft to the slip-ring unit.

## 2.5 Pressure Instrumentation

Measurements were also obtained using miniature silicon diaphragm pressure transducers located on the first-stage vane and the first-stage blade. The particular gages being used are Kulite Model LQ-062-600A with an active pressure area of 0.64 mm by 0.64 mm, and a frequency response of about 100 kHz in the installed configuration. Twenty-eight pressure transducers were installed on the vanes and twenty-four were installed on the blades. The pressure transducers were placed at 10%, 50%, and 90% span on the first vane and blade stages, and were distributed over several different vanes and blades so as to not disturb the integrity of the surface. No pressure transducers were installed in the second stage vane. The location of the surface mounted pressure transducers are summarized in the Appendix in section A.2. Figure 2.5.1 is a photograph of several of these transducers located at 10% span on the suction surface of the blade. Each of these transducers has four leads--two power leads and two output leads. The wires from the gages on the rotor are routed through the hollow shaft to the slip-ring unit.

Flowpath static pressure was measured on the outer wall of the turbine model at the inlet and exit to the turbine stages and between each blade row. The upstream static pressure was nearly equal to the upstream total pressure because the inlet Mach number was low (on the order of 0.1). The inlet Mach number was calculated and the inlet total

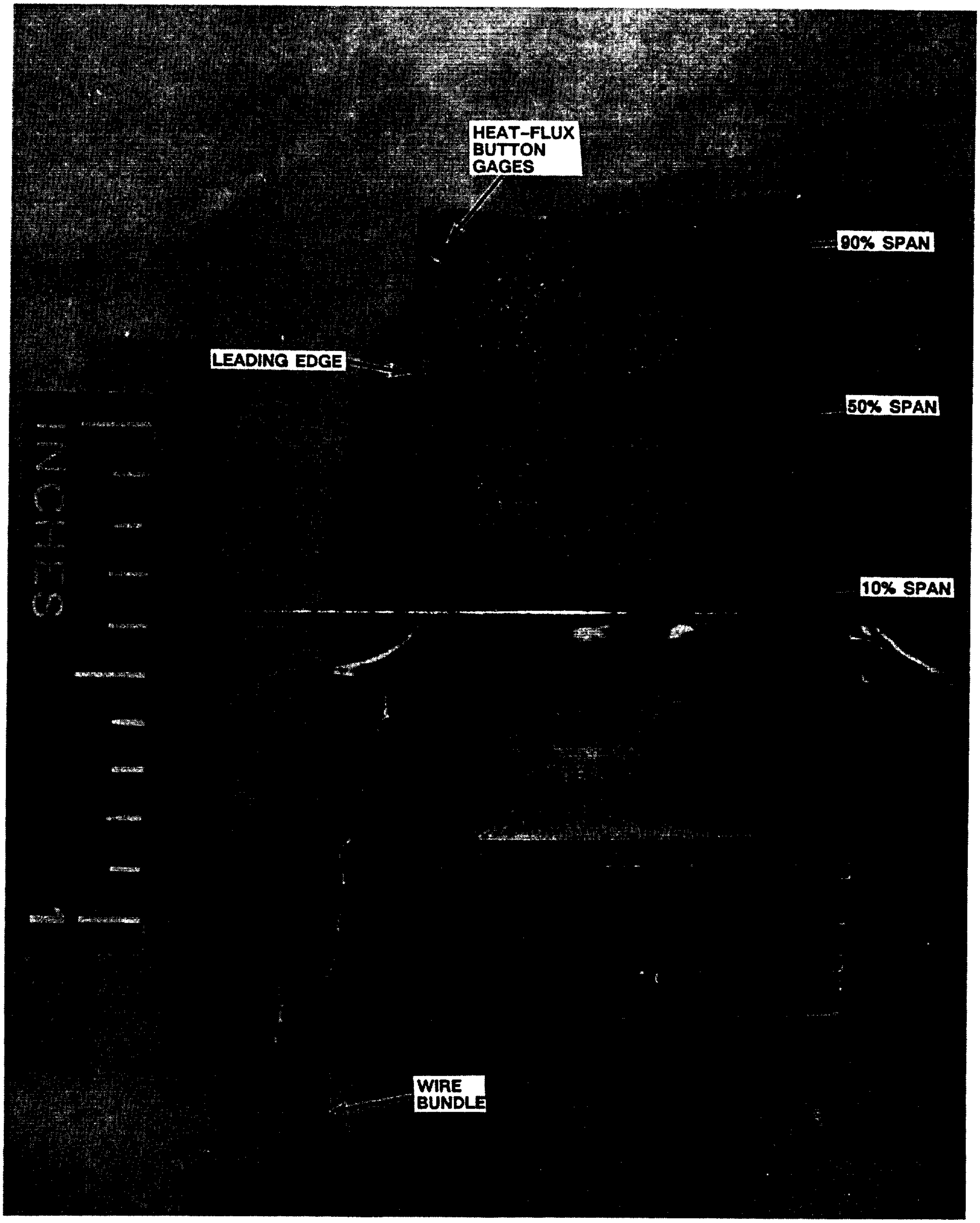


Figure 2.4.1 BUTTON-TYPE HEAT-FLUX GAGES ON FIRST-STAGE BLADE PRESSURE SURFACE

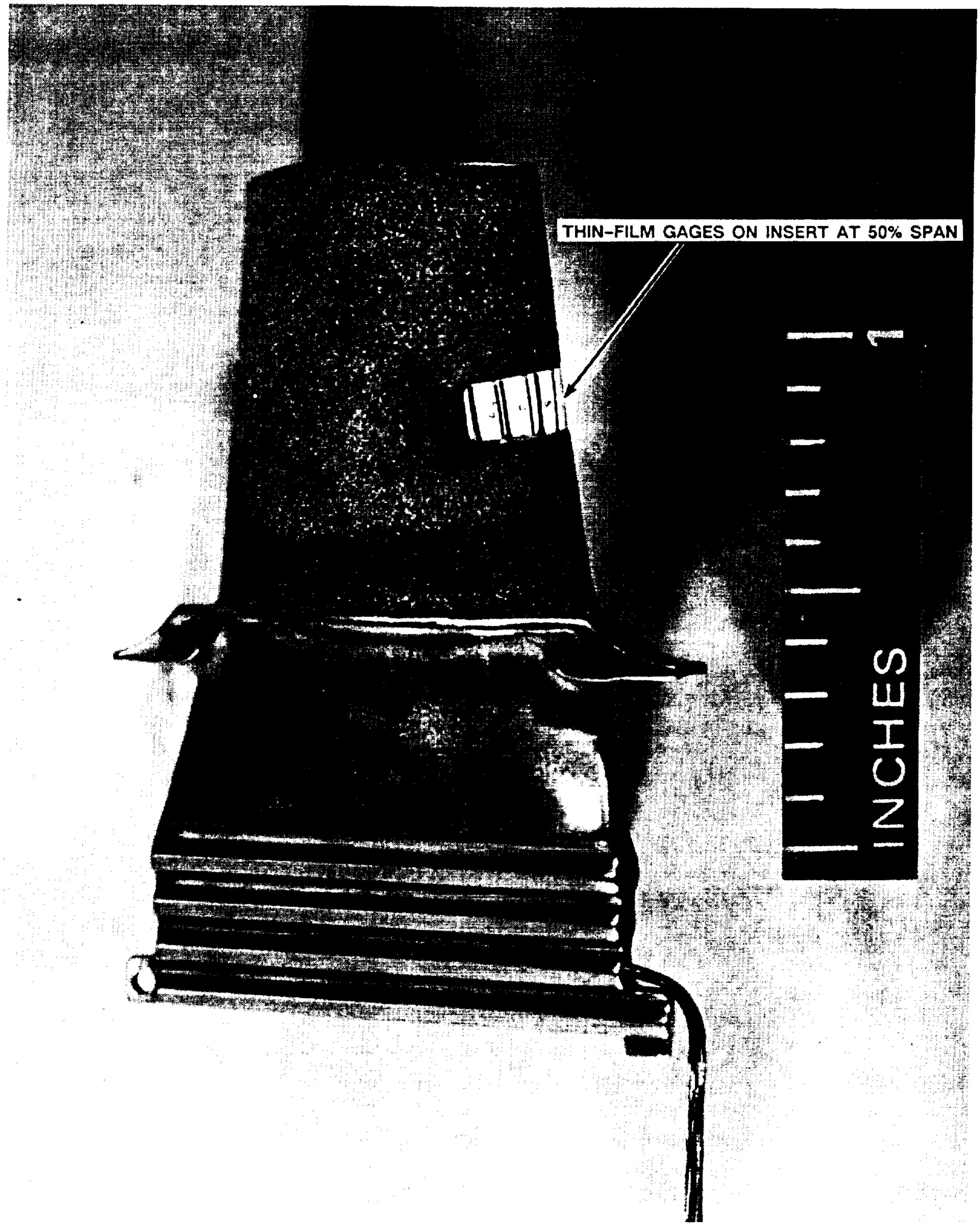


Figure 2.4.2 PHOTOGRAPH OF LEADING-EDGE INSERT HEAT-FLUX GAGES ON FIRST-STAGE BLADE

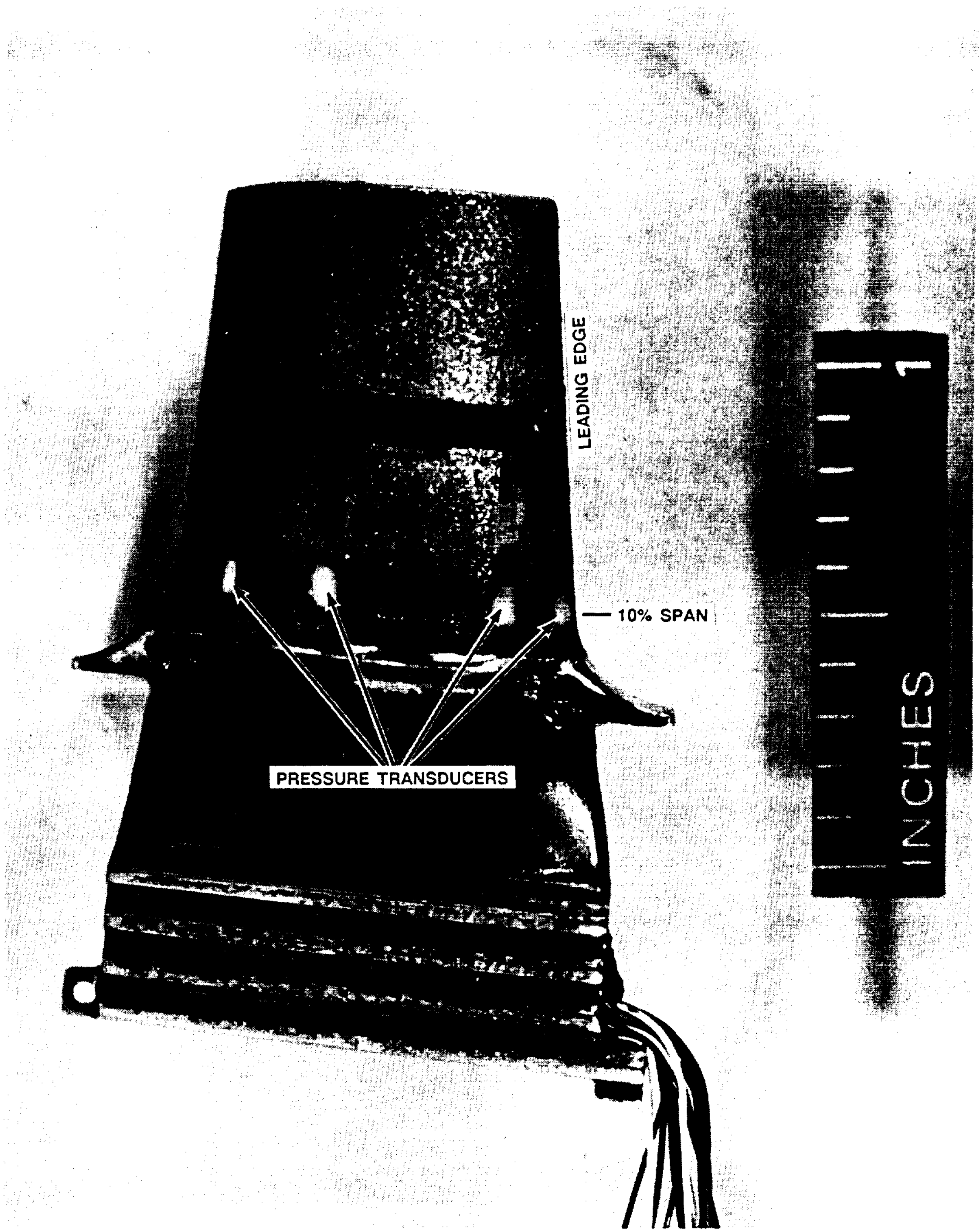


Figure 2.5.1 PHOTOGRAPH OF PRESSURE TRANSDUCERS AT 10% SPAN ON FIRST-STAGE BLADE SURFACE

pressure was obtained from the isentropic flow relationship. Total pressure was also measured in the passage downstream of the second rotor using two rakes of transducers.

## 2.6 High Speed Data Acquisition

An attempt was made to obtain time resolved data for selected heat transfer and pressure gages on the first stage rotor using a bank of 24 programmable, high-speed data recording units (Datalab DL6010 and DL6020). These units were configured so that a sample was recorded whenever a pulse was output by the shaft encoder, i.e., once every 0.36°. A separate timer box was used to measure the recording time after trigger. The data obtained using this bank of high-speed recorders were, however, contaminated with noise that was inadvertently introduced into the system. The unsteady pressure and heat transfer envelopes therefore could not be obtained. This problem will be rectified by start of the second phase of this program.

# SECTION 3

## EXPERIMENTAL RESULTS AND COMPARISON WITH PREDICTIONS

A total of thirteen runs were made during which several model configurations were used. Of these thirteen runs and different model configurations, eight runs produced data that could be used for the intentions of this research program. Some of the runs that did not produce useable data were lost because of shock-tube diaphragm failures. The remainder were lost in experimenting with the configuration of the model inlet duct. Table 1 summarizes the reflected shock conditions, the flow conditions at the turbine inlet, and the turbine speed for the eight runs to be discussed herein. Two shock tube conditions were run for these experiments; the first at a reflected-shock pressure and temperature of approximately $6.2 \times 10^3$ kPa (900 psia) and 544 K (980 °R), respectively, and the second at a reflected-shock pressure and temperature of approximately $10 \times 10^3$ kPa (1445 psia) and 602 K (1084 °R), respectively. For a given test condition, the range in reflected-shock pressure shown in Table 1 is the result of attempting to increase the test time by changing the relative amount of helium in the driver gas which also influences the incident shock Mach number and hence the reflected shock conditions. The two reflected-shock conditions result in first vane inlet Reynolds numbers (based on first vane chord) of approximately $1.4 \times 10^5$ and $2.5 \times 10^5$, respectively. Table 2(a) gives the measured upstream, interstage, and exit pressures, and Table 2(b) provides the pressure ratios for each of the vane and blade rows. The area of the downstream flow choke was changed so that data could be obtained at two values of stage pressure ratio, for each test condition. Measurements were obtained with the turbine speed set at 100%±1% of the design value or at approximately 103% of the design value. Limited data were obtained at off-design speed.

| Run | $\dot{W}$ [lbm/s] | $\left.\frac{P_{T,in}}{P_{s,out}}\right\|_{stage}$ | $P_{s,in}$ [psia] | Reflected shock pressure [psia] | Reflected shock temp. [°R] | $Re\|_{vc}$ ($\times 10^{-5}$)* | Actual speed [rpm] | % Design speed** |
|---|---|---|---|---|---|---|---|---|
| 1 | 9.52 | — | 90 | 865 | 949 | 2.39 | 6100 | 68 |
| 5 | 5.59 | 1.66 | 46.6 | 900 | 995 | 1.39 | 9075 | 99 |
| 6 | 5.81 | 1.65 | 48.3 | 929 | 990 | 1.44 | 9468 | 103 |
| 7 | 10.2 | 1.48 | 86 | 1519 | 1112 | 3.00 | 9612 | 99 |
| 8 | 9.74 | 1.38 | 89 | 1442 | 1084 | 2.69 | 9690 | 101 |
| 11 | 10.0 | 1.42 | 98 | 1369 | 1057 | 2.40 | 9585 | 101 |
| 12 | 5.83 | 1.54 | 48.3 | 925 | 981 | 1.45 | 9380 | 103 |
| 13 | 5.51 | 1.54 | 45.3 | 878 | 970 | 1.38 | 9365 | 103 |

*Reynolds number based on vane chord and vane inlet conditions.

** $N_{corr} = 291.4 \text{ rpm} / \sqrt{°R}$

Table 1--Summary of flow parameters.

| Run | $P_t$ into 1st vane (psia) | $P_s$ exiting 1st vane (psia) | $P_s$ exiting 1st rotor (psia) | $P_s$ exiting 2nd vane (psia) | $P_s$ exiting 2nd rotor (psia) | $P_t$ exiting 2nd rotor (psia) | $\left.\frac{P_{T,in}}{P_{s,out}}\right\rvert_{stage}$ | $\left.\frac{P_{T,in}}{P_{T,out}}\right\rvert_{stage}$ |
|---|---|---|---|---|---|---|---|---|
| 1 | 90.0 | 78.5 | 67.6 | — | — | — | — | — |
| 5 | 47.1 | 40.4 | 34.3 | 30.5 | 28.3 | 29.1 | 1.66 | 1.62 |
| 6 | 48.9 | 43.0 | 36.4 | 32.5 | 29.7 | 30.4 | 1.65 | 1.61 |
| 7 | 86 | 77 | 70 | 63 | 58.3 | 59.9 | 1.49 | 1.45 |
| 8 | 89 | 82 | 75 | 68 | 64.3 | 64.4 | 1.40 | 1.40 |
| 11 | 98 | 90 | 79 | 71.5 | 69.0 | 67.5 | 1.44 | 1.47 |
| 12 | 48.8 | 43.3 | 37.3 | 34.1 | 31.7 | 32.2 | 1.54 | 1.52 |
| 13 | 45.8 | 40.3 | 34.7 | 32.0 | 29.7 | 30.2 | 1.54 | 1.52 |

Table 2a--Measured interstage pressures. Static pressure were measured at the outer shroud.

| Run | First vane $\frac{P_{T,in}}{P_{s,out}}$ | First stage $\frac{P_{T,in}}{P_{s,out}}$ | Second vane $\frac{P_{s,in}}{P_{s,out}}$ | Second rotor $\frac{P_{s,in}}{P_{s,out}}$ |
|---|---|---|---|---|
| 1 | 1.15 | 1.33 | — | — |
| 5 | 1.17 | 1.37 | 1.12 | 1.08 |
| 6 | 1.14 | 1.34 | 1.12 | 1.09 |
| 7 | 1.13 | 1.24 | 1.11 | 1.08 |
| 8 | 1.10 | 1.20 | 1.10 | 1.06 |
| 11 | 1.10 | 1.26 | 1.10 | 1.04 |
| 12 | 1.13 | 1.31 | 1.09 | 1.08 |
| 13 | 1.14 | 1.32 | 1.08 | 1.08 |

Table 2b--Component pressure ratios. Static pressures were measured at the outer shroud.

The Stanton number results presented here for both of the vane rows and the first blade row are based on conditions at the first vane inlet. The relationship used to evaluate the Stanton number was

$$\mathrm{St} = \frac{\dot{q}(T)}{(\dot{W}/A)[H_o(T_o) - H_w(T)]} \tag{1}$$

The value of A used for this evaluation was $1.73 \times 10^{-2}$ m$^2$ (0.186 ft$^2$), and corresponds to the annular area upstream of the first stage vane. In this formulation, the heat flux and the wall enthalpy are both evaluated at the same temperature, T. If the cold-wall heat flux, $\dot{q}(T_w)$, is desired, then it can be obtained by multiplying the given Stanton number by $(\dot{W}/A)[H_0(T_0) - H_w(T_w)]$. The greatest contributor to the uncertainty in Stanton number is the uncertainty in the weight flow, $\dot{W}$. For these experiments, the weight flow was found from an experimentally determined flow calibration curve supplied by NASA MSFC which plotted the flow function as a function of the total to static pressure ratio across the first stage nozzle. The uncertainty in the vane row pressure measurement translate into an uncertainty in the flow function and the weight flow. An uncertainty of approximately 10% in the weight flow was found. Assuming an uncertainty in the heat flux and temperature measurements to be 5%, the expected error in the Stanton numbers can be calculated using the methodology of Kline and McClintock, 1953 to be 12%.

### 3.1 First Vane and First Blade Surface Pressure Results

The measured surface pressure distributions on the first vane at 10%, 50%, and 90% span along with the predicted pressure distributions are presented on Figures 3.1.1-3.1.3. These results are presented for two stage pressure ratios, approximately 1.54 and 1.65. The agreement between the data and the prediction at all three spanwise locations is not particularly good. The cause of the disagreement is in large part attributable to the uncertainty in the pressure measurement. Prior to the initial experiment, the pressure

Figure 3.1.1--Pressure distribution at 10% span on first vane.

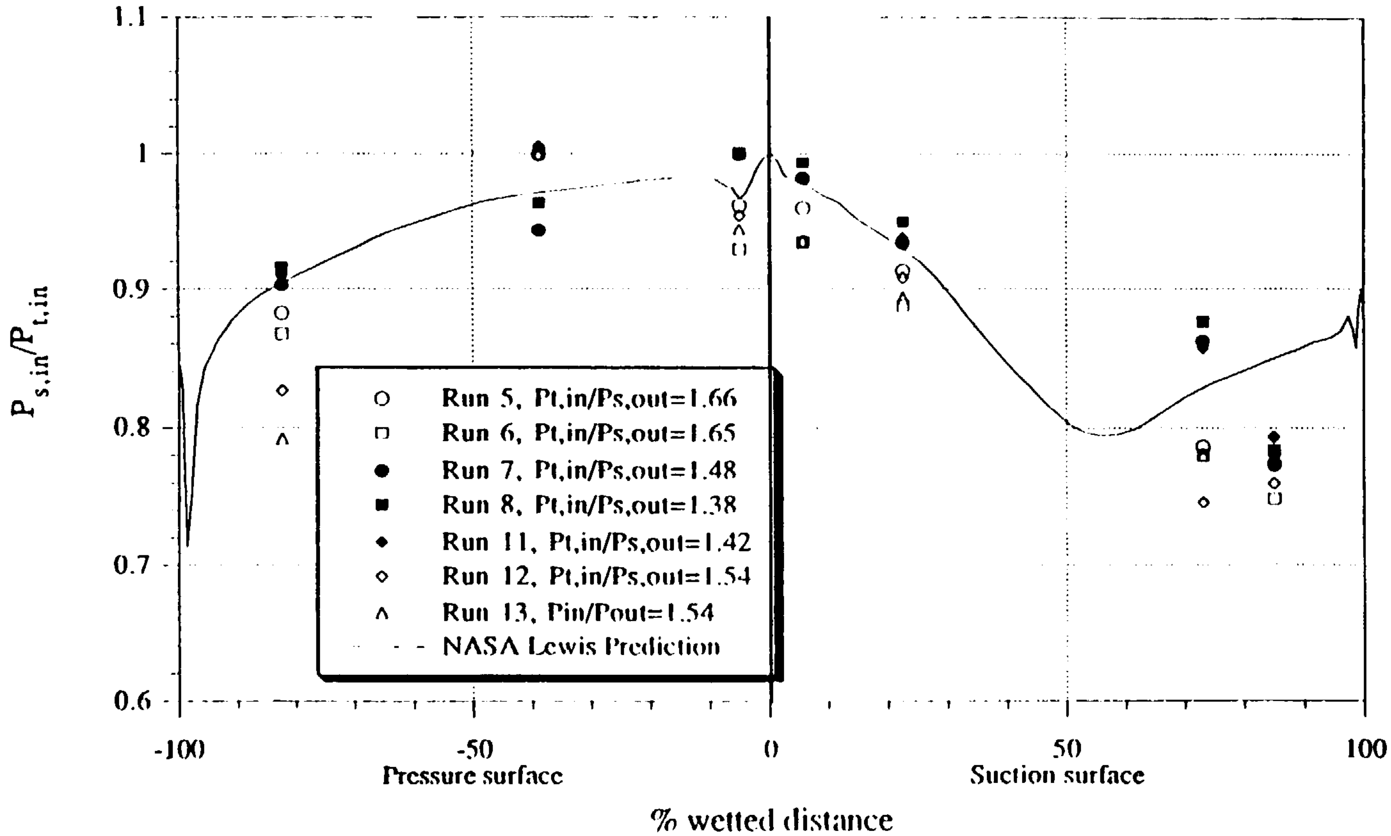

Figure 3.1.2--Pressure distribution at 50% span on first vane.

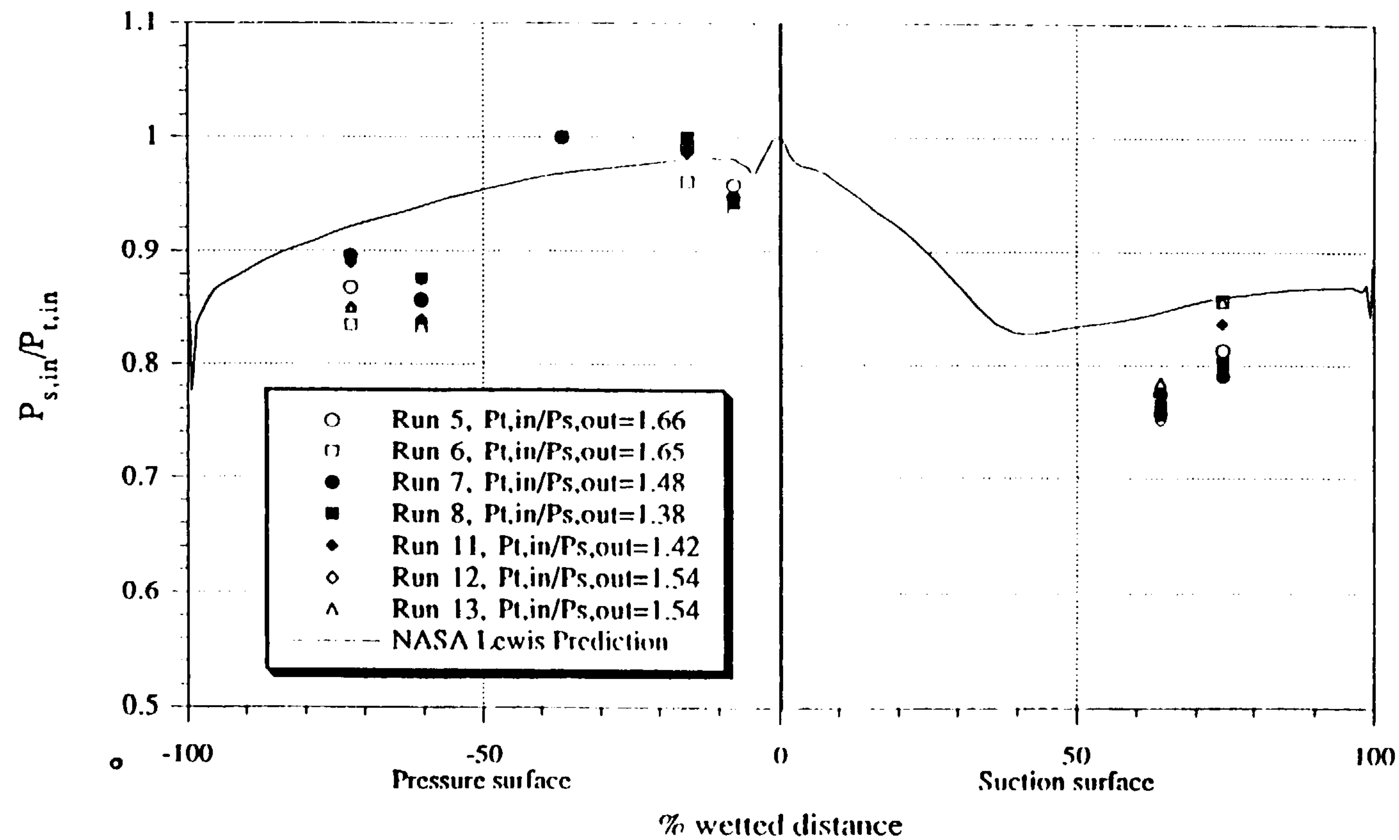

Figure 3.1.3--Pressure distribution at 90% span on first vane.

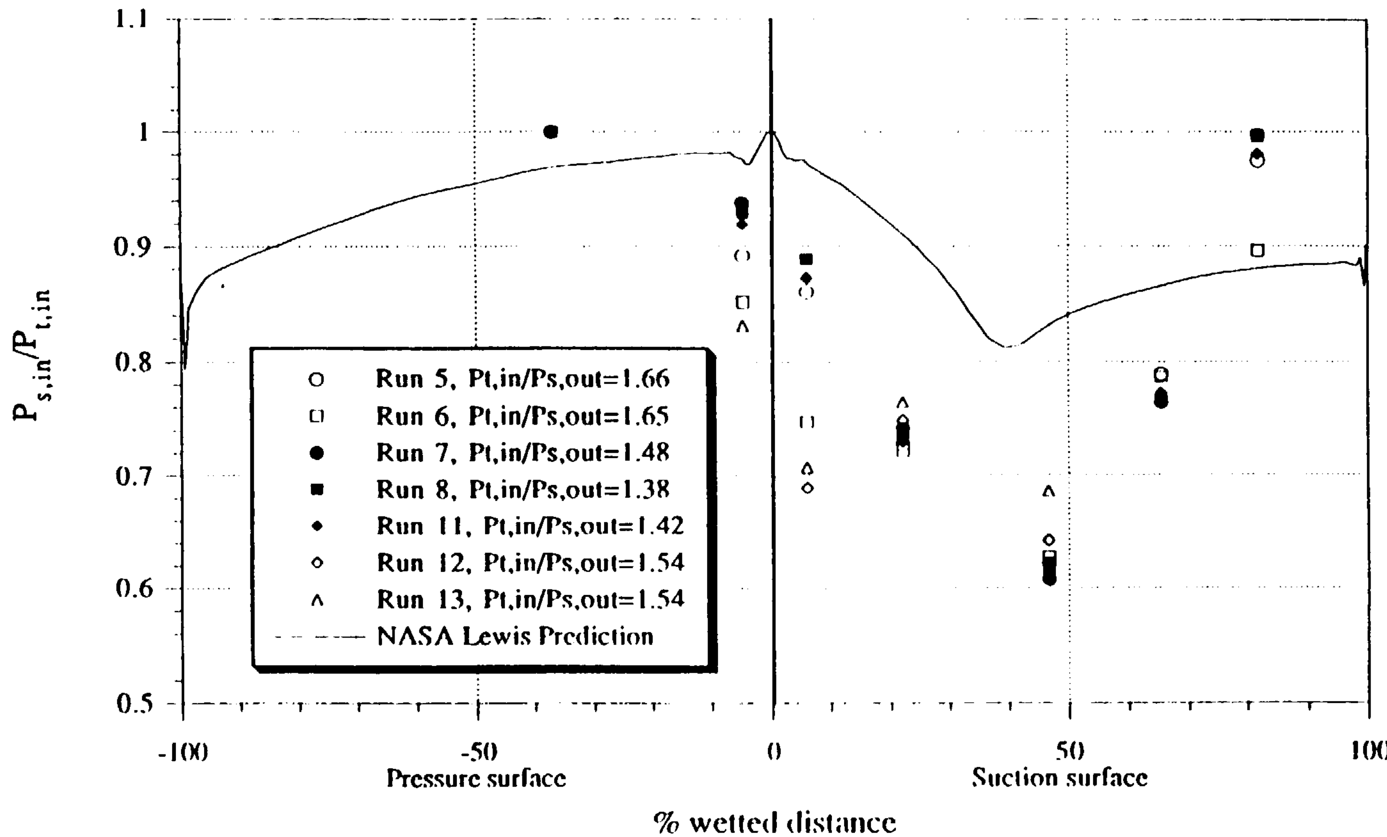

transducers were calibrated over the range from vacuum to 1.48 MPa (215 psia). During and after the experiments, they were calibrated again from vacuum to 0.655 MPa (95 psia). These latter calibrations were done by pressurizing the dump tank housing the turbine stage (see Figure 2.1.1). The pressure readings were recorded using the entire data recording system that is used during the experiment. For a given transducer, a linear fit was obtained for each data set over the pressure range of these experiments. The slope of the calibrations for most of the transducers was reproducible to within 3%. For a few others, the slope varied by as much as 5%. The pressure drop across the first vane row and the first blade row is relatively small for this turbine, being on the order of 10% to 15% of the inlet total pressure, which makes the uncertainty in the slope of the transducer calibration an important consideration. If a pressure measurement uncertainty of 3% due to variations in the slope of the calibration equation is assumed, along with a 2% uncertainty due to shock-tunnel reproducibility, the expected error in the normalized pressures ($P/P_T$) may be calculated using the methodology of Kline and McClintock (1953) to be 4.7%. The difficulty encountered here with the pressure measurements was unanticipated. A previous measurement program reported in Dunn, Bennett, Delaney, and Rao, 1990(a) demonstrated much better agreement between measurements and prediction. The calibration technique was the same in that work as used here. However, the transducers used in Dunn, et al., 1990a were 0 to 100 psia units while those used in this work were 0 to 600 psia units.

Figures 3.1.4, 3.1.5, and 3.1.6 present the measured surface pressure distributions on the first blade at the 10%, 50% and 90% locations at both values of stage pressure ratio. The same difficulties encountered with the vane pressure data described above were also encountered with the blade data. The disagreement between the measurements and the prediction are felt to be due to inaccuracy in the pressure measurement rather than problems with the prediction.

Figure 3.1.4--Pressure distribution at 10% span on first blade.

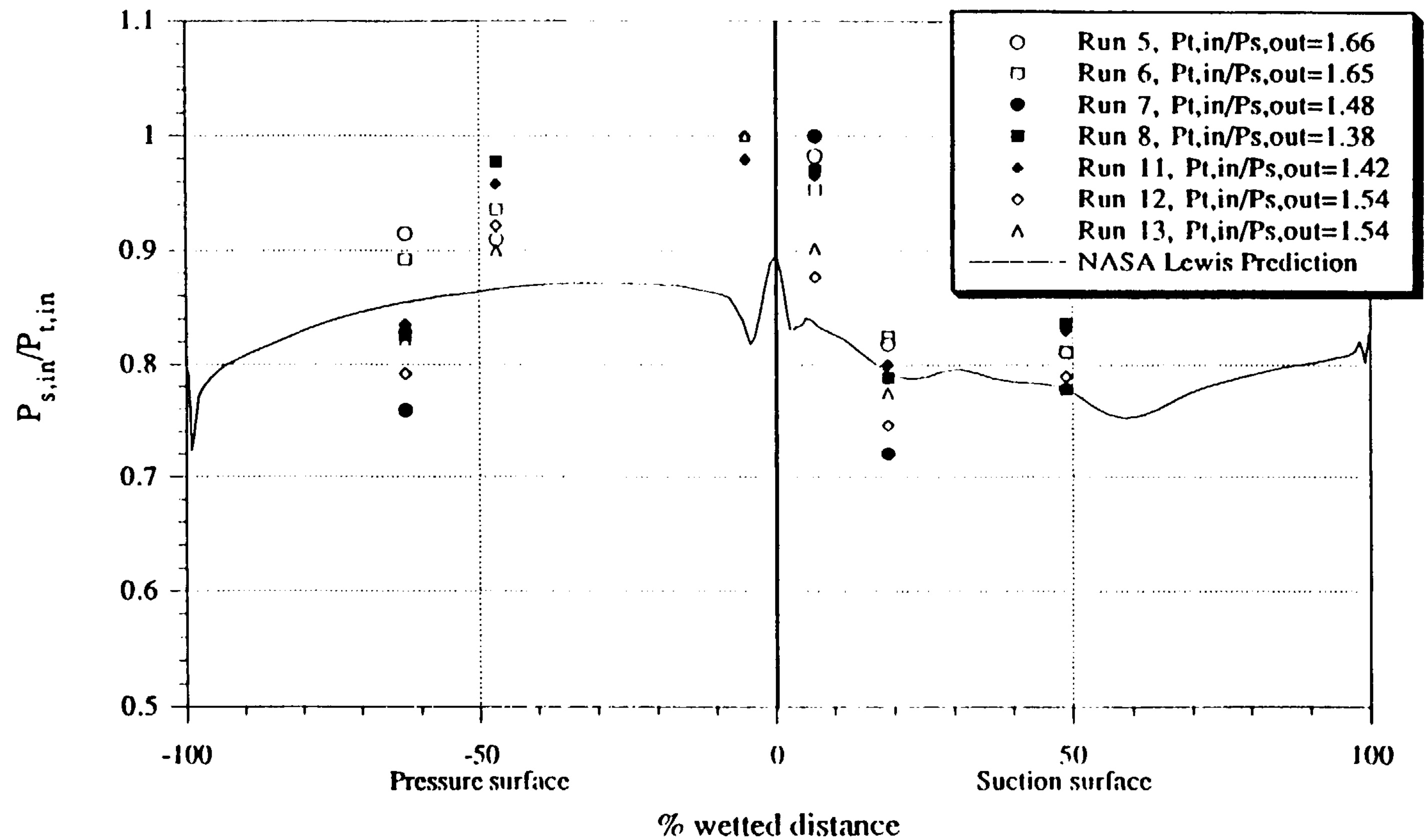

Figure 3.1.5--Pressure distribution at 50% span on first blade.

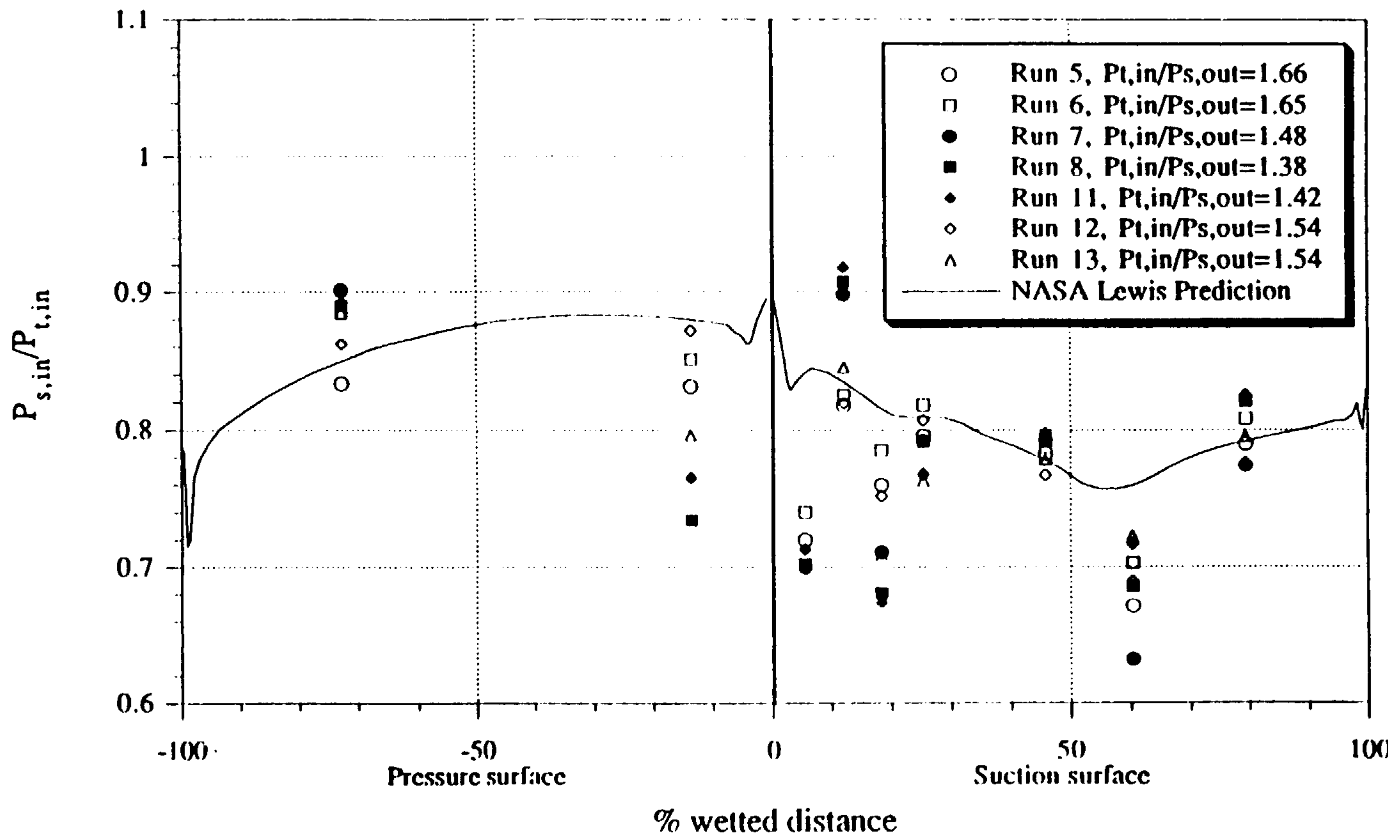

Figure 3.1.6--Pressure distribution at 90% span on first blade.

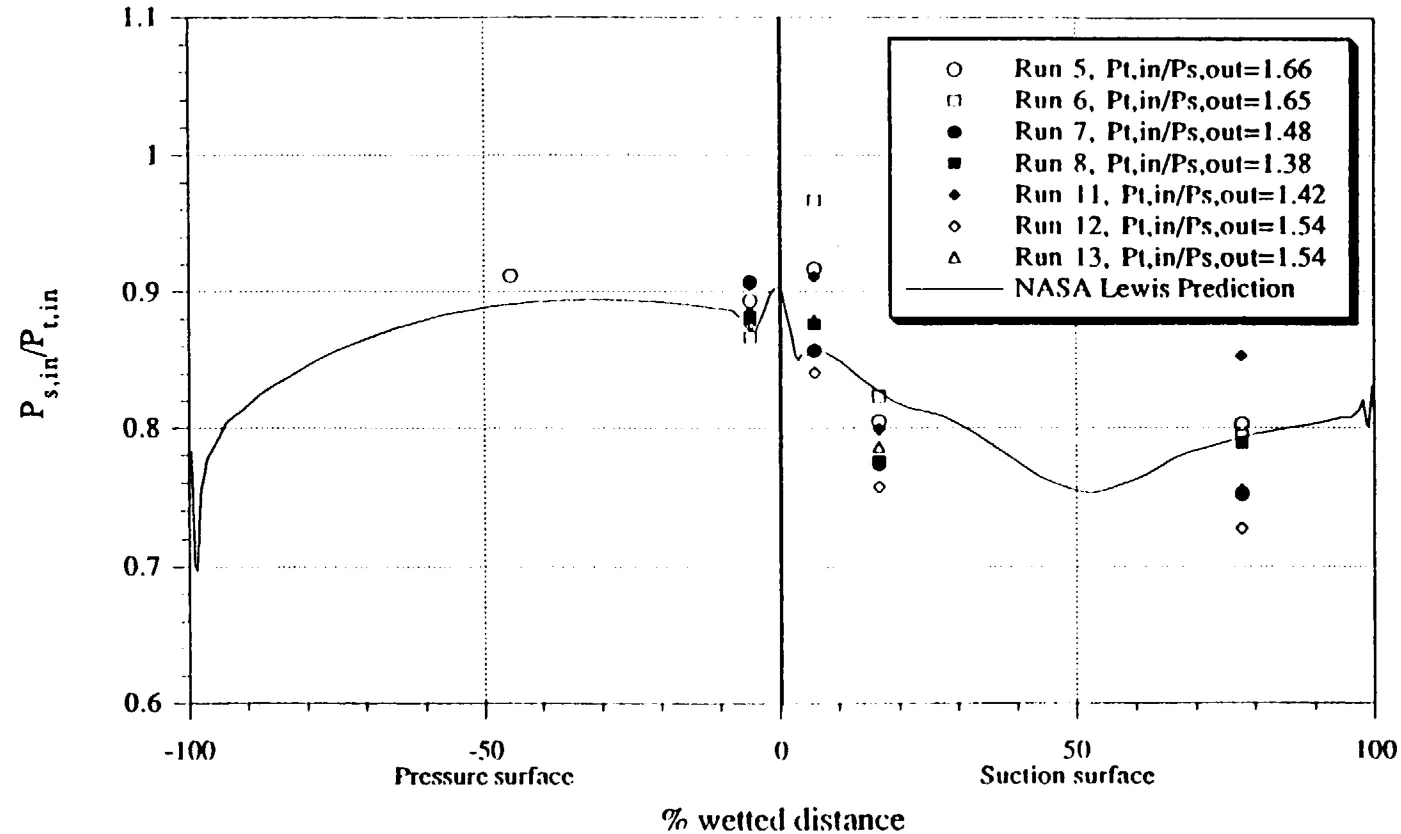

## 3.2 First Vane Surface Stanton Number Results

Figures 3.2.1 and 3.2.2 present the measured Stanton number distributions for the vane at 50% span for Reynolds numbers of 140,000 and 250,000, respectively. Figure 3.2.3 presents the Stanton number data for both Reynolds numbers at 10% span and Figure 3.2.4 presents data for both Reynolds numbers at 90% span. The low Reynolds number data were obtained at stage pressure ratios of 1.54 and 1.65 while the higher Reynolds number data were obtained at about 1.4 and 1.48. Inspection of the data suggests that the stage pressure ratio, in general, has little influence on the Stanton number distributions for the vane locations at which measurements were obtained.

The experimental results for the first vane presented in Figure 3.2.1 illustrate a rapid decrease in Stanton number on the suction surface from the stagnation point to about 15% wetted distance followed by a sharp increase near this location, then a peak at about 50% wetted distance. On the pressure surface, the data fall sharply from the stagnation point reaching a minimum at about 25% wetted distance, then increases steadily towards the trailing edge. This trend in the pressure surface data is consistent with that seen previously for the Garrett TFE731-2 HP turbine (Dunn, Rae and Holt, 1984), the Air Force LART (Dunn, Martin and Stanek, 1986) the Teledyne 702 turbine (Dunn and Chupp, 1988), as well as two other unpublished Calspan data sets. The peak Stanton number is shown to occur at the stagnation point and the maximum value reached on the suction and pressure surfaces are comparable with each other and equal to a little more than half of the stagnation value. Similar trends are seen at high Reynolds numbers (Figures 3.2.2) but with the minimums occurring closer to the stagnation point. Furthermore, the maximum in the suction surface data also occurs closer to the stagnation point.

Figure 3.2.1 also compares vane midspan experimental results with four predictions. Two of the predictions are for fully turbulent flow. The third and fourth predictions incorporate transition models. The two fully turbulent predictions were done

Figure 3.2.1. Stanton number distribution on first vane, 50% span, Re~140,000.

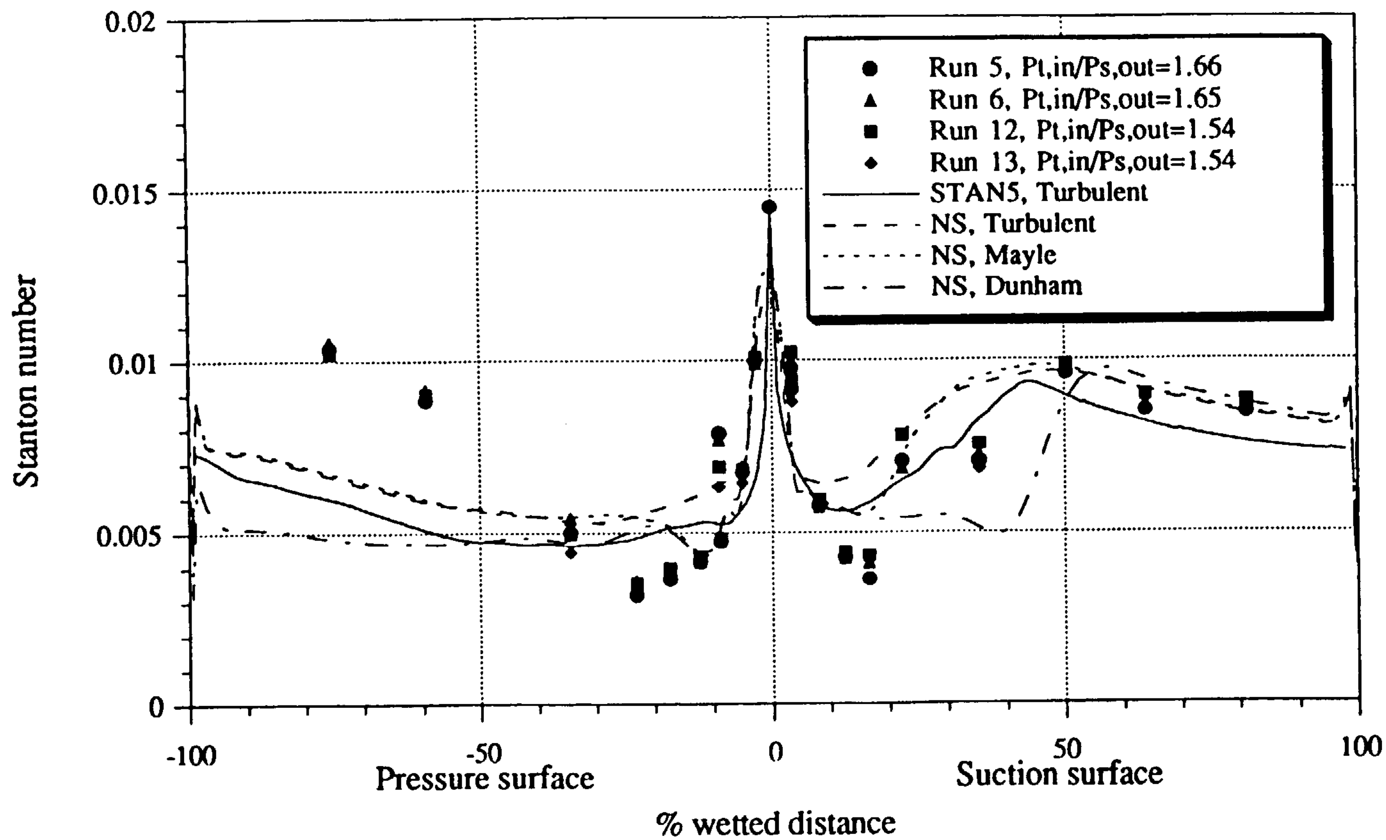

Figure 3.2.2. Stanton number distribution on first vane, 50% span, Re~250,000 results.

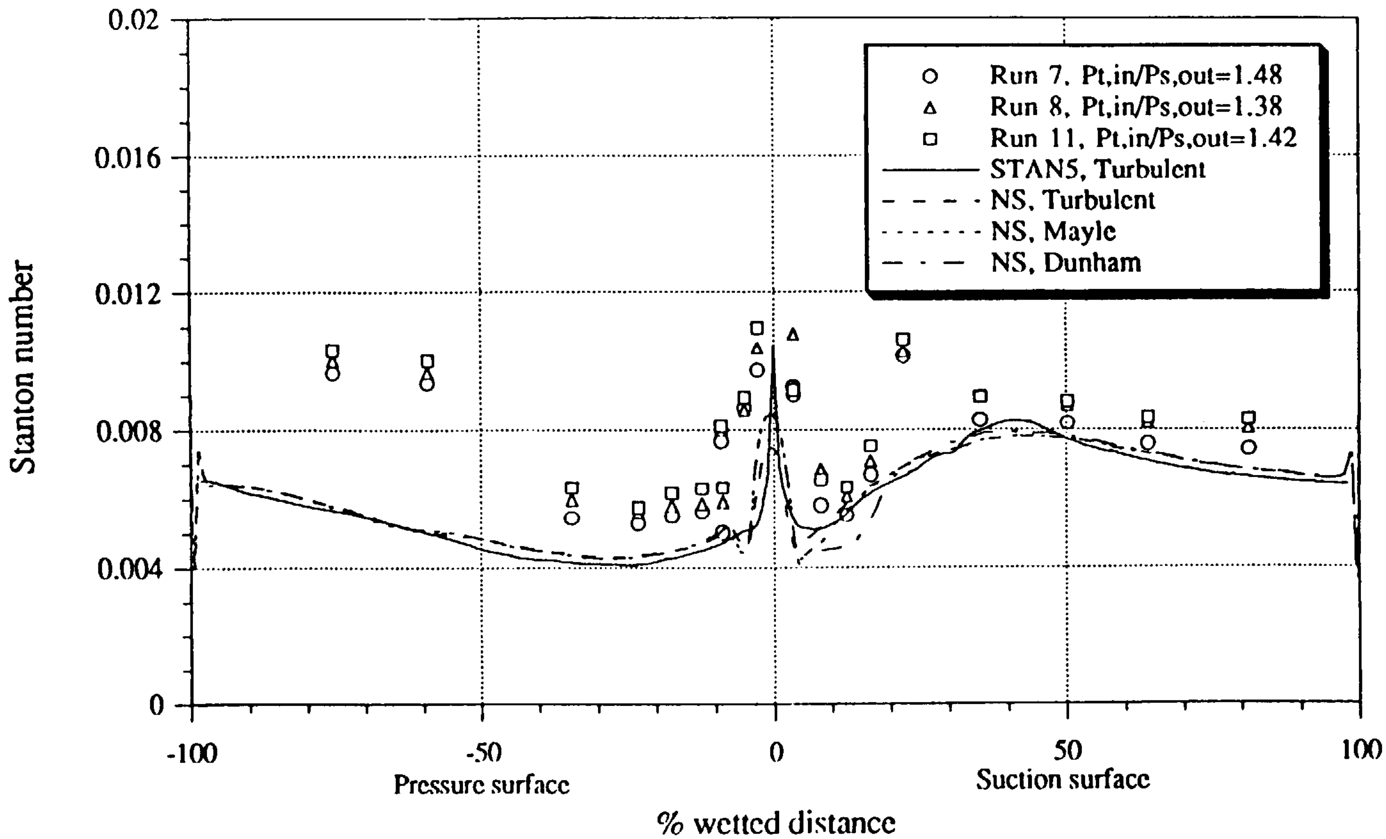

Figure 3.2.3. Stanton number distribution on first vane, 10% span. closed symbols: Re~140,000 data, open symbols: Re~250,000 data

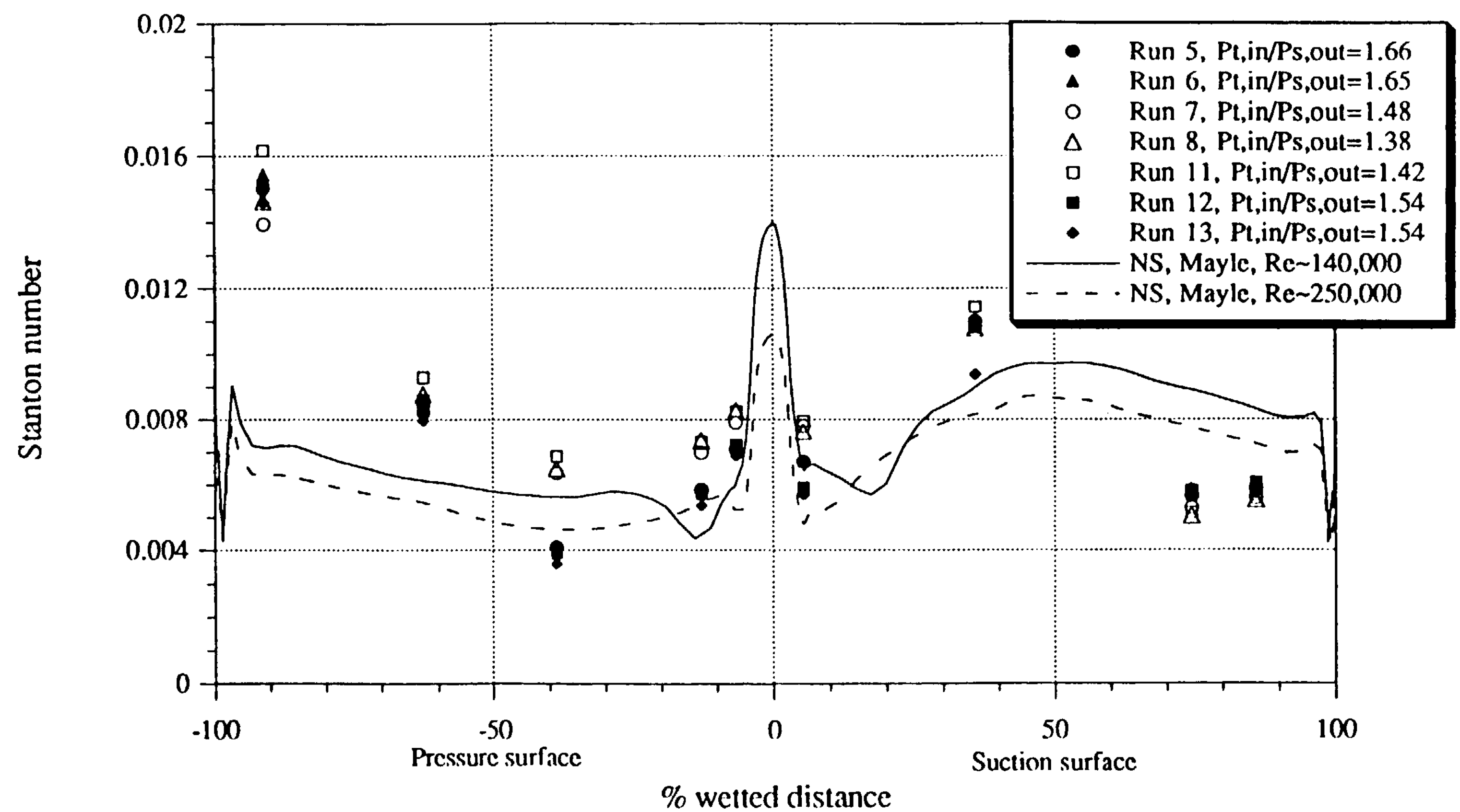

Figure 3.2.4. Stanton number distribution on first vane, 90% span
closed symbols: Re~140,000 data, open symbols: Re~250,000 data

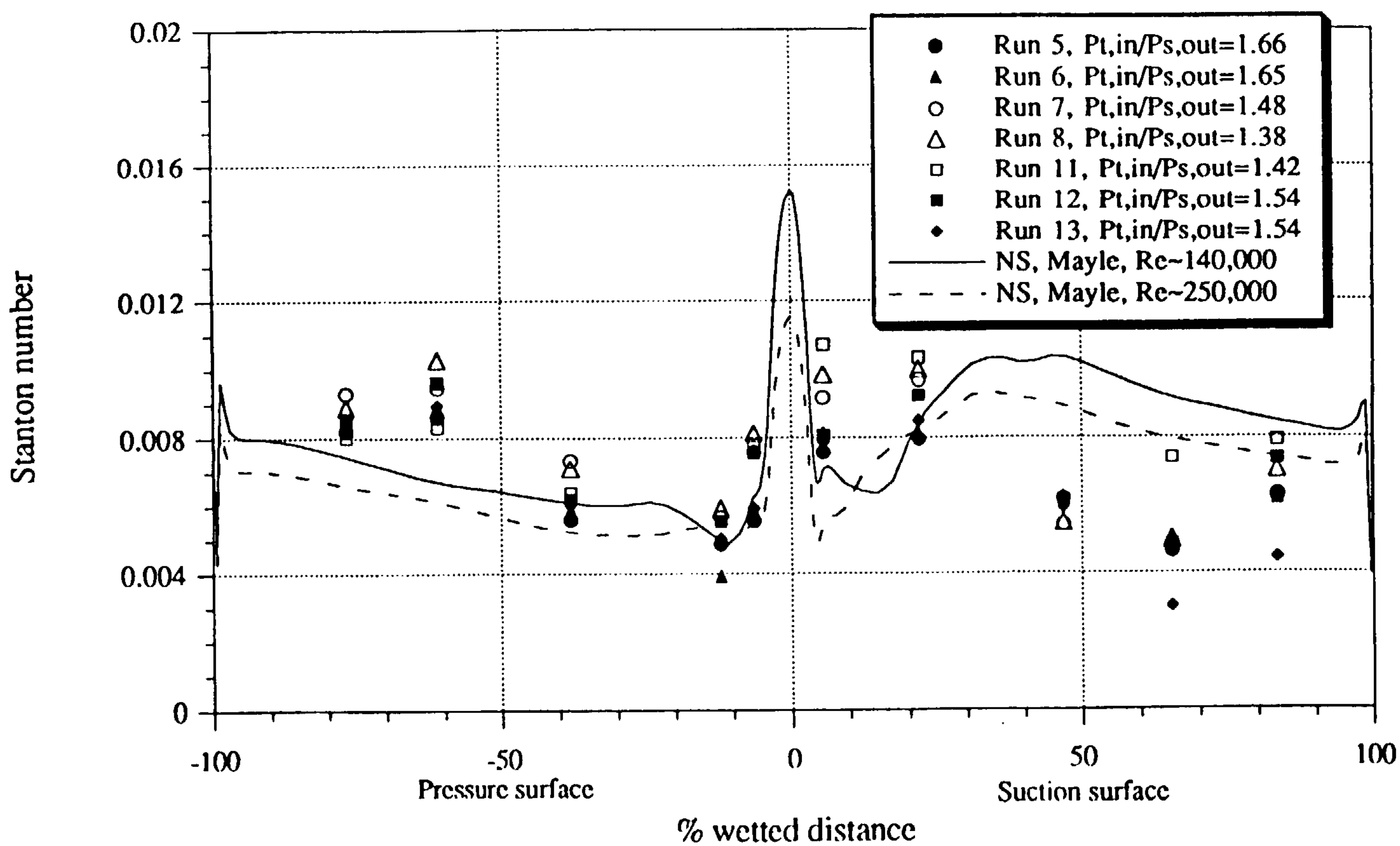

using the quasi-3D Navier-Stokes analysis described by Boyle (1991) and Gaugler's modified version the STAN5 boundary layer analysis of Crawford and Kays (1976). The predictions including transition were obtained by incorporating the transition model of Mayle, 1991 and the transition model due to Dunham, 1972 into the just noted Navier-Stokes analysis. Of the two fully turbulent predictions, the STAN5 prediction illustrates better overall agreement with the data. On the suction surface, the STAN5 prediction doesn't fall as low as the data in the vicinity of 15% wetted distance, and it doesn't climb as high as the data beyond 50% wetted distance. On the pressure surface, both of the fully turbulent predictions agree with the data reasonably well from the stagnation point to about 40% wetted distance. The data points at 60% and 80% wetted distance are significantly greater than the prediction. It was noted earlier in this section that this trend has been seen previously for full-stage turbines. This same trend was noted by Nealy, et al., 1984 for a vane ring downstream of a combustor. However, the Navier-Stokes analysis used here was applied to those data (Boyle, 1991) and reasonably good agreement between data and prediction was obtained. It is felt that the relatively high upstream turbulence in itself is not sufficient to account for the high pressure surface heat transfer, since the local turbulence level decreases significantly as the flow accelerates through the vane passage. The good agreement between the STAN5 boundary layer prediction and the Navier-Stokes fully turbulent analyses suggests that the numerical solutions of the analyses are not the source of the disagreement with the experimental data.

For the calculation incorporating the Dunham, 1972 transition model, transition occurs midway along the suction surface. However, the prediction is not in good agreement with the experimental data from about 7% wetted distance to 50% wetted distance. This analysis predicts Stanton numbers along the pressure surface that are generally in agreement with STAN5 over the initial 50% of that surface. Beyond 50%, the shape of the Dunham prediction deviates from the other two and falls below them and well below the data. This is because the flow never becomes fully turbulent with this model. Also included on Figure 3.3.1 is the Navier-Stokes prediction with the Mayle, 1991 transition model incorporated. This prediction is in much better agreement with the data than is the other prediction incorporating transition. Overall, the Navier-Stokes prediction which includes the Mayle transition model appears to be in better agreement with the data than any of the other predictions.

Figure 3.2.2 presents a comparison between the high Reynolds number data and the same four predictions described above. There is very little difference among the predictions at this higher Reynolds number except in the vicinity of the stagnation point and in the region of 5% to 20% on the suction surface. Both the N-S and the STAN5 solutions predict the stagnation region data reasonably well. The N-S solution with the Mayle transition model predicts the 5% to 20% wetted distance region better than the N-S solution with the Dunham model. On the pressure surface, all of the predictions are in reasonably good agreement with each other and all fall below the data from the stagnation point to about 40% wetted distance. The experimental results at 60% and 80% wetted distance are underpredicted by a significant amount by all four solutions. In summary, the predictions shown in Figures 3.2.1 and 3.2.2 show best agreement with the data when a fully turbulent analysis is used, even for the low Reynolds number cases. The transition models of both Mayle and of Dunham are highly dependent on the freestream turbulence intensity. Previous measurements gave an intensity of about 6% at the turbine inlet. At the low Reynolds number, Dunham's model predicts the start of transition too far downstream on the suction surface. Mayle's model agrees better with the data. At the high Reynolds number, transition occurs close to the leading edge, and there is little difference among the predictions.

Figures 3.2.3 and 3.2.4 present the first vane Stanton number results at 10% and 90% span, respectively. Both sets of Reynolds number data are included on these figures. The N-S prediction with the Mayle transition model has been selected for comparison with the experimental data. It would be anticipated that the high Reynolds number data set should be consistently lower than the low Reynolds number data by about 15% ($(2)^{0.2}=1.15$). There is sufficient uncertainty in the Stanton number results as described in Section 4 that generally, the data sets appear to overlap. The agreement between the suction surface prediction and the data is not as good as it was at midspan for either 10% or 90% span. In general, beyond 50% wetted distance, the prediction fell well above the data on the suction surface. The data point at 60% wetted distance is above the prediction, but no more so than the suction surface data points are below the prediction. The pressure surface data at 90% span are in as good agreement with the prediction as has been seen at any location on this vane.

## 3.3 First Blade Surface Stanton Number Results

### 3.3.1 Discussion of blade data

Figures 3.3.1 and 3.3.2 present the measured Stanton number distributions for the first blade at midspan for Reynolds numbers of 140,000 and 250,000, respectively. The Reynolds number data sets are both given on the same figure for the 10% span (Figure 3.3.3) and the 90% span (Figure 3.3.4) locations. The heat-flux values in the vicinity of the leading-edge region are known to be sensitive to incidence angle. However, the rotor speed range over which data were taken in these experiments (99% to 103% of design) was sufficiently small that it is unlikely that incidence angle had a significant effect. Likewise, the local Stanton number is sensitive to stage pressure ratio because of the change in incidence angle associated with the higher axial velocity (increased weight flow) at the lower value of pressure ratio. From the weight flow data presented in Table 1 it was difficult to obtain an estimate of the incidence angle variation resulting from the difference in pressure ratio. The experimental data (runs 5, 6, 12, and 13) at the 10% and 90% spanwise locations are consistent with each other near the leading edge in that the Stanton numbers for runs 5 and 6 are consistently greater than those for runs 12 and 13.

Figure 3.3.1. Stanton number distribution on first blade, 50% span, Re~140,000.

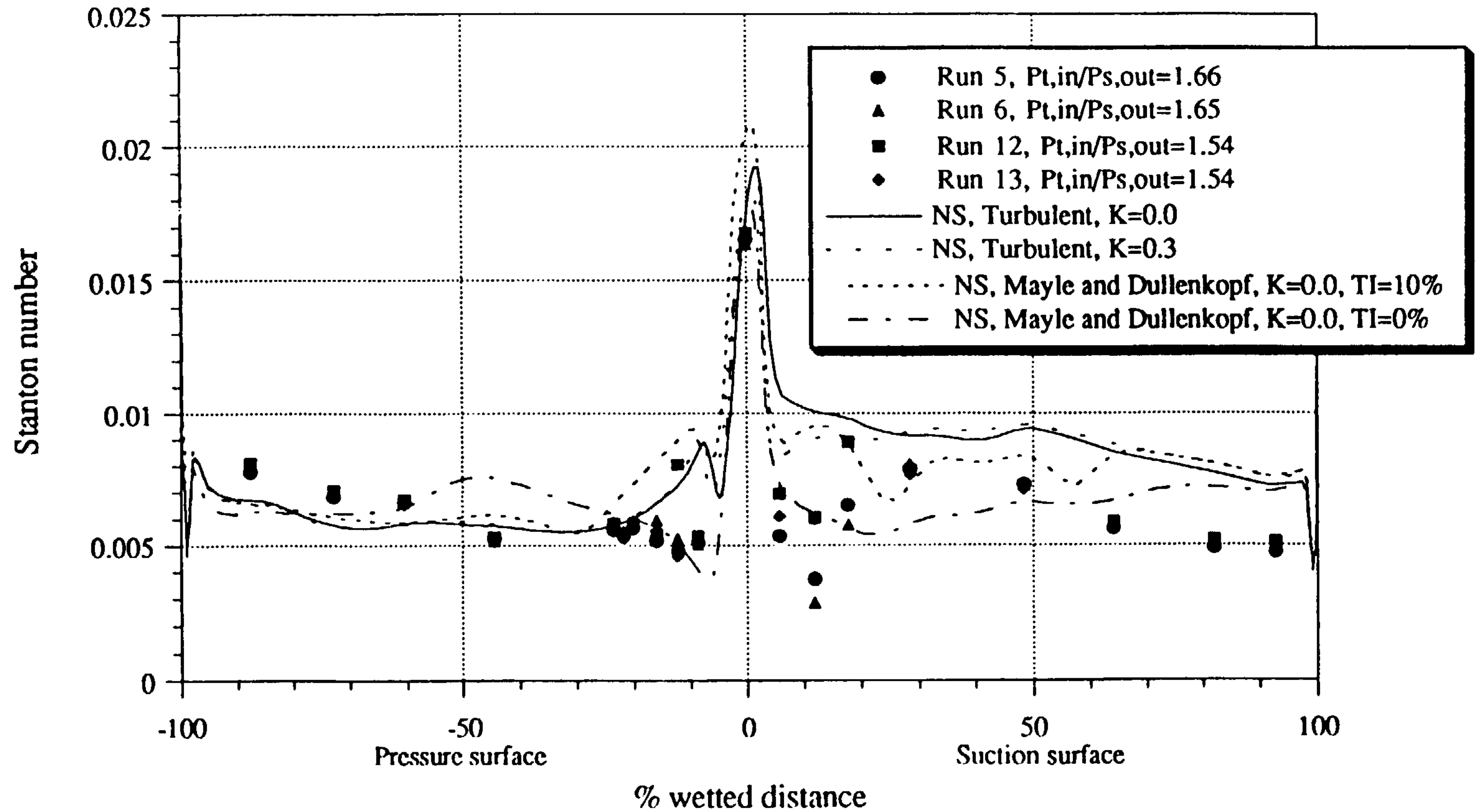

Figure 3.3.2. Stanton number distribution on first blade, 50% span, Re~250,000. Comparison with predictions for various roughness heights.

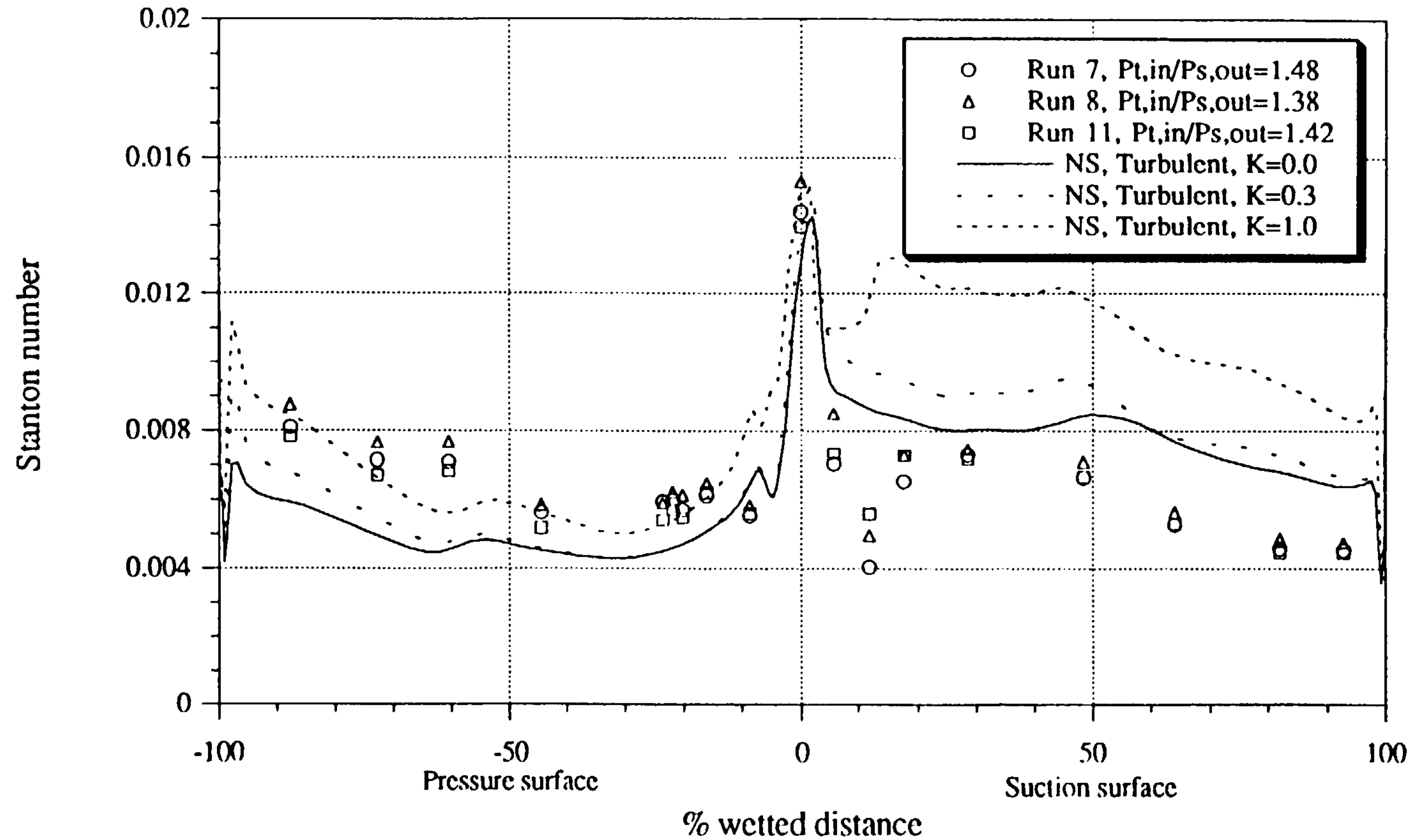

Figure 3.3.3. Stanton number distribution on first blade, 10% span
closed symbols: Re~140,000 data, open symbols: Re~250,000 data

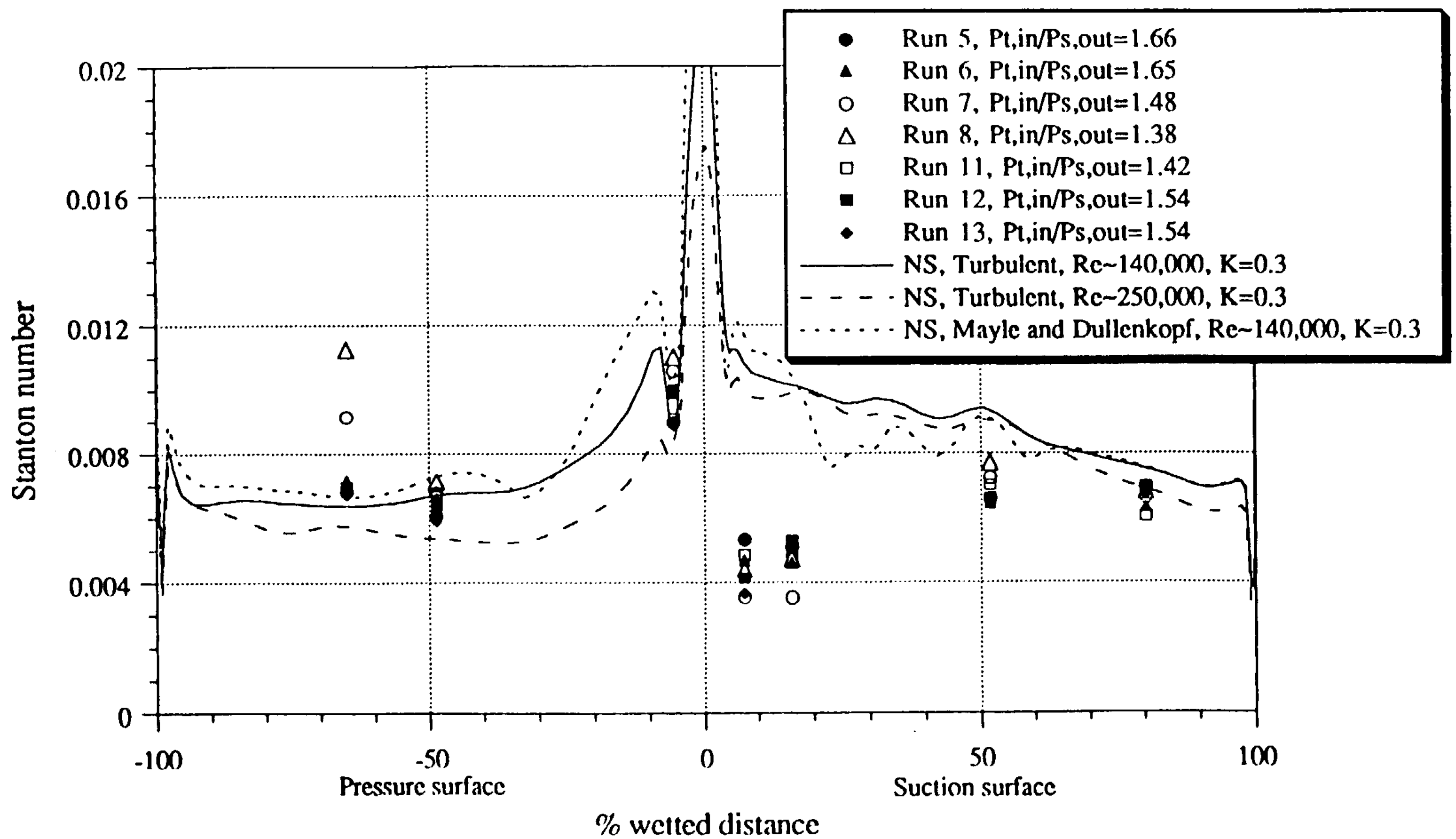

Figure 3.3.4. Stanton number distribution on first blade, 90% span
closed symbols: Re~140,000 data, open symbols: Re~250,000 data

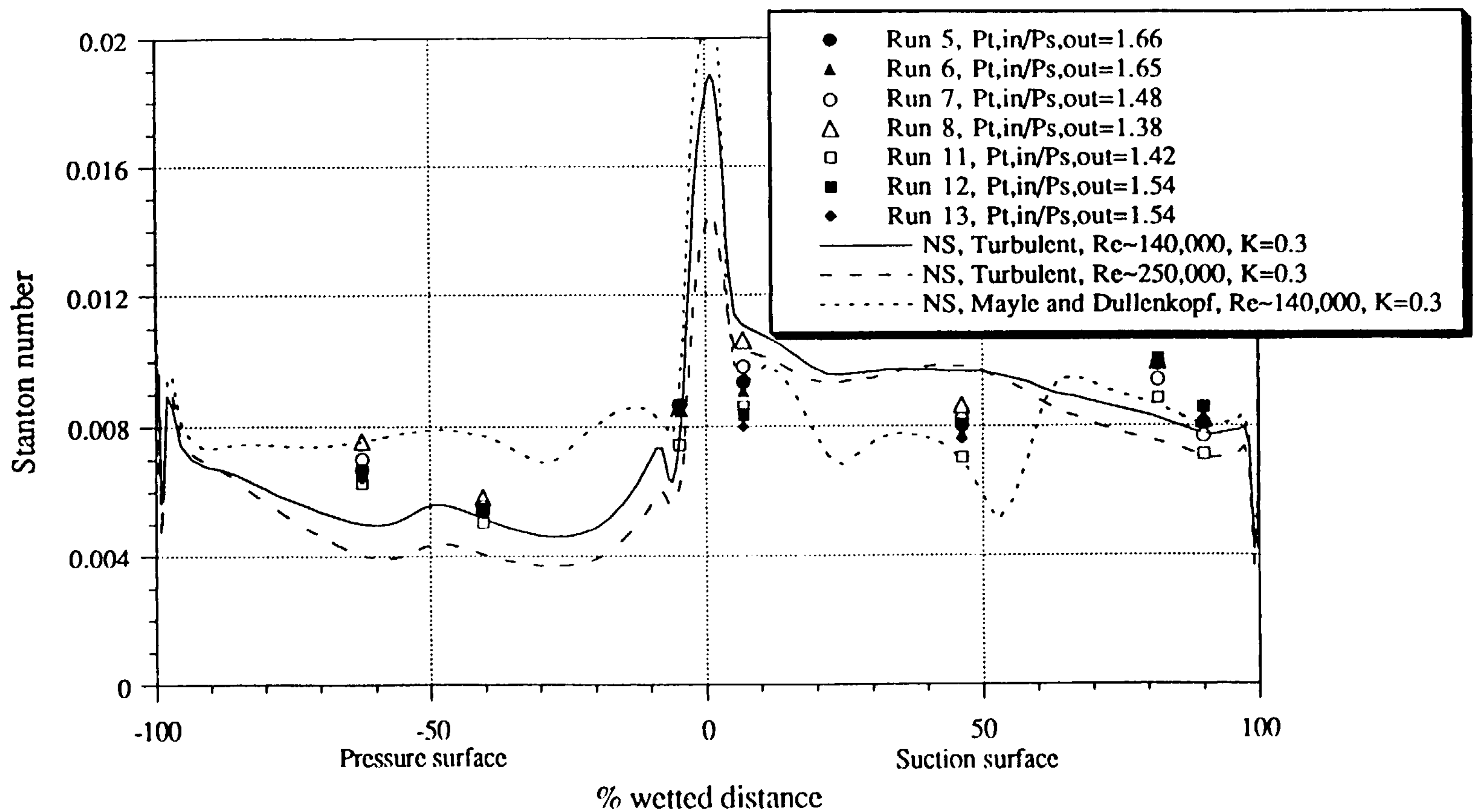

However, the trend in the Stanton number results from these same runs at midspan are opposite to that observed at 10% and 90% suggesting that if there was an influence, it didn't occur all along the leading edge. Another interpretation of the data would be that within the uncertainty of the data, no significant influence of pressure ratio or speed was observed for the range of conditions used here. Beyond 50% wetted distance, the results illustrate little influence on the Stanton number distribution for either the pressure or suction surface. Returning for a moment to the midspan results presented on Figure 3.3.1, at the stagnation point the experimental results are in agreement with each other, but immediately thereafter (from 0% to 15% wetted distance) on the suction surface and in the vicinity of 12% wetted distance the data do not coalesce. Three of the runs (run 6, 12, and 13) shown on this figure were for nominally 103% of design speed, and the other (run 5) for 99% of design speed. Two of the runs at 103% of design speed were for a stage pressure ratio of 1.54 (runs 12 and 13) while the other two runs were at a pressure ratio of about 1.65 (runs 5 and 6). At the 12% wetted distance location, two of the 103% speed points (runs 12 and 13 for the same stage pressure ratio) are in good agreement while the other one (run 6, higher pressure ratio) is low. Also note that runs 5 and 6, which are for the same stage pressure ratio but different speeds (99% and 103%), are in reasonably good agreement with each other suggesting that for this speed variation the influence on Stanton number distribution is not large.

The experimental data presented on Figure 3.3.1 show that the Stanton number fell rapidly from the stagnation point to about 10% wetted distance followed by a rapid increase, reaching a maximum value for the suction surface at about 25% wetted distance. On the pressure surface, the Stanton number increases from a minimum value in the vicinity of 15% wetted distance to a maximum near 90% wetted distance. The maximum values occurring on these two surfaces are comparable and well below the stagnation point value. Included on Figure 3.3.1 are two fully turbulent Navier-Stokes predictions, one for a rough airfoil and the other for a smooth airfoil, and a N-S prediction, with the

Mayle and Dullenkopf, 1989, 1990 intermittency model included, for a smooth airfoil. The STAN5 boundary layer analysis showed separation for the midspan pressure surface using the predicted inviscid flow field for a boundary condition and, therefore, the STAN5 prediction could not be obtained for the blade. The Navier-Stokes analyses do not indicate a significant increase in heat transfer due to blade surface roughness. On the pressure surface both of the fully turbulent analyses are in good agreement with the experimental data. However, on the suction surface these same predictions fall consistently above the data. The third prediction included on Figure 3.3.1 is in essential agreement with the fully turbulent predictions on the pressure surface. On the suction surface, it also overpredicts the data, but is closer than the fully turbulent predictions. The predicted heat transfer at the leading edge is higher than the experimental data. The average augmentation of the heat transfer in the laminar region was calculated assuming a turbulence intensity of 10%. The transition model used a background turbulence intensity of 2%. The intermittency model overpredicted the heat transfer at the leading edge by about 33%. This indicates that the augmentation due to freestream turbulence was excessive. The Froessling number at the stagnation region was calculated from the experimental results for this case, and using the cylinder in cross flow correlation of Traci and Wilcox, 1975 a freestream turbulence intensity of about 7% was estimated.

Along the entire pressure surface the fully turbulent predictions are nearly identical, and agree well with the experimental data. These predictions for the rotor are in contrast with those for the vane, where the pressure surface heat transfer exceeded the fully turbulent prediction. The transitioning prediction, which includes the effect of freestream turbulence, overpredicts the pressure surface heat transfer. The largest source of uncertainty in the heat transfer predictions is due to the uncertainty in the freestream turbulence for the augmentation of the laminar viscosity due to this freestream turbulence.

### 3.3.2 Blade surface roughness considerations

The first stage blade of this turbine appeared to be rough and there was concern that the roughness may enhance the heat transfer. Blair and Anderson, 1992 have illustrated that this enhancement can be significant. The influence of surface roughness on the blade data presented herein was therefore investigated.

Boyle and Civinskas, 1991, investigated the influence of surface roughness on the predicted heat transfer to the surface. The effective roughness height was strongly dependent on both the roughness and the density. The roughness density can be found from the trace shown in Figure 2.2.7. In this figure, the horizontal axis is compressed by more than a factor of ten over the vertical axis. Even though the blade shown in Figure 2.4,1, 2.4.2, and 2.5.1 are visibly rough, the peaks are not spaced closely together.

Comparing the two analyses shows that the effect of surface roughness is very small. This was not unexpected. The insensitivity to surface roughness is the result of both the low Reynolds number, and the effect of surface roughness density. In the Navier-Stokes analysis a reference $y^+$ was used for an a priori determination of the grid spacing. This reference value is given by

$$y^+_{REF} = 0.17y\, Re^{0.9}/s^{0.1}$$

where y is the distance from the surface, Re is the exit Reynolds number per unit length, and s is a characteristic distance.

An analogous reference roughness height is

$$k^+_{REF} = 0.17k\, Re^{0.9}/s^{0.1}$$

For the low Reynolds number case the exit unit Reynolds number was 1.28 x $10^7$/m (3.9 x $10^6$/ft).

The roughness height, k, in the above equations is not the actual roughness height, but rather the equivalent roughness height. The equivalent roughness height was estimated using the approach taken by Boyle and Civinskas, 1991 to be less than 0.3 of the actual roughness height. Even though the actual roughness height was ~150,000 Å (590 microinches), the value of $k^{+}_{REF}$ was calculated to be only 2.7. This value of the reference roughness height is only approximate since it is based on a friction factor for a smooth flat plate. Nonetheless, the value of $k^{+}$ is less than the value of 5 for a hydraulically smooth surface. Consequently, the rough and smooth heat transfer predictions are nearly identical. It should be noted that blades with this surface roughness, when operated in the SSME environment, are no longer hydraulically smooth due to the much higher Reynolds number of the actual engine. Calculations showed an increase in heat transfer of up to 25% due to surface roughness at the SSME operating conditions for K=0.3. The parameter K represents the ratio of the equivalent roughness height (k) to the actual roughness height.

Figure 3.3.2 presents the first blade midspan Stanton number data for the high Reynolds number case. Also included on this figure are three N-S predictions which were performed for different surface roughness heights. The N-S turbulent prediction with K=0 is consistently above the N-S prediction with the Mayle and Dullenkopf intermittency model. The value of Stanton number at the stagnation point is predicted reasonably well by the N-S solution. On the suction surface, the N-S turbulent prediction for a smooth surface (K=0) is consistently above the data. The prediction for K=0.3 is about 12% higher over the initial 50% of the surface, then about the same over the remainder of the surface. The prediction for K=1.0 represents a significant enhancement and is well above the data over the entire surface.

On the pressure surface of the blade, Figure 3.3.2 illustrates that the shape of the predictions is consistent with the data. The predictions for K=0 and K=0.3 both fall below the data. The prediction for K=1.0 is in reasonable good agreement with the data over the entire pressure surface.

Figures 3.3.3 and 3.3.4 present the experimental data and comparisons with predictions for the 10% span and the 90% span locations, respectively. Both sets of Reynolds number data are included on these figures. Figure 3.3.3 includes the fully turbulent N-S predictions for both Reynolds numbers and the N-S prediction with the Mayle and Dullenkopf intermittency model for the low Reynolds number. At the high Reynolds number, this prediction is essentially the same as the corresponding N-S fully turbulent prediction. For the suction surface, there is very little difference among the three predictions. The data between 5% and 15% wetted distance are substantially below the predictions, while the data between 50% and 80% are below, but in reasonable agreement with the predictions. For the pressure surface, the fully turbulent prediction is generally below the data while the intermittency model provides a reasonable representation of the data. The comparison presented in Figure 3.3.4 for the 90% span location demonstrates reasonably good agreement between the data and the intermittency model prediction for the suction surface and correspondingly good agreement on the pressure surface for the N-S fully turbulent prediction.

## 3.4 Second Vane Surface Stanton Number Results

The second vane Stanton number measurements are shown in Figures 3.4.1 for both Reynolds number cases and both stage pressure ratios. For the second vane, only midspan heat-flux data were taken. Figure 3.4.1 also includes the predicted midspan Stanton number distributions. A fully turbulent and an intermittency model prediction are shown. The high Reynolds number intermittency prediction provides a good prediction at the stagnation point. On the suction surface, the fully turbulent and the low Reynolds number intermittency model predictions are conservative over the entire surface. The high Reynolds number intermittency model prediction is a better representation of the

Figure 3.4.1. Stanton number distribution on second vane, 50% span
closed symbols: Re~140,000 data, open symbols: Re~250,000 data

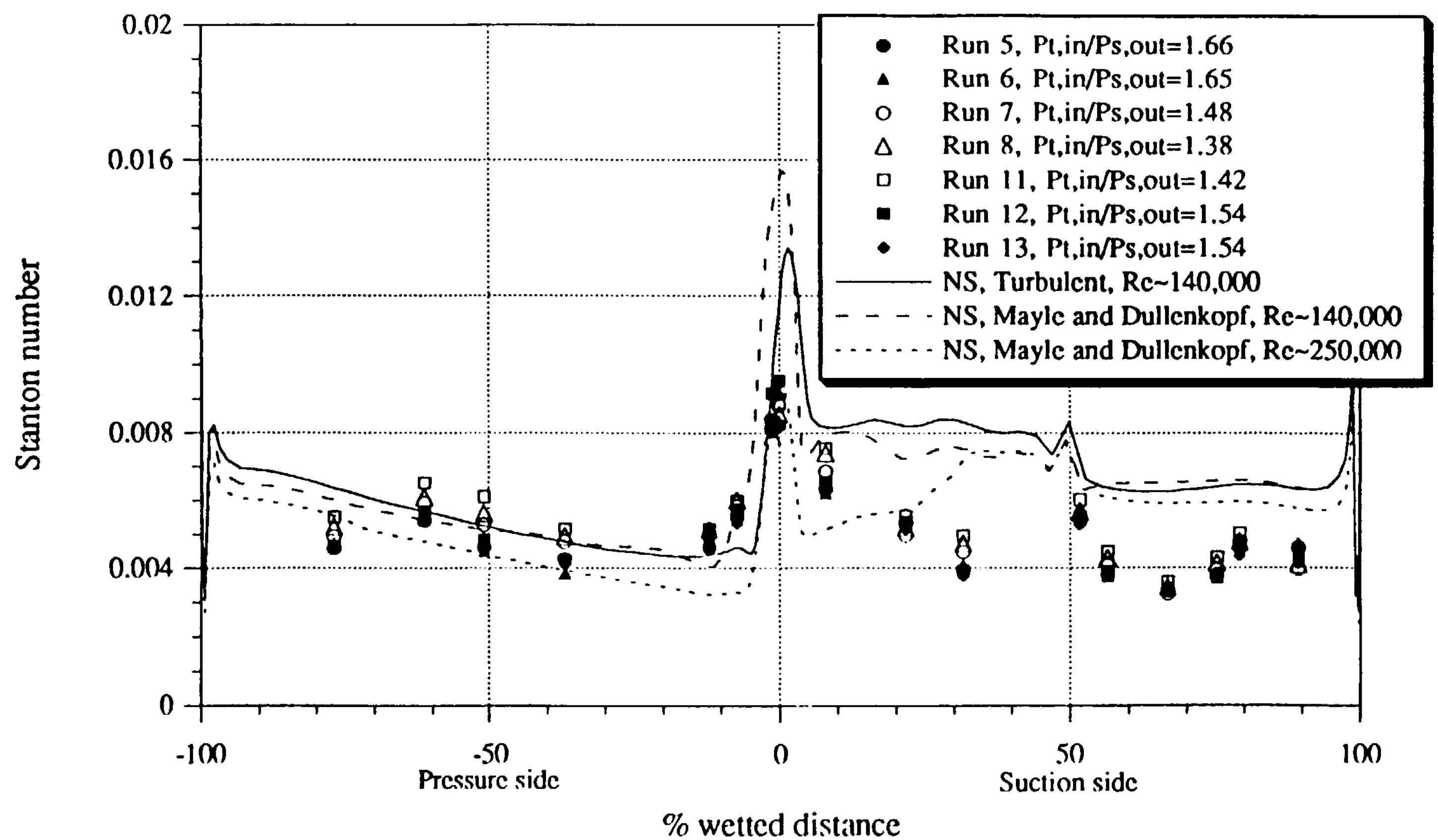

data. On the pressure surface, both the fully turbulent and the low Reynolds number intermittency models provide reasonable predictions of the data. The high Reynolds number intermittency model prediction on this surface is lower than the other two predictions by about 15% as would be anticipated.

### 3.5 Blade Platform, Blade Tip and Shroud Results for Design Speed Condition

Figures 3.5.1 and 3.5.2 present the blade platform Stanton number distribution for the low and high Reynolds number conditions, respectively, at three values of overall stage pressure ratio. At the higher Reynolds number, the data for the values of stage pressure ratio are in reasonable agreement. The low Reynolds number results presented in Figure 3.5.1 also suggest that the influence of pressure ratio is small. Further, the influence of Reynolds number appears to be small. For both Reynolds number cases, the trend of the data is to show a relatively small Stanton number increase in the chordwise direction. However, with only two measurement locations, it is difficult to determine anything more than this trend. The platform Stanton number values are of the same order as the blade midspan values.

Figures 3.5.3 and 3.5.4 present the Stanton number results obtained from the gages located in the blade tip at the low and high Reynolds number condition, respectively. The high Reynolds number results of runs 7, 8 and run 11 (Figure 3.5.4) were obtained at values of pressure ratio ranging from 1.38 to 1.48. The results of run 11 are shown to consistently fall below those of run 8. Run 7, which was performed at the larger value of stage pressure ratio, produced results at the 75% chord location which are not consistent with a well defined influence of pressure ratio on the tip Stanton number. There also appears to be a rather wide range in Stanton number value at the 39% tip-region measuring station. The low Reynolds number experiments (which were run at stage pressure ratios of 1.54 and 1.65) illustrate even a more pronounced variation in results at the 18% measuring station (shown on Figure 3.5.3) than was shown at 39% tip

Figure 3.5.1--Stanton number distribution on the blade platform, Re~140,000.

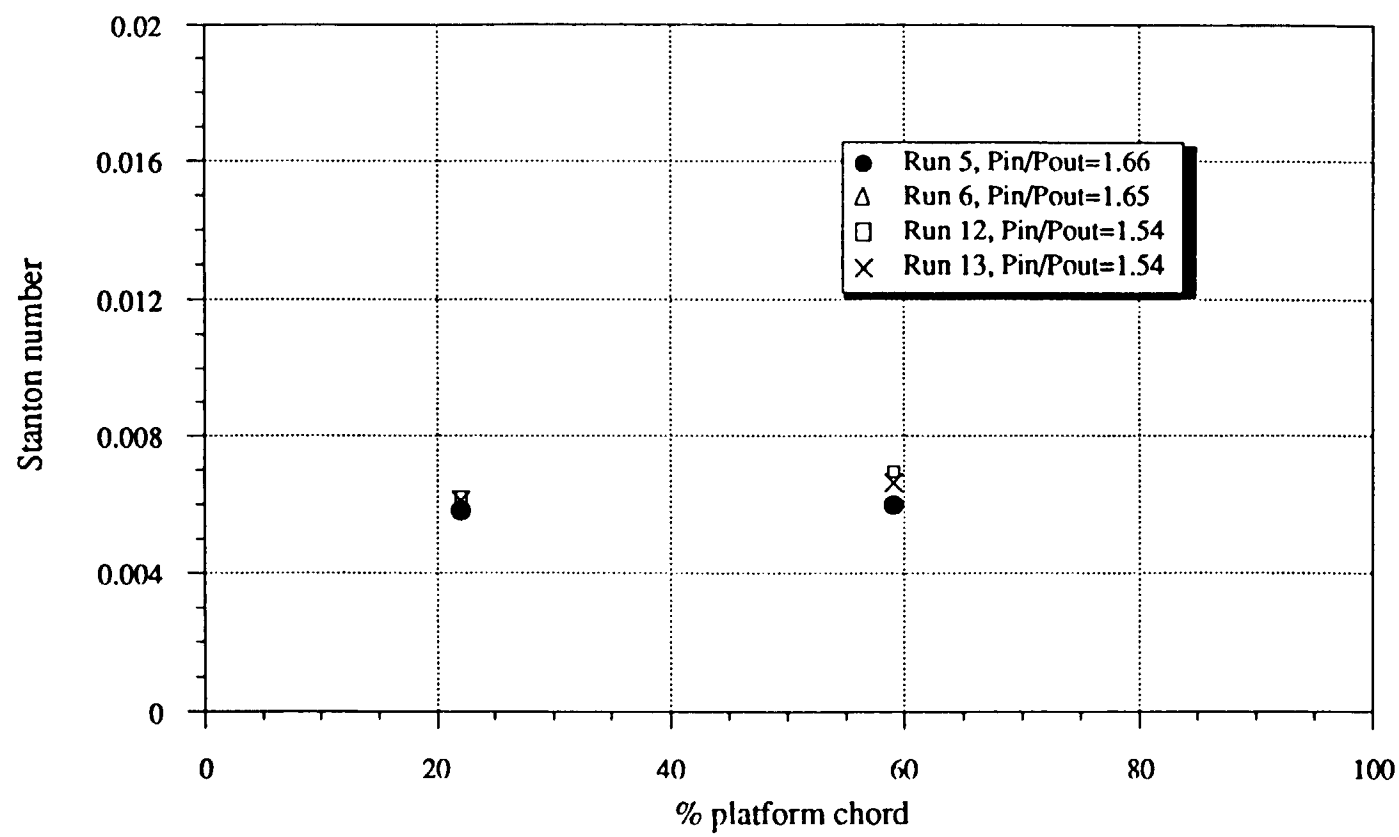

Figure 3.5.2--Stanton number distribution on the blade platform, Re~250,000.

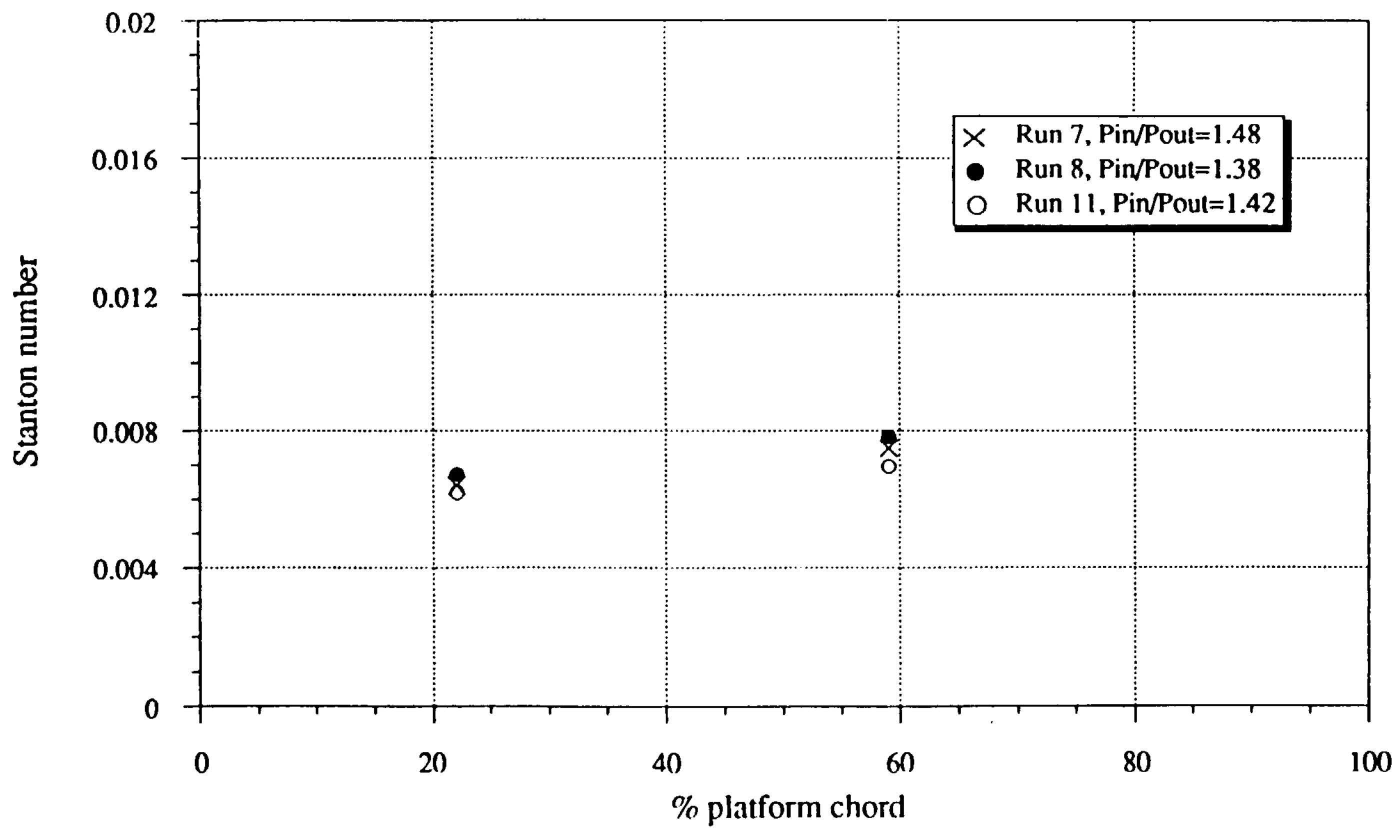

Figure 3.5.3--Stanton number distribution on the blade tip, Re~140,000.

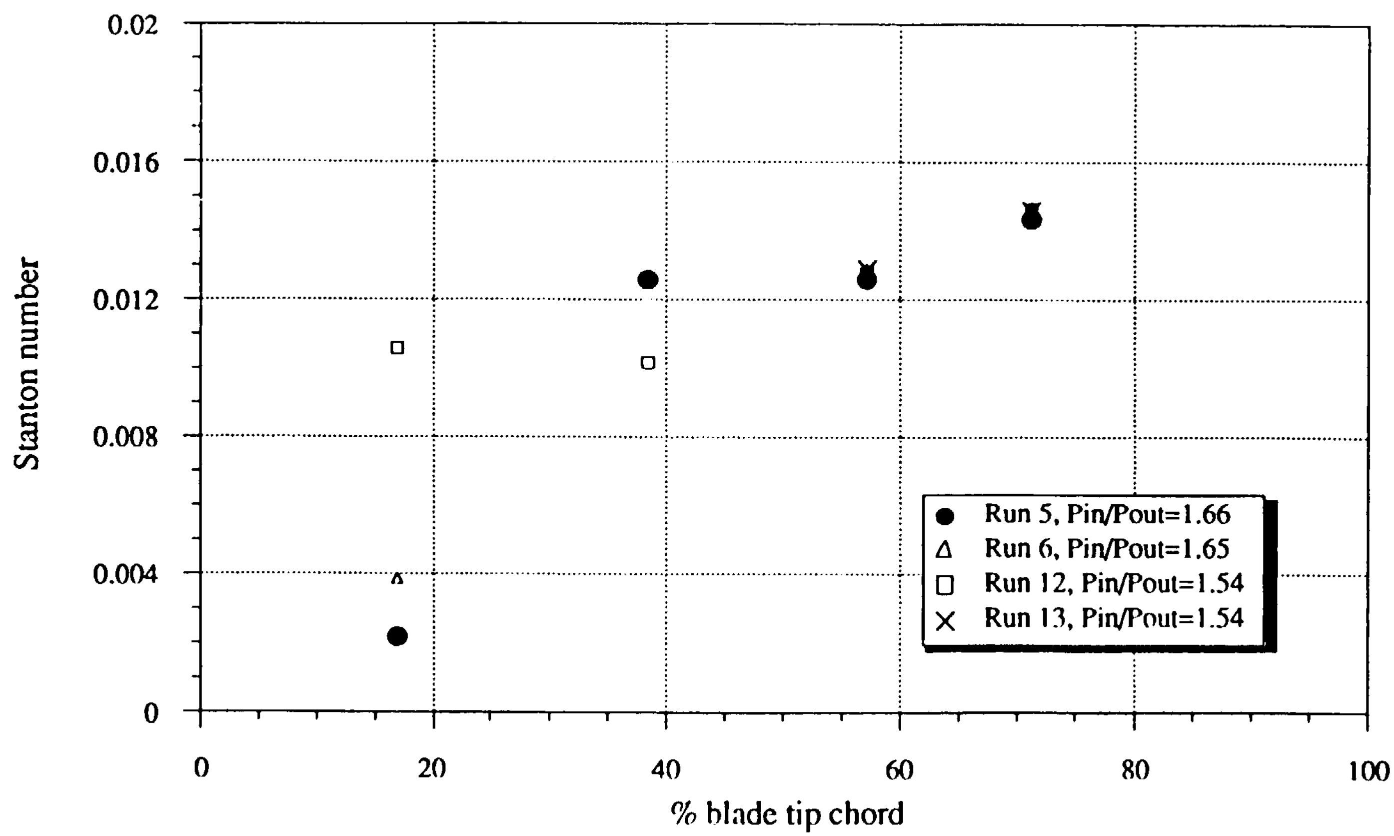

Figure 3.5.4--Stanton number distribution on the blade tip, Re~250,000.

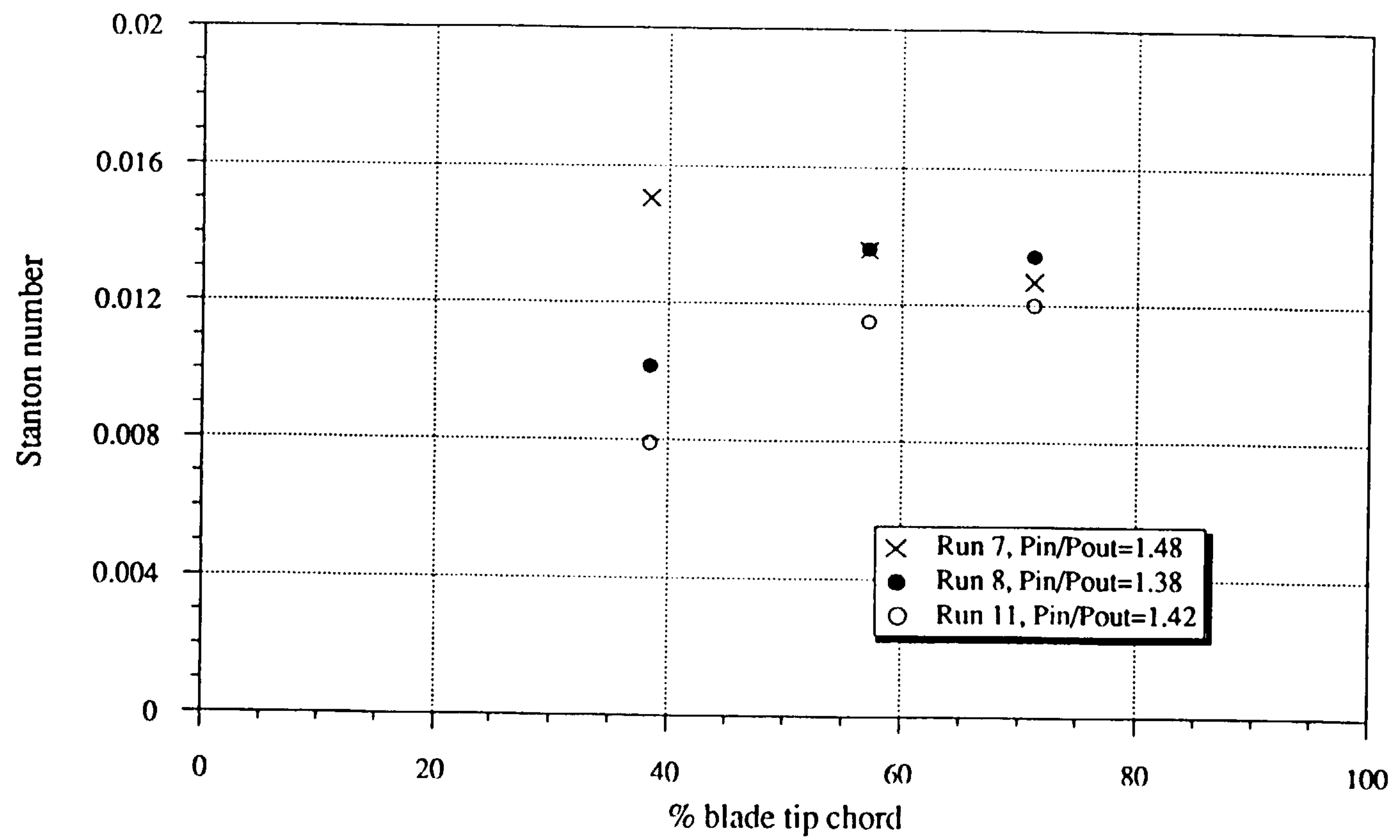

chord. There does not appear to be definitive influence of either Reynolds number or stage pressure ratio on the heat transfer results. For both Reynolds number cases, the tip region Stanton number values start out at small chord values with a rather wide variation, but converge near midchord. At chord values less than 40%, the tip Stanton numbers are on the order of the blade midspan values, but at large chord values the tip Stanton numbers rapidly approach the blade stagnation point value.

Figures 3.5.5 and 3.5.6 present the Stanton number distributions on the stationary shroud. The high Reynolds number data presented on Figure 3.5.6 illustrate a relatively high value of Stanton number over the entire region for which data were obtained. Stage pressure ratio does not appear to influence the results. Figure 3.5.5 presents corresponding results for the low Reynolds number test case. The results for both Reynolds numbers appear to be relatively independent of both Reynolds number and stage pressure ratio. For both Reynolds number cases, the shroud Stanton numbers are not as large as the blade stagnation point or tip values, but they are larger than the values measured at other blade locations.

Figures 3.5.7 and 3.5.8 are composite plots of the platform, tip and shroud Stanton number data as a function of blade chord. The root and tip locations are noted on the abscissa. For the data presented in both of these plots, the tip data are shown to be generally greater than either the platform or shroud data. The shroud data fall between the tip and the platform levels.

## 3.6 Vane and Blade Surface Results for Off-Design Speed (68% Design Speed)

Figures 3.6.1-3.6.3 plot the Stanton number distributions for the 50%, high Reynolds number runs on the first vane, first blade and second vane, respectively. These are included to complete the comparison between full speed and off-design speed data. As would be expected, speed has relatively little influence on the first vane for the vane pressure ratio of this turbine (Figure 3.6.1). Figure 3.6.2 presents the first blade data and

Figure 3.5.5--Stanton number distribution on the blade shroud, Re~140,000.

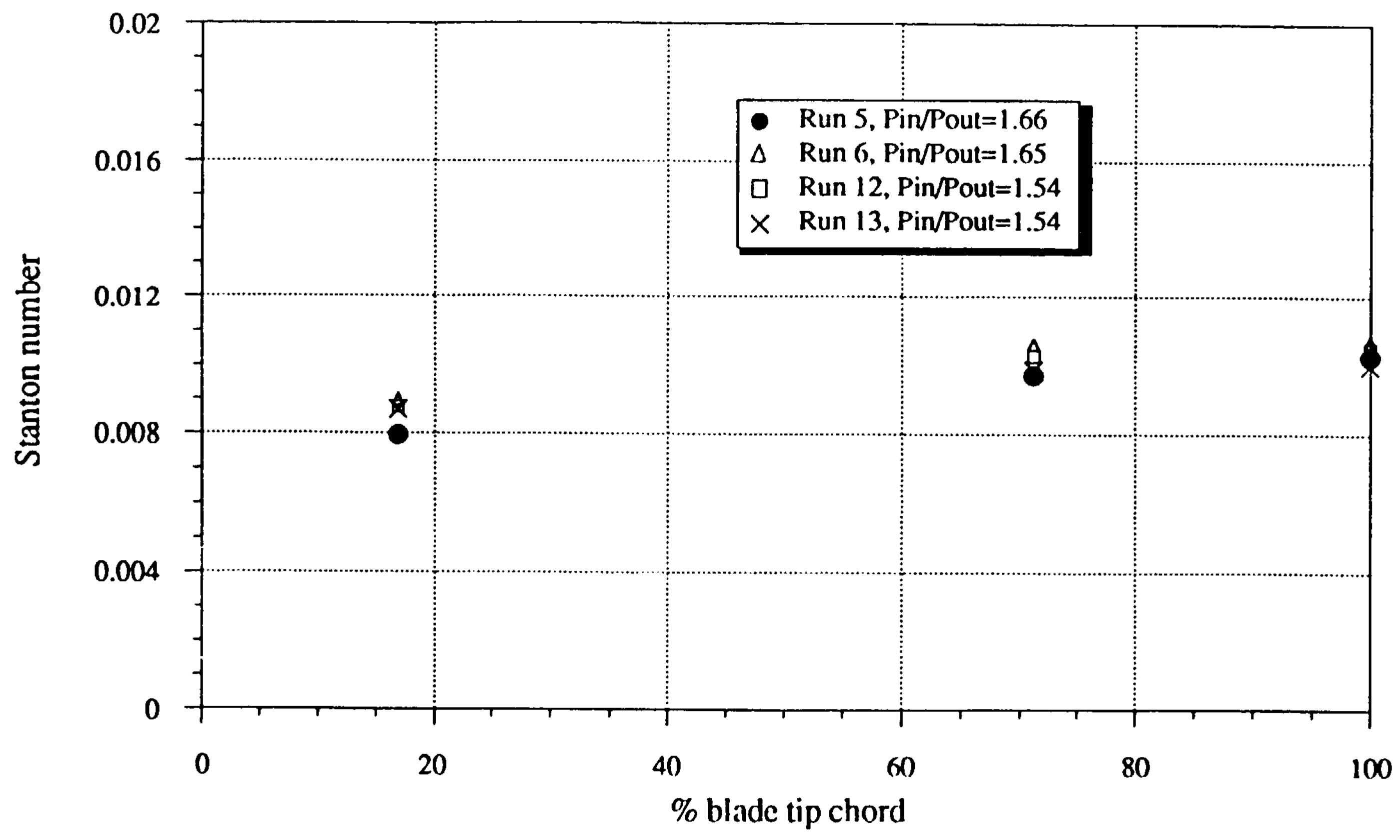

Figure 3.5.6--Stanton number distribution on the blade shroud, Re~250,000.

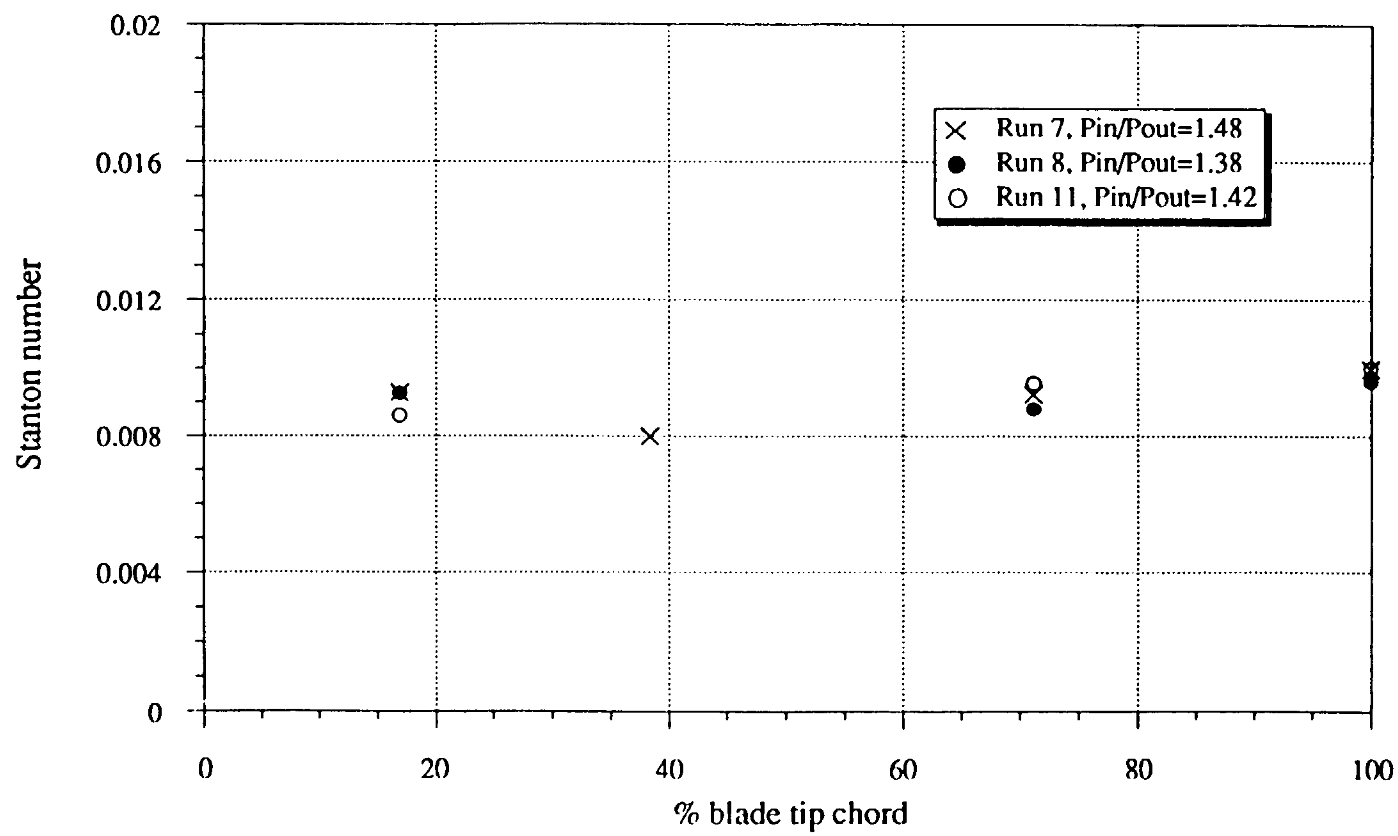

Figure 3.5.7--First blade tip, shroud, and platform, Rc~140,000 (Runs 5,6,12, and 13)

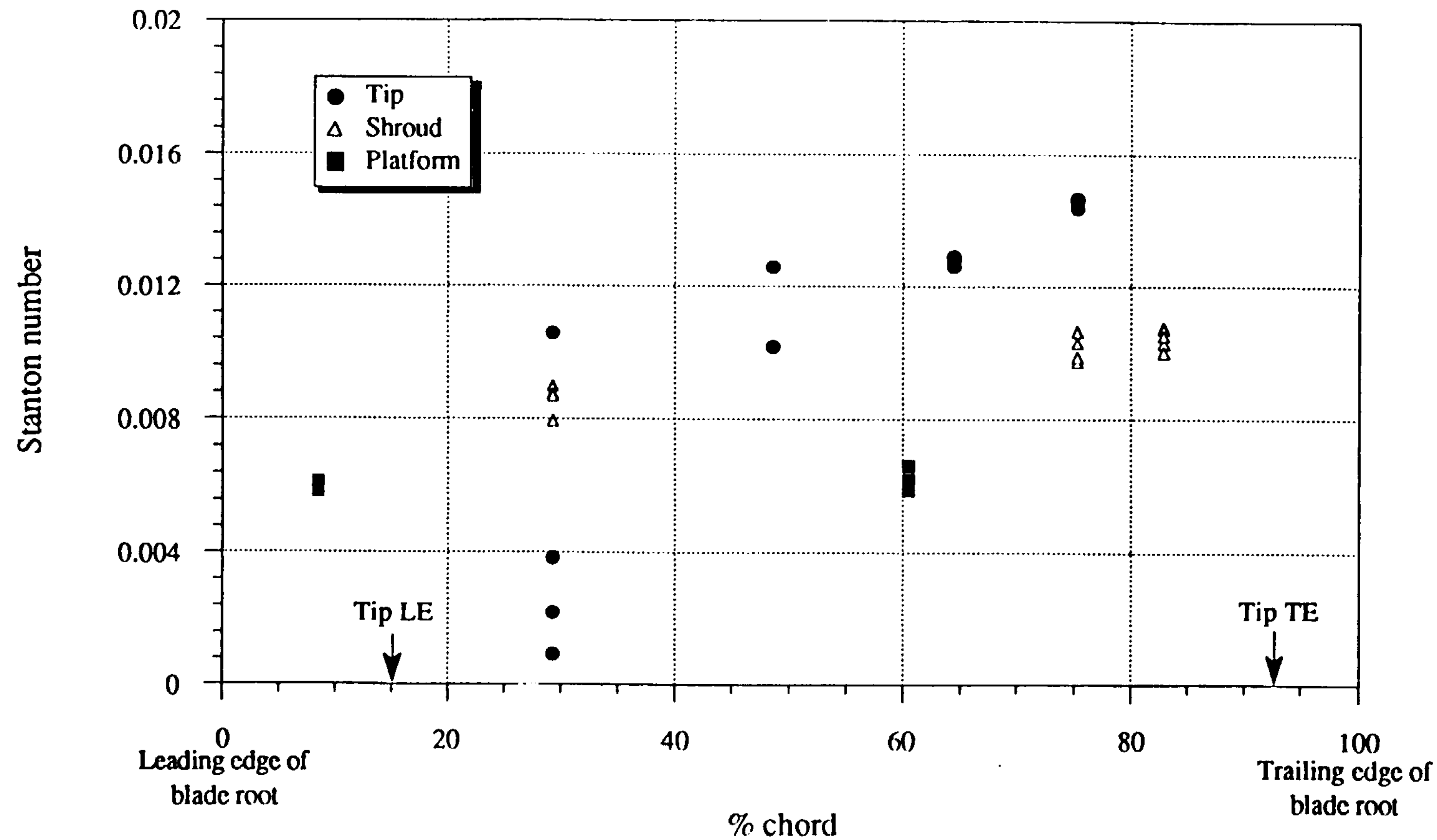

Figure 3.5.8--First blade tip, shroud, and platform, Re~250,000 (Runs 7,8, and 11)

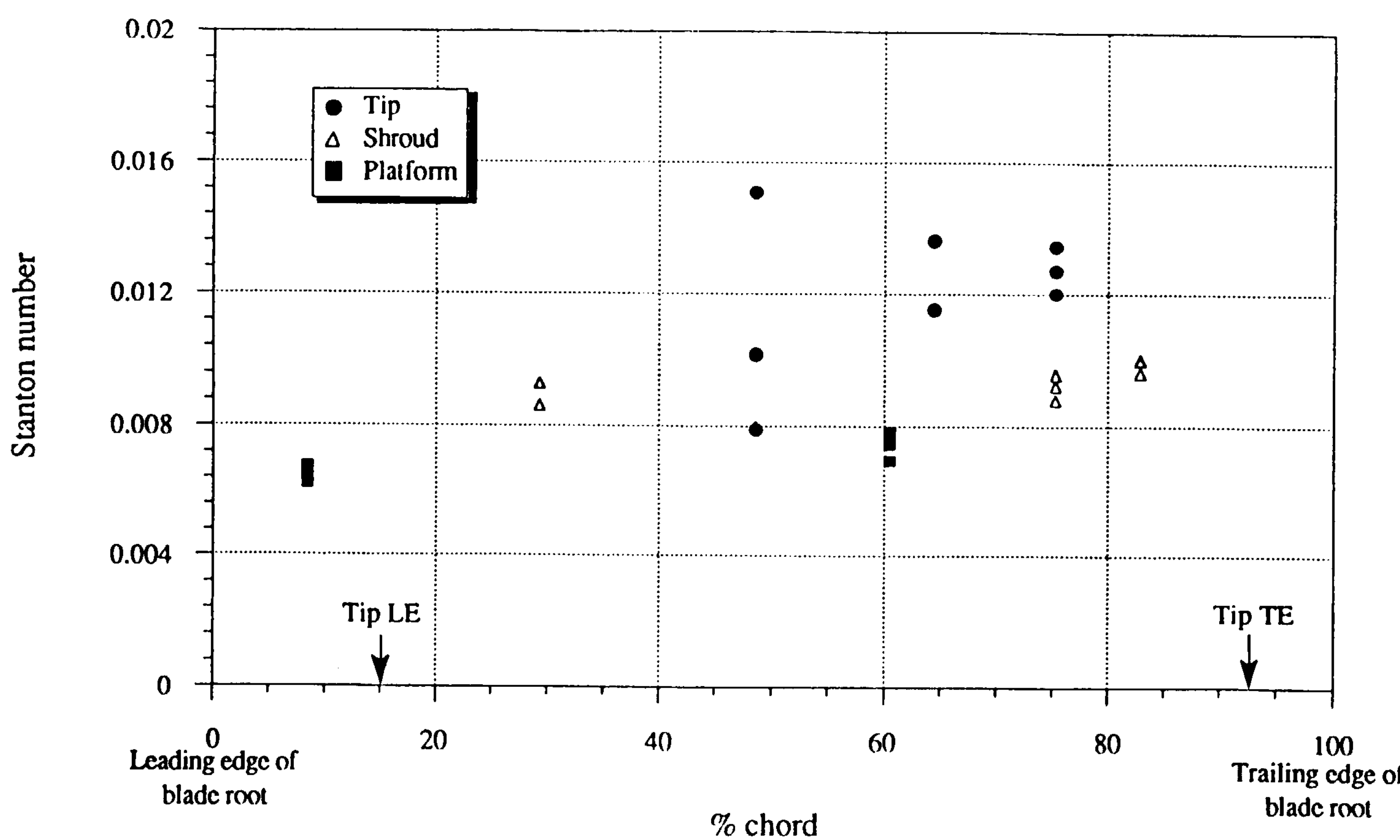

Figure 3.6.1--Stanton number distribution at 50% span on first vane, Re~250,000, comparison with off speed data.

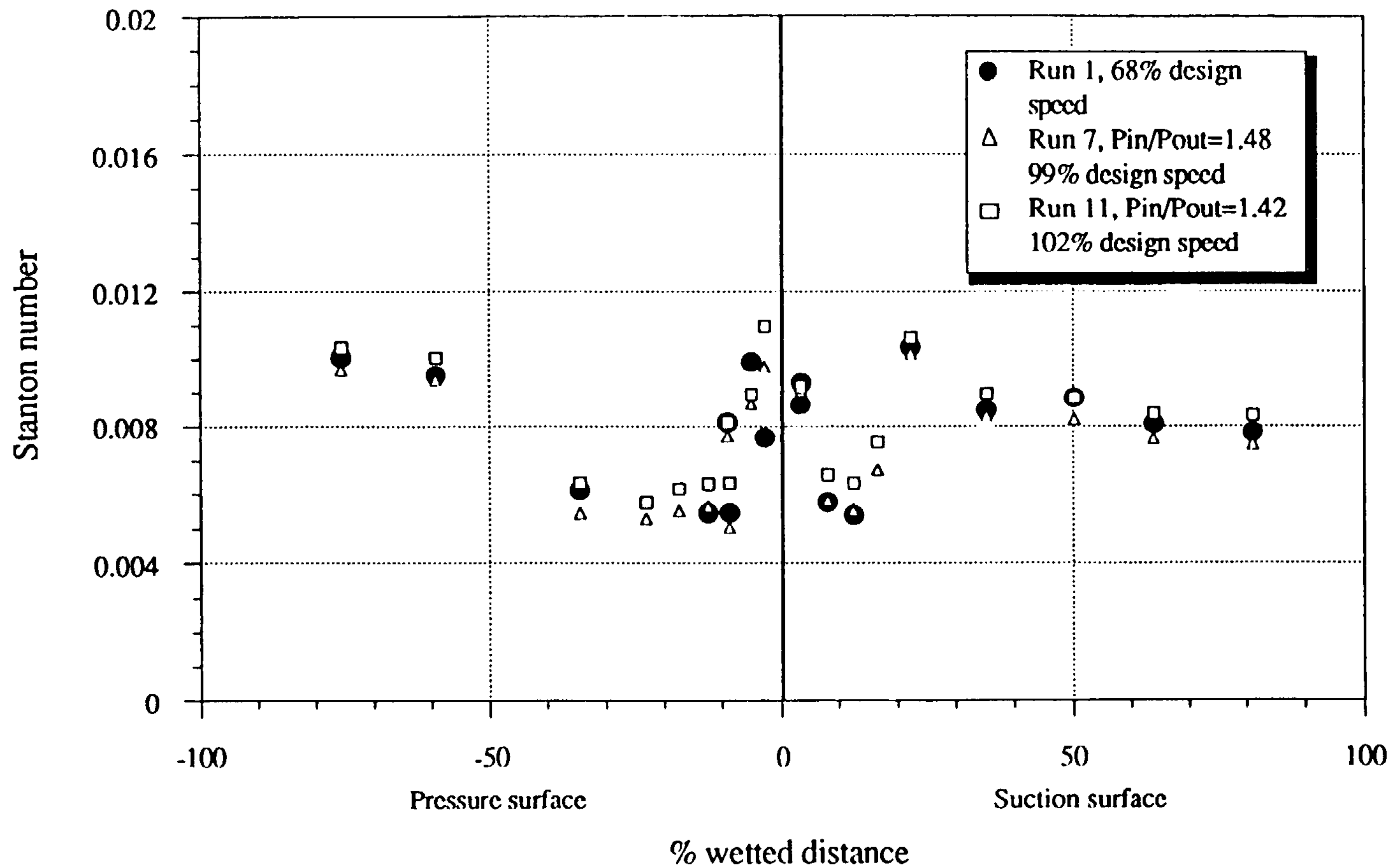

Figure 3.6.2--Stanton number distribution at 50% span on first blade, Re~250,000, comparison with off speed data.

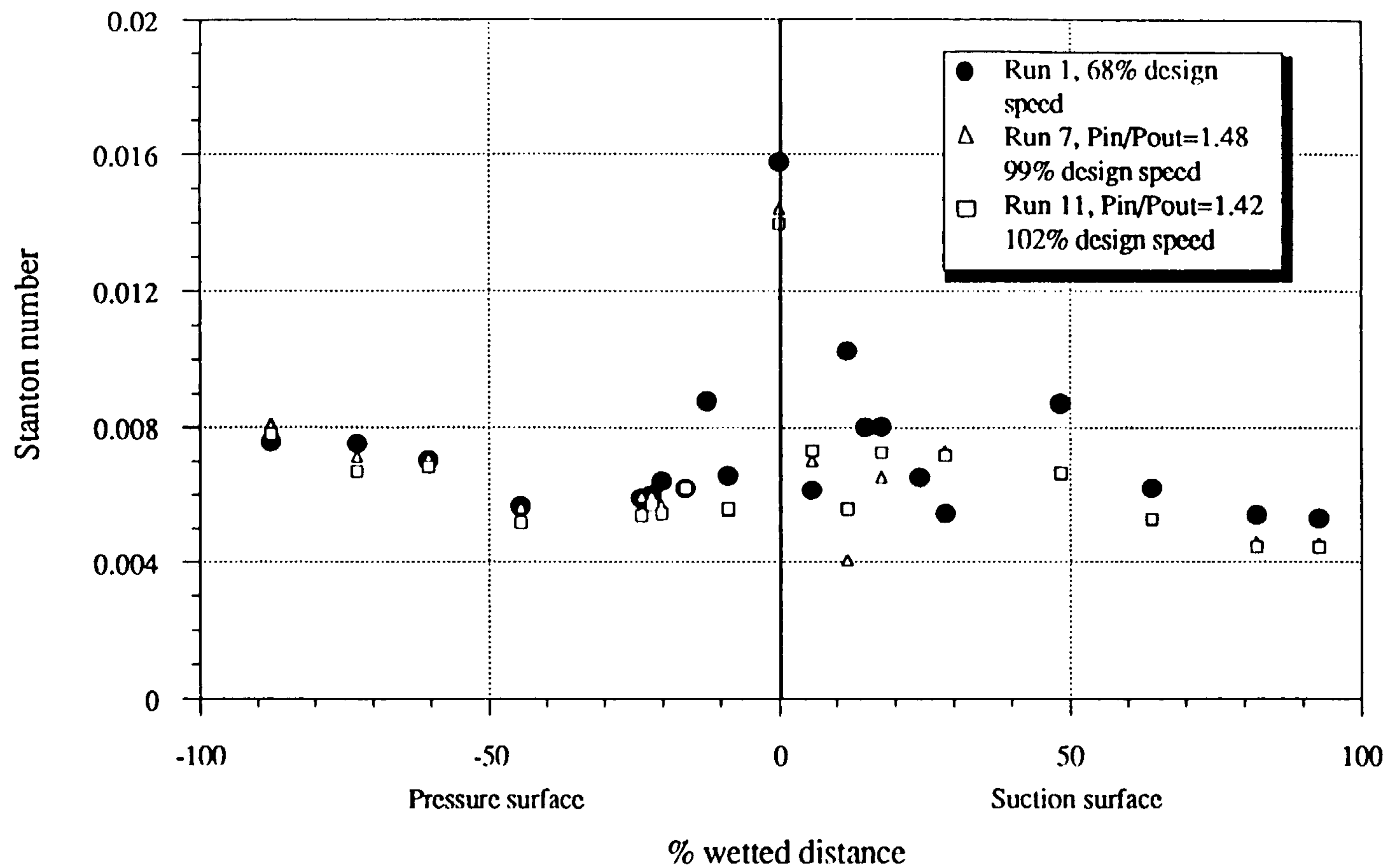

Figure 3.6.3--Stanton number distribution at 50% span on second vane, Re~250,000, comparison with off speed data.

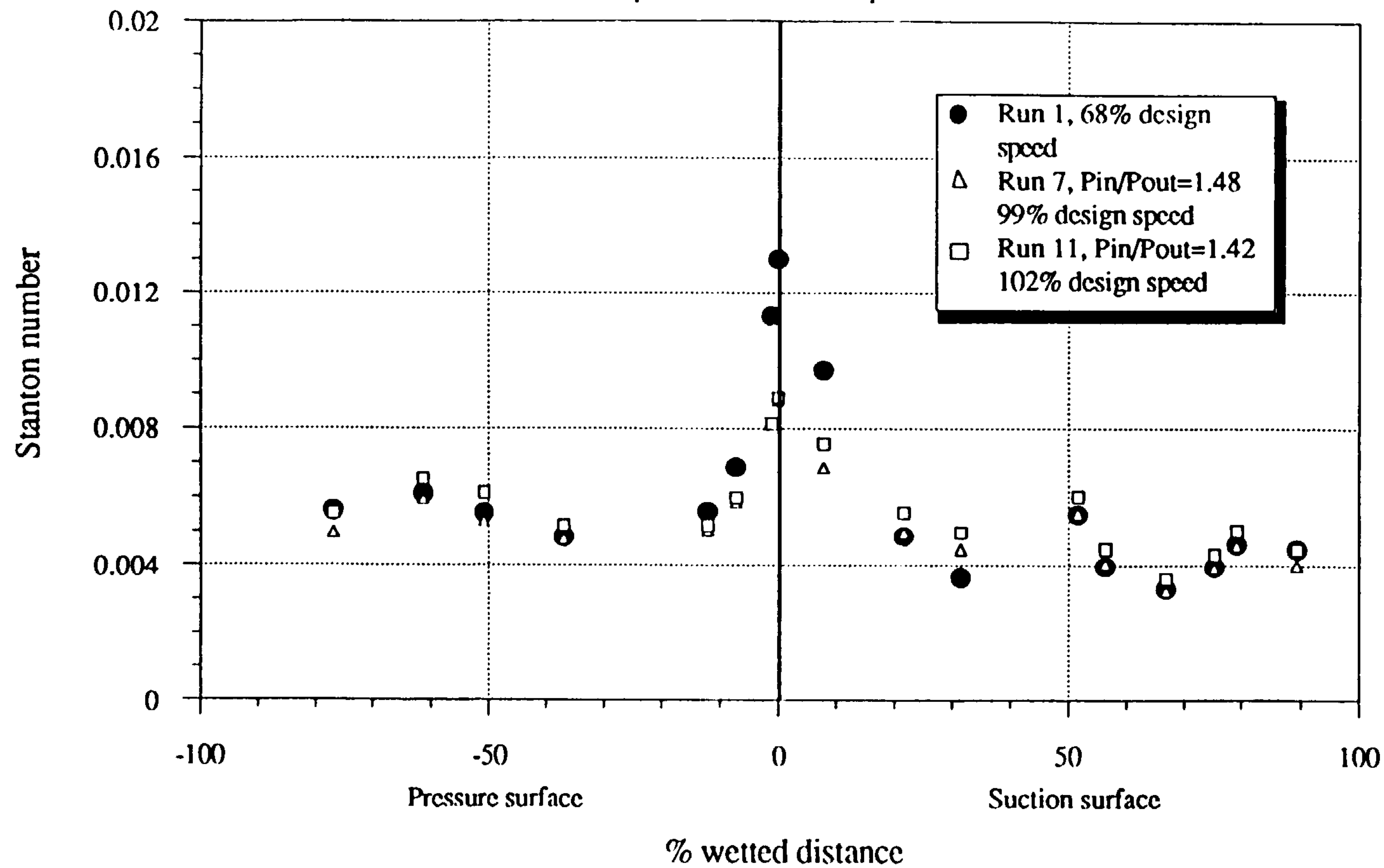

illustrates that in the vicinity of the leading edge, incidence angle has a noticeable influence on the magnitude of the Stanton number. Beyond 20% wetted distance on the pressure surface the influence of incidence angle is shown to be relatively small. For the suction surface at wetted distances less than 30%, the trend is not consistent apparently because of the transition location. At 50% wetted distance and beyond, the off-speed data are generally above the design speed data. Figure 3.6.3 presents the second vane Stanton number results. In the immediate region of the leading edge (5% to 10%), the off-design turbine speed appears to have an influence on the second vane Stanton number distribution. If there was going to be an influence, it is in this region that one would expect it to occur. However, on the second vane, the influence dies out much more rapidly than it did for the first blade, being essentially gone by about 5% wetted distance on the pressure surface and by 20% wetted distance on the suction surface.

### 3.7 Blade Platform, Tip and Shroud Results for Off-Design Speed

Figures 3.7.1 -3.7.3 present a comparison of the off speed (68% of design value) data with the design speed data for the blade platform, blade tip and the shroud, respectively. The data presented were obtained at the high Reynolds number at a stage pressure ratio of approximately 1.4 and 1.5. The results presented on Figure 3.7.1 for the platform illustrate that at each of the locations, the Stanton number results do not appear to be influenced by rotor speed. This is not surprising since both locations are sufficiently far from the stagnation point that incidence angle should not be important. Figure 3.7.2 compares the off speed and design speed tip region data. For this region, Metzger and Rued, 1989 have shown that blade relative motion should not have a significant influence on the average tip region heat transfer. At two measuring stations, the off speed results fall above the design speed values. However, at the third station, this is not true and thus the results are inconclusive. Figure 3.7.3 presents the time averaged shroud heat transfer results. The Stanton number is shown to have an increasing trend

Figure 3.7.1--Stanton number distribution on the blade platform, Re~250,000, comparison with off speed data.

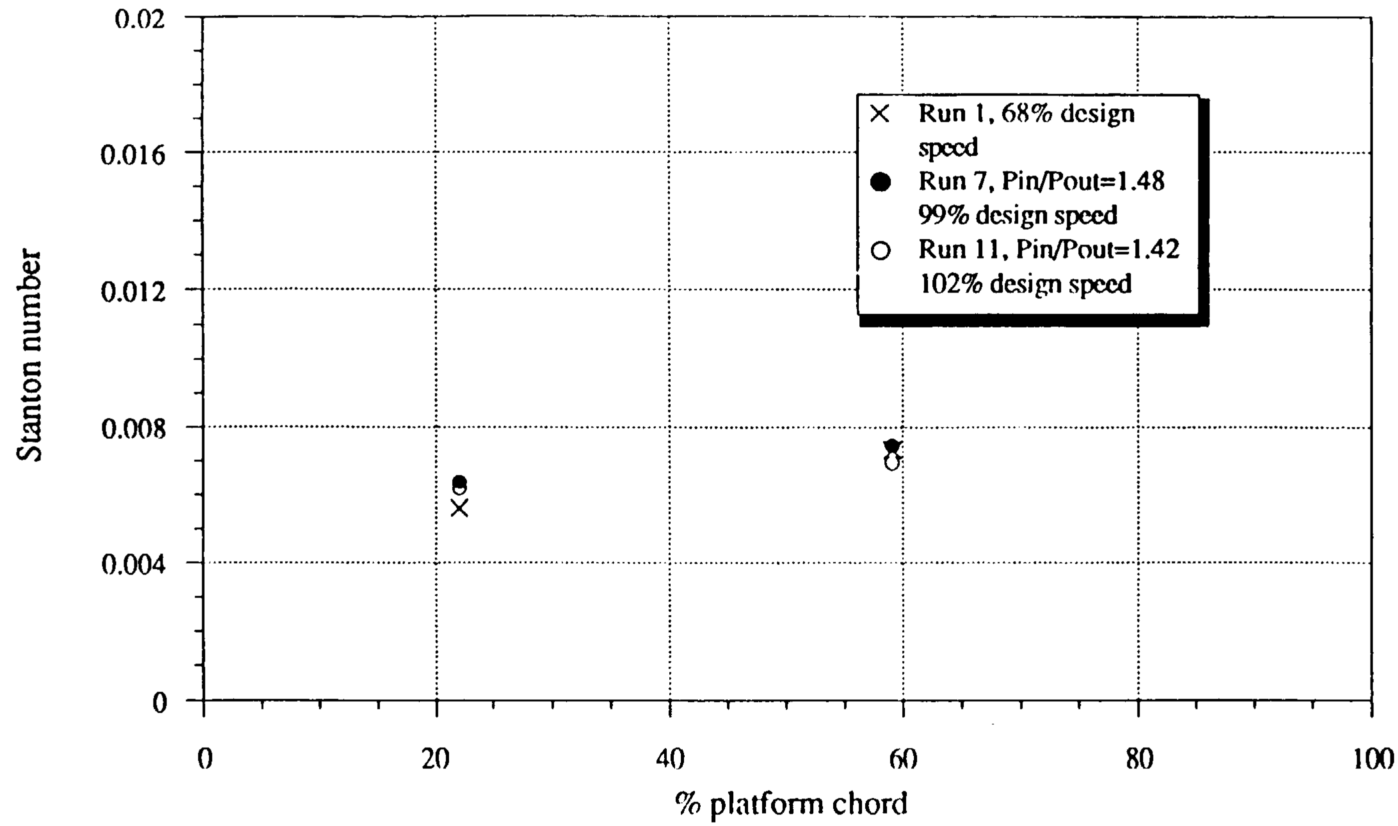

Figure 3.7.2--Stanton number distribution on the blade tip, Re~250,000, comparison with off speed data.

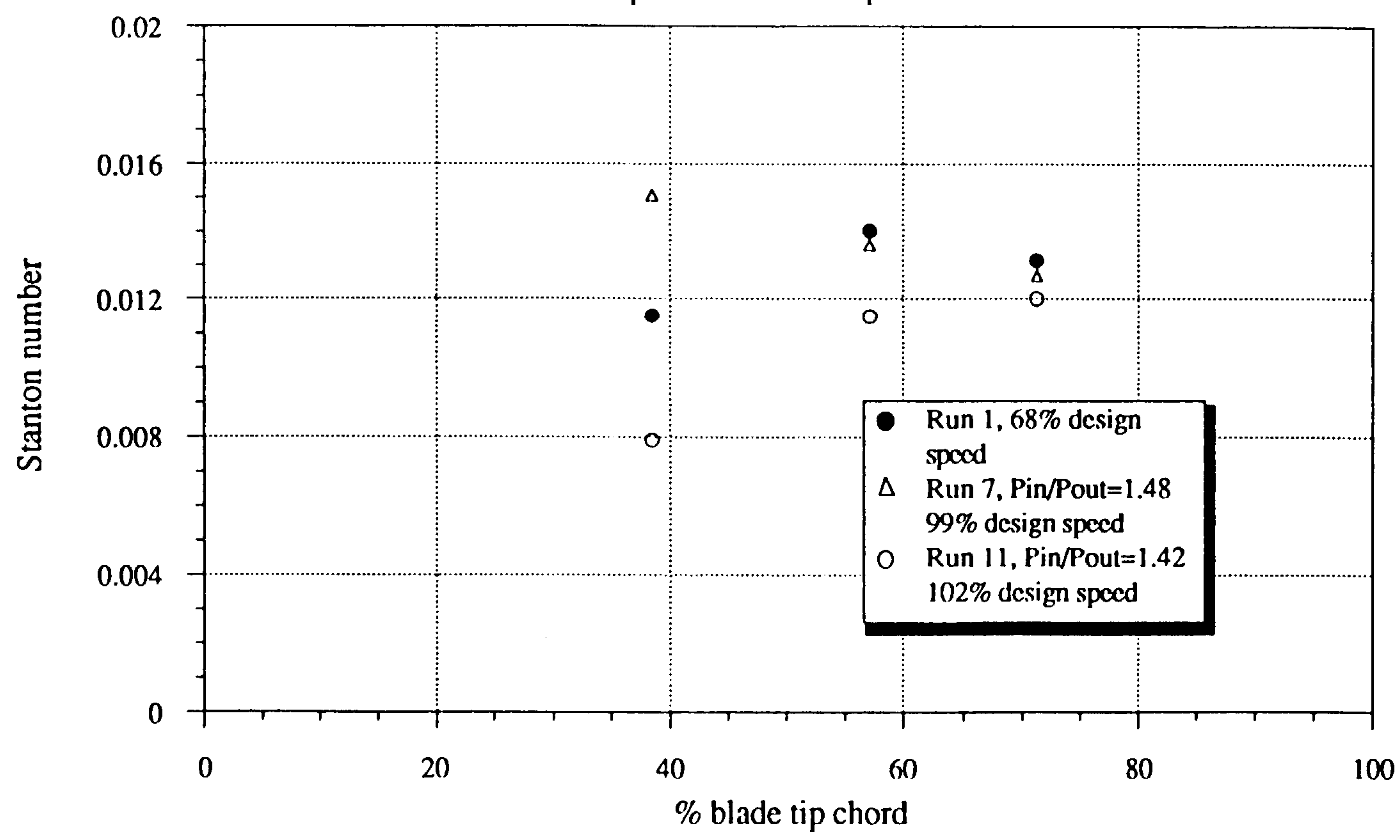

Figure 3.7.3--Stanton number distribution on the blade shroud, Re~250,000, comparison with off speed data.

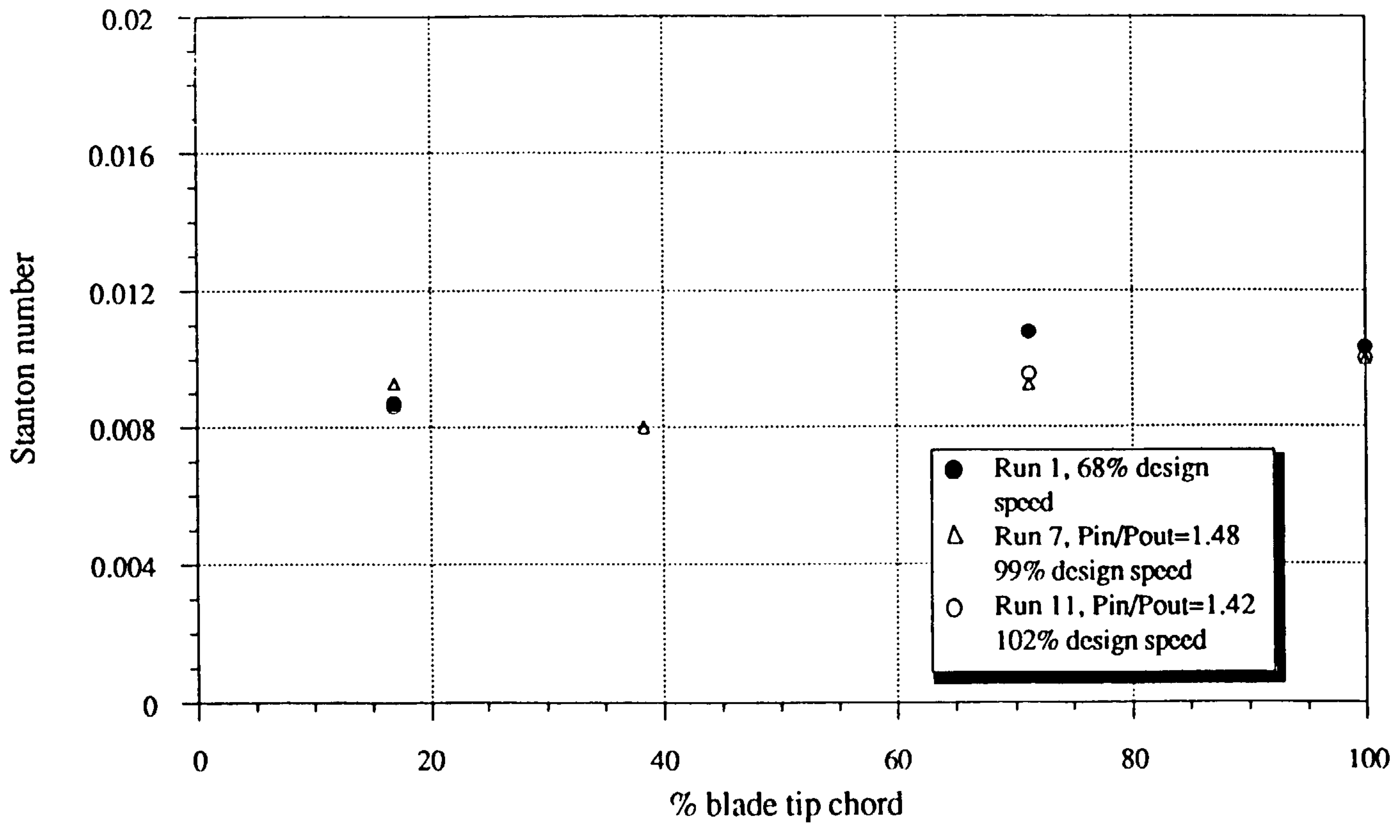

towards the blade trailing edge as would be anticipated because of the increasing driver pressure on the flow through the tip in moving from the leading edge towards the trailing edge. For a reduced rotor speed, a particular gage in the shroud would be exposed to the tip gap flow for a longer period of time (per rotor revolution) but it is also clear of the rotor tip for a longer period of time. The fraction of time for which the shroud gage is covered by the tip is the same as it is for the higher speed. If the gap flow is the same, then one would not expect to see a significant influence on Stanton number. However, because the influence of rotor speed on the blade surface pressure distribution in the tip region was not measured it is not possible to be certain that the tip flow was the same for both speeds and thus it is difficult to close the discussion of this point.

## SECTION 4
## CONCLUSIONS

Surface pressure and Stanton number distributions have been measured at selected locations on the first vane, first blade and second vane of a full two-stage turbine. The first vane and first blade pressure measurements have been compared with the prediction, but the agreement was not particularly good because of difficulties with the measurement. The measured Stanton number distributions at midspan for the first vane and the first blade have been compared with predictions obtained using a quasi-3D N-S code and a modified STAN5 technique. For the first vane, comparisons were presented for the fully turbulent case and for the transition case using two transition models (Mayle, 1991 and Dunham, 1972). At the low Reynolds number, the Mayle transition model and the fully turbulent prediction provided good agreement with the suction surface data. The fully turbulent, the Mayle transition model, and the Dunham transition model all provided good agreement with the suction surface data for the high Reynolds number case. The first vane pressure surface data were consistently underpredicted by all of the predictions. The sensitivity of the predictions to flow parameters such as turbulence intensity, coupled with the lack of agreement for the vane pressure surface heat transfer illustrates the importance of correctly modeling the actual flow field in any heat transfer analysis.

The first blade data were compared to N-S turbulent and N-S with the Mayle and Dullenkopf, 1989, 1990 intermittency model predictions. There is very little difference between the results of these two predictions. For the blade suction surface, the predictions were consistently above the data. The agreement between data and prediction for the pressure surface was reasonably good.

The surface of the blade used in these experiments appeared to be very rough. However, when the roughness density was accounted for, the analysis showed only a small increase in blade heat transfer due to surface roughness. The relatively good agreement between the measured and predicted rotor heat transfer supports this conclusion. In the analysis the effect of surface roughness is strongly dependent on Reynolds number. Consequently, for the actual SSME engine operating conditions the analysis predicts a significant increase in blade heat transfer due to surface roughness.

The second vane data were compared with N-S fully turbulent calculations and with a N-S solution including the Mayle and Dullenkopf intermittency model. For the suction surface, both calculations were generally conservative. However, for the pressure surface, the predicted Stanton number distributions were in good agreement with the experimental data.

The tip region was shown to exhibit high heat-transfer rates by comparison with the blade stagnation-point value. The shroud Stanton number values were less than the tip values, but higher than the platform values. Data were presented to illustrate the influence of off-design rotor speed on the vane and blade Stanton number distributions. The first vane Stanton number distribution was also not influenced by rotor speed. The tip and shroud distributions were not significantly influenced by rotor speed. However, both the first blade and the second vane were influenced by rotor speed in the vicinity of the leading edge. This influence persisted on the first blade over a greater portion of the surface than it did on the second vane.

## REFERENCES


Abhari, R.S., Guenette, G.R., Epstein, A.H., and Giles, M.B., 1991, "Comparison of Time-Resolved Turbine Rotor Blade Heat Transfer Measurements and Numerical Calculations," ASME Paper No. 91-GT-268.

Adamczyk, J.J., 1985, "Model Equation for Simulating Flows in Multistage Turbomachinery," ASME Paper No. 85-GT-226.

Adamczyk, J.J., 1986, "A Model for Closing the Inviscid Form of the Average-Passage Equation System," ASME Paper No. 86-GT-227.

Allen, H.W. and Kofskey, M.G., 1955, "Visualization Study of Secondary Flows in Turbine Rotor Tip Regions," NACA TN 3519.

Bindon, J.P., 1986, "Visualization of Axial Turbine Tip Clearance Using a Linear Cascade," Report No. CUED/A-Turbo TR122, Whittle Laboratory, Cambridge University, United Kingdom.

Blair, M.F., Dring, R.P., and Joslyn, H.D., 1988, "The Effects of Turbulence and Stator/Rotor Interaction on Turbine Heat Transfer, Part I: Design Operating Conditions," ASME Paper No. 88-GT-125.

Blair, M.F. and Anderson, O.L., 1989, "The Effects of Reynolds Number, Rotor Incidence Angle and Surface Roughness on the Heat Transfer Distribution in a Large-Scale Turbine Rotor Passage," UTRC Report No. UTRC-R89-957852-24.

Blair, M.F. and Anderson, O.L., 1992, "An Experimental Study of Heat Transfer in a Large Scale Turbine Rotor Passage," 37th International Gas Turbine Conference, Paper GT-92-.

Booth, T.C., Dodge, P.R. and Hepworth, H.K., 1982, "Rotor-Tip Leakage: Part I - Basic Methodology," Journal of Engineering for Power, Vol. 104, pp. 154-161.

Boyle, R.J., 1991, "Navier-Stokes Analysis of Turbine Blades Heat Transfer," Journal of Turbomachinery, pp. 392-403.

Boyle, R.J. and Civinskas, K.C., 1991, "Two-Dimensional Navier-Stokes Heat Transfer Analysis for Rough Turbine Blades," AIAA/SAE/ASME 27th Joint Propulsion Conference, Paper No. AIAA-91-2129.

Chima, R.V., 1986, "Development of an Explicit Multigrid Algorithm for Quasi-Three-Dimensional Flows in Turbomachinery", AIAA Paper No. 86-0032, NASA TM-87128.

Civinskas, K.C., Boyle, R.J. and McConnaughey, H.V., 1988, "Impact of ETO Propellants on the Aerothermodynamic Analyses of Propulsion Components," AIAA/ASME/SAE/ASEE 24th Joint Propulsion Conference, Paper No. AIAA-88-3091.

Crawford, M.E. and Kays, W.M., 1976, "STAN5 - A Program for Numerical Computation of Two-Dimensional Internal and External Boundary-Layer Flows," NASA CR-2742.

Dring, R.P. and Joslyn, H.D., 1986, "Through-Flow Analysis of a Multi-Stage Compressor, Part I - Aerodynamic Input," ASME Paper No. 86-GT-13.

Dunham, J. 1972, "Predictions of Boundary Layer Transition on Tubomachinery Blades", AGARD-AG-164.

Dunn, M.G. and Stoddard, F.J., "Measurement of Heat Transfer Rate to a Gas Turbine Stator," ASME Journal of Engineering for Power, Vol. 101, No. 2, April 1979.

Dunn, M.G. and Hause, A., 1982, "Measurement of Heat Flux and Pressure in a Turbine Stage," ASME Journal of Engineering for Power, Vol. 104, pp. 215-223.

Dunn, M.G., Rae, W.J. and Holt, J.L., 1984a, "Measurement and Analysis of Heat Flux Data in a Turbine Stage: Part I: Description of Experimental Apparatus and Data Analysis," Journal of Engineering for Power, Trans. ASME, Vol. 106, pp. 229-240.

Dunn, M.G., Rae, W.J., and Holt, J.L., 1984, "Measurement and Analyses of Heat Flux Data in a Turbine Stage: Part II - Discussion of Results and Comparison with Predictions," ASME Journal of Engineering for Gas Turbines and Power, Vol. 106, pp. 234-240.

Dunn, M.G., Martin, H.L., and Stanek, M.J., 1986, "Heat-Flux and Pressure Measurements and Comparison with Prediction for a Low Aspect Ratio Turbine Stage," ASME Journal of Turbomachinery, Vol. 108, pp. 108-115.

Dunn, M.G., 1986, "Heat-Flux Measurements for the Rotor of a Full-Stage Turbine: Part I - Time-Averaged Results," Journal of Turbomachinery, Vol. 108, pp. 90-97.

Dunn, M.G., George, W.K., Rae, W.J., Woodward, S.H., Moller, J.C., and Seymour, P.J., 1986, "Heat-Flux Measurments for the Rotor of a Full-Stage Turbine: Part II-Description of Analysis Technique and Typical Time-Resolved Measurements", Journal of Turbomachinery, Vol. 108, pp. 98-107.

Dunn, M.G. and Chupp, R.E., 1988, "Time-Averaged Heat-Flux Distributions and Comparison with Prediction for the Teledyne 702 hp Turbine Stage," ASME Journal of Turbomachinery, Vol. 110, pp. 51-56.

Dunn, M.G. and Chupp, R.E., 1989, "Influence of Vane/Blade Spacing and Injection on Stage Heat-Flux Distributions," AIAA Journal of Propulsion and Power, Vol. 5, No. 2, pp. 212-200.

Dunn, M.G., Seymour, P.J., Woodward, S.H., George, W.K., and Chupp, R.E., 1989, "Phase-Resolved Heat-Flux Measurements on the Blade of a Full-Scale Rotating Turbine", Journal of Turbomachinery, Vol. 111, pp. 8-19.

Dunn, M.G., Bennett, W., Delaney, R., and Rao, K., 1990(a), "Investigation of Unsteady Flow Through a Transonic Turbine Stage: Data/Prediction Comparison for Time-Averaged and Phase-Resolved Pressure Data," AIAA/SAE/ASME/ASEE 26th Joint Propulsion Conference, Orlando, FL, AIAA Paper No. 90-2409 (see also ASME J. of Turbomachinery, Vol. 114, pp. 91-99).

Dunn, M.G., 1989, "Phase and Time-Resolved Measurements of Unsteady Heat Transfer and Pressure in a Full-Stage Rotating Turbine," ASME Paper 89-GT-135.

Dunn, M.G. 1990, "Heat Transfer and Pressure Measurements for the SSME Fuel-Side Turbopump", Proceedings of the NASA 1990 Earth-to-Orbit Conference, Marshall Space Flight Center, AL.

Epstein, A.H., Guenette, G.R., Norton, R.J.G. and Yuzhang, C., 1985, "Time Resolved Measurements of a Turbine Rotor Stationary Tip Casing Pressure and Heat Transfer Field," AIAA Paper No. 85-1220.

Gaugler, R.E., 1981, "Some Modifications to, and Operating Experiences with, the Two-Dimensional Finite-Difference, Boundary-Layer Code STAN5," ASME Paper No. 81-GT-89.

George, W.K., Rae, W.J., and Woodward, S.H., 1991, "An Evaluation of Analog and Numerical Techniques for Unsteady Heat Transfer Measurements with Thin-Film Gauges in Transient Facilities", Experimental Thermal and Fluid Sciences, Vol. 4, pp. 333-342.

Giles, M.B., 1988, "Calculation of Unsteady Wake Rotor Interaction," AIAA Journal of Propulsion and Power, Vol. 4, No. 4, pp. 356-362.

Hah, C., 1984, "A Navier-Stokes Analysis of Three-Dimensional Turbulent Flows Inside Turbine Blade Rows at Design and Off-Design Conditions," Journal of Engineering for Power, Trans. ASME, 106, pp. 421-429.

Katsanis, T., 1969, "FORTRAN Program for Calculating Transonic Velocities on a Blade-to-Blade Stream Surface of a Turbomachine," NASA TN D-5427.

Katsanis, T and McNally, W.D., 1977, "Revised FORTRAN Program for Calculating Velocities and Streamlines on the Hub-Shroud Mid-Channel Stream Surface of an Axial-, Radial-, or Mixed-Flow Turbomachine or Annular Duct," Vol. I, User's Manual, Vol. II - Programmer's Manual," NASA TN D-8430, 8431.

Kline, S.J. and McClintock, 1953, "Describing Uncertainties in Single-Sampled Experiments", Mechanical Engineering, Vol. 75, pp. 3-8.

Mayle, R.E., 1991, "The Role of Laminar-Turbulent Transition in Gas Turbine Engines", paper presented at the 36th International Gas Turbine Conference, Paper No. 91-GT-261, Orlando, FL.

Mayle, R.E. and Dullenkopf, K., 1989, "A Theory of Wake Induced Transition", ASME J. of Turbomachinery, Vol. 112, pp. 188-195.

Mayle, R.E. and Dullenkopf, K., 1990, "More on the Turbulent-Strip Theory for Wake Induced Transition", paper presented at the 35th International Gas Turbine Conference, Paper No. 90-GT-137, Brussels, Belgium.

Mayle, R.E. and Metzger, D.E., 1982, "Heat Transfer at the Tip of an Unshrouded Turbine Blade," Proceedings, Seventh International Heat Transfer Conference, Vol. 3, pp. 87-92.

McFarland, E.R., 1984, "A Rapid Blade-to-Blade Solution for use in Turbomachinery Design," Journal of Engineering for Gas Turbines and Power, Vol. 105, No. 2, pp. 376-382.

Metzger, D.E., Dunn, M.G., and Hah, C., 1990, "Turbine Tip and Shroud Heat Transfer," Paper presented at the 35th ASME International Gas Turbine and Aerospace Congress, Paper No. 90-GT-333, Brussels, Belgium.

Metzger, D.E. and Rued, K., 1989, "The Influence of Turbine Clearance Gap Leakage on Flowpath Velocities and Heat Transfer, Part I: Sink Flow Effects on Blade Pressure Sides," Journal of Turbomachinery, Trans. ASME, Vol. 111, pp. 284-292.

McNally, W.D., 1970, "Fortran Program for Calculating Compressible Laminar and Turbulent Boundary Layers in Arbitrary Pressure Gradients," NASA TND-5681.

Moore, J. and Tilton, J.S., 1988, "Tip Leakage Flow in a Linear Turbine Cascade," Journal of Turbomachinery, Trans. ASME, Vol. 110, pp. 18-26.

Nealy, D.A., Milele, M.S., Hylton, L.D., and Gladden, H.J., 1984, "Measurements of Heat Transfer Distribution Over the Surfaces of Highly Loaded Turbine Nozzle Guide Vanes", J. of Engineering for Gas Turbines and Power, Vol. 106, pp. 149-158.

Rae, W.J., Taulbee, D.B., Civinskas, K.C., and Dunn, M.G., 1988, "Turbine-Stage Heat Transfer: Comparison of Short Duration Measurements with State-of-the-Art Predictions", Journal of Propulsion and Power, Vol. 4, No. 6, pp. 541-548.

Rai, M.M., 1987, "Navier-Stokes Simulations of Rotor/Stator Interaction Using Patched and Overlaid Grids," Journal of Propulsion, No. 3, pp. 387-396.

Rai, M.M. and Madavan, K.K., 1988, "Multi Airfoil Navier Stokes Simulation of Turbine Rotor-Stator Interaction," AIAA Paper No. 88-0361.

Rao, K.V. and Delaney, R.A., 1990, "Investigation of Unsteady Flow Through a Transonic Turbine Stage, Part I - Analysis," AIAA/SAE/ASME/ASEE 26th Joint Propulsion Conference, Orlando, FL, AIAA Paper No. 90-2408.

Taulbee, D.B., Tran, L., and Dunn, M.G., 1988, "Stagnation Point and Surface Heat Transfer for a Turbine Stage: Prediction and Comparison with Data", ASME 33rd International Gas Turbine Conference, Paper 88-GT-30, Amsterdam.

Traci, R.M. and Wilcox, D.C., 1975, "Freestream Turbulence Effects on Stagnation Heat Transfer," AIAA Journal, Vol. 13, No. 7, pp. 890-896.

Tran, L and Taulbee, D.B., 1991, "Prediction of Unsteady Rotor-Surface Pressure and Heat Transfer from Wake Passings", ASME 36th International Gas Turbine Conference, Paper No. 91-GT-267, Orlando, Florida.

Wadia, A.R. and Booth, T.C., 1982, "Rotor-Tip Leakage: Part II - Design Optimization Through Viscous Analysis and Experiment," Journal of Engineering for Power, Trans. ASME, Vol. 104, 1982, pp. 162-169.

# APPENDIX

A.1 Vane and Blade Coordinates

A.1.1 First Nozzle Coordinates

First nozzle, hub

| | x [in] | y[in] |
|---|---|---|
| 1 | 0.00013213 | 0.85099 |
| 2 | 0.00052741 | 0.84738 |
| 3 | 0.0011839 | 0.84380 |
| 4 | 0.0020981 | 0.84027 |
| 5 | 0.0032653 | 0.83683 |
| 6 | 0.0046793 | 0.83347 |
| 7 | 0.0063326 | 0.83023 |
| 8 | 0.0082165 | 0.82712 |
| 9 | 0.010321 | 0.82415 |
| 10 | 0.012636 | 0.82134 |
| 11 | 0.015147 | 0.81870 |
| 12 | 0.017843 | 0.81626 |
| 13 | 0.020710 | 0.81402 |
| 14 | 0.023731 | 0.81199 |
| 15 | 0.026891 | 0.81018 |
| 16 | 0.030173 | 0.80861 |
| 17 | 0.033561 | 0.80728 |
| 18 | 0.037036 | 0.80620 |
| 19 | 0.040580 | 0.80538 |
| 20 | 0.057465 | 0.80198 |
| 21 | 0.074350 | 0.79836 |
| 22 | 0.091235 | 0.79453 |
| 23 | 0.10812 | 0.79048 |
| 24 | 0.12500 | 0.78620 |
| 25 | 0.14189 | 0.78169 |
| 26 | 0.15877 | 0.77696 |
| 27 | 0.17566 | 0.77199 |
| 28 | 0.19254 | 0.76678 |
| 29 | 0.20943 | 0.76133 |
| 30 | 0.22631 | 0.75564 |
| 31 | 0.24320 | 0.74969 |
| 32 | 0.26008 | 0.74349 |
| 33 | 0.27697 | 0.73703 |
| 34 | 0.29385 | 0.73031 |
| 35 | 0.31074 | 0.72331 |
| 36 | 0.32762 | 0.71603 |
| 37 | 0.34451 | 0.70847 |
| 38 | 0.36139 | 0.70062 |
| 39 | 0.37828 | 0.69246 |
| 40 | 0.39516 | 0.68401 |
| 41 | 0.41205 | 0.67523 |
| 42 | 0.42893 | 0.66613 |
| 43 | 0.44582 | 0.65670 |
| 44 | 0.46270 | 0.64692 |
| 45 | 0.47959 | 0.63678 |
| 46 | 0.49647 | 0.62627 |
| 47 | 0.51336 | 0.61539 |
| 48 | 0.53024 | 0.60410 |
| 49 | 0.54713 | 0.59240 |
| 50 | 0.56401 | 0.58027 |
| 51 | 0.58090 | 0.56769 |
| 52 | 0.59778 | 0.55464 |
| 53 | 0.61467 | 0.54110 |
| 54 | 0.63155 | 0.52705 |
| 55 | 0.64844 | 0.51244 |
| 56 | 0.66532 | 0.49727 |
| 57 | 0.68220 | 0.48148 |
| 58 | 0.69909 | 0.46504 |
| 59 | 0.71597 | 0.44791 |
| 60 | 0.73286 | 0.43004 |
| 61 | 0.74974 | 0.41137 |
| 62 | 0.76663 | 0.39184 |
| 63 | 0.78351 | 0.37136 |
| 64 | 0.80040 | 0.34986 |
| 65 | 0.81728 | 0.32721 |
| 66 | 0.83417 | 0.30331 |
| 67 | 0.85105 | 0.27798 |
| 68 | 0.86794 | 0.25103 |
| 69 | 0.88482 | 0.22221 |
| 70 | 0.90171 | 0.19120 |
| 71 | 0.91859 | 0.15755 |
| 72 | 0.93547 | 0.12064 |
| 73 | 0.95226 | 0.079845 |
| 74 | 0.95938 | 0.061524 |
| 75 | 0.96650 | 0.043204 |
| 76 | 0.97361 | 0.024884 |
| 77 | 0.98073 | 0.0065631 |
| 78 | 0.98230 | 0.0038427 |
| 79 | 0.98463 | 0.0017172 |
| 80 | 0.98750 | 0.00039538 |
| 81 | 0.99063 | 4.5100e-06 |
| 82 | 0.99374 | 0.00058252 |
| 83 | 0.99652 | 0.0020755 |
| 84 | 0.99872 | 0.0043429 |
| 85 | 1.0001 | 0.0071712 |
| 86 | 1.0006 | 0.010294 |
| 87 | 1.0006 | 0.011143 |
| 88 | 1.0005 | 0.011986 |
| 89 | 1.0003 | 0.012818 |
| 90 | 1.0001 | 0.013632 |
| 91 | 0.98945 | 0.044610 |
| 92 | 0.97884 | 0.075588 |
| 93 | 0.96823 | 0.10657 |

| | | |
|---|---|---|
| 94 | 0.95762 | 0.13754 |
| 95 | 0.94701 | 0.16852 |
| 96 | 0.93640 | 0.19950 |
| 97 | 0.92579 | 0.23047 |
| 98 | 0.91517 | 0.26145 |
| 99 | 0.90456 | 0.29243 |
| 100 | 0.89579 | 0.31792 |
| 101 | 0.88691 | 0.34341 |
| 102 | 0.87803 | 0.36860 |
| 103 | 0.86915 | 0.39346 |
| 104 | 0.86027 | 0.41799 |
| 105 | 0.85139 | 0.44216 |
| 106 | 0.84251 | 0.46596 |
| 107 | 0.83363 | 0.48935 |
| 108 | 0.82475 | 0.51232 |
| 109 | 0.81587 | 0.53485 |
| 110 | 0.80700 | 0.55689 |
| 111 | 0.79812 | 0.57842 |
| 112 | 0.78924 | 0.59939 |
| 113 | 0.78036 | 0.61975 |
| 114 | 0.76852 | 0.64546 |
| 115 | 0.75657 | 0.66951 |
| 116 | 0.74463 | 0.69194 |
| 117 | 0.73269 | 0.71293 |
| 118 | 0.72075 | 0.73262 |
| 119 | 0.70881 | 0.75107 |
| 120 | 0.69686 | 0.76840 |
| 121 | 0.68492 | 0.78470 |
| 122 | 0.67298 | 0.80004 |
| 123 | 0.66104 | 0.81450 |
| 124 | 0.64910 | 0.82813 |
| 125 | 0.63716 | 0.84099 |
| 126 | 0.62521 | 0.85311 |
| 127 | 0.61327 | 0.86455 |
| 128 | 0.60133 | 0.87533 |
| 129 | 0.58939 | 0.88549 |
| 130 | 0.57745 | 0.89505 |
| 131 | 0.56551 | 0.90404 |
| 132 | 0.55357 | 0.91249 |
| 133 | 0.54162 | 0.92041 |
| 134 | 0.52968 | 0.92783 |
| 135 | 0.51774 | 0.93476 |
| 136 | 0.50580 | 0.94121 |
| 137 | 0.49386 | 0.94720 |
| 138 | 0.48192 | 0.95275 |
| 139 | 0.46998 | 0.95787 |
| 140 | 0.45803 | 0.96256 |
| 141 | 0.44609 | 0.96683 |
| 142 | 0.43415 | 0.97070 |
| 143 | 0.42221 | 0.97418 |
| 144 | 0.41027 | 0.97726 |
| 145 | 0.39833 | 0.97997 |
| 146 | 0.38638 | 0.98230 |
| 147 | 0.37444 | 0.98426 |
| 148 | 0.36250 | 0.98585 |
| 149 | 0.35056 | 0.98708 |
| 150 | 0.33862 | 0.98796 |
| 151 | 0.32668 | 0.98848 |
| 152 | 0.31474 | 0.98865 |
| 153 | 0.30462 | 0.98856 |
| 154 | 0.29439 | 0.98827 |
| 155 | 0.28417 | 0.98779 |
| 156 | 0.27395 | 0.98712 |
| 157 | 0.26373 | 0.98626 |
| 158 | 0.25351 | 0.98521 |
| 159 | 0.24329 | 0.98396 |
| 160 | 0.23307 | 0.98252 |
| 161 | 0.22285 | 0.98088 |
| 162 | 0.21263 | 0.97903 |
| 163 | 0.20241 | 0.97698 |
| 164 | 0.19219 | 0.97472 |
| 165 | 0.18197 | 0.97224 |
| 166 | 0.17174 | 0.96954 |
| 167 | 0.16152 | 0.96661 |
| 168 | 0.15130 | 0.96344 |
| 169 | 0.14108 | 0.96003 |
| 170 | 0.13086 | 0.95635 |
| 171 | 0.12064 | 0.95241 |
| 172 | 0.11042 | 0.94819 |
| 173 | 0.10020 | 0.94367 |
| 174 | 0.089978 | 0.93883 |
| 175 | 0.079757 | 0.93365 |
| 176 | 0.069536 | 0.92810 |
| 177 | 0.059316 | 0.92215 |
| 178 | 0.049095 | 0.91577 |
| 179 | 0.038874 | 0.90891 |
| 180 | 0.028653 | 0.90151 |
| 181 | 0.018432 | 0.89349 |
| 182 | 0.016656 | 0.89197 |
| 183 | 0.014952 | 0.89037 |
| 184 | 0.013325 | 0.88869 |
| 185 | 0.011778 | 0.88693 |
| 186 | 0.010314 | 0.88511 |
| 187 | 0.0089374 | 0.88322 |
| 188 | 0.0076500 | 0.88126 |
| 189 | 0.0064551 | 0.87925 |
| 190 | 0.0053553 | 0.87719 |
| 191 | 0.0043528 | 0.87507 |
| 192 | 0.0034499 | 0.87292 |
| 193 | 0.0026486 | 0.87072 |
| 194 | 0.0019505 | 0.86849 |
| 195 | 0.0013573 | 0.86622 |
| 196 | 0.00087012 | 0.86393 |
| 197 | 0.00049012 | 0.86163 |
| 198 | 0.00021811 | 0.85930 |
| 199 | 5.4660e-05 | 0.85697 |
| 200 | 1.4000e-07 | 0.85463 |

First nozzle, midspan

| | x [in] | y[in] |
|---|---|---|
| 1 | 0.00013143 | 0.87560 |
| 2 | 0.00052459 | 0.87200 |
| 3 | 0.0011775 | 0.86843 |
| 4 | 0.0020869 | 0.86491 |
| 5 | 0.0032478 | 0.86147 |
| 6 | 0.0046542 | 0.85813 |
| 7 | 0.0062986 | 0.85489 |
| 8 | 0.0081725 | 0.85179 |
| 9 | 0.010266 | 0.84882 |
| 10 | 0.012568 | 0.84602 |
| 11 | 0.015066 | 0.84339 |
| 12 | 0.017748 | 0.84094 |
| 13 | 0.020599 | 0.83870 |
| 14 | 0.023603 | 0.83667 |
| 15 | 0.026747 | 0.83486 |
| 16 | 0.030012 | 0.83329 |
| 17 | 0.033381 | 0.83195 |
| 18 | 0.036838 | 0.83086 |
| 19 | 0.040363 | 0.83003 |
| 20 | 0.057963 | 0.82639 |
| 21 | 0.075563 | 0.82253 |
| 22 | 0.093164 | 0.81843 |
| 23 | 0.11076 | 0.81408 |
| 24 | 0.12836 | 0.80950 |
| 25 | 0.14596 | 0.80467 |
| 26 | 0.16356 | 0.79959 |
| 27 | 0.18117 | 0.79426 |
| 28 | 0.19877 | 0.78868 |
| 29 | 0.21637 | 0.78283 |
| 30 | 0.23397 | 0.77673 |
| 31 | 0.25157 | 0.77035 |
| 32 | 0.26917 | 0.76370 |
| 33 | 0.28677 | 0.75678 |
| 34 | 0.30437 | 0.74957 |
| 35 | 0.32197 | 0.74207 |
| 36 | 0.33957 | 0.73427 |
| 37 | 0.35717 | 0.72618 |
| 38 | 0.37477 | 0.71778 |
| 39 | 0.39237 | 0.70906 |
| 40 | 0.40997 | 0.70002 |
| 41 | 0.42757 | 0.69065 |
| 42 | 0.44517 | 0.68093 |
| 43 | 0.46277 | 0.67087 |
| 44 | 0.48037 | 0.66044 |
| 45 | 0.49797 | 0.64964 |
| 46 | 0.51557 | 0.63846 |
| 47 | 0.53317 | 0.62687 |
| 48 | 0.55077 | 0.61488 |
| 49 | 0.56837 | 0.60246 |
| 50 | 0.58597 | 0.58959 |
| 51 | 0.60357 | 0.57627 |
| 52 | 0.62117 | 0.56245 |
| 53 | 0.63877 | 0.54814 |
| 54 | 0.65637 | 0.53329 |
| 55 | 0.67397 | 0.51789 |
| 56 | 0.69157 | 0.50191 |
| 57 | 0.70917 | 0.48530 |
| 58 | 0.72677 | 0.46804 |
| 59 | 0.74437 | 0.45009 |
| 60 | 0.76197 | 0.43139 |
| 61 | 0.77957 | 0.41189 |
| 62 | 0.79717 | 0.39153 |
| 63 | 0.81477 | 0.37025 |
| 64 | 0.83237 | 0.34795 |
| 65 | 0.84997 | 0.32454 |
| 66 | 0.86757 | 0.29991 |
| 67 | 0.88517 | 0.27391 |
| 68 | 0.90277 | 0.24636 |
| 69 | 0.92037 | 0.21706 |
| 70 | 0.93796 | 0.18573 |
| 71 | 0.95556 | 0.15198 |
| 72 | 0.97316 | 0.11533 |
| 73 | 0.99066 | 0.075653 |
| 74 | 0.99808 | 0.058299 |
| 75 | 1.0055 | 0.040945 |
| 76 | 1.0129 | 0.023591 |
| 77 | 1.0203 | 0.0062364 |
| 78 | 1.0219 | 0.0036896 |
| 79 | 1.0242 | 0.0016451 |
| 80 | 1.0271 | 0.00037010 |
| 81 | 1.0302 | 6.9900e-06 |
| 82 | 1.0333 | 0.00059956 |
| 83 | 1.0360 | 0.0020971 |
| 84 | 1.0382 | 0.0043615 |
| 85 | 1.0396 | 0.0071818 |
| 86 | 1.0401 | 0.010294 |
| 87 | 1.0400 | 0.011221 |
| 88 | 1.0399 | 0.012141 |
| 89 | 1.0397 | 0.013047 |
| 90 | 1.0394 | 0.013931 |
| 91 | 1.0284 | 0.043257 |
| 92 | 1.0173 | 0.072584 |
| 93 | 1.0063 | 0.10191 |
| 94 | 0.99527 | 0.13124 |
| 95 | 0.98424 | 0.16056 |
| 96 | 0.97320 | 0.18989 |
| 97 | 0.96217 | 0.21921 |
| 98 | 0.95113 | 0.24853 |
| 99 | 0.94010 | 0.27786 |
| 100 | 0.93097 | 0.30205 |
| 101 | 0.92174 | 0.32639 |
| 102 | 0.91250 | 0.35059 |
| 103 | 0.90327 | 0.37464 |
| 104 | 0.89403 | 0.39854 |
| 105 | 0.88480 | 0.42227 |

| | | |
|---|---|---|
| 106 | 0.87557 | 0.44583 |
| 107 | 0.86633 | 0.46921 |
| 108 | 0.85710 | 0.49239 |
| 109 | 0.84786 | 0.51537 |
| 110 | 0.83863 | 0.53813 |
| 111 | 0.82940 | 0.56065 |
| 112 | 0.82016 | 0.58292 |
| 113 | 0.81092 | 0.60474 |
| 114 | 0.79861 | 0.63284 |
| 115 | 0.78619 | 0.65993 |
| 116 | 0.77377 | 0.68587 |
| 117 | 0.76134 | 0.71073 |
| 118 | 0.74892 | 0.73442 |
| 119 | 0.73650 | 0.75655 |
| 120 | 0.72408 | 0.77724 |
| 121 | 0.71166 | 0.79658 |
| 122 | 0.69924 | 0.81467 |
| 123 | 0.68681 | 0.83160 |
| 124 | 0.67439 | 0.84745 |
| 125 | 0.66197 | 0.86227 |
| 126 | 0.64955 | 0.87615 |
| 127 | 0.63713 | 0.88912 |
| 128 | 0.62471 | 0.90125 |
| 129 | 0.61229 | 0.91258 |
| 130 | 0.59987 | 0.92316 |
| 131 | 0.58745 | 0.93301 |
| 132 | 0.57503 | 0.94219 |
| 133 | 0.56261 | 0.95072 |
| 134 | 0.55019 | 0.95863 |
| 135 | 0.53777 | 0.96595 |
| 136 | 0.52535 | 0.97271 |
| 137 | 0.51293 | 0.97894 |
| 138 | 0.50051 | 0.98465 |
| 139 | 0.48809 | 0.98986 |
| 140 | 0.47567 | 0.99460 |
| 141 | 0.46325 | 0.99888 |
| 142 | 0.45083 | 1.0027 |
| 143 | 0.43840 | 1.0061 |
| 144 | 0.42598 | 1.0091 |
| 145 | 0.41356 | 1.0117 |
| 146 | 0.40114 | 1.0140 |
| 147 | 0.38872 | 1.0158 |
| 148 | 0.37630 | 1.0173 |
| 149 | 0.36388 | 1.0185 |
| 150 | 0.35146 | 1.0193 |
| 151 | 0.33904 | 1.0197 |
| 152 | 0.32662 | 1.0199 |
| 153 | 0.31609 | 1.0197 |
| 154 | 0.30546 | 1.0194 |
| 155 | 0.29483 | 1.0188 |
| 156 | 0.28420 | 1.0180 |
| 157 | 0.27357 | 1.0170 |
| 158 | 0.26294 | 1.0158 |
| 159 | 0.25231 | 1.0144 |

| | | |
|---|---|---|
| 160 | 0.24168 | 1.0127 |
| 161 | 0.23105 | 1.0109 |
| 162 | 0.22042 | 1.0088 |
| 163 | 0.20979 | 1.0065 |
| 164 | 0.19916 | 1.0040 |
| 165 | 0.18853 | 1.0012 |
| 166 | 0.17789 | 0.99829 |
| 167 | 0.16726 | 0.99509 |
| 168 | 0.15663 | 0.99166 |
| 169 | 0.14600 | 0.98797 |
| 170 | 0.13537 | 0.98403 |
| 171 | 0.12474 | 0.97981 |
| 172 | 0.11411 | 0.97532 |
| 173 | 0.10348 | 0.97052 |
| 174 | 0.092848 | 0.96541 |
| 175 | 0.082217 | 0.95996 |
| 176 | 0.071586 | 0.95414 |
| 177 | 0.060955 | 0.94792 |
| 178 | 0.050325 | 0.94126 |
| 179 | 0.039694 | 0.93412 |
| 180 | 0.029063 | 0.92642 |
| 181 | 0.018432 | 0.91809 |
| 182 | 0.016656 | 0.91656 |
| 183 | 0.014952 | 0.91496 |
| 184 | 0.013325 | 0.91328 |
| 185 | 0.011778 | 0.91153 |
| 186 | 0.010314 | 0.90970 |
| 187 | 0.0089374 | 0.90781 |
| 188 | 0.0076500 | 0.90586 |
| 189 | 0.0064551 | 0.90385 |
| 190 | 0.0053553 | 0.90178 |
| 191 | 0.0043528 | 0.89967 |
| 192 | 0.0034499 | 0.89751 |
| 193 | 0.0026486 | 0.89532 |
| 194 | 0.0019505 | 0.89308 |
| 195 | 0.0013573 | 0.89082 |
| 196 | 0.00087012 | 0.88853 |
| 197 | 0.00049013 | 0.88623 |
| 198 | 0.00021811 | 0.88390 |
| 199 | 5.4660e-05 | 0.88157 |
| 200 | 1.4000e-07 | 0.87923 |

First nozzle, tip

| | x [in] | y [in] |
|---|---|---|
| 1 | 0.00013073 | 0.90027 |
| 2 | 0.00052177 | 0.89667 |
| 3 | 0.0011712 | 0.89311 |
| 4 | 0.0020757 | 0.88961 |
| 5 | 0.0032303 | 0.88618 |
| 6 | 0.0046291 | 0.88284 |
| 7 | 0.0062647 | 0.87961 |
| 8 | 0.0081285 | 0.87651 |
| 9 | 0.010211 | 0.87355 |
| 10 | 0.012500 | 0.87075 |
| 11 | 0.014985 | 0.86812 |
| 12 | 0.017652 | 0.86568 |
| 13 | 0.020488 | 0.86344 |
| 14 | 0.023476 | 0.86140 |
| 15 | 0.026603 | 0.85959 |
| 16 | 0.029850 | 0.85801 |
| 17 | 0.033202 | 0.85667 |
| 18 | 0.036639 | 0.85557 |
| 19 | 0.040145 | 0.85472 |
| 20 | 0.058460 | 0.85086 |
| 21 | 0.076775 | 0.84674 |
| 22 | 0.095090 | 0.84237 |
| 23 | 0.11341 | 0.83774 |
| 24 | 0.13172 | 0.83285 |
| 25 | 0.15004 | 0.82769 |
| 26 | 0.16835 | 0.82227 |
| 27 | 0.18667 | 0.81658 |
| 28 | 0.20498 | 0.81062 |
| 29 | 0.22330 | 0.80438 |
| 30 | 0.24161 | 0.79786 |
| 31 | 0.25993 | 0.79105 |
| 32 | 0.27824 | 0.78395 |
| 33 | 0.29656 | 0.77656 |
| 34 | 0.31487 | 0.76887 |
| 35 | 0.33319 | 0.76087 |
| 36 | 0.35150 | 0.75256 |
| 37 | 0.36982 | 0.74393 |
| 38 | 0.38813 | 0.73498 |
| 39 | 0.40645 | 0.72570 |
| 40 | 0.42476 | 0.71607 |
| 41 | 0.44308 | 0.70610 |
| 42 | 0.46139 | 0.69577 |
| 43 | 0.47971 | 0.68507 |
| 44 | 0.49802 | 0.67400 |
| 45 | 0.51634 | 0.66254 |
| 46 | 0.53465 | 0.65068 |
| 47 | 0.55297 | 0.63840 |
| 48 | 0.57128 | 0.62570 |
| 49 | 0.58960 | 0.61255 |
| 50 | 0.60791 | 0.59895 |
| 51 | 0.62623 | 0.58487 |
| 52 | 0.64454 | 0.57030 |
| 53 | 0.66286 | 0.55520 |
| 54 | 0.68117 | 0.53957 |
| 55 | 0.69949 | 0.52337 |
| 56 | 0.71780 | 0.50657 |
| 57 | 0.73612 | 0.48915 |
| 58 | 0.75443 | 0.47107 |
| 59 | 0.77275 | 0.45229 |
| 60 | 0.79106 | 0.43276 |
| 61 | 0.80938 | 0.41243 |
| 62 | 0.82769 | 0.39125 |
| 63 | 0.84601 | 0.36915 |
| 64 | 0.86432 | 0.34606 |
| 65 | 0.88264 | 0.32188 |
| 66 | 0.90095 | 0.29652 |
| 67 | 0.91927 | 0.26984 |
| 68 | 0.93759 | 0.24171 |
| 69 | 0.95590 | 0.21192 |
| 70 | 0.97422 | 0.18026 |
| 71 | 0.99253 | 0.14642 |
| 72 | 1.0108 | 0.11002 |
| 73 | 1.0291 | 0.071462 |
| 74 | 1.0368 | 0.055074 |
| 75 | 1.0445 | 0.038686 |
| 76 | 1.0522 | 0.022298 |
| 77 | 1.0599 | 0.0059098 |
| 78 | 1.0615 | 0.0035365 |
| 79 | 1.0638 | 0.0015731 |
| 80 | 1.0666 | 0.00034483 |
| 81 | 1.0697 | 9.4700e-06 |
| 82 | 1.0728 | 0.00061660 |
| 83 | 1.0755 | 0.0021187 |
| 84 | 1.0777 | 0.0043802 |
| 85 | 1.0791 | 0.0071925 |
| 86 | 1.0795 | 0.010294 |
| 87 | 1.0795 | 0.011300 |
| 88 | 1.0794 | 0.012297 |
| 89 | 1.0791 | 0.013276 |
| 90 | 1.0788 | 0.014229 |
| 91 | 1.0673 | 0.041904 |
| 92 | 1.0558 | 0.069580 |
| 93 | 1.0444 | 0.097256 |
| 94 | 1.0329 | 0.12493 |
| 95 | 1.0215 | 0.15261 |
| 96 | 1.0100 | 0.18028 |
| 97 | 0.99853 | 0.20796 |
| 98 | 0.98707 | 0.23564 |
| 99 | 0.97561 | 0.26331 |
| 100 | 0.96612 | 0.28622 |
| 101 | 0.95653 | 0.30942 |
| 102 | 0.94694 | 0.33264 |
| 103 | 0.93735 | 0.35589 |
| 104 | 0.92776 | 0.37916 |
| 105 | 0.91816 | 0.40247 |

| | | | | | |
|---|---|---|---|---|---|
| 106 | 0.90857 | 0.42580 | 154 | 0.31652 | 1.0506 |
| 107 | 0.89898 | 0.44917 | 155 | 0.30548 | 1.0499 |
| 108 | 0.88939 | 0.47258 | 156 | 0.29444 | 1.0490 |
| 109 | 0.87980 | 0.49602 | 157 | 0.28340 | 1.0479 |
| 110 | 0.87020 | 0.51950 | 158 | 0.27236 | 1.0465 |
| 111 | 0.86061 | 0.54302 | 159 | 0.26132 | 1.0448 |
| 112 | 0.85102 | 0.56657 | 160 | 0.25028 | 1.0430 |
| 113 | 0.84143 | 0.58987 | 161 | 0.23924 | 1.0409 |
| 114 | 0.82864 | 0.62037 | 162 | 0.22820 | 1.0386 |
| 115 | 0.81574 | 0.65049 | 163 | 0.21716 | 1.0361 |
| 116 | 0.80284 | 0.67992 | 164 | 0.20612 | 1.0333 |
| 117 | 0.78994 | 0.70864 | 165 | 0.19507 | 1.0303 |
| 118 | 0.77705 | 0.73632 | 166 | 0.18403 | 1.0271 |
| 119 | 0.76415 | 0.76214 | 167 | 0.17299 | 1.0237 |
| 120 | 0.75125 | 0.78617 | 168 | 0.16195 | 1.0200 |
| 121 | 0.73835 | 0.80855 | 169 | 0.15091 | 1.0160 |
| 122 | 0.72545 | 0.82939 | 170 | 0.13987 | 1.0118 |
| 123 | 0.71255 | 0.84878 | 171 | 0.12883 | 1.0073 |
| 124 | 0.69966 | 0.86684 | 172 | 0.11779 | 1.0025 |
| 125 | 0.68676 | 0.88363 | 173 | 0.10675 | 0.99746 |
| 126 | 0.67386 | 0.89925 | 174 | 0.095713 | 0.99208 |
| 127 | 0.66096 | 0.91376 | 175 | 0.084673 | 0.98635 |
| 128 | 0.64806 | 0.92724 | 176 | 0.073633 | 0.98026 |
| 129 | 0.63516 | 0.93974 | 177 | 0.062593 | 0.97377 |
| 130 | 0.62226 | 0.95133 | 178 | 0.051553 | 0.96683 |
| 131 | 0.60936 | 0.96205 | 179 | 0.040513 | 0.95940 |
| 132 | 0.59647 | 0.97195 | 180 | 0.029472 | 0.95141 |
| 133 | 0.58357 | 0.98109 | 181 | 0.018432 | 0.94276 |
| 134 | 0.57067 | 0.98949 | 182 | 0.016656 | 0.94123 |
| 135 | 0.55777 | 0.99722 | 183 | 0.014952 | 0.93963 |
| 136 | 0.54487 | 1.0043 | 184 | 0.013325 | 0.93795 |
| 137 | 0.53197 | 1.0107 | 185 | 0.011778 | 0.93619 |
| 138 | 0.51907 | 1.0166 | 186 | 0.010314 | 0.93437 |
| 139 | 0.50617 | 1.0219 | 187 | 0.0089374 | 0.93248 |
| 140 | 0.49327 | 1.0267 | 188 | 0.0076500 | 0.93053 |
| 141 | 0.48038 | 1.0310 | 189 | 0.0064551 | 0.92851 |
| 142 | 0.46748 | 1.0348 | 190 | 0.0053553 | 0.92645 |
| 143 | 0.45458 | 1.0382 | 191 | 0.0043528 | 0.92434 |
| 144 | 0.44168 | 1.0411 | 192 | 0.0034499 | 0.92218 |
| 145 | 0.42878 | 1.0436 | 193 | 0.0026486 | 0.91998 |
| 146 | 0.41588 | 1.0457 | 194 | 0.0019505 | 0.91775 |
| 147 | 0.40298 | 1.0475 | 195 | 0.0013573 | 0.91548 |
| 148 | 0.39008 | 1.0489 | 196 | 0.00087013 | 0.91320 |
| 149 | 0.37718 | 1.0499 | 197 | 0.00049013 | 0.91089 |
| 150 | 0.36429 | 1.0506 | 198 | 0.00021811 | 0.90856 |
| 151 | 0.35139 | 1.0511 | 199 | 5.4670e-05 | 0.90623 |
| 152 | 0.33849 | 1.0512 | 200 | 1.5000e-07 | 0.90389 |
| 153 | 0.32756 | 1.0510 | | | |

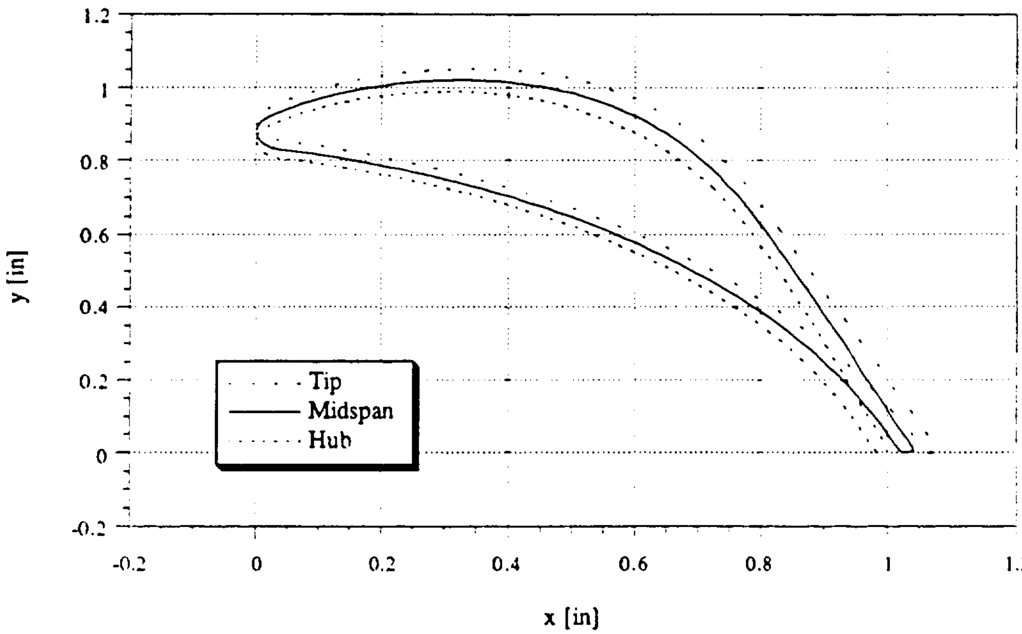


Figure A..1.1--First nozzle: tip, midspan, and hub

A.1.2 First Rotor Coordinates

First rotor, hub

| | x [in] | y[in] |
|---|---|---|
| 1 | 0.12085 | 0.22903 |
| 2 | 0.12139 | 0.22218 |
| 3 | 0.12192 | 0.21942 |
| 4 | 0.12246 | 0.21733 |
| 5 | 0.12299 | 0.21558 |
| 6 | 0.12352 | 0.21406 |
| 7 | 0.12406 | 0.21270 |
| 8 | 0.12459 | 0.21146 |
| 9 | 0.12513 | 0.21031 |
| 10 | 0.12556 | 0.20943 |
| 11 | 0.13846 | 0.18586 |
| 12 | 0.15136 | 0.16523 |
| 13 | 0.16426 | 0.14691 |
| 14 | 0.17716 | 0.13049 |
| 15 | 0.19007 | 0.11568 |
| 16 | 0.20297 | 0.10227 |
| 17 | 0.21587 | 0.090094 |
| 18 | 0.22877 | 0.079021 |
| 19 | 0.24167 | 0.068951 |
| 20 | 0.25457 | 0.059799 |
| 21 | 0.26747 | 0.051497 |
| 22 | 0.28037 | 0.043990 |
| 23 | 0.29327 | 0.037227 |
| 24 | 0.30617 | 0.031170 |
| 25 | 0.31907 | 0.025784 |
| 26 | 0.33197 | 0.021040 |
| 27 | 0.34487 | 0.016912 |
| 28 | 0.35777 | 0.013379 |
| 29 | 0.37067 | 0.010424 |
| 30 | 0.38357 | 0.0080306 |
| 31 | 0.39648 | 0.0061865 |
| 32 | 0.40938 | 0.0048812 |
| 33 | 0.42228 | 0.0041060 |
| 34 | 0.43518 | 0.0038545 |
| 35 | 0.44808 | 0.0041218 |
| 36 | 0.46098 | 0.0049050 |
| 37 | 0.47388 | 0.0062027 |
| 38 | 0.48678 | 0.0080152 |
| 39 | 0.49968 | 0.010344 |
| 40 | 0.51258 | 0.013194 |
| 41 | 0.52548 | 0.016569 |
| 42 | 0.53838 | 0.020478 |
| 43 | 0.55128 | 0.024929 |
| 44 | 0.56418 | 0.029933 |
| 45 | 0.57708 | 0.035504 |
| 46 | 0.58998 | 0.041659 |
| 47 | 0.60288 | 0.048416 |
| 48 | 0.61579 | 0.055799 |
| 49 | 0.62869 | 0.063833 |
| 50 | 0.64159 | 0.072549 |
| 51 | 0.65449 | 0.081985 |
| 52 | 0.66739 | 0.092182 |
| 53 | 0.68029 | 0.10319 |
| 54 | 0.69319 | 0.11508 |
| 55 | 0.70609 | 0.12791 |
| 56 | 0.71899 | 0.14177 |
| 57 | 0.73189 | 0.15679 |
| 58 | 0.74479 | 0.17309 |
| 59 | 0.75759 | 0.19071 |
| 60 | 0.76711 | 0.20483 |
| 61 | 0.77662 | 0.21971 |
| 62 | 0.78613 | 0.23524 |
| 63 | 0.79565 | 0.25133 |
| 64 | 0.80516 | 0.26791 |
| 65 | 0.81468 | 0.28492 |
| 66 | 0.82419 | 0.30232 |
| 67 | 0.83371 | 0.32006 |
| 68 | 0.84322 | 0.33812 |
| 69 | 0.85273 | 0.35647 |
| 70 | 0.86225 | 0.37509 |
| 71 | 0.87176 | 0.39394 |
| 72 | 0.88128 | 0.41303 |
| 73 | 0.89079 | 0.43232 |
| 74 | 0.90030 | 0.45180 |
| 75 | 0.90982 | 0.47147 |
| 76 | 0.91933 | 0.49130 |
| 77 | 0.92885 | 0.51130 |
| 78 | 0.93826 | 0.53123 |
| 79 | 0.93867 | 0.53225 |
| 80 | 0.93897 | 0.53331 |
| 81 | 0.93915 | 0.53439 |
| 82 | 0.93921 | 0.53549 |
| 83 | 0.93879 | 0.53836 |
| 84 | 0.93756 | 0.54099 |
| 85 | 0.93563 | 0.54316 |
| 86 | 0.93316 | 0.54468 |
| 87 | 0.93035 | 0.54543 |
| 88 | 0.92745 | 0.54534 |
| 89 | 0.92470 | 0.54442 |
| 90 | 0.92233 | 0.54274 |
| 91 | 0.92053 | 0.54046 |
| 92 | 0.90538 | 0.51508 |
| 93 | 0.89012 | 0.49148 |
| 94 | 0.87486 | 0.46955 |
| 95 | 0.85960 | 0.44909 |
| 96 | 0.84435 | 0.42991 |
| 97 | 0.82909 | 0.41190 |
| 98 | 0.81383 | 0.39494 |
| 99 | 0.79857 | 0.37895 |
| 100 | 0.78331 | 0.36386 |
| 101 | 0.76806 | 0.34960 |

| | | |
|---|---|---|
| 102 | 0.75280 | 0.33613 |
| 103 | 0.73754 | 0.32339 |
| 104 | 0.72228 | 0.31135 |
| 105 | 0.70703 | 0.29999 |
| 106 | 0.69177 | 0.28927 |
| 107 | 0.67651 | 0.27916 |
| 108 | 0.66125 | 0.26964 |
| 109 | 0.64599 | 0.26071 |
| 110 | 0.63074 | 0.25233 |
| 111 | 0.61548 | 0.24451 |
| 112 | 0.60022 | 0.23721 |
| 113 | 0.58496 | 0.23045 |
| 114 | 0.56971 | 0.22420 |
| 115 | 0.55445 | 0.21845 |
| 116 | 0.53919 | 0.21322 |
| 117 | 0.52393 | 0.20849 |
| 118 | 0.50867 | 0.20425 |
| 119 | 0.49342 | 0.20051 |
| 120 | 0.47816 | 0.19727 |
| 121 | 0.46290 | 0.19452 |
| 122 | 0.44764 | 0.19228 |
| 123 | 0.43238 | 0.19054 |
| 124 | 0.41713 | 0.18931 |
| 125 | 0.40187 | 0.18860 |
| 126 | 0.38661 | 0.18841 |
| 127 | 0.37135 | 0.18875 |
| 128 | 0.35610 | 0.18964 |
| 129 | 0.34084 | 0.19109 |
| 130 | 0.32558 | 0.19311 |
| 131 | 0.31032 | 0.19572 |
| 132 | 0.29506 | 0.19895 |
| 133 | 0.27981 | 0.20281 |
| 134 | 0.26455 | 0.20734 |
| 135 | 0.24929 | 0.21257 |
| 136 | 0.23403 | 0.21852 |
| 137 | 0.21878 | 0.22526 |
| 138 | 0.20352 | 0.23282 |
| 139 | 0.18826 | 0.24127 |
| 140 | 0.17300 | 0.25067 |
| 141 | 0.17157 | 0.25157 |
| 142 | 0.17003 | 0.25247 |
| 143 | 0.16849 | 0.25330 |
| 144 | 0.16696 | 0.25406 |
| 145 | 0.16542 | 0.25476 |
| 146 | 0.16388 | 0.25540 |
| 147 | 0.16234 | 0.25597 |
| 148 | 0.16081 | 0.25649 |
| 149 | 0.15927 | 0.25694 |
| 150 | 0.15773 | 0.25733 |
| 151 | 0.15620 | 0.25767 |
| 152 | 0.15466 | 0.25794 |
| 153 | 0.15312 | 0.25814 |
| 154 | 0.15159 | 0.25829 |
| 155 | 0.15005 | 0.25837 |
| 156 | 0.14851 | 0.25838 |
| 157 | 0.14698 | 0.25832 |
| 158 | 0.14544 | 0.25820 |
| 159 | 0.14390 | 0.25799 |
| 160 | 0.14237 | 0.25771 |
| 161 | 0.14083 | 0.25734 |
| 162 | 0.13929 | 0.25687 |
| 163 | 0.13776 | 0.25631 |
| 164 | 0.13622 | 0.25565 |
| 165 | 0.13468 | 0.25486 |
| 166 | 0.13315 | 0.25393 |
| 167 | 0.13161 | 0.25285 |
| 168 | 0.13007 | 0.25158 |
| 169 | 0.12854 | 0.25008 |
| 170 | 0.12700 | 0.24830 |
| 171 | 0.12546 | 0.24612 |
| 172 | 0.12393 | 0.24334 |
| 173 | 0.12239 | 0.23944 |

First rotor, midspan

| | x [in] | y[in] |
|---|---|---|
| 1 | 0.17979 | 0.15760 |
| 2 | 0.18048 | 0.15051 |
| 3 | 0.18117 | 0.14765 |
| 4 | 0.18186 | 0.14549 |
| 5 | 0.18255 | 0.14370 |
| 6 | 0.18325 | 0.14215 |
| 7 | 0.18394 | 0.14077 |
| 8 | 0.18463 | 0.13953 |
| 9 | 0.18532 | 0.13838 |
| 10 | 0.18588 | 0.13752 |
| 11 | 0.19747 | 0.11992 |
| 12 | 0.20907 | 0.10432 |
| 13 | 0.22066 | 0.090363 |
| 14 | 0.23226 | 0.077786 |
| 15 | 0.24386 | 0.066406 |
| 16 | 0.25546 | 0.056082 |
| 17 | 0.26706 | 0.046707 |
| 18 | 0.27866 | 0.038194 |
| 19 | 0.29026 | 0.030473 |
| 20 | 0.30186 | 0.023488 |
| 21 | 0.31346 | 0.017191 |
| 22 | 0.32506 | 0.011543 |
| 23 | 0.33667 | 0.0065094 |
| 24 | 0.34827 | 0.0020632 |
| 25 | 0.35987 | -0.0018200 |
| 26 | 0.37147 | -0.0051603 |
| 27 | 0.38308 | -0.0079749 |
| 28 | 0.39468 | -0.010278 |
| 29 | 0.40628 | -0.012082 |
| 30 | 0.41789 | -0.013396 |
| 31 | 0.42949 | -0.014227 |
| 32 | 0.44109 | -0.014583 |
| 33 | 0.45269 | -0.014466 |
| 34 | 0.46430 | -0.013880 |
| 35 | 0.47590 | -0.012825 |
| 36 | 0.48750 | -0.011300 |
| 37 | 0.49911 | -0.0093034 |
| 38 | 0.51071 | -0.0068301 |
| 39 | 0.52231 | -0.0038744 |
| 40 | 0.53392 | -0.00042857 |
| 41 | 0.54552 | 0.0035173 |
| 42 | 0.55712 | 0.0079753 |
| 43 | 0.56873 | 0.012960 |
| 44 | 0.58033 | 0.018489 |
| 45 | 0.59193 | 0.024584 |
| 46 | 0.60353 | 0.031268 |
| 47 | 0.61514 | 0.038571 |
| 48 | 0.62674 | 0.046529 |
| 49 | 0.63834 | 0.055183 |
| 50 | 0.64995 | 0.064584 |
| 51 | 0.66155 | 0.074794 |
| 52 | 0.67315 | 0.085889 |
| 53 | 0.68476 | 0.097967 |
| 54 | 0.69636 | 0.11116 |
| 55 | 0.70796 | 0.12560 |
| 56 | 0.71956 | 0.14120 |
| 57 | 0.73117 | 0.15788 |
| 58 | 0.74277 | 0.17563 |
| 59 | 0.75428 | 0.19430 |
| 60 | 0.76284 | 0.20889 |
| 61 | 0.77140 | 0.22401 |
| 62 | 0.77996 | 0.23958 |
| 63 | 0.78851 | 0.25556 |
| 64 | 0.79707 | 0.27189 |
| 65 | 0.80563 | 0.28854 |
| 66 | 0.81418 | 0.30549 |
| 67 | 0.82274 | 0.32269 |
| 68 | 0.83130 | 0.34014 |
| 69 | 0.83986 | 0.35780 |
| 70 | 0.84841 | 0.37567 |
| 71 | 0.85697 | 0.39373 |
| 72 | 0.86553 | 0.41197 |
| 73 | 0.87408 | 0.43037 |
| 74 | 0.88264 | 0.44893 |
| 75 | 0.89120 | 0.46763 |
| 76 | 0.89975 | 0.48647 |
| 77 | 0.90831 | 0.50544 |
| 78 | 0.91677 | 0.52432 |
| 79 | 0.91715 | 0.52530 |
| 80 | 0.91742 | 0.52631 |
| 81 | 0.91759 | 0.52735 |
| 82 | 0.91764 | 0.52839 |
| 83 | 0.91722 | 0.53127 |
| 84 | 0.91598 | 0.53391 |
| 85 | 0.91403 | 0.53608 |
| 86 | 0.91154 | 0.53760 |
| 87 | 0.90871 | 0.53833 |
| 88 | 0.90578 | 0.53822 |
| 89 | 0.90301 | 0.53725 |
| 90 | 0.90061 | 0.53550 |
| 91 | 0.89881 | 0.53307 |
| 92 | 0.88521 | 0.50815 |
| 93 | 0.87153 | 0.48428 |
| 94 | 0.85784 | 0.46148 |
| 95 | 0.84416 | 0.43968 |
| 96 | 0.83047 | 0.41879 |
| 97 | 0.81679 | 0.39876 |
| 98 | 0.80310 | 0.37956 |
| 99 | 0.78942 | 0.36116 |
| 100 | 0.77573 | 0.34353 |
| 101 | 0.76205 | 0.32665 |
| 102 | 0.74836 | 0.31053 |
| 103 | 0.73468 | 0.29513 |
| 104 | 0.72099 | 0.28046 |

| | | |
|---|---|---|
| 105 | 0.70731 | 0.26652 |
| 106 | 0.69362 | 0.25330 |
| 107 | 0.67994 | 0.24079 |
| 108 | 0.66625 | 0.22899 |
| 109 | 0.65257 | 0.21790 |
| 110 | 0.63888 | 0.20751 |
| 111 | 0.62520 | 0.19783 |
| 112 | 0.61151 | 0.18884 |
| 113 | 0.59783 | 0.18053 |
| 114 | 0.58414 | 0.17291 |
| 115 | 0.57046 | 0.16596 |
| 116 | 0.55677 | 0.15967 |
| 117 | 0.54309 | 0.15404 |
| 118 | 0.52940 | 0.14905 |
| 119 | 0.51572 | 0.14468 |
| 120 | 0.50204 | 0.14094 |
| 121 | 0.48835 | 0.13781 |
| 122 | 0.47467 | 0.13527 |
| 123 | 0.46098 | 0.13331 |
| 124 | 0.44730 | 0.13193 |
| 125 | 0.43361 | 0.13111 |
| 126 | 0.41993 | 0.13085 |
| 127 | 0.40624 | 0.13113 |
| 128 | 0.39256 | 0.13194 |
| 129 | 0.37887 | 0.13328 |
| 130 | 0.36519 | 0.13515 |
| 131 | 0.35151 | 0.13754 |
| 132 | 0.33782 | 0.14044 |
| 133 | 0.32414 | 0.14387 |
| 134 | 0.31045 | 0.14782 |
| 135 | 0.29677 | 0.15230 |
| 136 | 0.28309 | 0.15731 |
| 137 | 0.26941 | 0.16288 |
| 138 | 0.25572 | 0.16900 |
| 139 | 0.24204 | 0.17572 |
| 140 | 0.22836 | 0.18304 |
| 141 | 0.22703 | 0.18375 |
| 142 | 0.22559 | 0.18445 |
| 143 | 0.22416 | 0.18507 |
| 144 | 0.22273 | 0.18564 |
| 145 | 0.22130 | 0.18614 |
| 146 | 0.21987 | 0.18658 |
| 147 | 0.21844 | 0.18696 |
| 148 | 0.21701 | 0.18728 |
| 149 | 0.21558 | 0.18754 |
| 150 | 0.21415 | 0.18775 |
| 151 | 0.21271 | 0.18790 |
| 152 | 0.21128 | 0.18799 |
| 153 | 0.20985 | 0.18802 |
| 154 | 0.20842 | 0.18799 |
| 155 | 0.20699 | 0.18790 |
| 156 | 0.20556 | 0.18775 |
| 157 | 0.20413 | 0.18753 |
| 158 | 0.20270 | 0.18724 |
| 159 | 0.20126 | 0.18689 |
| 160 | 0.19983 | 0.18645 |
| 161 | 0.19840 | 0.18594 |
| 162 | 0.19697 | 0.18535 |
| 163 | 0.19554 | 0.18466 |
| 164 | 0.19411 | 0.18387 |
| 165 | 0.19268 | 0.18297 |
| 166 | 0.19124 | 0.18194 |
| 167 | 0.18981 | 0.18077 |
| 168 | 0.18838 | 0.17943 |
| 169 | 0.18695 | 0.17787 |
| 170 | 0.18552 | 0.17605 |
| 171 | 0.18409 | 0.17386 |
| 172 | 0.18265 | 0.17113 |
| 173 | 0.18122 | 0.16736 |

First rotor, tip

| | x [in] | y [in] |
|---|---|---|
| 1 | 0.23860 | 0.086311 |
| 2 | 0.23945 | 0.078986 |
| 3 | 0.24030 | 0.076022 |
| 4 | 0.24115 | 0.073796 |
| 5 | 0.24200 | 0.071961 |
| 6 | 0.24285 | 0.070380 |
| 7 | 0.24370 | 0.068984 |
| 8 | 0.24455 | 0.067731 |
| 9 | 0.24540 | 0.066594 |
| 10 | 0.24609 | 0.065741 |
| 11 | 0.25639 | 0.054062 |
| 12 | 0.26670 | 0.043481 |
| 13 | 0.27700 | 0.033867 |
| 14 | 0.28731 | 0.025118 |
| 15 | 0.29762 | 0.017155 |
| 16 | 0.30792 | 0.0099103 |
| 17 | 0.31823 | 0.0033318 |
| 18 | 0.32853 | -0.0026254 |
| 19 | 0.33884 | -0.0079985 |
| 20 | 0.34914 | -0.012819 |
| 21 | 0.35945 | -0.017113 |
| 22 | 0.36975 | -0.020902 |
| 23 | 0.38006 | -0.024207 |
| 24 | 0.39036 | -0.027043 |
| 25 | 0.40067 | -0.029424 |
| 26 | 0.41098 | -0.031360 |
| 27 | 0.42128 | -0.032861 |
| 28 | 0.43159 | -0.033935 |
| 29 | 0.44189 | -0.034587 |
| 30 | 0.45220 | -0.034822 |
| 31 | 0.46250 | -0.034641 |
| 32 | 0.47281 | -0.034047 |
| 33 | 0.48311 | -0.033039 |
| 34 | 0.49342 | -0.031615 |
| 35 | 0.50372 | -0.029772 |
| 36 | 0.51403 | -0.027506 |
| 37 | 0.52434 | -0.024810 |
| 38 | 0.53464 | -0.021675 |
| 39 | 0.54495 | -0.018093 |
| 40 | 0.55525 | -0.014051 |
| 41 | 0.56556 | -0.0095350 |
| 42 | 0.57586 | -0.0045274 |
| 43 | 0.58617 | 0.00099160 |
| 44 | 0.59647 | 0.0070458 |
| 45 | 0.60678 | 0.013663 |
| 46 | 0.61708 | 0.020877 |
| 47 | 0.62739 | 0.028727 |
| 48 | 0.63770 | 0.037260 |
| 49 | 0.64800 | 0.046534 |
| 50 | 0.65831 | 0.056619 |
| 51 | 0.66861 | 0.067602 |
| 52 | 0.67892 | 0.079595 |
| 53 | 0.68922 | 0.092741 |
| 54 | 0.69953 | 0.10724 |
| 55 | 0.70983 | 0.12330 |
| 56 | 0.72014 | 0.14063 |
| 57 | 0.73044 | 0.15898 |
| 58 | 0.74075 | 0.17816 |
| 59 | 0.75098 | 0.19790 |
| 60 | 0.75858 | 0.21295 |
| 61 | 0.76618 | 0.22830 |
| 62 | 0.77378 | 0.24392 |
| 63 | 0.78138 | 0.25979 |
| 64 | 0.78898 | 0.27588 |
| 65 | 0.79658 | 0.29217 |
| 66 | 0.80418 | 0.30866 |
| 67 | 0.81178 | 0.32532 |
| 68 | 0.81938 | 0.34215 |
| 69 | 0.82698 | 0.35913 |
| 70 | 0.83458 | 0.37626 |
| 71 | 0.84218 | 0.39353 |
| 72 | 0.84978 | 0.41092 |
| 73 | 0.85738 | 0.42844 |
| 74 | 0.86498 | 0.44607 |
| 75 | 0.87258 | 0.46381 |
| 76 | 0.88018 | 0.48165 |
| 77 | 0.88778 | 0.49959 |
| 78 | 0.89530 | 0.51744 |
| 79 | 0.89564 | 0.51837 |
| 80 | 0.89588 | 0.51933 |
| 81 | 0.89603 | 0.52032 |
| 82 | 0.89608 | 0.52131 |
| 83 | 0.89565 | 0.52421 |
| 84 | 0.89440 | 0.52685 |
| 85 | 0.89244 | 0.52903 |
| 86 | 0.88993 | 0.53054 |
| 87 | 0.88708 | 0.53126 |
| 88 | 0.88413 | 0.53112 |
| 89 | 0.88133 | 0.53011 |
| 90 | 0.87892 | 0.52829 |
| 91 | 0.87709 | 0.52569 |
| 92 | 0.86506 | 0.50124 |
| 93 | 0.85295 | 0.47709 |
| 94 | 0.84083 | 0.45343 |
| 95 | 0.82872 | 0.43028 |
| 96 | 0.81661 | 0.40767 |
| 97 | 0.80449 | 0.38564 |
| 98 | 0.79238 | 0.36419 |
| 99 | 0.78027 | 0.34338 |
| 100 | 0.76815 | 0.32321 |
| 101 | 0.75604 | 0.30373 |
| 102 | 0.74393 | 0.28494 |
| 103 | 0.73181 | 0.26689 |
| 104 | 0.71970 | 0.24960 |

| | | |
|---|---|---|
| 105 | 0.70759 | 0.23308 |
| 106 | 0.69547 | 0.21736 |
| 107 | 0.68336 | 0.20245 |
| 108 | 0.67125 | 0.18837 |
| 109 | 0.65913 | 0.17513 |
| 110 | 0.64702 | 0.16274 |
| 111 | 0.63490 | 0.15119 |
| 112 | 0.62279 | 0.14051 |
| 113 | 0.61068 | 0.13067 |
| 114 | 0.59856 | 0.12168 |
| 115 | 0.58645 | 0.11352 |
| 116 | 0.57434 | 0.10618 |
| 117 | 0.56222 | 0.099647 |
| 118 | 0.55011 | 0.093900 |
| 119 | 0.53800 | 0.088917 |
| 120 | 0.52588 | 0.084676 |
| 121 | 0.51377 | 0.081152 |
| 122 | 0.50166 | 0.078319 |
| 123 | 0.48954 | 0.076149 |
| 124 | 0.47743 | 0.074617 |
| 125 | 0.46532 | 0.073693 |
| 126 | 0.45320 | 0.073351 |
| 127 | 0.44109 | 0.073563 |
| 128 | 0.42898 | 0.074301 |
| 129 | 0.41686 | 0.075540 |
| 130 | 0.40475 | 0.077254 |
| 131 | 0.39264 | 0.079418 |
| 132 | 0.38052 | 0.082008 |
| 133 | 0.36841 | 0.085002 |
| 134 | 0.35630 | 0.088377 |
| 135 | 0.34418 | 0.092112 |
| 136 | 0.33207 | 0.096189 |
| 137 | 0.31996 | 0.10059 |
| 138 | 0.30784 | 0.10529 |
| 139 | 0.29573 | 0.11028 |
| 140 | 0.28362 | 0.11554 |
| 141 | 0.28238 | 0.11607 |
| 142 | 0.28105 | 0.11656 |
| 143 | 0.27972 | 0.11698 |
| 144 | 0.27840 | 0.11735 |
| 145 | 0.27707 | 0.11765 |
| 146 | 0.27574 | 0.11789 |
| 147 | 0.27442 | 0.11808 |
| 148 | 0.27309 | 0.11821 |
| 149 | 0.27176 | 0.11829 |
| 150 | 0.27044 | 0.11831 |
| 151 | 0.26911 | 0.11828 |
| 152 | 0.26778 | 0.11819 |
| 153 | 0.26646 | 0.11804 |
| 154 | 0.26513 | 0.11784 |
| 155 | 0.26381 | 0.11758 |
| 156 | 0.26248 | 0.11726 |
| 157 | 0.26115 | 0.11688 |
| 158 | 0.25983 | 0.11644 |
| 159 | 0.25850 | 0.11593 |
| 160 | 0.25717 | 0.11536 |
| 161 | 0.25585 | 0.11471 |
| 162 | 0.25452 | 0.11398 |
| 163 | 0.25319 | 0.11316 |
| 164 | 0.25187 | 0.11225 |
| 165 | 0.25054 | 0.11124 |
| 166 | 0.24921 | 0.11011 |
| 167 | 0.24789 | 0.10885 |
| 168 | 0.24656 | 0.10743 |
| 169 | 0.24523 | 0.10582 |
| 170 | 0.24391 | 0.10396 |
| 171 | 0.24258 | 0.10177 |
| 172 | 0.24125 | 0.099068 |
| 173 | 0.23993 | 0.095429 |

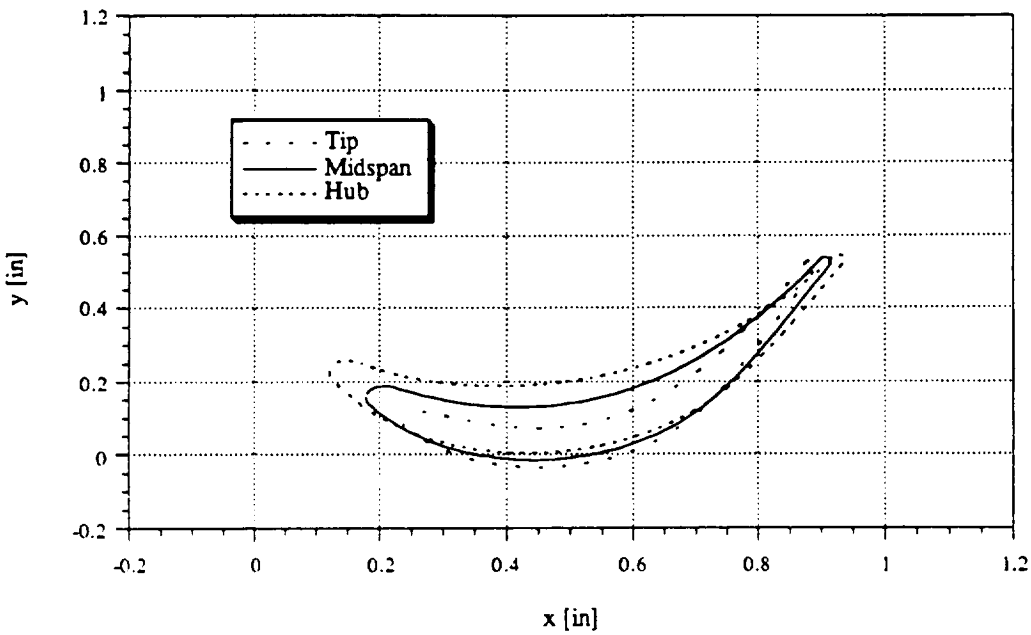


Figure A.1.2--First rotor: tip, midspan, hub.

### A.1.3 Second Nozzle Coordinates

Second nozzle, hub

| | x [in] | y[in] |
|---|---|---|
| 1 | 0.067200 | 0.71990 |
| 2 | 0.067500 | 0.71690 |
| 3 | 0.068000 | 0.71390 |
| 4 | 0.068700 | 0.71100 |
| 5 | 0.069500 | 0.70800 |
| 6 | 0.070600 | 0.70520 |
| 7 | 0.071800 | 0.70240 |
| 8 | 0.073100 | 0.69970 |
| 9 | 0.074700 | 0.69710 |
| 10 | 0.076400 | 0.69460 |
| 11 | 0.078300 | 0.69220 |
| 12 | 0.080300 | 0.68990 |
| 13 | 0.082400 | 0.68780 |
| 14 | 0.084700 | 0.68580 |
| 15 | 0.087100 | 0.68390 |
| 16 | 0.089600 | 0.68220 |
| 17 | 0.092200 | 0.68070 |
| 18 | 0.094900 | 0.67930 |
| 19 | 0.097700 | 0.67810 |
| 20 | 0.10060 | 0.67710 |
| 21 | 0.10350 | 0.67630 |
| 22 | 0.10650 | 0.67560 |
| 23 | 0.10950 | 0.67520 |
| 24 | 0.11250 | 0.67490 |
| 25 | 0.11550 | 0.67480 |
| 26 | 0.11850 | 0.67490 |
| 27 | 0.12150 | 0.67520 |
| 28 | 0.12450 | 0.67570 |
| 29 | 0.12750 | 0.67640 |
| 30 | 0.14540 | 0.68050 |
| 31 | 0.16330 | 0.68380 |
| 32 | 0.18120 | 0.68620 |
| 33 | 0.19900 | 0.68770 |
| 34 | 0.21690 | 0.68850 |
| 35 | 0.23480 | 0.68850 |
| 36 | 0.25270 | 0.68780 |
| 37 | 0.27060 | 0.68630 |
| 38 | 0.28850 | 0.68410 |
| 39 | 0.30640 | 0.68130 |
| 40 | 0.32430 | 0.67780 |
| 41 | 0.34220 | 0.67360 |
| 42 | 0.36000 | 0.66880 |
| 43 | 0.37790 | 0.66340 |
| 44 | 0.39580 | 0.65730 |
| 45 | 0.41370 | 0.65070 |
| 46 | 0.43160 | 0.64340 |
| 47 | 0.44950 | 0.63550 |
| 48 | 0.46740 | 0.62690 |
| 49 | 0.48530 | 0.61780 |
| 50 | 0.50310 | 0.60810 |
| 51 | 0.52100 | 0.59770 |
| 52 | 0.53890 | 0.58670 |
| 53 | 0.55680 | 0.57510 |
| 54 | 0.57470 | 0.56290 |
| 55 | 0.59260 | 0.55000 |
| 56 | 0.61050 | 0.53650 |
| 57 | 0.62840 | 0.52230 |
| 58 | 0.64630 | 0.50740 |
| 59 | 0.66410 | 0.49180 |
| 60 | 0.68200 | 0.47560 |
| 61 | 0.69990 | 0.45860 |
| 62 | 0.71780 | 0.44080 |
| 63 | 0.73570 | 0.42220 |
| 64 | 0.75360 | 0.40290 |
| 65 | 0.77150 | 0.38260 |
| 66 | 0.78940 | 0.36150 |
| 67 | 0.80730 | 0.33940 |
| 68 | 0.82510 | 0.31630 |
| 69 | 0.84300 | 0.29210 |
| 70 | 0.86090 | 0.26680 |
| 71 | 0.87880 | 0.24020 |
| 72 | 0.89670 | 0.21230 |
| 73 | 0.91460 | 0.18290 |
| 74 | 0.93250 | 0.15180 |
| 75 | 0.95040 | 0.11890 |
| 76 | 0.96830 | 0.083800 |
| 77 | 0.98610 | 0.046300 |
| 78 | 1.0039 | 0.0060000 |
| 79 | 1.0046 | 0.0048000 |
| 80 | 1.0054 | 0.0036000 |
| 81 | 1.0064 | 0.0026000 |
| 82 | 1.0075 | 0.0017000 |
| 83 | 1.0087 | 0.0010000 |
| 84 | 1.0101 | 0.00050000 |
| 85 | 1.0115 | 1.0000e-04 |
| 86 | 1.0129 | 0.0000 |
| 87 | 1.0143 | 1.0000e-04 |
| 88 | 1.0157 | 0.00040000 |
| 89 | 1.0170 | 0.00080000 |
| 90 | 1.0183 | 0.0015000 |
| 91 | 1.0194 | 0.0024000 |
| 92 | 1.0205 | 0.0034000 |
| 93 | 1.0213 | 0.0045000 |
| 94 | 1.0220 | 0.0057000 |
| 95 | 1.0225 | 0.0071000 |
| 96 | 1.0228 | 0.0085000 |
| 97 | 1.0229 | 0.0099000 |
| 98 | 1.0229 | 0.010300 |
| 99 | 1.0229 | 0.010600 |
| 100 | 1.0229 | 0.011000 |
| 101 | 1.0228 | 0.011400 |

| | | |
|---|---|---|
| 102 | 1.0227 | 0.011800 |
| 103 | 1.0227 | 0.012100 |
| 104 | 1.0226 | 0.012500 |
| 105 | 1.0225 | 0.012800 |
| 106 | 1.0223 | 0.013200 |
| 107 | 1.0047 | 0.062800 |
| 108 | 0.98700 | 0.11240 |
| 109 | 0.96930 | 0.16200 |
| 110 | 0.95160 | 0.21160 |
| 111 | 0.93400 | 0.26120 |
| 112 | 0.91630 | 0.31070 |
| 113 | 0.89860 | 0.36030 |
| 114 | 0.88090 | 0.40990 |
| 115 | 0.86320 | 0.45950 |
| 116 | 0.85820 | 0.47360 |
| 117 | 0.85300 | 0.48760 |
| 118 | 0.84790 | 0.50150 |
| 119 | 0.84280 | 0.51510 |
| 120 | 0.83760 | 0.52840 |
| 121 | 0.83250 | 0.54140 |
| 122 | 0.82730 | 0.55420 |
| 123 | 0.82220 | 0.56680 |
| 124 | 0.81700 | 0.57900 |
| 125 | 0.81190 | 0.59100 |
| 126 | 0.80670 | 0.60260 |
| 127 | 0.80160 | 0.61400 |
| 128 | 0.79640 | 0.62500 |
| 129 | 0.79130 | 0.63580 |
| 130 | 0.77680 | 0.66370 |
| 131 | 0.76210 | 0.68850 |
| 132 | 0.74750 | 0.71090 |
| 133 | 0.73290 | 0.73110 |
| 134 | 0.71830 | 0.74950 |
| 135 | 0.70360 | 0.76640 |
| 136 | 0.68900 | 0.78200 |
| 137 | 0.67440 | 0.79630 |
| 138 | 0.65980 | 0.80960 |
| 139 | 0.64520 | 0.82190 |
| 140 | 0.63050 | 0.83320 |
| 141 | 0.61590 | 0.84370 |
| 142 | 0.60130 | 0.85340 |
| 143 | 0.58670 | 0.86230 |
| 144 | 0.57210 | 0.87050 |
| 145 | 0.55740 | 0.87800 |
| 146 | 0.54280 | 0.88480 |
| 147 | 0.52820 | 0.89100 |
| 148 | 0.51360 | 0.89660 |
| 149 | 0.49900 | 0.90150 |
| 150 | 0.48430 | 0.90580 |
| 151 | 0.46970 | 0.90960 |
| 152 | 0.45510 | 0.91280 |
| 153 | 0.44050 | 0.91540 |
| 154 | 0.42580 | 0.91740 |
| 155 | 0.41120 | 0.91880 |
| 156 | 0.39660 | 0.91970 |
| 157 | 0.38200 | 0.92000 |
| 158 | 0.36740 | 0.91970 |
| 159 | 0.35270 | 0.91890 |
| 160 | 0.33810 | 0.91740 |
| 161 | 0.32350 | 0.91540 |
| 162 | 0.30890 | 0.91270 |
| 163 | 0.29430 | 0.90930 |
| 164 | 0.27960 | 0.90530 |
| 165 | 0.26500 | 0.90060 |
| 166 | 0.25040 | 0.89520 |
| 167 | 0.23580 | 0.88910 |
| 168 | 0.22110 | 0.88210 |
| 169 | 0.20650 | 0.87430 |
| 170 | 0.19190 | 0.86560 |
| 171 | 0.17730 | 0.85590 |
| 172 | 0.16270 | 0.84520 |
| 173 | 0.14800 | 0.83320 |
| 174 | 0.13340 | 0.82000 |
| 175 | 0.11880 | 0.80520 |
| 176 | 0.10420 | 0.78880 |
| 177 | 0.089600 | 0.77030 |
| 178 | 0.074900 | 0.74920 |
| 179 | 0.073300 | 0.74660 |
| 180 | 0.071900 | 0.74380 |
| 181 | 0.070700 | 0.74100 |
| 182 | 0.069600 | 0.73810 |
| 183 | 0.068700 | 0.73520 |
| 184 | 0.068000 | 0.73220 |
| 185 | 0.067500 | 0.72910 |
| 186 | 0.067200 | 0.72610 |
| 187 | 0.067100 | 0.72300 |

Second nozzle, midspan

| | x [in] | y[in] |
|---|---|---|
| 1 | 0.022600 | 0.81050 |
| 2 | 0.022900 | 0.80750 |
| 3 | 0.023300 | 0.80450 |
| 4 | 0.024000 | 0.80160 |
| 5 | 0.024800 | 0.79880 |
| 6 | 0.025800 | 0.79600 |
| 7 | 0.026900 | 0.79320 |
| 8 | 0.028300 | 0.79050 |
| 9 | 0.029800 | 0.78800 |
| 10 | 0.031400 | 0.78550 |
| 11 | 0.033200 | 0.78310 |
| 12 | 0.035200 | 0.78090 |
| 13 | 0.037300 | 0.77870 |
| 14 | 0.039500 | 0.77670 |
| 15 | 0.041800 | 0.77490 |
| 16 | 0.044200 | 0.77320 |
| 17 | 0.046800 | 0.77160 |
| 18 | 0.049400 | 0.77020 |
| 19 | 0.052100 | 0.76900 |
| 20 | 0.054800 | 0.76800 |
| 21 | 0.057700 | 0.76710 |
| 22 | 0.060500 | 0.76640 |
| 23 | 0.063400 | 0.76580 |
| 24 | 0.066300 | 0.76550 |
| 25 | 0.069300 | 0.76530 |
| 26 | 0.072200 | 0.76530 |
| 27 | 0.075100 | 0.76550 |
| 28 | 0.078000 | 0.76590 |
| 29 | 0.080900 | 0.76640 |
| 30 | 0.10060 | 0.77000 |
| 31 | 0.12040 | 0.77260 |
| 32 | 0.14010 | 0.77410 |
| 33 | 0.15990 | 0.77460 |
| 34 | 0.17960 | 0.77420 |
| 35 | 0.19940 | 0.77300 |
| 36 | 0.21910 | 0.77090 |
| 37 | 0.23890 | 0.76800 |
| 38 | 0.25860 | 0.76430 |
| 39 | 0.27840 | 0.75990 |
| 40 | 0.29820 | 0.75480 |
| 41 | 0.31790 | 0.74900 |
| 42 | 0.33770 | 0.74240 |
| 43 | 0.35740 | 0.73520 |
| 44 | 0.37720 | 0.72730 |
| 45 | 0.39690 | 0.71880 |
| 46 | 0.41670 | 0.70960 |
| 47 | 0.43640 | 0.69980 |
| 48 | 0.45620 | 0.68940 |
| 49 | 0.47590 | 0.67830 |
| 50 | 0.49570 | 0.66660 |
| 51 | 0.51540 | 0.65420 |
| 52 | 0.53520 | 0.64120 |
| 53 | 0.55490 | 0.62760 |
| 54 | 0.57470 | 0.61330 |
| 55 | 0.59450 | 0.59830 |
| 56 | 0.61420 | 0.58270 |
| 57 | 0.63400 | 0.56640 |
| 58 | 0.65370 | 0.54950 |
| 59 | 0.67350 | 0.53180 |
| 60 | 0.69320 | 0.51340 |
| 61 | 0.71300 | 0.49430 |
| 62 | 0.73270 | 0.47440 |
| 63 | 0.75250 | 0.45370 |
| 64 | 0.77220 | 0.43220 |
| 65 | 0.79200 | 0.40980 |
| 66 | 0.81170 | 0.38650 |
| 67 | 0.83150 | 0.36230 |
| 68 | 0.85120 | 0.33710 |
| 69 | 0.87100 | 0.31080 |
| 70 | 0.89080 | 0.28330 |
| 71 | 0.91050 | 0.25460 |
| 72 | 0.93030 | 0.22460 |
| 73 | 0.95000 | 0.19310 |
| 74 | 0.96980 | 0.15990 |
| 75 | 0.98950 | 0.12490 |
| 76 | 1.0093 | 0.087800 |
| 77 | 1.0290 | 0.048200 |
| 78 | 1.0487 | 0.0059000 |
| 79 | 1.0493 | 0.0046000 |
| 80 | 1.0501 | 0.0035000 |
| 81 | 1.0511 | 0.0025000 |
| 82 | 1.0522 | 0.0017000 |
| 83 | 1.0535 | 0.0010000 |
| 84 | 1.0548 | 0.00040000 |
| 85 | 1.0562 | 1.0000e-04 |
| 86 | 1.0576 | 0.0000 |
| 87 | 1.0590 | 1.0000e-04 |
| 88 | 1.0604 | 0.00040000 |
| 89 | 1.0617 | 0.00090000 |
| 90 | 1.0630 | 0.0015000 |
| 91 | 1.0641 | 0.0024000 |
| 92 | 1.0651 | 0.0034000 |
| 93 | 1.0660 | 0.0045000 |
| 94 | 1.0667 | 0.0057000 |
| 95 | 1.0672 | 0.0071000 |
| 96 | 1.0675 | 0.0085000 |
| 97 | 1.0676 | 0.0099000 |
| 98 | 1.0676 | 0.010300 |
| 99 | 1.0675 | 0.010700 |
| 100 | 1.0675 | 0.011100 |
| 101 | 1.0674 | 0.011500 |
| 102 | 1.0674 | 0.011900 |
| 103 | 1.0673 | 0.012400 |
| 104 | 1.0672 | 0.012800 |

| | | |
|---|---|---|
| 105 | 1.0670 | 0.013100 |
| 106 | 1.0669 | 0.013500 |
| 107 | 1.0476 | 0.062100 |
| 108 | 1.0282 | 0.11070 |
| 109 | 1.0089 | 0.15930 |
| 110 | 0.98960 | 0.20780 |
| 111 | 0.97030 | 0.25640 |
| 112 | 0.95100 | 0.30500 |
| 113 | 0.93170 | 0.35350 |
| 114 | 0.91240 | 0.40210 |
| 115 | 0.89310 | 0.45070 |
| 116 | 0.88750 | 0.46450 |
| 117 | 0.88190 | 0.47850 |
| 118 | 0.87630 | 0.49230 |
| 119 | 0.87070 | 0.50610 |
| 120 | 0.86510 | 0.51970 |
| 121 | 0.85940 | 0.53320 |
| 122 | 0.85380 | 0.54660 |
| 123 | 0.84820 | 0.55980 |
| 124 | 0.84260 | 0.57290 |
| 125 | 0.83690 | 0.58570 |
| 126 | 0.83130 | 0.59830 |
| 127 | 0.82570 | 0.61070 |
| 128 | 0.82010 | 0.62290 |
| 129 | 0.81440 | 0.63480 |
| 130 | 0.79860 | 0.66660 |
| 131 | 0.78260 | 0.69630 |
| 132 | 0.76660 | 0.72370 |
| 133 | 0.75060 | 0.74880 |
| 134 | 0.73470 | 0.77190 |
| 135 | 0.71870 | 0.79310 |
| 136 | 0.70270 | 0.81280 |
| 137 | 0.68670 | 0.83110 |
| 138 | 0.67080 | 0.84800 |
| 139 | 0.65480 | 0.86380 |
| 140 | 0.63880 | 0.87850 |
| 141 | 0.62280 | 0.89210 |
| 142 | 0.60690 | 0.90480 |
| 143 | 0.59090 | 0.91660 |
| 144 | 0.57490 | 0.92760 |
| 145 | 0.55890 | 0.93770 |
| 146 | 0.54300 | 0.94700 |
| 147 | 0.52700 | 0.95560 |
| 148 | 0.51100 | 0.96340 |
| 149 | 0.49510 | 0.97050 |
| 150 | 0.47910 | 0.97680 |
| 151 | 0.46310 | 0.98250 |
| 152 | 0.44710 | 0.98750 |
| 153 | 0.43120 | 0.99180 |
| 154 | 0.41520 | 0.99540 |
| 155 | 0.39920 | 0.99840 |
| 156 | 0.38320 | 1.0007 |
| 157 | 0.36730 | 1.0023 |
| 158 | 0.35130 | 1.0033 |
| 159 | 0.33530 | 1.0036 |
| 160 | 0.31930 | 1.0032 |
| 161 | 0.30340 | 1.0021 |
| 162 | 0.28740 | 1.0002 |
| 163 | 0.27140 | 0.99770 |
| 164 | 0.25540 | 0.99440 |
| 165 | 0.23950 | 0.99030 |
| 166 | 0.22350 | 0.98540 |
| 167 | 0.20750 | 0.97970 |
| 168 | 0.19150 | 0.97310 |
| 169 | 0.17560 | 0.96560 |
| 170 | 0.15960 | 0.95710 |
| 171 | 0.14360 | 0.94750 |
| 172 | 0.12760 | 0.93690 |
| 173 | 0.11170 | 0.92500 |
| 174 | 0.095700 | 0.91180 |
| 175 | 0.079700 | 0.89710 |
| 176 | 0.063700 | 0.88070 |
| 177 | 0.047800 | 0.86240 |
| 178 | 0.031800 | 0.84180 |
| 179 | 0.029900 | 0.83900 |
| 180 | 0.028200 | 0.83610 |
| 181 | 0.026700 | 0.83310 |
| 182 | 0.025400 | 0.82990 |
| 183 | 0.024400 | 0.82670 |
| 184 | 0.023500 | 0.82350 |
| 185 | 0.023000 | 0.82020 |
| 186 | 0.022600 | 0.81680 |
| 187 | 0.022500 | 0.81350 |

Second nozzle, tip

| | x [in] | y [in] |
|---|---|---|
| 1 | -0.022100 | 0.90100 |
| 2 | -0.021800 | 0.89810 |
| 3 | -0.021400 | 0.89520 |
| 4 | -0.020800 | 0.89230 |
| 5 | -0.020000 | 0.88950 |
| 6 | -0.019000 | 0.88670 |
| 7 | -0.017900 | 0.88400 |
| 8 | -0.016600 | 0.88140 |
| 9 | -0.015100 | 0.87880 |
| 10 | -0.013500 | 0.87640 |
| 11 | -0.011800 | 0.87400 |
| 12 | -0.0099000 | 0.87180 |
| 13 | -0.0079000 | 0.86970 |
| 14 | -0.0058000 | 0.86770 |
| 15 | -0.0035000 | 0.86580 |
| 16 | -0.0012000 | 0.86410 |
| 17 | 0.0013000 | 0.86260 |
| 18 | 0.0038000 | 0.86120 |
| 19 | 0.0064000 | 0.85990 |
| 20 | 0.0091000 | 0.85880 |
| 21 | 0.011800 | 0.85790 |
| 22 | 0.014600 | 0.85710 |
| 23 | 0.017400 | 0.85650 |
| 24 | 0.020200 | 0.85610 |
| 25 | 0.023000 | 0.85580 |
| 26 | 0.025900 | 0.85570 |
| 27 | 0.028700 | 0.85580 |
| 28 | 0.031500 | 0.85600 |
| 29 | 0.034200 | 0.85640 |
| 30 | 0.055900 | 0.85950 |
| 31 | 0.077500 | 0.86130 |
| 32 | 0.099100 | 0.86190 |
| 33 | 0.12070 | 0.86140 |
| 34 | 0.14230 | 0.85990 |
| 35 | 0.16390 | 0.85740 |
| 36 | 0.18560 | 0.85400 |
| 37 | 0.20720 | 0.84970 |
| 38 | 0.22880 | 0.84450 |
| 39 | 0.25040 | 0.83850 |
| 40 | 0.27200 | 0.83180 |
| 41 | 0.29370 | 0.82430 |
| 42 | 0.31530 | 0.81600 |
| 43 | 0.33690 | 0.80700 |
| 44 | 0.35850 | 0.79740 |
| 45 | 0.38010 | 0.78700 |
| 46 | 0.40170 | 0.77590 |
| 47 | 0.42340 | 0.76420 |
| 48 | 0.44500 | 0.75180 |
| 49 | 0.46660 | 0.73880 |
| 50 | 0.48820 | 0.72510 |
| 51 | 0.50980 | 0.71070 |
| 52 | 0.53150 | 0.69570 |
| 53 | 0.55310 | 0.68000 |
| 54 | 0.57470 | 0.66370 |
| 55 | 0.59630 | 0.64660 |
| 56 | 0.61790 | 0.62900 |
| 57 | 0.63950 | 0.61060 |
| 58 | 0.66120 | 0.59150 |
| 59 | 0.68280 | 0.57170 |
| 60 | 0.70440 | 0.55120 |
| 61 | 0.72600 | 0.53000 |
| 62 | 0.74760 | 0.50790 |
| 63 | 0.76930 | 0.48510 |
| 64 | 0.79090 | 0.46150 |
| 65 | 0.81250 | 0.43700 |
| 66 | 0.83410 | 0.41150 |
| 67 | 0.85570 | 0.38250 |
| 68 | 0.87730 | 0.35780 |
| 69 | 0.89900 | 0.32940 |
| 70 | 0.92060 | 0.29980 |
| 71 | 0.94220 | 0.26900 |
| 72 | 0.96380 | 0.23680 |
| 73 | 0.98540 | 0.20320 |
| 74 | 1.0071 | 0.16800 |
| 75 | 1.0287 | 0.13090 |
| 76 | 1.0503 | 0.091700 |
| 77 | 1.0719 | 0.050000 |
| 78 | 1.0934 | 0.0057000 |
| 79 | 1.0941 | 0.0045000 |
| 80 | 1.0949 | 0.0034000 |
| 81 | 1.0958 | 0.0025000 |
| 82 | 1.0970 | 0.0016000 |
| 83 | 1.0982 | 0.00090000 |
| 84 | 1.0995 | 0.00040000 |
| 85 | 1.1009 | 1.0000e-04 |
| 86 | 1.1023 | 0.0000 |
| 87 | 1.1037 | 1.0000e-04 |
| 88 | 1.1051 | 0.00040000 |
| 89 | 1.1064 | 0.00090000 |
| 90 | 1.1077 | 0.0015000 |
| 91 | 1.1088 | 0.0024000 |
| 92 | 1.1098 | 0.0034000 |
| 93 | 1.1107 | 0.0045000 |
| 94 | 1.1113 | 0.0058000 |
| 95 | 1.1118 | 0.0071000 |
| 96 | 1.1121 | 0.0085000 |
| 97 | 1.1122 | 0.0099000 |
| 98 | 1.1122 | 0.010300 |
| 99 | 1.1122 | 0.010800 |
| 100 | 1.1122 | 0.011200 |
| 101 | 1.1121 | 0.011700 |
| 102 | 1.1120 | 0.012100 |
| 103 | 1.1119 | 0.012600 |
| 104 | 1.1117 | 0.013000 |

| | | | | | |
|---|---|---|---|---|---|
| 105 | 1.1116 | 0.013400 | 147 | 0.52580 | 1.0201 |
| 106 | 1.1114 | 0.013900 | 148 | 0.50850 | 1.0302 |
| 107 | 1.0905 | 0.061400 | 149 | 0.49120 | 1.0394 |
| 108 | 1.0695 | 0.10900 | 150 | 0.47380 | 1.0478 |
| 109 | 1.0486 | 0.15650 | 151 | 0.45650 | 1.0554 |
| 110 | 1.0276 | 0.20410 | 152 | 0.43920 | 1.0622 |
| 111 | 1.0067 | 0.25170 | 153 | 0.42180 | 1.0682 |
| 112 | 0.98570 | 0.29920 | 154 | 0.40450 | 1.0735 |
| 113 | 0.96480 | 0.34680 | 155 | 0.38720 | 1.0780 |
| 114 | 0.94380 | 0.39430 | 156 | 0.36990 | 1.0817 |
| 115 | 0.92290 | 0.44190 | 157 | 0.35250 | 1.0847 |
| 116 | 0.91690 | 0.45550 | 158 | 0.33520 | 1.0869 |
| 117 | 0.91080 | 0.46940 | 159 | 0.31790 | 1.0883 |
| 118 | 0.90470 | 0.48320 | 160 | 0.30060 | 1.0889 |
| 119 | 0.89860 | 0.49720 | 161 | 0.28320 | 1.0888 |
| 120 | 0.89250 | 0.51110 | 162 | 0.26590 | 1.0878 |
| 121 | 0.88640 | 0.52500 | 163 | 0.24860 | 1.0860 |
| 122 | 0.88030 | 0.53900 | 164 | 0.23120 | 1.0834 |
| 123 | 0.87420 | 0.55300 | 165 | 0.21390 | 1.0799 |
| 124 | 0.86810 | 0.56690 | 166 | 0.19660 | 1.0756 |
| 125 | 0.86200 | 0.58060 | 167 | 0.17930 | 1.0703 |
| 126 | 0.85590 | 0.59420 | 168 | 0.16190 | 1.0641 |
| 127 | 0.84980 | 0.60760 | 169 | 0.14460 | 1.0568 |
| 128 | 0.84370 | 0.62080 | 170 | 0.12730 | 1.0486 |
| 129 | 0.83760 | 0.63380 | 171 | 0.11000 | 1.0392 |
| 130 | 0.82040 | 0.66970 | 172 | 0.092600 | 1.0286 |
| 131 | 0.80300 | 0.70410 | 173 | 0.075300 | 1.0168 |
| 132 | 0.78570 | 0.73660 | 174 | 0.058000 | 1.0036 |
| 133 | 0.76840 | 0.76660 | 175 | 0.040600 | 0.98890 |
| 134 | 0.75110 | 0.79430 | 176 | 0.023300 | 0.97260 |
| 135 | 0.73370 | 0.81990 | 177 | 0.0060000 | 0.95450 |
| 136 | 0.71640 | 0.84370 | 178 | -0.011300 | 0.93440 |
| 137 | 0.69910 | 0.86580 | 179 | -0.013600 | 0.93150 |
| 138 | 0.68170 | 0.88650 | 180 | -0.015500 | 0.92830 |
| 139 | 0.66440 | 0.90570 | 181 | -0.017300 | 0.92510 |
| 140 | 0.64710 | 0.92380 | 182 | -0.018800 | 0.92180 |
| 141 | 0.62980 | 0.94060 | 183 | -0.020000 | 0.91830 |
| 142 | 0.61240 | 0.95630 | 184 | -0.020900 | 0.91480 |
| 143 | 0.59510 | 0.97100 | 185 | -0.021600 | 0.91120 |
| 144 | 0.57780 | 0.98470 | 186 | -0.022000 | 0.90760 |
| 145 | 0.56050 | 0.99740 | 187 | -0.022200 | 0.90390 |
| 146 | 0.54310 | 1.0092 | | | |

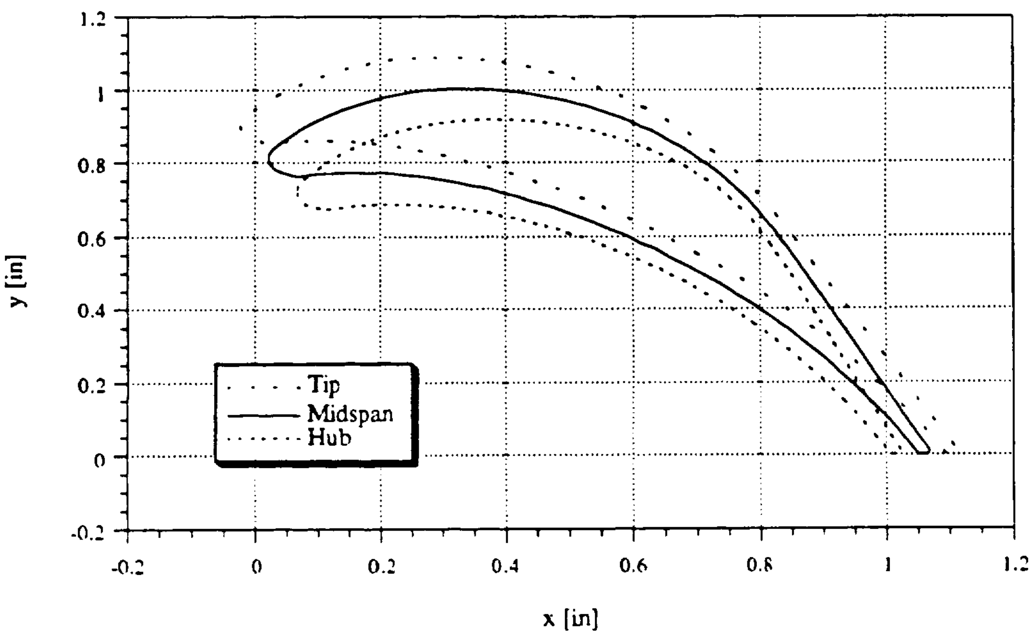


Figure A.1.3--Second nozzle, tip, midspan, hub.

A.3 Listing of Instrumentation Locations

| Position No. | Location | $\Sigma$ ₤/₤ | % Wetted Distance |
|---|---|---|---|
| 44 | Pressure, 90%, $S_T$ = 1.426 | 0.091 | 6.38 |
| 45 | Pressure, 90%, $S_T$ = 1.426 | 0.173 | 12.13 |
| 46 | Pressure, 90%, $S_T$ = 1.426 | 0.543 | 38.08 |
| 47 | Pressure, 90%, $S_T$ = 1.426 | 0.872 | 61.15 |
| 48 | Pressure, 90%, $S_T$ = 1.426 | 1.096 | 76.86 |
| | | | |
| 80 | Pressure, 50%, $S_T$ = 1.386 | 0 | 0 |
| 81 | Pressure, 50%, $S_T$ = 1.386 | 0.0385 | 2.78 |
| 49 | Pressure, 50%, $S_T$ = 1.386 | 0.070 | 5.05 |
| 82 | Pressure, 50%, $S_T$ = 1.386 | 0.123 | 8.87 |
| 50 | Pressure, 50%, $S_T$ = 1.386 | 0.125 | 9.02 |
| 83 | Pressure, 50%, $S_T$ = 1.386 | 0.173 | 12.48 |
| 84 | Pressure, 50%, $S_T$ = 1.386 | 0.244 | 17.61 |
| 85 | Pressure, 50%, $S_T$ = 1.386 | 0.3235 | 23.34 |
| 51 | Pressure, 50%, $S_T$ = 1.386 | 0.477 | 34.42 |
| 52 | Pressure, 50%, $S_T$ = 1.386 | 0.821 | 59.24 |
| 53 | Pressure, 50%, $S_T$ = 1.386 | 1.048 | 75.61 |
| 54 | Pressure, 50%, $S_T$ = 1.386 | 1.119 | 85.86 |
| | | | |
| 55 | Pressure, 23%, $S_T$ = 1.374 | 1.244 | 90.54 |
| | | | |
| 56 | Pressure, 10%, $S_T$ = 1.282 | 0.084 | 6.55 |
| 57 | Pressure, 10%, $S_T$ = 1.282 | 0.164 | 12.79 |
| 58 | Pressure, 10%, $S_T$ = 1.282 | 0.496 | 38.69 |
| 59 | Pressure, 10%, $S_T$ = 1.282 | 0.802 | 62.56 |
| 60 | Pressure, 10%, $S_T$ = 1.282 | 1.047 | 81.67 |
| 61 | Pressure, 10%, $S_T$ = 1.282 | 1.169 | 91.19 |

Table A.2.1--Heat flux instrumentation, first stage nozzle guide vane, pressure side.

| Position No. | Location | $\Sigma \pounds/\pounds$ | % Wetted Distance |
|---|---|---|---|
| 62 | Suction, 90%, $S_T$ = 1.726 | 0.095 | 5.50 |
| 63 | Suction, 90%, $S_T$ = 1.726 | 0.376 | 21.78 |
| 64 | Suction, 90%, $S_T$ = 1.726 | 0.809 | 46.87 |
| 65 | Suction, 90%, $S_T$ = 1.726 | 1.127 | 65.30 |
| 66 | Suction, 90%, $S_T$ = 1.726 | 1.435 | 83.20 |
| | | | |
| 80 | Suction, 50%, $S_T$ = 1.706 | 0.000 | 0 |
| 86 | Suction, 50%, $S_T$ = 1.706 | 0.0585 | 3.43 |
| 67 | Suction, 50%, $S_T$ = 1.706 | 0.060 | 3.52 |
| 87 | Suction, 50%, $S_T$ = 1.706 | 0.1385 | 8.12 |
| 88 | Suction, 50%, $S_T$ = 1.706 | 0.215 | 12.60 |
| 89 | Suction, 50%, $S_T$ = 1.706 | 0.285 | 16.71 |
| 90 | Suction, 50%, $S_T$ = 1.706 | 0.363 | 21.28 |
| 68 | Suction, 50%, $S_T$ = 1.706 | 0.381 | 22.33 |
| 69 | Suction, 50%, $S_T$ = 1.706 | 0.603 | 35.35 |
| 70 | Suction, 50%, $S_T$ = 1.706 | 0.857 | 50.23 |
| 71 | Suction, 50%, $S_T$ = 1.706 | 1.090 | 63.89 |
| 72 | Suction, 50%, $S_T$ = 1.706 | 1.385 | 81.18 |
| | | | |
| 73 | Suction, 31%, $S_T$ = 1.685 | 1.579 | 93.71 |
| | | | |
| 74 | Suction, 19%, $S_T$ = 1.609 | 1.489 | 92.54 |
| | | | |
| 75 | Suction, 10%, $S_T$ = 1.580 | 0.085 | 5.38 |
| 76 | Suction, 10%, $S_T$ = 1.580 | 0.367 | 23.23 |
| 77 | Suction, 10%, $S_T$ = 1.580 | 0.567 | 35.87 |
| 78 | Suction, 10%, $S_T$ = 1.580 | 1.177 | 74.49 |
| 79 | Suction, 10%, $S_T$ = 1.580 | 1.357 | 85.89 |

Table A.2.2--Heat flux instrumenatation, first stage nozzle guide vane, suction side.

| Position No. | Location | $\Sigma$ £/£ | % Wetted Distance |
|---|---|---|---|
| 33 | Tip, $S_T$ = 0.985 | 0.1665 | 16.9 |
| 34 | Tip, $S_T$ = 0.985 | 0.379 | 38.48 |
| 35 | Tip, $S_T$ = 0.985 | 0.563 | 57.16 |
| 36 | Tip, $S_T$ = 0.985 | 0.702 | 71.27 |
| | | | |
| 12 | Suction, 90%, $S_T$ = 1.101 | 0.075 | 6.81 |
| 13 | Suction, 90%, $S_T$ = 1.101 | 0.509 | 46.23 |
| 37 | Suction, 90%, $S_T$ = 1.101 | 0.632 | 57.40 |
| 38 | Suction, 90%, $S_T$ = 1.101 | 0.767 | 69.66 |
| 14 | Suction, 90%, $S_T$ = 1.101 | 0.900 | 81.74 |
| 39 | Suction, 90%, $S_T$ = 1.101 | 0.991 | 90.01 |
| | | | |
| 1 | Pressure, 90%, $S_T$ = 0.898 | 0.043 | 4.79 |
| 2 | Pressure, 90%, $S_T$ = 0.898 | 0.406 | 45.21 |
| 3 | Pressure, 90%, $S_T$ = 0.898 | 0.561 | 62.47 |
| | | | |
| 20 | Suction, 10%, $S_T$ = 1.232 | 0.090 | 7.31 |
| 21 | Suction, 10%, $S_T$ = 1.232 | 0.198 | 16.07 |
| 22 | Suction, 10%, $S_T$ = 1.232 | 0.636 | 51.62 |
| 23 | Suction, 10%, $S_T$ = 1.232 | 0.988 | 80.19 |
| | | | |
| 9 | Pressure, 10%, $S_T$ = 0.955 | 0.052 | 5.45 |
| 10 | Pressure, 10%, $S_T$ = 0.955 | 0.464 | 48.59 |
| 11 | Pressure, 10%, $S_T$ = 0.955 | 0.622 | 65.13 |

Table A.2.3a--Heat flux instrumentation, first stage rotor.

| Position No. | Location | $\Sigma$ £/£ | % Wetted Distance |
|---|---|---|---|
| 24 | Platform | 0.222 | 22.05 |
| 25 | Platform | 0.595 | 59.09 |
| | | | |
| 26 | Suction 50%, $S_T$ = 1.158 | 0 | 0 |
| 30 | Suction 50%, $S_T$ = 1.158 | 0.067 | 5.79 |
| 31 | Suction 50%, $S_T$ = 1.158 | 0.137 | 11.83 |
| 32 | Suction 50%, $S_T$ = 1.158 | 0.205 | 17.71 |
| 15 | Suction 50%, $S_T$ = 1.158 | 0.330 | 28.51 |
| 16 | Suction 50%, $S_T$ = 1.158 | 0.560 | 48.38 |
| 17 | Suction 50%, $S_T$ = 1.158 | 0.742 | 64.10 |
| 18 | Suction 50%, $S_T$ = 1.158 | 0.949 | 81.99 |
| 19 | Suction 50%, $S_T$ = 1.158 | 1.074 | 92.79 |
| | | | |
| 27 | Pressure, 50%, $S_T$ = 0.919 | 0.080 | 8.71 |
| 28 | Pressure, 50%, $S_T$ = 0.919 | 0.148 | 16.10 |
| 29 | Pressure, 50%, $S_T$ = 0.919 | 0.201 | 21.87 |
| 4 | Pressure, 50%, $S_T$ = 0.919 | 0.217 | 23.61 |
| 5 | Pressure, 50%, $S_T$ = 0.919 | 0.409 | 44.50 |
| 6 | Pressure, 50%, $S_T$ = 0.919 | 0.556 | 60.50 |
| 7 | Pressure, 50%, $S_T$ = 0.919 | 0.669 | 72.80 |
| 8 | Pressure, 50%, $S_T$ = 0.919 | 0.806 | 87.70 |

Table A.2.3b--Heat flux instrumentation, first stage rotor (cont'd).

| Position No. | Location | $\Sigma$ £/£ | % Wetted Distance |
|---|---|---|---|
| 91 | Pressure, 50%, $S_T = 1.392$ | 0.016 | 1.15 |
| 92 | Pressure, 50%, $S_T = 1.392$ | 0.101 | 7.26 |
| 93 | Pressure, 50%, $S_T = 1.392$ | 0.168 | 12.07 |
| 94 | Pressure, 50%, $S_T = 1.392$ | 0.514 | 36.93 |
| 95 | Pressure, 50%, $S_T = 1.392$ | 0.707 | 50.79 |
| 96 | Pressure, 50%, $S_T = 1.392$ | 0.855 | 61.42 |
| 97 | Pressure, 50%, $S_T = 1.392$ | 1.071 | 76.94 |
| | | | |
| 98 | Suction, 50%, $S_T = 1.729$ | 0.00 | 0 |
| 99 | Suction, 50%, $S_T = 1.729$ | 0.137 | 7.92 |
| 100 | Suction, 50%, $S_T = 1.729$ | 0.375 | 21.69 |
| 101 | Suction, 50%, $S_T = 1.729$ | 0.545 | 31.52 |
| 102 | Suction, 50%, $S_T = 1.729$ | 0.893 | 51.65 |
| 103 | Suction, 50%, $S_T = 1.729$ | 0.975 | 56.39 |
| 104 | Suction, 50%, $S_T = 1.729$ | 1.155 | 66.80 |
| 105 | Suction, 50%, $S_T = 1.729$ | 1.302 | 75.30 |
| 106 | Suction, 50%, $S_T = 1.729$ | 1.369 | 79.18 |
| 107 | Suction, 50%, $S_T = 1.729$ | 1.546 | 89.42 |

Table A.2.3c--Heat flux instrumentation, first stage rotor (cont'd).

| Position No. | Location | Σ £/£ | % Wetted Distance |
|---|---|---|---|
| P1 | Pressure, 90%, $S_T$ = 0.891 | 0.044 | 4.94 |
| P2 | Pressure, 90%, $S_T$ = 0.891 | 0.403 | 45.23 |
| P3 | Pressure, 90%, $S_T$ = 0.891 | 0.563 | 63.19 |
| | | | |
| P4 | Suction, 90%, $S_T$ = 1.125 | 0.068 | 6.00 |
| P5 | Suction, 90%, $S_T$ = 1.125 | 0.187 | 16.62 |
| P6 | Suction, 90%, $S_T$ = 1.125 | 0.875 | 77.78 |
| | | | |
| P7 | Pressure, 50%, $S_T$ = 0.921 | 0.040 | 4.34 |
| P8 | Pressure, 50%, $S_T$ = 0.921 | 0.125 | 13.57 |
| P9 | Pressure, 50%, $S_T$ = 0.921 | 0.402 | 43.65 |
| P10 | Pressure, 50%, $S_T$ = 0.921 | 0.670 | 72.75 |
| | | | |
| P11 | Suction, 50%, $S_T$ = 1.165 | 0.065 | 5.54 |
| P12 | Suction, 50%, $S_T$ = 1.165 | 0.141 | 12.06 |
| P13 | Suction, 50%, $S_T$ = 1.165 | 0.214 | 18.37 |
| P14 | Suction, 50%, $S_T$ = 1.165 | 0.296 | 25.41 |
| P15 | Suction, 50%, $S_T$ = 1.165 | 0.534 | 45.84 |
| P16 | Suction, 50%, $S_T$ = 1.165 | 0.702 | 60.26 |
| P17 | Suction, 50%, $S_T$ = 1.165 | 0.925 | 79.40 |
| | | | |

Table A.2.4a--Pressure Instrumentation, first stage rotor.

| | | | |
|---|---|---|---|
| P18 | Pressure, 10%, $S_T$ = 0.948 | 0.047 | 4.96 |
| P19 | Pressure, 10%, $S_T$ = 0.948 | 0.445 | 46.94 |
| P20 | Pressure, 10%, $S_T$ = 0.948 | 0.593 | 62.55 |
| | | | |
| P21 | Suction, 10%, $S_T$ = 1.215 | 0.083 | 6.83 |
| P22 | Suction, 10%, $S_T$ = 1.215 | 0.231 | 19.01 |
| P23 | Suction, 10%, $S_T$ = 1.215 | 0.594 | 48.89 |
| P24 | Suction, 10%, $S_T$ = 1.215 | 0.896 | 73.74 |

Table A.2.4b--Pressure Instrumentation, first stage rotor (cont'd).

| Position No. | Location | Σ £/£ | % Wetted Distance |
|---|---|---|---|
| P25 | Pressure, 90%, $S_T$ = 1.433 | 0.068 | 4.75 |
| P26 | Pressure, 90%, $S_T$ = 1.433 | 0.528 | 36.85 |
| P30 | Pressure, 90%, $S_T$ = 1.433 | 1.064 | 74.25 |
| | | | |
| P33 | Pressure, 50%, $S_T$ = 1.425 | 0.108 | 7.58 |
| P34 | Pressure, 50%, $S_T$ = 1.425 | 0.218 | 15.30 |
| P35 | Pressure, 50%, $S_T$ = 1.425 | 0.518 | 36.35 |
| P36 | Pressure, 50%, $S_T$ = 1.425 | 0.860 | 60.35 |
| P37 | Pressure, 50%, $S_T$ = 1.425 | 1.031 | 72.35 |
| | | | |
| P45 | Pressure, 10%, $S_T$ = 1.241 | 0.061 | 4.92 |
| P46 | Pressure, 10%, $S_T$ = 1.241 | 0.480 | 38.68 |
| P47 | Pressure, 10%, $S_T$ = 1.241 | 1.023 | 82.43 |

Table A.2.5a--Pressure Instrumentation, first stage vane.

| Position No. | Location | Σ £/£ | % Wetted Distance |
|---|---|---|---|
| P28 | Suction, 90%, $S_T$ = 1.662 | 0.100 | 6.02 |
| P29 | Suction, 90%, $S_T$ = 1.662 | 0.367 | 22.08 |
| P30 | Suction, 90%, $S_T$ = 1.662 | 0.775 | 46.63 |
| P31 | Suction, 90%, $S_T$ = 1.662 | 1.088 | 65.46 |
| P32 | Suction, 90%, $S_T$ = 1.662 | 1.359 | 81.77 |
| | | | |
| P38 | Suction, 50%, $S_T$ = 1.728 | 0.114 | 6.60 |
| P39 | Suction, 50%, $S_T$ = 1.728 | 0.252 | 14.58 |
| P40 | Suction, 50%, $S_T$ = 1.728 | 0.400 | 23.15 |
| P41 | Suction, 50%, $S_T$ = 1.728 | 0.592 | 34.26 |
| P42 | Suction, 50%, $S_T$ = 1.728 | 0.847 | 49.02 |
| P43 | Suction, 50%, $S_T$ = 1.728 | 1.108 | 64.12 |
| P44 | Suction, 50%, $S_T$ = 1.728 | 1.491 | 86.28 |
| | | | |
| P48 | Suction, 10%, $S_T$ = 1.568 | 0.091 | 5.80 |
| P49 | Suction, 10%, $S_T$ = 1.568 | 0.354 | 22.58 |
| P50 | Suction, 10%, $S_T$ = 1.568 | 0.563 | 35.91 |
| P51 | Suction, 10%, $S_T$ = 1.568 | 1.148 | 73.21 |
| P52 | Suction, 10%, $S_T$ = 1.568 | 1.333 | 85.01 |

Table A.2.5b--Pressure Instrumentation, first stage vane (cont'd).

| Position No. | Location |
|---|---|
| P53 | Hub wall, near midpassage, 0.062 aft of leading edge |
| P54 | Hub wall, 0.145 from suction surface, 0.062 aft of leading edge |
| P55 | Hub wall, 0.604 from leading edge, near pressure surface of vane #1 |
| | |
| P56 | Hub wall, 0.575 from leading edge, near pressure surface of vane #7 |
| | |
| P57 | Hub wall, 0.086 from trailing edge, near pressure surface of vane #7 (in region where vane trailing edge has been removed |

Table A.2.5c--Pressure Instrumentation, first stage vane (cont'd).

A.4 Listing of Data: Pressure and Stanton numbers

| % wetted distance | Run 5 | Run 6 | Run 7 | Run 8 | Run 11 | Run 12 | Run 13 |
|---|---|---|---|---|---|---|---|
| -82.4 | 0.88276 | 0.86732 | 0.90313 | 0.91504 | 0.90972 | 0.82652 | 0.79142 |
| -38.7 | 1.0000 | 1.0000 | 0.94244 | 0.96289 | 1.0049 | 1.0000 | 1.0000 |
| -4.9000 | 0.96158 | 0.92878 | 0.99996 | 1.0000 | 1.0000 | 0.95414 | 0.94347 |
| 5.8000 | 0.95961 | 0.93366 | 0.98175 | 0.99316 | 0.98234 | 0.93519 | 0.93470 |
| 22.600 | 0.91330 | 0.88780 | 0.93381 | 0.94922 | 0.93719 | 0.90828 | 0.89376 |
| 73.200 | 0.78621 | 0.77951 | 0.86190 | 0.87598 | 0.85672 | 0.74576 | 0.78070 |
| 85.000 | 0.77438 | 0.74829 | 0.77274 | 0.78320 | 0.79293 | 0.75972 | 0.77778 |

Table A.3.1--Pressure ratio distribution, first vane, 10% span. % wetted distances less than zero are on pressure surface, % wetted distances greater than zero are on suction surface.

| % wetted distance | Run 5 | Run 6 | Run 7 | Run 8 | Run 11 | Run 12 | Run 13 |
|---|---|---|---|---|---|---|---|
| -72.400 | 0.86831 | 0.83445 | 0.89595 | 0.89234 | 0.88943 | 0.85020 | 0.84981 |
| -60.400 | 0.85767 | 0.83254 | 0.85645 | 0.87585 | 0.87378 | 0.83929 | 0.83624 |
| -36.400 | 0.99996 | 1.0000 | 1.0000 | 1.0000 | 1.0000 | 1.0000 | 1.0000 |
| -15.300 | 0.99319 | 0.96172 | 0.98844 | 1.0000 | 0.99804 | 0.98611 | 0.99031 |
| -7.6000 | 0.95931 | 0.93971 | 0.94798 | 0.94277 | 0.94423 | | |
| 34.300 | | | | | | | |
| 64.100 | 0.77442 | 0.76364 | 0.75723 | 0.76431 | 0.77397 | 0.75099 | 0.78488 |
| 74.700 | 0.81410 | 0.85742 | 0.79094 | 0.80213 | 0.83659 | 0.79663 | 0.85659 |

Table A.3.2--Pressure ratio distribution, first vane, 50% span. % wetted distances less than zero are on pressure surface, % wetted distances greater than zero are on suction surface.

| % wetted distance | Run 5 | Run 6 | Run 7 | Run 8 | Run 11 | Run 12 | Run 13 |
|---|---|---|---|---|---|---|---|
| -36.800 | 1.0000 | 1.0000 | 0.99998 | 1.0000 | 1.0000 | | |
| -4.7000 | 0.89197 | 0.85129 | 0.93754 | 0.92958 | 0.91932 | 0.93100 | 0.83100 |
| 6.0000 | 0.86042 | 0.74738 | | 0.88826 | 0.87242 | 0.68900 | 0.70700 |
| 22.100 | 0.72753 | 0.72164 | 0.74183 | 0.73709 | 0.72889 | 0.74900 | 0.76500 |
| 46.600 | 0.62141 | 0.62726 | 0.60763 | 0.61502 | 0.62101 | 0.64200 | 0.68600 |
| 65.500 | 0.78967 | 0.78646 | 0.76420 | 0.76526 | 0.77205 | 0.77000 | |
| 81.800 | 0.97514 | 0.89609 | 0.99718 | 0.99624 | 0.98030 | | |

Table A.3.3--Pressure ratio distribution, first vane, 90% span. % wetted distances less than zero are on pressure surface, % wetted distances greater than zero are on suction surface.

| % wetted distance | Run 5 | Run 6 | Run 7 | Run 8 | Run 11 | Run 12 | Run 13 |
|---|---|---|---|---|---|---|---|
| -62.600 | 0.91500 | 0.89200 | 0.75936 | 0.82600 | 0.83500 | 0.79187 | 0.82190 |
| -46.900 | 0.91000 | 0.93600 | | 0.97700 | 0.95800 | 0.92170 | 0.90000 |
| -5.0000 | | | | | 0.97900 | 0.99823 | 0.99978 |
| 6.8000 | 0.98300 | 0.95300 | 1.00103 | 0.97000 | 0.96500 | 0.87711 | 0.90190 |
| 19.000 | 0.81900 | 0.82500 | 0.72097 | 0.78800 | 0.80000 | 0.74628 | 0.77429 |
| 48.900 | 0.81100 | 0.81200 | 0.77809 | 0.83600 | 0.83000 | 0.78989 | 0.77714 |

Table A.3.4--Pressure ratio distribution, first blade, 10% span. % wetted distances less than zero are on pressure surface, % wetted distances greater than zero are on suction surface.

| % wetted distance | Run 5 | Run 6 | Run 7 | Run 8 | Run 11 | Run 12 | Run 13 |
|---|---|---|---|---|---|---|---|
| -72.700 | 0.83400 | 0.88400 | 0.90100 | 0.89000 | 0.89900 | 0.86200 | 0.88500 |
| -13.600 | 0.83200 | 0.85100 | | 0.73400 | 0.76500 | 0.87200 | 0.79600 |
| 5.6000 | 0.72000 | 0.74000 | 0.70000 | 0.70200 | 0.71300 | | |
| 12.100 | 0.81800 | 0.82500 | 0.89800 | 0.90700 | 0.91800 | 0.81900 | 0.84500 |
| 18.400 | 0.76000 | 0.78500 | 0.71100 | 0.68100 | 0.67400 | 0.75200 | 0.70900 |
| 25.400 | 0.79600 | 0.81800 | 0.79200 | 0.79100 | 0.76800 | 0.80700 | 0.76300 |
| 45.800 | 0.78300 | 0.77900 | 0.79200 | 0.79100 | 0.79700 | 0.76700 | 0.77800 |
| 60.300 | 0.67200 | 0.70300 | 0.63200 | 0.68600 | 0.71700 | 0.69000 | 0.72200 |
| 79.400 | 0.79000 | 0.80800 | 0.77400 | 0.82000 | 0.82500 | 0.77600 | 0.79500 |

Table A.3.5--Pressure ratio distribution, first blade, 50% span. % wetted distances less than zero are on pressure surface, % wetted distances greater than zero are on suction surface.

| % wetted distance | Run 5 | Run 6 | Run 7 | Run 8 | Run 11 | Run 12 | Run 13 |
|---|---|---|---|---|---|---|---|
| -45.200 | 0.91200 | | | | | | |
| -4.9000 | 0.89400 | 0.86700 | 0.90700 | 0.88200 | 0.88500 | 0.87600 | 0.88100 |
| 6.0000 | 0.91700 | 0.96700 | 0.85700 | 0.87600 | 0.91100 | 0.84100 | 0.87900 |
| 16.600 | 0.80500 | 0.82300 | 0.77400 | 0.77500 | 0.79900 | 0.75700 | 0.78600 |
| 77.800 | 0.80300 | 0.79400 | 0.75200 | 0.78900 | 0.85300 | 0.72700 | 0.75400 |

Table A.3.6--Pressure ratio distribution, first blade, 90% span. % wetted distances less than zero are on pressure surface, % wetted distances greater than zero are on suction surface.

| % wetted distance | Run 1 | Run 5 | Run 6 | Run 7 | Run 8 | Run 11 | Run 12 | Run 13 |
|---|---|---|---|---|---|---|---|---|
| -91.190 | 0.013191 | 0.015026 | 0.015452 | 0.013966 | 0.014661 | 0.016170 | 0.015130 | 0.014617 |
| -81.670 | | | 0.022809 | 0.025479 | 0.025560 | 0.027150 | 0.023096 | 0.021765 |
| -62.560 | 0.0079545 | 0.0082174 | 0.0083739 | 0.0084706 | 0.0087706 | 0.0092800 | 0.0086087 | 0.0079565 |
| -38.690 | 0.0055909 | 0.0040957 | 0.0040435 | 0.0063529 | 0.0064862 | 0.0068700 | 0.0039043 | 0.0035913 |
| -12.790 | 0.0070364 | 0.0058348 | 0.0057652 | 0.0069832 | 0.0073486 | 0.0073000 | 0.0057043 | 0.0053565 |
| -6.5500 | 0.0088909 | 0.0070870 | 0.0070870 | 0.0079160 | 0.0082569 | 0.0082500 | 0.0072000 | 0.0068783 |
| 5.3800 | 0.0075000 | 0.0067043 | 0.0066957 | 0.0077983 | 0.0076147 | 0.0079500 | 0.0058870 | 0.0056783 |
| 23.230 | | | | | | | | |
| 35.870 | 0.010964 | 0.011009 | 0.010870 | 0.010866 | 0.010798 | 0.011440 | 0.010800 | 0.0093739 |
| 74.490 | 0.0060455 | 0.0056522 | 0.0058435 | 0.0052941 | 0.0050550 | 0.0051300 | 0.0058000 | 0.0056609 |
| 85.890 | 0.0063000 | 0.0058870 | 0.0059913 | 0.0056050 | 0.0055229 | 0.0056800 | 0.0060609 | 0.0057565 |

Table A.3.7--Stanton number distribution, first vane, 10% span. % wetted distances less than zero are on pressure surface, % wetted distances greater than zero are on suction surface.

| % wetted distance | Run 1 | Run 5 | Run 6 | Run 7 | Run 8 | Run 11 | Run 12 | Run 13 |
|---|---|---|---|---|---|---|---|---|
| -75.610 | 0.010036 | 0.010365 | 0.010522 | 0.0096639 | 0.010037 | 0.010320 | 0.010200 | 0.010252 |
| -59.240 | 0.0095000 | 0.0088522 | 0.0091304 | 0.0093697 | 0.0096789 | 0.010020 | 0.0090087 | 0.0088348 |
| -34.420 | 0.0061182 | 0.0050174 | 0.0054000 | 0.0054622 | 0.0059725 | 0.0063300 | 0.0049304 | 0.0044348 |
| -23.020 | | 0.0032087 | 0.0032696 | 0.0052941 | 0.0056239 | 0.0057500 | 0.0035304 | 0.0035826 |
| -17.360 | | 0.0036522 | 0.0038609 | 0.0055210 | 0.0058073 | 0.0061600 | 0.0039478 | 0.0039304 |
| -12.300 | 0.0054545 | 0.0041652 | 0.0041565 | 0.0056555 | 0.0058624 | 0.0063000 | 0.0042957 | 0.0042696 |
| -9.0200 | 0.0081182 | 0.0078870 | 0.0076696 | 0.0076975 | 0.0080092 | 0.0081100 | 0.0068870 | 0.0063130 |
| -8.7500 | 0.0054636 | 0.0047478 | 0.0047391 | 0.0050420 | 0.0059174 | 0.0063300 | 0.0048174 | 0.0048348 |
| -5.0500 | 0.0099091 | 0.0067565 | 0.0068870 | 0.0086555 | 0.0085780 | 0.0089400 | 0.0068087 | 0.0064261 |
| -2.7400 | 0.0076636 | 0.0099739 | 0.0098783 | 0.0097647 | 0.010385 | 0.010960 | 0.010078 | 0.0100000 |
| 0.0000 | | 0.014504 | 0.014522 | | | | | |
| 3.4100 | 0.0086273 | 0.0097826 | 0.0097652 | 0.0092773 | 0.010780 | 0.0091400 | 0.010217 | 0.010191 |
| 3.5200 | 0.0092818 | 0.0091391 | 0.0092087 | 0.0090336 | 0.0092661 | | 0.0093739 | 0.0087826 |
| 8.0700 | 0.0057818 | 0.0057913 | 0.0057043 | 0.0058235 | 0.0068440 | 0.0065700 | 0.0059217 | 0.0059217 |
| 12.520 | 0.0053909 | 0.0042870 | 0.0042435 | 0.0055462 | 0.0060826 | 0.0063300 | 0.0043913 | 0.0043652 |
| 16.600 | | 0.0036522 | 0.0041130 | 0.0067143 | 0.0070917 | 0.0075300 | 0.0043130 | 0.0042696 |
| 22.330 | 0.010345 | 0.0070435 | 0.0068348 | 0.010151 | 0.010275 | 0.010620 | 0.0077913 | |
| 35.350 | 0.0084727 | 0.0070435 | 0.0072348 | 0.0082941 | 0.0089633 | 0.0089500 | 0.0075304 | 0.0068174 |
| 50.230 | 0.0088273 | 0.0096000 | 0.0098174 | 0.0082017 | 0.0087156 | 0.0088200 | 0.0098435 | 0.0097217 |
| 63.890 | 0.0080727 | 0.0085217 | 0.0086696 | 0.0076134 | 0.0082018 | 0.0083600 | 0.0089565 | 0.0088696 |
| 81.180 | 0.0078091 | 0.0084609 | 0.0086957 | 0.0074538 | 0.0080459 | 0.0083100 | 0.0087826 | 0.0086609 |

Table A.3.8--Stanton number distribution, first vane, 50% span. % wetted distances less than zero are on pressure surface, % wetted distances greater than zero are on suction surface.

| % wetted distance | Run 1 | Run 5 | Run 6 | Run 7 | Run 8 | Run 11 | Run 12 | Run 13 |
|---|---|---|---|---|---|---|---|---|
| -76.860 | 0.0081364 | 0.0082087 | 0.0084957 | 0.0093277 | 0.0088991 | 0.0080100 | 0.0085739 | 0.0085130 |
| -61.150 | 0.0092545 | 0.0086435 | 0.0088783 | 0.0094958 | 0.010303 | 0.0083200 | 0.0096435 | 0.0089652 |
| -38.080 | 0.0070545 | 0.0056087 | 0.0058696 | 0.0073445 | 0.0071101 | 0.0063900 | 0.0061913 | 0.0060435 |
| -12.130 | 0.0076909 | 0.0048870 | 0.0039304 | 0.0056723 | 0.0059083 | 0.0055500 | 0.0055304 | 0.0050435 |
| -6.3800 | 0.010009 | 0.0055565 | 0.0058174 | 0.0075882 | 0.0081284 | 0.0077900 | 0.0075391 | 0.0059217 |
| 5.5000 | 0.0090727 | 0.0075826 | 0.0081478 | 0.0091933 | 0.0098440 | 0.010710 | 0.0080783 | 0.0078783 |
| 21.780 | | 0.0079565 | 0.0081217 | 0.0096975 | 0.010009 | 0.010340 | 0.0092261 | 0.0085043 |
| 46.870 | 0.0060000 | 0.0062087 | 0.0062696 | 0.0054706 | 0.0054954 | 0.0061600 | 0.0061565 | 0.0059391 |
| 65.300 | 0.0054545 | 0.0046522 | 0.0048696 | 0.0048487 | 0.0049817 | 0.0074000 | 0.0048609 | 0.0030174 |
| 83.200 | 0.0073909 | 0.0062522 | 0.0061739 | 0.0063361 | 0.0070367 | 0.0079000 | 0.0073739 | 0.0044522 |

Table A.3.9--Stanton number distribution, first vane, 90% span. % wetted distances less than zero are on pressure surface, % wetted distances greater than zero are on suction surface.

| % wetted distance | Run 1 | Run 5 | Run 6 | Run 7 | Run 8 | Run 11 | Run 12 | Run 13 |
|---|---|---|---|---|---|---|---|---|
| -65.130 | 0.0071273 | 0.0068261 | 0.0071739 | 0.0091597 | 0.011275 | 0.0069300 | 0.0069652 | 0.0067391 |
| -48.590 | 0.0066455 | 0.0060522 | 0.0065913 | 0.0067815 | 0.0071376 | 0.0066600 | 0.0063304 | 0.0058870 |
| -5.4500 | 0.010309 | 0.0089739 | 0.0098870 | 0.010588 | 0.011028 | 0.0090900 | 0.0099913 | 0.0089826 |
| 7.3100 | 0.010482 | 0.0053304 | 0.0046870 | 0.0035882 | 0.0044128 | 0.0048500 | 0.0041304 | 0.0036696 |
| 16.070 | 0.0074091 | 0.0050870 | 0.0046000 | 0.0035714 | 0.0047431 | 0.0047400 | 0.0052783 | 0.0051739 |
| 51.620 | | 0.0065652 | 0.0064348 | 0.0072353 | 0.0077064 | 0.0070000 | 0.0065913 | 0.0064261 |
| 80.170 | 0.0068727 | 0.0069391 | 0.0063130 | 0.0066387 | 0.0067982 | 0.0060300 | 0.0069478 | 0.0067043 |

Table A.3.10--Stanton number distribution, first blade, 10% span. % wetted distances less than zero are on pressure surface, % wetted distances greater than zero are on suction surface.

| % wetted distance | Run 1 | Run 5 | Run 6 | Run 7 | Run 8 | Run 11 | Run 12 | Run 13 |
|---|---|---|---|---|---|---|---|---|
| -87.700 | 0.0076000 | 0.0077739 | 0.0079739 | 0.0081008 | 0.0087431 | 0.0078200 | 0.0080957 | 0.0079652 |
| -72.800 | 0.0075455 | 0.0068348 | 0.0070087 | 0.0071513 | 0.0076514 | 0.0067000 | 0.0070435 | 0.0067652 |
| -60.500 | 0.0070455 | 0.0066174 | 0.0066348 | 0.0071092 | 0.0076697 | 0.0068300 | 0.0067043 | 0.0065217 |
| -44.500 | 0.0056727 | 0.0052522 | 0.0051652 | 0.0056471 | 0.0058440 | 0.0051700 | 0.0052783 | 0.0051391 |
| -23.610 | 0.0059000 | 0.0055478 | 0.0058609 | 0.0059580 | 0.0058899 | 0.0053900 | 0.0058087 | 0.0055217 |
| -21.870 | 0.0060364 | 0.0053217 | 0.0055043 | 0.0059832 | 0.0062202 | 0.0057100 | 0.0054261 | 0.0054261 |
| -20.200 | 0.0064182 | 0.0056435 | 0.0057043 | 0.0057059 | 0.0061284 | 0.0054600 | 0.0057652 | 0.0058957 |
| -16.100 | 0.0062182 | 0.0051826 | 0.0059304 | 0.0061345 | 0.0064679 | 0.0062100 | 0.0053739 | 0.0055391 |
| -12.300 | 0.0087909 | 0.0048000 | 0.0052087 | | | | 0.0080348 | 0.0045739 |
| -8.7100 | 0.0065909 | 0.0051217 | 0.0050522 | 0.0055378 | 0.0058349 | 0.0056100 | 0.0053043 | 0.0050609 |
| 0.0000 | 0.015782 | 0.016539 | 0.016365 | 0.014429 | 0.015321 | 0.013980 | 0.016800 | 0.016478 |
| 5.7000 | 0.0061545 | 0.0053565 | 0.0053739 | 0.0070420 | 0.0084954 | 0.0073300 | 0.0069217 | 0.0060957 |
| 11.830 | 0.010255 | 0.0037478 | 0.0028522 | 0.0040504 | 0.0049541 | 0.0055900 | 0.0060348 | 0.0059652 |
| 15.000 | 0.0080182 | | | | | | | |
| 17.710 | 0.0080364 | 0.0065130 | 0.0057478 | 0.0065378 | 0.0072936 | 0.0072700 | 0.0088870 | 0.0088870 |
| 24.200 | 0.0065455 | | | | | | | |
| 28.510 | 0.0054636 | 0.0078957 | 0.0080522 | 0.0073109 | 0.0074587 | 0.0071800 | 0.0078174 | 0.0076609 |
| 48.380 | 0.0087273 | 0.0072957 | 0.0072870 | 0.0066471 | 0.0071009 | 0.0066600 | 0.0072522 | 0.0070870 |
| 64.100 | 0.0062182 | 0.0056435 | 0.0056609 | 0.0052689 | 0.0056422 | 0.0052900 | 0.0058870 | 0.0057652 |
| 81.990 | 0.0054091 | 0.0049130 | 0.0050522 | 0.0045882 | 0.0048624 | 0.0044600 | 0.0052000 | 0.0049826 |
| 92.790 | 0.0053273 | 0.0047652 | 0.0048348 | 0.0045546 | 0.0047431 | 0.0044500 | 0.0050870 | 0.0048261 |

Table A.3.11--Stanton number distribution, first blade, 50% span. % wetted distances less than zero are on pressure surface, % wetted distances greater than zero are on suction surface.

| % wetted distance | Run 1 | Run 5 | Run 6 | Run 7 | Run 8 | Run 11 | Run 12 | Run 13 |
|---|---|---|---|---|---|---|---|---|
| -62.470 | 0.0073455 | 0.0066696 | 0.0065217 | 0.0070084 | 0.0075413 | 0.0062500 | 0.0066348 | 0.0064087 |
| -40.420 | | 0.0053913 | 0.0054174 | 0.0055294 | 0.0058165 | 0.0050300 | 0.0054522 | 0.0054087 |
| -4.7900 | 0.0099545 | 0.0086522 | 0.0085391 | | 0.0085505 | 0.0074300 | 0.0086174 | 0.0084783 |
| 6.8100 | 0.0077818 | 0.0093478 | 0.0090609 | 0.0098151 | 0.010606 | 0.0085800 | 0.0083391 | 0.0079826 |
| 46.230 | 0.0084364 | 0.0080087 | 0.0077391 | 0.0082017 | 0.0086147 | 0.0070200 | 0.0080348 | 0.0076000 |
| 57.400 | 0.0074545 | | | | | | | |
| 69.660 | 0.010464 | | | | | | | |
| 81.740 | 0.0088545 | 0.0098783 | 0.0098783 | 0.0094118 | 0.0099358 | 0.0088400 | 0.010017 | 0.0098609 |
| 90.010 | 0.0079000 | 0.0080696 | 0.0081913 | 0.0076891 | 0.0081743 | 0.0071200 | 0.0085391 | 0.0081913 |

Table A.3.12--Stanton number distribution, first blade, 90% span. % wetted distances less than zero are on pressure surface, % wetted distances greater than zero are on suction surface.

| % wetted distance | Run 1 | Run 5 | Run 6 | Run 7 | Run 8 | Run 11 | Run 12 | Run 13 |
|---|---|---|---|---|---|---|---|---|
| -76.940 | 0.0056091 | 0.0046087 | 0.0047217 | 0.0049580 | 0.0052385 | 0.0055100 | 0.0046348 | 0.0046870 |
| -61.420 | 0.0061000 | 0.0054087 | 0.0056000 | 0.0059412 | 0.0061101 | 0.0065100 | 0.0056696 | 0.0056435 |
| -50.790 | 0.0055455 | 0.0046348 | 0.0044783 | 0.0052941 | 0.0056239 | 0.0061200 | 0.0048348 | 0.0048783 |
| -36.930 | 0.0048364 | 0.0042783 | 0.0038435 | 0.0047899 | 0.0049450 | 0.0051600 | 0.0042348 | 0.0041043 |
| -12.070 | 0.0055818 | 0.0046435 | 0.0047130 | 0.0050336 | 0.0051376 | 0.0051600 | 0.0049826 | 0.0045130 |
| -7.2600 | 0.0068636 | 0.0055130 | 0.0054696 | 0.0058403 | 0.0060000 | 0.0059800 | 0.0057391 | 0.0053130 |
| -1.1500 | 0.011309 | 0.0084000 | 0.0080000 | 0.0081597 | 0.0079083 | 0.0081300 | 0.0091739 | 0.0082435 |
| 0.0000 | 0.013000 | 0.0082348 | 0.0082522 | 0.0088319 | 0.0085596 | 0.0088900 | 0.0095217 | 0.0091130 |
| 7.9200 | 0.0097091 | 0.0063304 | 0.0062087 | 0.0068571 | 0.0074037 | 0.0075400 | 0.0065391 | 0.0063130 |
| 21.690 | 0.0048545 | 0.0053391 | 0.0053043 | 0.0049664 | 0.0052018 | 0.0055200 | 0.0053652 | 0.0051478 |
| 31.520 | 0.0036545 | 0.0039391 | 0.0040609 | 0.0044790 | 0.0047339 | 0.0049700 | 0.0039043 | 0.0037739 |
| 51.650 | 0.0055000 | 0.0054522 | 0.0057739 | 0.0055210 | 0.0056697 | 0.0060200 | 0.0055130 | 0.0052783 |
| 56.390 | 0.0039909 | 0.0038261 | 0.0037913 | 0.0040588 | 0.0043028 | 0.0045000 | 0.0037478 | 0.0038696 |
| 66.800 | 0.0033273 | 0.0033565 | 0.0034174 | 0.0032605 | 0.0034404 | 0.0036200 | 0.0033826 | 0.0033913 |
| 75.300 | 0.0039636 | 0.0037913 | 0.0038087 | 0.0039412 | 0.0041560 | 0.0043200 | 0.0037130 | 0.0037478 |
| 79.180 | 0.0046273 | 0.0047826 | 0.0047739 | 0.0045966 | 0.0047890 | 0.0050400 | 0.0046348 | 0.0043478 |
| 89.420 | 0.0044818 | 0.0046261 | 0.0047043 | 0.0040000 | 0.0041193 | 0.0044700 | 0.0042348 | 0.0041304 |

Table A.3.13--Stanton number distribution, second vane, 50% span. % wetted distances less than zero are on pressure surface, % wetted distances greater than zero are on suction surface.

# PART II: PHASE-RESOLVED SURFACE-PRESSURE AND HEAT-FLUX MEASUREMENTS ON THE FIRST-STAGE VANE AND BLADE OF THE SSME FUEL-SIDE TURBINE

by

M.G. Dunn and C.W. Haldeman
Calspan-UB Research Center
Buffalo, New York 14225

CUBRC Final Report No. 640 II

Prepared for:

NASA Lewis Research Center
21000 Brookpark Rd.
Cleveland, OH 44135

May 1994

# ABSTRACT

Time-averaged surface pressure and heat-flux distributions have been measured for the first-stage vane, the first-stage blade, and the second-stage vane of the SSME fuel-side turbine. The previously obtained time averaged results are presented in Part I of this report. Part II will concentrate on the recent phase-resolved surface pressure, phase-resolved heat-flux, and unsteady pressure and unsteady heat-flux loading measurements for the first-stage blade row. Measurements were made at 10%, 50%, and 90% span on both the pressure and suction surfaces of the blade. For the results described herein, five separate experiments were performed at a single operating condition: turbine inlet total pressure of 345.6 kPa (50.5 psia), turbine inlet total temperature of 513 K (923 R ), turbine corrected speed of 101%, and a total-to-total stage pressure ratio of 1.41.

A shock tube is used as a short-duration source of heated and pressurized air to which the turbine is subjected. Miniature silicone-diaphragm pressure transducers are used to obtain the pressure measurements and platinum thin-film gauges are used to obtain the heat-flux measurements. The measured unsteady pressure envelope is compared to the results of two separate prediction techniques: (a) a Rocketdyne (turbine manufacturer) prediction and (b) a NASA Lewis prediction.

## ACKNOWLEDGMENTS

This research was supported under Grant NAG3-581 and monitored by Dr. Raymond Gaugler and Mr. Kas Civinskas of the NASA Lewis Research Center, Cleveland, Ohio. The authors would like to extend our appreciation to Tony Eastland, of the Rocketdyne Division of Rockwell International, and to Eric McFarland, of the NASA Lewis Research Center, for providing us with the unsteady pressure-envelope predictions. This work would not have been possible without the contributions of the many Calspan engineers and technicians, especially John R. Mosselle, Jeffrey L. Barton, and Robert M. Field.

## TABLE OF CONTENTS

## LIST OF FIGURES

# LIST OF TABLES

# SECTION 1
# INTRODUCTION

The time-averaged surface-pressure and heat-flux results for this turbine were previously presented by Dunn, Kim, Civinskas, and Boyle, 1992 and are described in detail in Part I of the final report for Grant NAG3-581. The results reported in Part II represent a data set that is in addition to the one reported in Part I. This report includes an updated time-averaged surface-pressure data set for the first blade. However, because the time-averaged heat-flux results obtaind for these measurements were nearly identical to those reported earlier, they will not be presented again. The intent of this measurement program was to obtain the unsteady heat-flux loading and to significantly improve the accuracy of the surface-pressure measurements in order to be able to obtain phase-resolved (unsteady) surface-pressure data on the first blade. The second blade row was not instrumented. Because there is a small pressure change across each vane or blade row for this particular turbine, careful calibration of the pressure transducers was an important issue in this measurement program. As will be demonstrated, the transducer calibration accuracy for this set of experiments is very good.

The flow and heat transfer that occur in a turbine stage represent one of the most complicated environments seen in any practical machine: the flow is always unsteady, can be transonic, is generally three-dimensional, and is subjected to strong body forces. Despite these problems, satisfactory designs have been achieved over the years due to advances in materials and manufacturing processes, as well as to the development of a sound analytical understanding of the flow and heat-transfer mechanics that define performance. These analytical developments were made possible by a series of approximations, in which the level of detail retained in the modeling was sufficient to reveal important physical effects, while still allowing solutions to be found by available analytical/numerical methods.

The major milestones in the development of these methods have been the approximations that flow through each blade row is steady in coordinates fixed to the blades, that three-dimensionally can be handled by treating a series of two-dimensional flows in hub-to-shroud and blade-to-blade surfaces, and that the effects of viscosity can be estimated by non-interacting boundary-layer calculations and by loss models to account for secondary flow.

During the past several years, there has been significant progress made in development of analytical methods to describe the unsteady flow existing in a compressor or turbine stage. Calibration of these analytical methods so that models describing the fluid dynamics can be developed is dependent upon having a representative experimental data base.

The unsteady internal flow of a gas turbine has been the subject of several experimental and analytical investigations during the time that the associated analytical methods were being developed. The problem is obviously a very difficult one to solve requiring significant interaction between the experimental and analytical communities. Just as there are many different analytical tools that can be used to attack this problem, there are also many different experimental facilities. The method of attacking the problem from an experimental viewpoint is subdivided by those groups using full-scale engine-like hardware and those groups simulating the physics by some other means. The facilities that can accommodate engine-like hardware can be further divided into two classes; (1) long duration, incompressible flow facilities or (2) short duration, compressible flow facilities. Examples of long-duration facilities are; (a) the large low speed rig at United Technologies Research Center (UTRC) in which some of the pioneering rotor/stator interaction research (referenced below) was performed, and (b) the more recent blow-down facility at Marshall Space Flight Center (MSFC). Examples of short-duration (those with run times less than a second or two) facilities in approximate ascending order of test time are; (c) the shock-tunnel facilities at Calspan, (d) the isentropic light-piston compression tube at Oxford, (e) the isentropic light-piston compression tube at VKI, (f) the blow-down facility at MIT, (g) the large isentropic light-piston compression tube at Pyestock, and (h) the large blow-down facility at Wright-Patterson Air Force Base.

Test time and turbine hardware alone are not the important parameters on which to make a decision regarding choice of facility for a measurement program. Each of these experimental facilities has associated with it a suite of instrumentation, instrument calibration technique, and other capabilities that may or may not be applicable to and/or available at other facilities. The choice of which facility and instrumentation package is most appropriate depends upon the particular application and must be made by the user.

The UTRC low speed rotating rig has been utilized to obtain unsteady pressure and heat transfer data as reported by Dring, Blair, and Joslyn, 1980; Dring and Joslyn, 1981; and Dring, Joslyn, Hardin, and Wagner, 1982; and Blair, Dring, and Joslyn, 1988. The facility at MSFC has been used to obtain performance measurements for the SSME turbine stage (a machine essentially the same as the one used for the experiments reported in this paper) as reported by Hudson, Gaddis, Johnson, and Boynton, 1991. Additional information regarding this facility can be found in Bordelon, Kauffman, and Heaman, 1993.

The short-duration shock-tunnel facilities at Calspan have been used for several previous measurement programs to obtain time-resolved heat-flux or surface-pressure data on the blade of a high-pressure turbine at high rotational speed, but for different turbine stages, e.g., Dunn, et al. 1986; Dunn, et al., 1988; Dunn, 1989; Dunn, Bennett, Delaney, and Rao, 1990. This last reference concentrated on time-resolved surface-pressure measurements for the blade of a high-pressure turbine and comparison of the data with prediction. More recently, Rao, Delaney, and Dunn, 1994 have extended the analysis and presented a further comparison of the time-resolved pressure data (Part I) and a comparison with the time-resolved heat-flux data (Part II).

Researchers at the MIT Gas Turbine Laboratory have developed a blow-down turbine facility and have been actively investigating the unsteady flow within a high-pressure turbine stage at high rotational speed. Several papers have appeared in the literature describing their work, e.g. Epstein, Guenette, Norton, and Cao, 1985; Abhari, Guenette, Epstein, and Giles, 1991; and Abhari and Epstein, 1992.

Oxford University and Pyestock researchers have also been active in the general area of unsteady turbine flows. As was noted above, the facility of choice for both of these groups is the isentropic light-piston compression tube. Results of some of their work relevant to unsteady flow in turbines are given in the following references ; Hilditch and Ainsworth, 1990; Ainsworth, Dietz, and Nunn, 1991; Dietz and Ainsworth, 1992; and Sheard, Dietz, and Ainsworth, 1992.

The Von Karman Institute also has an isentropic light-piston compression tube that is used to create a source of heated and pressurized gas that can be used to supply incoming flow to a turbine cascade or stage. Time-averaged results from VKI have been reported by Consigny and Richards, 1982, by Camci and Arts, 1985, and by Arts and Bourguignon, 1989 to note but a few.

Another facility that is now becoming operational is the Advanced Turbine Aerothermal Research Rig (currently referred to as the Turbine Research Facility) at Wright Patterson Air Force Base. This facility is a large blow-down type that is capable of handling a full-stage turbine with a rotor diameter on the order of 1-meter. A description of this facility is given in Haldeman, Dunn, MacArthur, and Murawski, 1992.

An alternate experimental technique that has been used by several groups to study the physics of the unsteady rotor-stator interaction is the rotating bar technique. This technique is relatively inexpensive, the interaction produced is readily amenable to many different diagnostic tools, and it illustrates some of the basic physics known to be present in a turbine stage. Some of the earliest reported work using the rotating bar technique is that of Pfeil, Herbst, and Schroeder, 1982; Doorly and Oldfield, 1985; and Doorly, Oldfield, and Scrivener, 1985. More recently, several other groups built similar units and reported their results, e.g. O'Brien, Simoneau, LaGraff, and Morehouse, 1986; O'Brien, 1988; Dullenkopf, Schulz, and Wittig, 1990; Ou, Han, and Mehendale, 1993.

# SECTION 2
# DESCRIPTION OF THE EXPERIMENTAL TECHNIQUE, THE TURBINE FLOW PATH AND THE INSTRUMENTATION

**2.1 The Experimental Technique.** The measurements are performed utilizing a reflected-shock tunnel to produce a short-duration source of heated and pressurized gas that subsequently passes through the turbine. Air was used as the test gas for these experiments. A schematic of the experimental apparatus illustrating the shock tube, an expansion nozzle, a large dump tank and a device that houses the turbine stage and provides the flow path geometry is shown in Figure 1. The shock tube has a 0.47-m (18.5-inch) diameter by 12.2-m (40-feet) long driver tube and 0.47-m (18.5-inch) diameter by 18.3-m (60-feet) long driven tube. The driver tube was designed to be sufficiently long so that the wave system reflected from the driver endwall (at the left-hand end of the sketch) would not terminate the test time prematurely. At the flow conditions to be run for these measurements, the test time is very long for a short-duration shock-tunnel facility being on the order of 35 milliseconds. Depending upon the size and configuration of the turbine stage and the associated hardware that houses the turbine, the time required to establish steady flow in the turbine may be on the order of 5 to 10 milliseconds which leaves ample time to complete the measurements.

In order to initiate an experiment, the test section is evacuated while the driver, the double diaphragm section, and the driven tube are pressurized to predetermined values. Pressure values are selected to duplicate the design flow conditions. The flow function ($\dot{w}\sqrt{\theta}/\delta$), wall-to-total temperature ratio ($T_W/T_O$), stage total to total pressure ratio, and corrected speed are duplicated. The shock-tunnel facility has the advantage that the value of $T_O$ can be set at almost any desired value in the range of 800°R to 3500°R, and the test gas can be selected to duplicate the desired specific heat ratio. The design pressure ratio across the turbine is established by altering the throat diameter of the flow-control nozzle located downstream of the turbine exit. A geometry difference between this set of experiments and the ones previously reported is that the flow-control nozzle for this series of measurements was moved much closer to the turbine exit as is illustrated in Figure 2.

**2.2 The Turbine Flow Path.** Figure 2 is a sketch of the turbine stage illustrating the new position of the flow control nozzle mentioned above and the extent to which the flow path of the SSME hardware has been reproduced. One of the requirements of the experiment was that the as-flown geometry of the turbine be faithfully reproduced. The first stage vane row (41 vanes) and the first stage rotor row (63 blades), as well as the second stage vane row (39 vanes) and the second stage rotor row (59 blades) are shown. The first stage vane has a significant cut back at the trailing edge which extends from the hub to about 35% span as illustrated in the photograph of Figure 3. The pre-burner dome and bolt, the 13 struts upstream of the first-stage vane, the 12 flow straighteners, and 6 struts downstream of the second rotor have been included. Flow path static pressure was measured on the outer wall at the inlet and exit to the turbine stages and between each blade row. Examples of these interstage pressure measurements will be shown later in the paper. Since the Mach number of the flow upstream of the first vane is on the order of 0.15, the measured upstream static pressure is nearly equal to the upstream total pressure. The inlet Mach number was calculated and the inlet total pressure was obtained from the isentropic flow relationship. Total pressure was measured downstream of the second rotor using 7 pressure transducers across the passage. The reader is referred to Dunn and Kim, 1992 for details of the configuration and the coordinates of the vanes and blades.

**2.3 Surface-Pressure Instrumentation.** Surface-pressure measurements were obtained using twenty-four miniature silicon diaphragm pressure transducers mounted in the blade skin and flush with the contour of the blade. The particular transducers being used are Kulite Model LQ-062-600A with an active pressure area of 0.64 mm by 0.64 mm and a frequency response of about 100 kHz in the installed configuration. Only the active chip is installed in the blades, thus there is no cavity or screen over the chip. These chips are installed approximately 0.2 mm below the surface and are covered with a layer of RTV (a silastic material) to make them flush with the surface. The thin layer of RTV acts both as a thermal barrier and as a particle barrier to protect the chip from damage. As demonstrated by the fast response of the transducer to flow (see Figures 13-15), the dynamic response of the sensor has not been compromised. External temperature compensation was used with these transducers.

For the particular measurement program reported here, one would not have selected 600 psi transducers if one had the option of designing the instrumentation for the experiment reported. However, the 600A transducers were selected because the measurement program was designed to be extended to an inlet pressure consistent with the 4,137 kPa (600 psi) value. The pressure transducers were placed at 10%, 50%, and 90% span at the locations given in Dunn and Kim, 1992, and were distributed over several different blades (at relative positions with respect to a stage index marker that will be described later) so as to not disturb the integrity of the surface. Figure 4 is a photograph of several transducers located on the suction surface of a blade at 90% span.

**2.4 Heat-Flux Instrumentation.** The heat-flux measurements were performed using thin-film resistance thermometers. The thin-film gauges are made of platinum (~100 Å thick) and are hand painted on an insulating Pyrex 7740 substrate in the form of a strip that is approximately 1.02 x $10^{-4}$-m (0.004-in) wide by about 5.08 x $10^{-4}$-m (0.020-in) long. The response time of these thin films is on the order of $10^{-8}$ s (Vidal, 1956). The substrate onto which the gauge is painted can be made in many sizes and shapes. The substrates are held within the base metal of the turbine stage by use of epoxy.

Both button-type gauges and contoured leading-edge inserts were installed on the vane and blade of the SSME turbine. Figure 5(a) is a photograph of a rotor blade that has been instrumented with button-types gauges and Figure 5(b) is a photograph of a blade containing a contoured leading-edge insert. A detailed listing of the gauge locations is given in Dunn and Kim, 1992.

The heat-flux gauges were calibrated and reduced using standard Calspan techniques (Vidal, 1956). In essence, there is a calibration which converts the resistance change in the heat-flux sensor to temperature. This calibration is updated every run by recording the resistance of the sensor, and scaling the calibration factor by any increase in resistance. Since the thermal properties of the substrate are well known, the heat-flux can be determined from the temperature-time trace using a semi-infinite model (Cook-Felderman, 1966). The accuracy of the heat-flux data reported herein is on the order of ±2.5%.

## 2.5 Pressure-Transducer Calibration Technique and Results

The blade, flowpath, and flowpath rake pressure transducers were calibrated simultaneously through the entire data acquisition system prior to each run. In general, one run was done each day, and the pre-run calibration served as the post-run calibration for the previous run. Although there was one occasion where two runs were done on one day and the pre-run calibration done at the beginning of the day served both runs. The pressure standard used was an Omega transducer which had been calibrated several times over the previous year against an NIST traceable, 1379 kPa MKS Baratron unit. The total variation in the Omega was less than the ±0.7 kPa calibration accuracy over this time span.

Pressure data obtained during the experiments is converted to engineering units using a relative scheme where the only important calibration constant is the scale of the transducer (output in kPa/volt). In this type of system, the base-line at the beginning of a run is averaged to create a set voltage level, and a secondary pressure measurement system (the Omega transducer) provides a pressure measurement in the test section immediately before a run. The voltage readings are converted to pressure by subtracting the base-line voltage from the voltage at any point in time, multiplying this voltage difference by the scale factor, and then adding the measured offset pressure (which is generally quite close to zero).

This system is more impervious to electronic drift, but does require good calibrations over the entire pressure range from vacuum to maximum anticipated pressure and not just over the pressure range expected on the blade surfaces. For these measurements, the pressure fluctuations were expected to vary between 140 and 345 kPa. Because there was a chance that experiments would be run at a higher pressure condition, the calibration was done from 0 to 483 kPa. The calibration was performed by pressurizing the test section (see Figure 1), and then opening a small valve and allowing the tank to bleed while sampling the transducers at fixed time intervals (generally 5 seconds). Each of these data points is the average of 100 data points sampled at 1 kHz for 0.1 seconds (although these values can be changed by the user). Several different types of calibrations were done to examine the effects of different procedures on the calibration results, several pressurization and de-pressurization cycles were checked at levels both above and below atmospheric conditions. Some hysteresis was noted in the system, but it was on the order of the calibration accuracy. Generally, several hundred data points were used. Calibration was done by performing a linear least-squares regression on the data and plotting the residuals.

Calibration accuracy can be shown in two forms. Figure 6 is a plot of how the best estimate of the scale factor changed from run to run. This is shown as a percent of reading. One can see that for a majority of the transducers fall within a ±0.5% of reading span, and that these transducers are relatively tight, indicating that little is changing in the transducer. Figure 7 shows the 95% range of the absolute values of the deviation from the measured pressure standard for each calibration. For every calibration, the deviations are averaged and the standard deviation ($\sigma$) is generated. Assuming that the distribution is Gaussian, then 95% of the data should exist within $\pm 2\sigma$. Figure 7 represents the positive side of this data.

Comparing figures 6 and 7, one can see that the deviation of the calibrations is by far the largest contributor to the overall uncertainty of the pressure measurements, and that in fact, the variation in the scale factor is probably largely due to the deviations of these calibrations. It is however, quite important to realize that even for the bad sensors (4 kPa variations), this is an overall accuracy of ±0.1% of full-scale for the transducers, and that for the majority of the sensors which have accuracy's of ± 1 kPa, this is an overall accuracy of ±0.02% of full-scale reading.

In addition to the pressure calibrations just described, at the end of the experiments checks were performed on the system by examining the effects of rotation on the pressure transducers and the effects of temperature. Some of the transducers were found to have had the protective RTV coating compromised during the testing sequence. This has probably been the single most important cause in the long-term drift of the pressure-transducers. The overall effect of this accuracy on the experimental results presented is not significant since any temperature effects would only change the DC level of the transducer readings and not the unsteady component.

## 2.6 Experimental Conditions

Table 1 provides a summary of the reflected-shock conditions, the full turbine total-to-total pressure ratio, the turbine weight flow, the average speed during the data collection period, and the percent of corrected turbine speed. These experiments were performed at a reflected-shock pressure and temperature of approximately 6.44 x $10^3$ kPa (936 psia) and 513°K (923°R), respectively. This reflected-shock condition results in a first vane inlet Reynolds numbers (based on first vane axial chord) of approximately 1.4 x $10^5$. Measurements were obtained with the turbine speed set at 101% $\pm$ 1% of the design value. For this turbine, the corrected speed is 291.36 rpm as indicated below Table 1.

Table 1 Summary of flow parameters.

| Run # | $\dot{W}$ * (kgm/s) | Full turbine $\frac{P_{T,in}}{P_{T,out}}$ | Reflected shock pressure (kpa) | Reflected shock temperature (°K) | Average Speed (rpm) | % Design speed ** (%) |
|---|---|---|---|---|---|---|
| 22 | 2.34 | 1.42 | 6412 | 507 | 9000 | 102 |
| 24 | 2.54 | 1.46 | 6855 | 521 | 8991 | 101 |
| 26 | 2.10 | 1.39 | 6228 | 510 | 9031 | 102 |
| 27 | 2.26 | 1.40 | 6438 | 514 | 8885 | 100 |
| 28 | 2.25 | 1.38 | 6289 | 512 | 9010 | 102 |

* obtained from vane flow rig data at experimental value of $P_{T,in} / P_{S,out}$ for first vane (see Table 2)

** $N_{corr} = N_{phy} / \sqrt{T_T} = 291.36$ rpm

Table 2 presents the inlet total pressure, the first vane total-to-static pressure ratio, the first stage total-to-static pressure ratio, and the overall turbine total-to-total pressure ratio. The average inlet total pressure for the 5 runs was 346 kPa, the average first vane pressure ratio was 1.11, the average first stage pressure ratio was 1.24, and the average total-to-total pressure ratio was 1.41. The target pressure ratio was 1.45, which could have been achieved by altering the flow-control nozzle throat area. However, for the purposes of this measurement program, it was not necessary to make a throat area change. The first blade tip clearance was 2.14% of blade height (0.0187 in.).

Table 2 Component pressure ratios.

| Run # | $P_T$ into 1st vane (kpa) | First vane * $\frac{P_{T,in}}{P_{S,out}}$ | First stage $\frac{P_{T,in}}{P_{S,out}}$ | Full turbine $\frac{P_{T,in}}{P_{T,out}}$ ** |
|---|---|---|---|---|
| 22 | 345 | 1.11 | 1.25 | 1.42 |
| 24 | 366 | 1.12 | 1.27 | 1.46 |
| 26 | 334 | 1.10 | 1.22 | 1.39 |
| 27 | 348 | 1.11 | 1.23 | 1.40 |
| 28 | 335 | 1.11 | 1.22 | 1.38 |

* Static pressures were measured at the outer shroud.
** $P_{T,out}$ is average pressure from 7 flowpath transducers

# SECTION 3
# EXPERIMENTAL RESULTS

This portion of the final report will concentrate on the following; (a) the time-averaged surface-pressure data at 10%, 50%, and 90% span on the blade, (b) the ensemble averaged surface pressure on the blade as it passes through a vane passage, (c) the unsteady envelope of surface pressure on the blade, (d) the ensemble averaged surface heat flux on the blade as it passes through a vane passage, and (e) the unsteady envelope of surface heat flux on the blade.

**3.1 Reservoir and Flow Path Pressure Histories.** Prior to presenting the time-averaged pressure results for the blade, the time-resolved blade surface pressure, and the time-resolved heat-flux measurements for the blade, the uniformity of the reservoir being used to feed the turbine flow, and the uniformity of the turbine stage pressure field for the time during which the measurements to be described were obtained will be demonstrated. Figures 8 (a) through (e) are pressure time histories sampled at a frequency of 100 kHz with an anti-aliasing Bessel filter at 40 kHz for the following locations in the experiment: 8(a) the shock tube reflected-shock reservoir; static pressure measurements taken at the outer wall along the flow path at the following locations, 8(b) just upstream of the vane entrance, 8(c) between the first vane and the first blade, 8(d) between the first blade and the second vane, and 8(e) downstream of the second blade. On Figures (b) through (e) the time required to establish local steady flow is noted on the figure. During the flow establishment time, the wave system being established between the flow-control nozzle and the inlet which determines the turbine weight flow and the bypass flow can be clearly seen in the pressure data. A one dimensional calculation can be performed to demonstrate that the wave system moves through the stage at approximately the local speed of sound. After flow has been established in the stage, the interstage pressure remains relatively uniform. The occasional spike on the trace is the result of electronic interference which does not affect the result, but could not be eliminated from the electrical circuit without excessive filtering, which was not desirable.

**3.2 Blade Time-Averaged Surface-Pressure Results.** Blade surface-pressure measurements were obtained at 10%, 50%, and 90% span. Figure 3 illustrated that there is a significant cut back of the first vane that extends from the hub to nearly 35% of the span. This feature of the vane appears to have a significant influence on the vane pressure at the 10% span location and perhaps some influence on the midspan results as will be demonstrated in this section. The surface-pressure measurements are compared with both the Dunn, Kim, Civinskas, and Boyle, 1992 and the Boyle, 1994 predictions. The technique used to obtain the 1994 predictions is reported in Boyle and Giel, 1994. Their analysis uses a steady-state, three-dimensional, thin-layer Navier-Stokes code developed by Chima, 1991 and Chima and Yokota, 1988. The code, known as RVC3D, uses an explicit time marching algorithm, employing implicit residual smoothing. A four-stage Runge-Kutta scheme is used in the calculation. The prediction of Boyle for the SSME configuration includes the influence of the vane cut back.

Figure 9 is a comparison of the 1992 prediction (see Part I of this report) with the 1994 prediction. In general, the previous predictions are lower than the more recent ones, but not by a significant amount for the purposes of this comparison. Figure 10 presents a comparison of the pressure measurements and the 1994 prediction for the 90% span location. This figure contains both the current experimental data and those reported in the previous publication. The measured and predicted pressure levels are shown to be in reasonable agreement for this particular location. Figure 11 presents a comparable comparison for the 10% span location. This comparison is not nearly as good as was demonstrated for the 90% span location. The reason for this lack of agreement is felt to be the result of the vane cut back illustrated in Figure 3. This disturbance in vane contour is in the immediate upstream proximity of the blade transducers. For example, at the 70% wetted distance location on the suction surface the disagreement between the prediction and the data is significant. The data from all five runs are plotted and shown to be very repeatable. The calibration of all of the transducers from which data were obtained for this figure were carefully checked and found to be consistent with the results of Figures 6 and 7 and were verified not to be sensitive to either acceleration effects or diaphragm heating effects. The data are felt to be correct and the deviation from the prediction is felt to be the result of the vane geometry. Figure 12 presents the comparison between the experimental data and the recent prediction. The data point at 55% on the suction surface is particularly interesting since the calibration is good, the data are repeatable, the transducer is not sensitive to either acceleration or heating effects and still there is a significant disagreement between the data and the prediction. The reason for this disagreement is not clear, but it is possible that the vane cut back is having an influence on the mid span data.

**3.3 Blade Phase-Resolved Surface-Pressure Results.** Phase-resolved measurements are taken by describing the circumferential position of the blade leading edge within the vane passage. Phase-averaged results are presented as a percentage of the passage from 0 to 100%, where 100% would correspond to 8.78 degrees.

Figures 13, 14, and 15 present time histories of blade pressure at 10% span (48.9% wetted distance), 50% span (45.8% wetted distance), and 90% span (16.6% wetted distance) from which the phase-resolved pressure histories to be presented in this section have been derived. These pressure transducers have been sampled at a frequency of 100 kHz with a 40 kHz anti-aliasing Bessel filter and no other filtering has been done to these traces. Once again, the occasional electrical spike mentioned in the previous paragraph appears in the data trace.

Figure 16 is an FFT for a blade pressure transducer (run 27) located at mid span on the suction surface at 18.37% wetted distance. The rotor speed for this run was 8885 rpm which corresponds to a passage cutting frequency of 6.07kHz. Figure 16 illustrates the presence of vane passage cutting at this frequency, but the harmonic at 12.14 kHz is buried in the background signal. The signature at 6.07 kHz suggests that the unsteady component of the blade pressure signal is the result of vane passage cutting. Because of the relatively small magnitude of the unsteady pressure signal for this particular turbine, the FFT is not sharp and clean as was shown for the previous experiments reported by Dunn et al., 1990 for which the magnitude of the unsteady pressure signal was more than an order of magnitude greater than it was for this turbine.

Before discussing the phase-resolved data, it is important to note that the pressure and heat-flux instrumentation is distributed among several different blades and that in order to compare phase-resolved data from different blades, the relative location of this instrumentation must be indexed to a common reference point in the turbine. To accomplish this, a once per revolution marker is derived from the shaft encoder which is initially adjusted to correspond to the time at which the blade containing the contoured leading edge heat-flux gauge insert (blade no. 1) is aligned with the trailing edge of a vane as illustrated in Figure 17. The vane pitch is 8.7805° and the blade pitch is 5.714°. This figure also provides a listing by blade number of the remaining blade instrumentation. The information provided on this figure was used to reference all of the phase-resolved pressure and heat-flux data to a consistent passage location.

Blade surface-pressure data similar to those presented in Figures 13-15 were used to obtain passage average pressure profiles and the corresponding unsteady pressure envelope. In ensemble averaging the blade data, the blade pressure histories (traces similar to those presented in Figures 13-15) were filtered at 20 kHz (approximately three times the vane passage cutting frequency). For many cases, the surface-pressure data were sufficiently steady to allow the ensemble average to be performed over a time period corresponding to one, two, three, or four revolutions. However, it was found in performing the data analysis that ensemble averaging over one or two revolutions provided essentially the same result as averaging over four revolutions as is illustrated in Figure 18 for the blade pressure data at a position of 90% span at 16.6% wetted distance. The unsteady pressure variation (maximum minus mimimum pressure at the particular location) is plotted as a function of percent of vane passage with 0% and 100% corresponding to the vane trailing edge as illustrated in Figure 17. A revolution of the rotor requires approximately 6.7 milliseconds to complete which corresponds to a vane-passage cutting frequency of about 6.15 kHz. It was noted earlier that the rotor speed increases by about two per cent over the entire test time. The initial rotor speed is set so that the speed during the test time is the desired speed ±1% which results in a change in the incidence angle. The results presented in Figure 18 reflect this change in incidence angle.

Figures 19, 20, and 21 are three additional ensemble averaged surface pressure results for two locations at mid span and another one at 90% span. On all three of these figures the data from all five runs have been included. The ordinate on these figures is tha difference between the maximum and the minimum pressure at the particular location. Because the individual runs have a slightly different vane inlet total pressure, only the unsteady component of the pressure is presented in these figures. For the results presented in Figure 19 the run-to-run variation in ensemble averaged pressure is relatively small and the results from individual runs are in good agreement except for the results of run 24. It should be noted that run 24 was performed for the largest mass flow and the largest pressure ratio and when this is accounted for, the results are consistent. Figure 20 is a corresponding plot for a location further along the suction surface at mid span. In general, the ensemble averaged pressure at this location over the duration of the measurement program are in reasonably good agreement with each other. Figure 21 presents the ensemble averaged pressure data at 48.89% wetted distance and 90% span on the suction surface. The passage averaged pressure shown in these figures is reasonably consistent from run to run.

**3.4 Unsteady Pressure Envelope on First Blade.** Figure 22 presents the measured first-stage blade unsteady pressure envelope compared to the mid span prediction supplied by Eastland, 1994. The prediction was made by Chen using an unsteady potential flow panel method ( Chen, 1989) with the upstream blade wake modeled with the wake profile of Lakshminarayana and Davino, 1980, and the effect of the downstream blade row included in a quasi-steady fashion. The comparison presented here is a blind comparison since this envelope was available well in advance of the measurements having been performed. No attempt has been made by Chen to refine the calculations for the various parameters within his calculation which could be varied to obtain a better agreement with the experimental result. The ordinate of this plot is the maximum pressure minus the minimum pressure divided by the first vane inlet total pressure and the abscissa is the wetted distance along the blade surface. Experimental data from all spanwise locations have been included on Figure 22.

A second prediction provided to us by McFarland (1994) is also included on Figure 22 for comparison with the experimental data. This prediction was obtained using a multi-blade, multi-stage panel method as described in McFarland (1993). The calculation is for a steady inviscid flow and includes potential interference effects from all four blade rows. Viscous wake effects were not included which would tend to result in a lower than anticipated unsteady pressure envelope. The blade count for the calculation was changed from 41:63:39:59 to 3:2:3:2. Figure 22 illustrates that the experimental data are bound almost entirely by these two predictions.

It was mentioned earlier in the report that there is relatively little pressure change across the various components of this turbine which results in the magnitude of the unsteady pressure envelope being small and difficult to measure. By comparison, the magnitude of the unsteady pressure envelope for the measurements (using an Allison turbine with a vane exit Mach number greater than one ) reported in Dunn, et al. 1990 was more than fifty times larger. On the pressure surface of the blade the magnitude of the unsteady pressure is predicted by Chen to be on the order of 1.4% to 2% with a peak of 2.6% occurring at the 95% span location where there was not a pressure transducer located. The magnitude of the unsteady envelope on the suction surface is predicted to be in the vicinity of 2% at 5% wetted distance and the data suggest a value on the order of about 1.5%. At 10% wetted distance, the predicted value is on the order of 1.2% and the data cluster around 0.8%. A suction surface peak is predicted to occur around 35% wetted distance, but a pressure transducer was not located at this particular location. At about 50%, the envelope is predicted to fall to about 1.5% and the data suggest a value on the order of 1%. Beyond 50% wetted distance, the predicted envelope increases in value whereas the data remain at about the 0.5% level out to the 75% wetted distance position which is the farthest location at which a pressure transducer was located. The unsteady envelope is predicted to increase greatly beyond 90% wetted distance. Overall, considering that the prediction was performed well in advance of the experiment and that there has been no attempt by Chen to legitimately improve upon the agreement between the predicted and measured unsteady envelope, it is concluded that the agreement presented is reasonably good.

Concerning the prediction of McFarland, on the suction surface at wetted distances less than 40% the predicted magnitude of the unsteady envelope is about as much below the data as the prediction of Chen is above the data. From 40% wetted distance on, the McFarland prediction is in reasonably good agreement with the experimental data. For the pressure side of the blade, the McFarland prediction is consistently below the data, but it is a bit closer the measured values than is the Chen prediction. The McFarland prediction does not include the potential influence of the pressure field fluctuations caused by the viscous wakes. For this reason it is felt that the McFarland technique will generally under predict the magnitude of the unsteady pressure envelope. Overall, it was concluded that the McFarland prediction, like the Chen prediction, also provided a reasonably good representation of the experimental data. The experimental results are shown to be bounded by the results of the two predictions.

**3.5 Blade Time-Resolved Heat-Flux Results** Figure 23 illustrates the surface heat flux (for run 27) on the suction surface of the blade at mid span and 17.71% wetted distance for a time period of a little over two revolutions of the rotor. Thin-film gauges were placed at 10% , 50%, and 90% span and in the tip of the blade. The heat-flux history for each gauge was calculated from the temperature-time history of the thin-film gauge (which is derived from the gauge voltage history and the gauge calibration data) using a technique described by Cook and Felderman, 1966. The thin-film gauge voltage history was recorded at a sampling frequency of 100 kHz. The resulting temperature history was then filtered at 20 kHz prior to calculating the heat-flux history which was subsequently used to obtain the unsteady heat-flux envelope and the phase-resolved heat-flux profile for selected locations on the blade as a function of position within the passage.

The magnitude of the time-averaged heat flux shown in Figure 23 is consistent with the results of the earlier measurements reported by Dunn et al., 1992. The spikes in the trace seen at approximately 31.5 ms, 33.6 ms, 38.8 ms, and 43.5 ms are electrical interference and are not associated with the turbine aerodynamics.

Two specific locations were selected at the mid span location on the suction surface of the first-stage blade in order to compare the qualitative behavior of the phase-resolved surface pressure with the surface heat flux; one position in a region of a strongly favorable pressure gradient for this turbine (approximately 18% wetted distance) and a second position in a region of a mildly unfavorable pressure gradient (approximately 47% wetted distance). The predicted mid span pressure distribution for this blade is given in Figure 5 of Dunn, Kim, Civinskas, and Boyle, 1992 and that figure illustrates that the pressure gradient is mildly favorable over that portion of the suction surface from 0% to 33% wetted distance, and unfavorable from 33% to 100% wetted distance on the suction surface. The vane exit Mach number is subsonic (on the order of 0.5 or less). There are a large number of upstream struts associated with this engine configuration which tend to confuse the issue a little. However, the FFT of the blade surface-pressure (see Figure 16) and heat-flux (see Figure 24) data suggest that the unsteady behavior on the blade for this turbine is dominated by the vane wakes. For these turbine conditions, one would anticipate that the influences of the inviscid flow field would b e transmitted through the boundary layer with little or no phase lag and thus one should anticipate the phase-resolved pressure and heat-flux profiles to be qualitatively similar.

Figure 25 presents a comparison of the phase-resolved heat flux with the corresponding phase-resolved surface pressure at the 18% wetted distance location which is in the region of a strong favorable pressure gradient on the suction surface of the blade. This comparison indicates that the pressure and heat flux are qualitatively in phase. The heat-flux data point at about 61% of the vane exit passage is higher than would have been anticipated.

Figure 26 is a similar comparison between the phase-resolved heat flux and the phase-resolved surface pressure for a location a little further along on the blade where the pressure gradient is unfavorable instead of favorable. With the exception of the data point at approximately 50% of the passage, the two profiles are in qualitative agreement with each other. Comparisons similar to those shown in Figures 25 and 26 were found generally to have a point within the passage that didn't line up to give unequivocal agreement between the two profiles. This is felt to be due to the small reaction of the individual blade rows of the SSME turbine which produces relatively small unsteady effects which, in turn, make resolution of the events difficult.

**3.6 Blade Unsteady Heat-Flux Envelope** Figure 27 presents the unsteady heat-flux envelope for the first blade. This figure presents the maximum minus the minimum heat flux normalized by the stagnation value for the particular run as a function of wetted distance on the blade. Data from all five runs and 10%, 50%, and 90% span are included on this plot. These results were obtained from data records like that presented in Figure 23. The magnitude of the unsteady envelope on the suction surface is relatively independent of location on the blade and reflects the unsteady pressure envelope results presented earlier on Figure 22. For the pressure surface, the unsteady heat-flux envelope appears to be rather small (by comparison with the suction surface) in the region from 0% to 30% wetted distance and then becomes of comparable magnitude from 40% to 70% wetted distance. Beyond 70% wetted distance on the pressure surface, the magnitude of the unsteady heat-flux envelope is small by comparison to any other location on the blade. Whereas an average value for the unsteady pressure was less than 1%, the average of the unsteady heat flux is on the order of 10% . This result is qualitatively consistent with the results of the measurement program for the much more reactive Allison turbine that are reported in Rao, Delaney and Dunn, 1994.

# SECTION 4
# CONCLUSIONS

Time histories of the reservoir of gas reservoir and the turbine flow path pressures have been presented to demonstrate the flow environment within which the data were obtained. The interstage pressure histories illustrate the initial flow establishment time within the turbine and the uniformity of the turbine pressure field during the test time. The measurements were performed at the design flow function, stage pressure ratio, and corrected speed.

The unsteady envelope of surface pressure and heat flux along with the corresponding phase-resolved (in moving through a vane passage) pressure and heat-flux profiles have been measured for the first blade of the SSME fuel-side two-stage turbine. The unsteady pressure envelope was found to be bounded by the predictions of Chen and McFarland. A prediction of the unsteady heat-flux envelope was not available, but the relative magnitude of the heat-flux envelope was found to be significantly larger than the pressure envelope which is consistent with previous measurements.

Measurements obtained at several different blade locations were presented to demonstrate that the ensemble average of the phase-resolved surface pressure data was well defined and the run-to-run variation at a given location on the blade was relatively small.

Representative comparisons between the phase-resolved surface pressure and heat-flux have been obtained for two locations on the blade suction surface; one in the region of a favorable pressure gradient and the other in a region of an unfavorable pressure gradient. For this subsonic turbine, these two quantities are qualitatively in phase with each other.

The measurements described here were capable of resolving the unsteadiness associated with the first stage vane-blade interaction. More importantly, the variation within the experimental data is completely within the band predicted by two different calculations. While some increase in accuracy of the measurement could be achieved by replacing the pressure transducers with ones more aligned with the expected pressure level on the blade, the experimental inaccuracies are felt to be less than the numerical ones.

# SECTION 5
# REFERENCES


Abhari, R.S. and Epstein, A.H., 1992, "An Experimental Study of Film Cooling in a Rotating Transonic Turbine," ASME paper no. 92-GT-201 (see also ASME Journal of Turbomachinery, Vol. 116, pp.818-827, Jan. 1994).

Abhari, R.S., Guenette, G.R., Epstein, A.H., and Giles, M.B., 1992, "Comparison of Time-Resolved Measurements and Numerical Calculations," ASME J. of Turbomachinery, Vol. 114, pp.818-827.

Ainsworth, R.W., Dietz, A.J., and Nunn, T.A., 1990, "The Use of Semi-Conductor Sensors for Blade Surface Pressure Measurement in a Model Turbine Stage," ASME paper no. 90-GT-346.

Arts, T. and Bourguignon, A.E., 1989, "Behaviour of a Two Rows of Holes Coolant Film Along the Pressure Side of a High Pressure Nozzle Guide Vane," ASME paper no. 89-GT-186.

Blair, M.F., Dring, R.P., and Joslyn, H.D., 1988, "The Effects of Turbulence and Stator/Rotor Interaction on Turbine Heat Transfer: Part II - Effects of Reynolds Number and Incidence," ASME paper no. 88-GT-5.

Bordelon, W.J., Kauffman, W.J., and Heaman, J.P., 1993, "The Marshall Space Flight Center Turbine Test Equipment; Description and Performance," ASME paper no. 93-GT-380.

Boyle, R. J, 1994, private communication R. Boyle to M. Dunn.

Boyle, R.J. and Giel, P.W., 1992, "Three-Dimensional Navier-Stokes Heat Transfer Predictions for Turbine Blade Rows," AIAA paper no. AIAA-92-3068

Camci, C. and Arts, T., 1985, "Experimental Heat Transfer Investigation Around the Film-Cooled Leading Edge of a High-Pressure Gas Turbine Rotor Blade," ASME paper no. 85-GT-114.

Chen, S.H., 1989, "Turbomachinery Unsteady Load Predictions with Non uniform Inflow," AIAA paper no. 89-0450 (see also AIAA J. of Propulsion and Power, pp 667-673, May-June 1992).

Chima, 1991, "Viscous Three-Dimensional Calculations of Transonic Fan Performance," AGARD Propulsion and Energetics Symposium on Computational Fluid Mechanics for Propulsion, San Antonio, TX.

Chima, R.V. and Yokota, J.W., 1988, "Numerical Analysis of Three-Dimensional Viscous Internal Flows," AIAA paper no. AIAA-88-3522, (also NASA TM-100878)

Consigny, H. and Richards, B.E., 1982, "Short Duration Measurements of Heat-Transfer Rate to a Gas Turbine Rotor Blade," ASME J. of Engineering for Power, Vol. 104, pp.542-551.

Cook, W.J. and Felderman, E.J., 1966, "Reduction of Data From Thin-Film Heat-Flux Gages: A Concise Numerical Technique," AIAA Journal, pp 561-562.

Dietz, A.J. and Ainsworth, R.W., 1992,"Unsteady Measurements on the Rotor of a Model Turbine Stage in a Transient Flow Facility," ASME paper no. 92-GT-156.

Doorly, D.J. and Oldfield, M.L.G., 1985, "Simulation of the Effects of Shock Wave Passing on a Turbine Rotor Blade," ASME paper no. 85-GT-112.

Doorly, D.J., Oldfield, M.L.G., and Scrivener, C.T.J., 1985, "Wake Passing in a Turbine Rotor Cascade," Heat Transfer and Cooling in Gas Turbines, AGARD Conf. preprint no. AGARD-CP-390.

Dring, R.P., Blair, M.F., and Joslyn, H.D., 1980, "An Experimental Investigation of Film Cooling on a Turbine Rotor Blade," ASME J. of Engineering for Power, Vol. 102, pp. 81-87.

Dring, R.P. and Joslyn, H.D., 1981, "Measurement of Turbine Rotor Blade Flows," ASME J. of Engineering for Power, Vol. 103, pp.400-405.

Dring, R.P., Joslyn, H.D., Hardin, L.W., and Wagner, J.H., 1982, "Turbine Rotor-Stator Interaction," ASME J. of Engineering for Power, Vol. 104, pp. 729-742.

Dullenkopf, K., Schulz, A., and Wittig, S., 1990, "The Effect of Incident Wake Conditions on the Mean Heat Transfer of an Airfoil," ASME paper no. 90-GT-121.

Dunn, M.G., George, W.K., Rae,W.J., Woodward, S.H., Moller, J.C., and Seymour, P.J., 1986, "Heat-Flux Measurements for the Rotor of a Full-Stage Turbine: Part II- Description of Analysis Technique and Typical Time-Resolved Measurements," ASME paper no. 86-GT-78 (see also ASME J. of Turbomachinery, Vol. 108, pp.98-107, 1986).

Dunn, M.G., Seymour, P.J., Woodward, S.J., George, W.K., and Chupp, R.E., 1988, "Phase-Resolved Heat-Flux Measurements on the Blade of a Full-Scale Rotating Turbine," ASME paper no. 88-GT-173, (see also ASME J. of Turbomachinery, Vol. 111, pp. 8-19, 1989.

Dunn, M.G., 1989, "Phase and Time-Resolved Measurements of Unsteady Heat Transfer and Pressure in a Full-Stage Rotating Turbine," ASME paper no. 89-GT-135 (see also ASME J. of Turbomachinery, Vol. 112, pp. 531-538, 1990)

Dunn, M.G., Bennett, W., Delaney, R., and Rao, K., 1990, "Investigation of Unsteady Flow Through a Transonic Turbine Stage: Part II - Data/Prediction Comparison for Time-Averaged and Phase-Resolved Pressure Data," AIAA/SAE/ASME/ASEE 26th Joint Propulsion Conference, Orlando, FL, AIAA Paper No. 90-2409, (see also ASME J. of Turbomachinery, Vol. 114, pp. 91-99, 1992)

Dunn, M.G., Kim, J., Civinskas, K.C., and Boyle, R.J., 1992 (a), "Time-Averaged Heat Transfer and Pressure Measurements and Comparison With Prediction for a Two-Stage Turbine," ASME paper no. 92-GT-194, (see also ASME J. of Turbomachinery, Vol. 116, pp. 14-22, 1994)

Dunn, M.G. and Kim, J., 1992(b), "Time Averaged and Phase-Resolved Heat-Transfer and Pressure Measurements for the Turbine of the SSME Fuel Side Turbopump," CUBRC Report No. 640I.

Eastland, A., 1994, Rocketdyne Division of Rockwell International, private communication with M.Dunn.

Epstein, A.H., Guenette, G.R., Norton, R.J.G., and Cao, Y., 1985, "Time-Resolved Measurements of a Turbine Rotor Stationary Tip Casing Pressure and Heat Transfer Field," AIAA paper no. AIAA-85-1220.

Haldeman, C.W., Dunn, M.G., MacArthur, C.D., and Murawski, C.G., 1992, "The USAF Advanced Turbine Aerothermal Research Rig (ATARR)," Conf. preprint for the 1992 AGARD Meeting on Heat Transfer and Advanced Cooling for Gas Turbine Engines, AGARD-CP-527.

Hilditch, M.A. and Ainsworth, R.W., 1990, "Unsteady Heat Transfer Measurements on a Rotating Gas Turbine Blade," ASME paper no. 90-GT-175.

Hudson, S.T., Gaddis, S.W., Johnson, P.D., and Boynton, J.L., 1991, "Cold Flow Testing of the Space Shuttle Main Engine High Pressure Fuel Turbine Model," AIAA paper no. 91-2503.

Lakshminarayana, B. and Davino, R., 1980, "Mean Velocity and Decay Characteristics in the Guidevane and Stator Blade Wake of an Axial Flow Compressor," Journal of Engineering for Power, Vol. 102, pp. 50-60.

McFarland, E.R., 1994, NASA Lewis Research Center, private communication with M.Dunn.

McFarland, E.R., 1993, "An Integral Equation Solution for Multi-Stage Turbomachinery Design Calculations," ASME paper no. 93-GT-41.

O'Brien, J.E., 1988, "Effects of Wake Passing on Stagnation Region Heat Transfer," paper presented at the Heat Transfer in Gas Turbine Engines and Three-Dimensional Flows Conference, ASME Winter Annual Meeting.

O'Brien, J.E., Simoneau, R.J., LaGraff, J.E., and Morehouse, K.A., 1986, "Unsteady Heat Transfer and Direct Comparison to Steady-State Measurements in a Rotor-Wake Experiment," NASA Technical Memorandum 87220.

Ou, S., Han, J.C., and Mehendale, A.B., 1993, "Unsteady Wake Over A Linear Turbine Blade Cascade With Air and CO2 Film Injection:Part I- Effects on Heat Transfer Coefficient," ASME paper no. 93-GT-210.

Pfeil, H., Herbst, R., and Schroeder, T., 1982, "Investigation of the Laminar-Turbulent Transition of Boundary Layers Disturbed by Wakes," ASME paper no. 82-GT-124.

Rao, K.V., Delaney, R.A., and Dunn, M.G., 1994, "Vane-Blade Interaction in a Transonic Turbine, Part I - Aerodynamics and Part II - Heat Transfer," to be published in the AIAA J. of Propulsion and Power.

Sheard, A.G., Dietz, A.J., and Ainsworth, R.W., 1992, "The Dynamic Characteristics of a High Pressure Turbine Stage in a Transient Wind Tunnel," ASME paper no. 92-GT-166.

Vidal, R.J., 1956, "Model Instrumentation Techniques for Heat Transfer and Force Measurements in a Hypersonic Shock Tunnel", Cornell Aeronautical Laboratory Report AD-917-A-1.

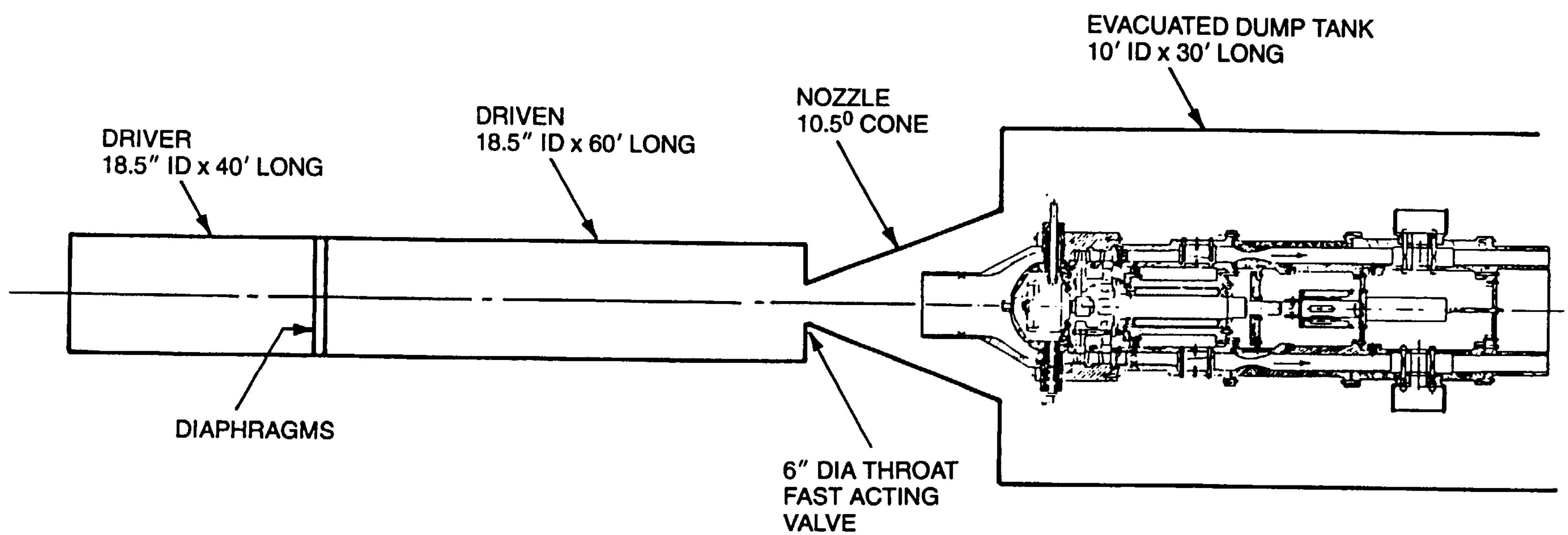


**Fig. 1 Sketch of the SSME turbine stage located in the shock– tunnel**

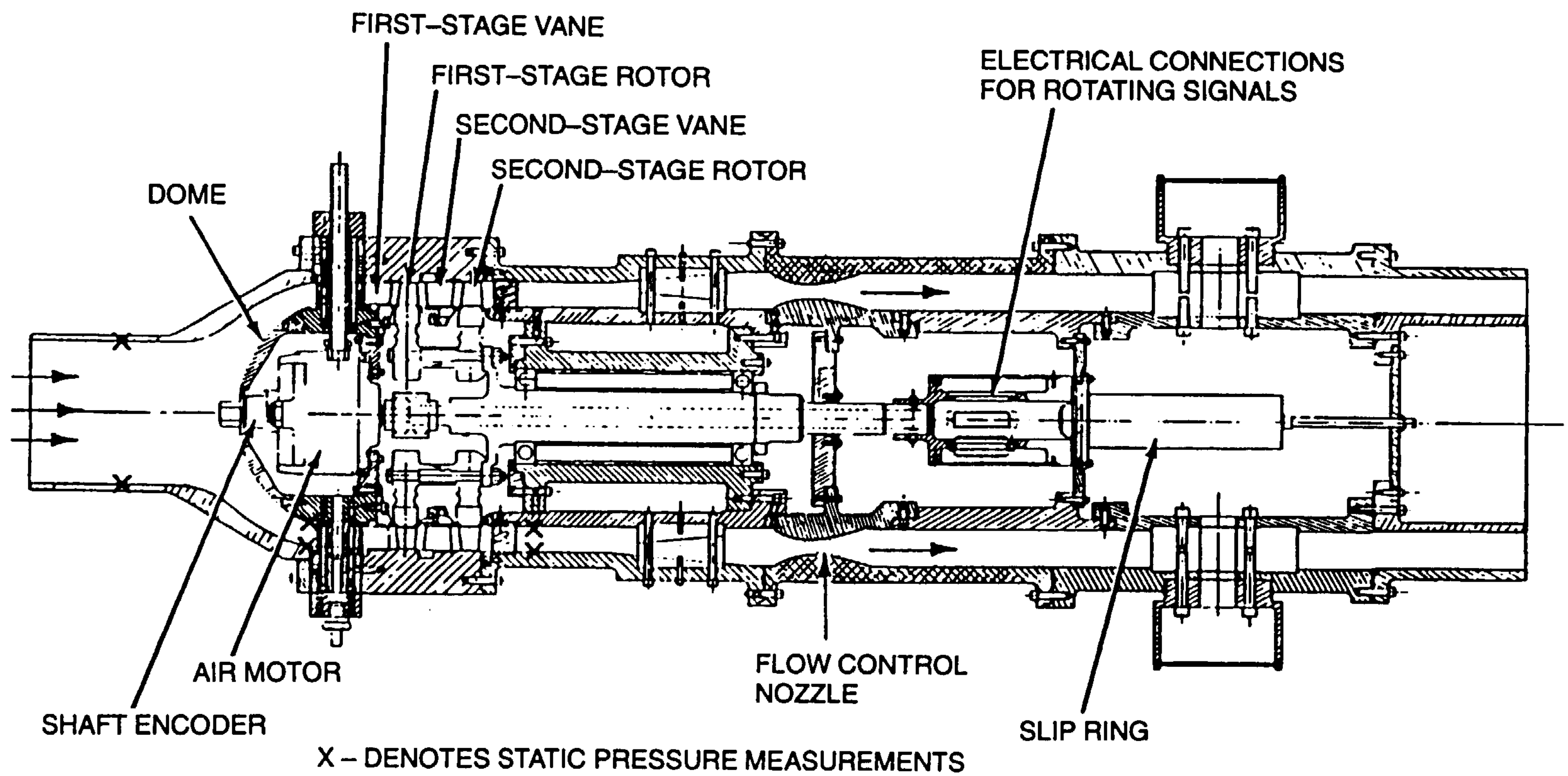


**Fig. 2 Sketch of device housing SSME turbine stage**

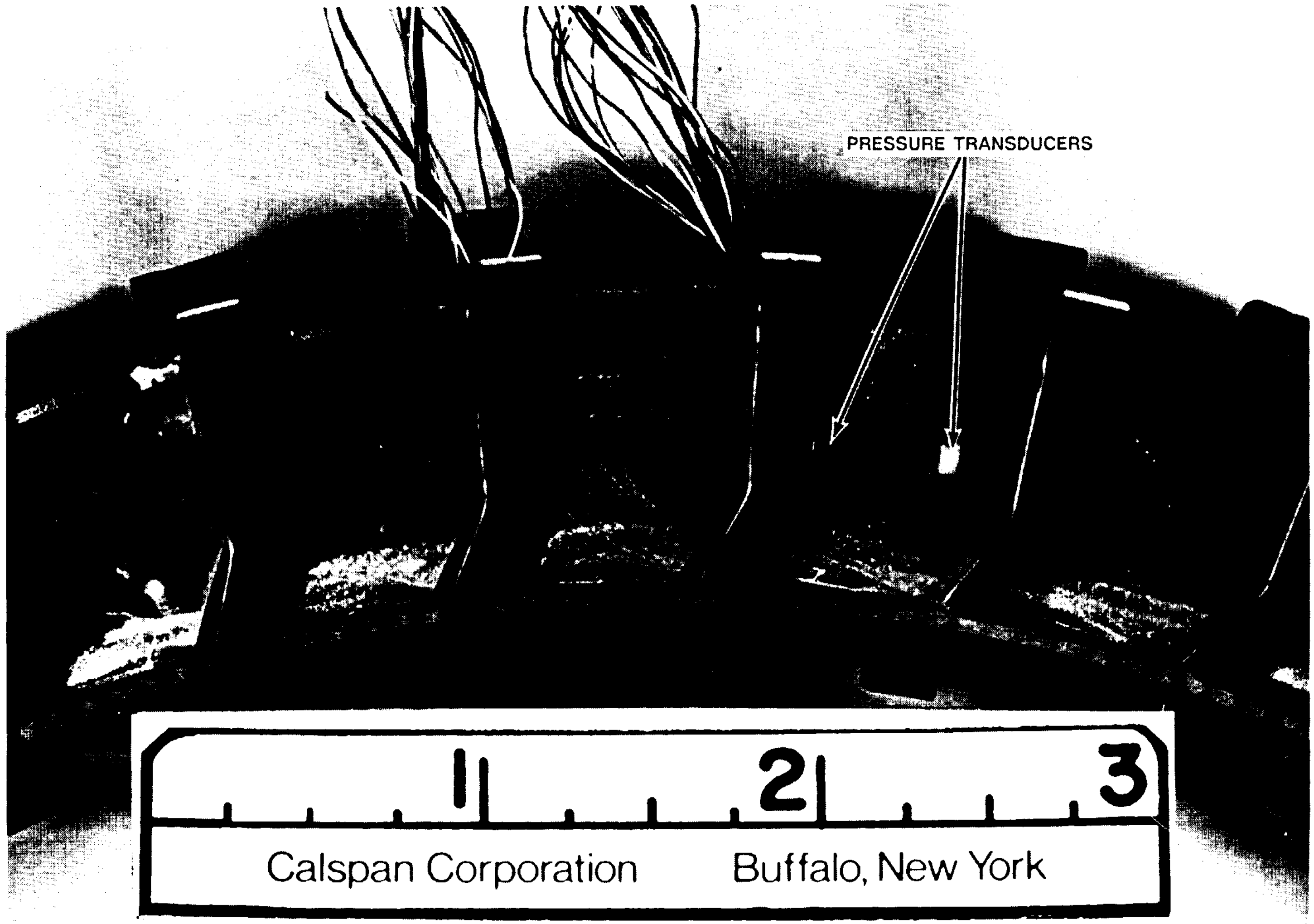


Fig. 3 Photograph of first stage vane showing cut back

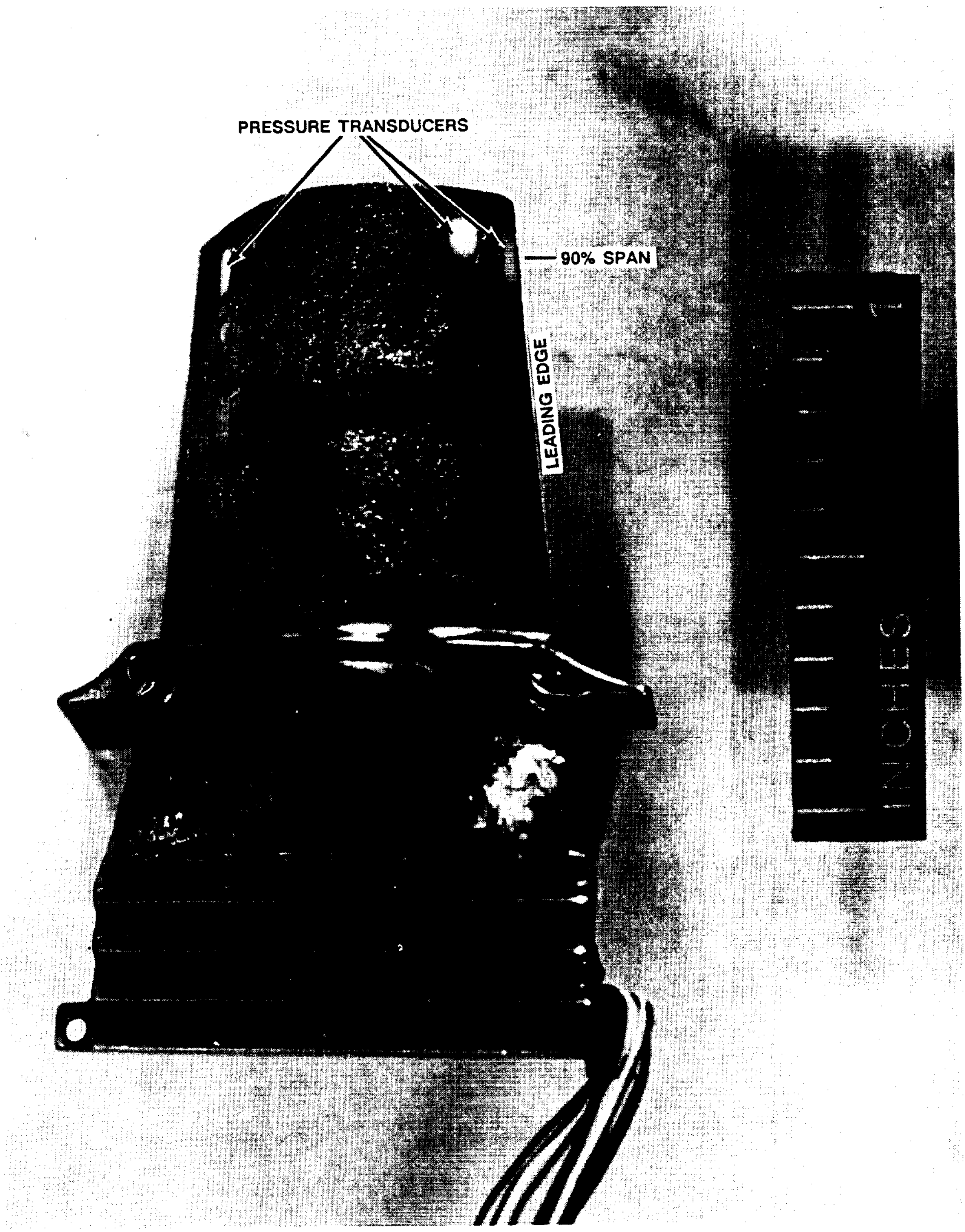


Fig. 4 Photograph of pressure transducers at 90% span on first–stage blade suction surface

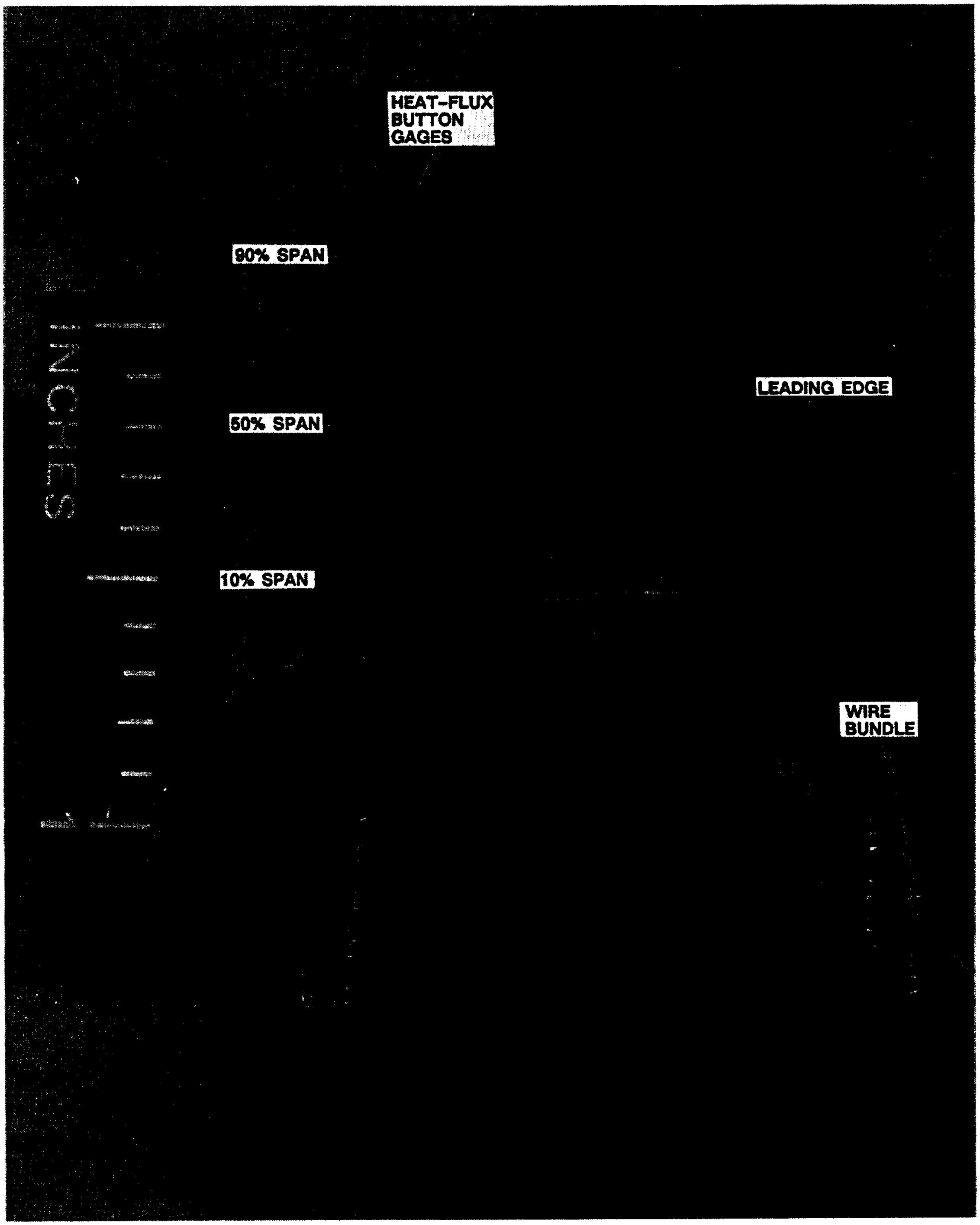


**Fig. 5(a) Button–type heat–flux gages on first–stage blade suction surface**

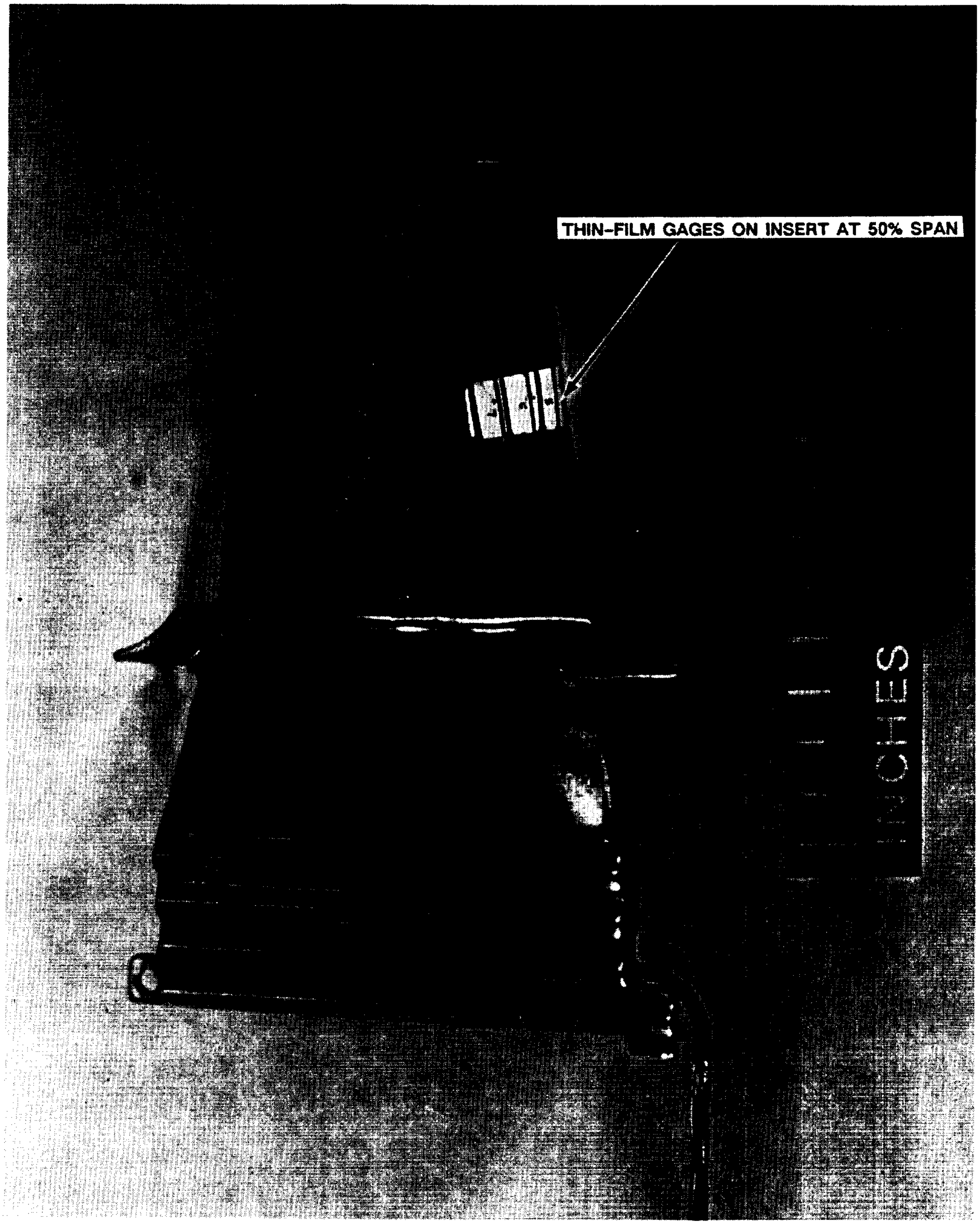


**Fig. 5(b) Photograph of leading–edge insert heat–flux gages on first–stage blade**

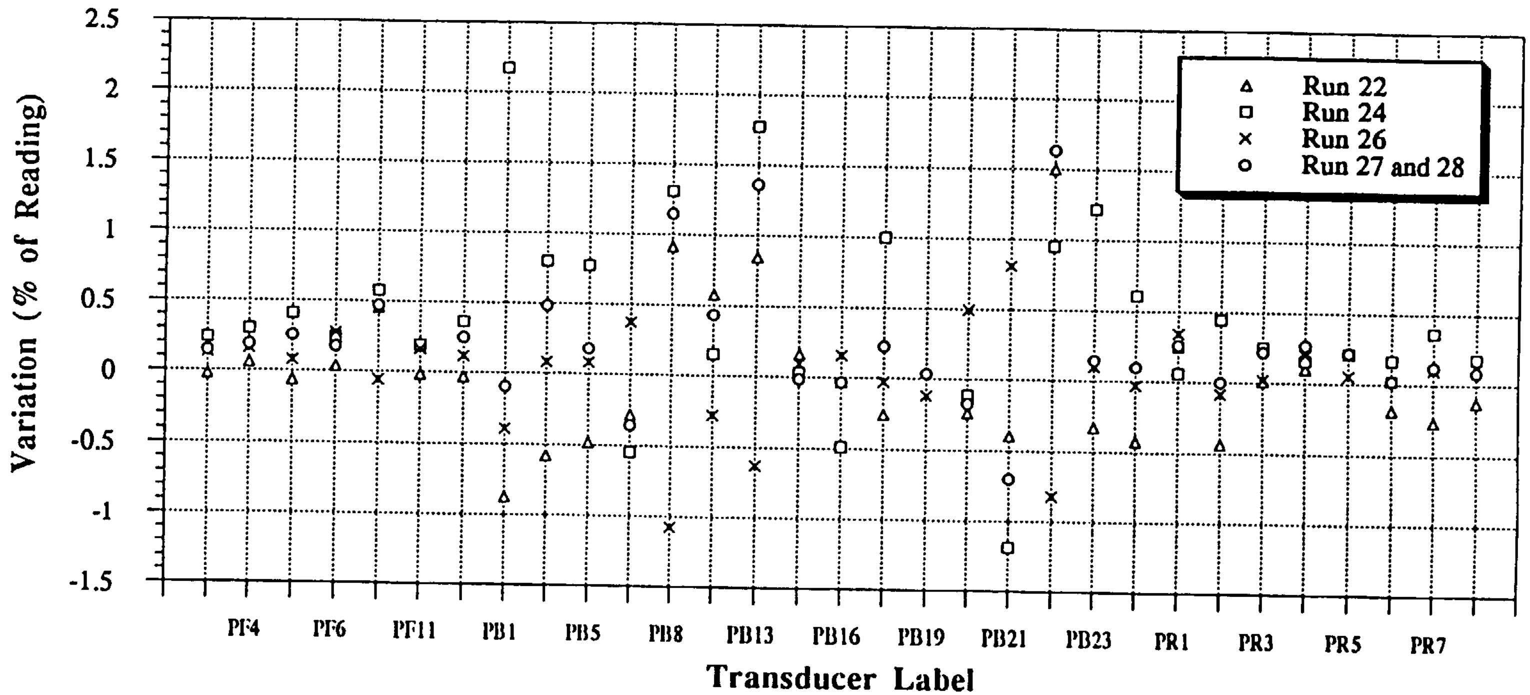


**Fig. 6** Long-range drift in scale factors of flow path, first-stage blade, and pressure-rake transducers (variation is described as a percent of reading from test to test)

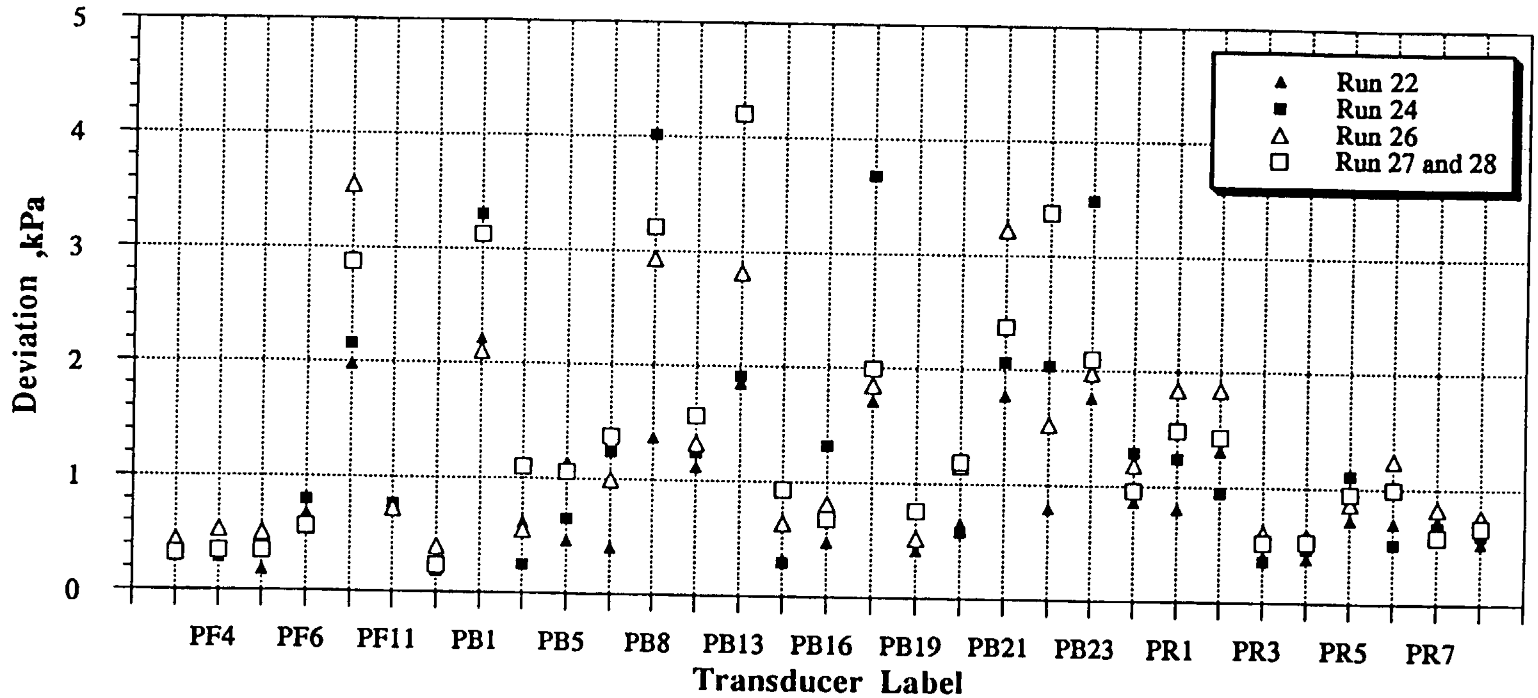


**Fig. 7** **Calibration accuracy range (95% or +2σ), positive side shown**

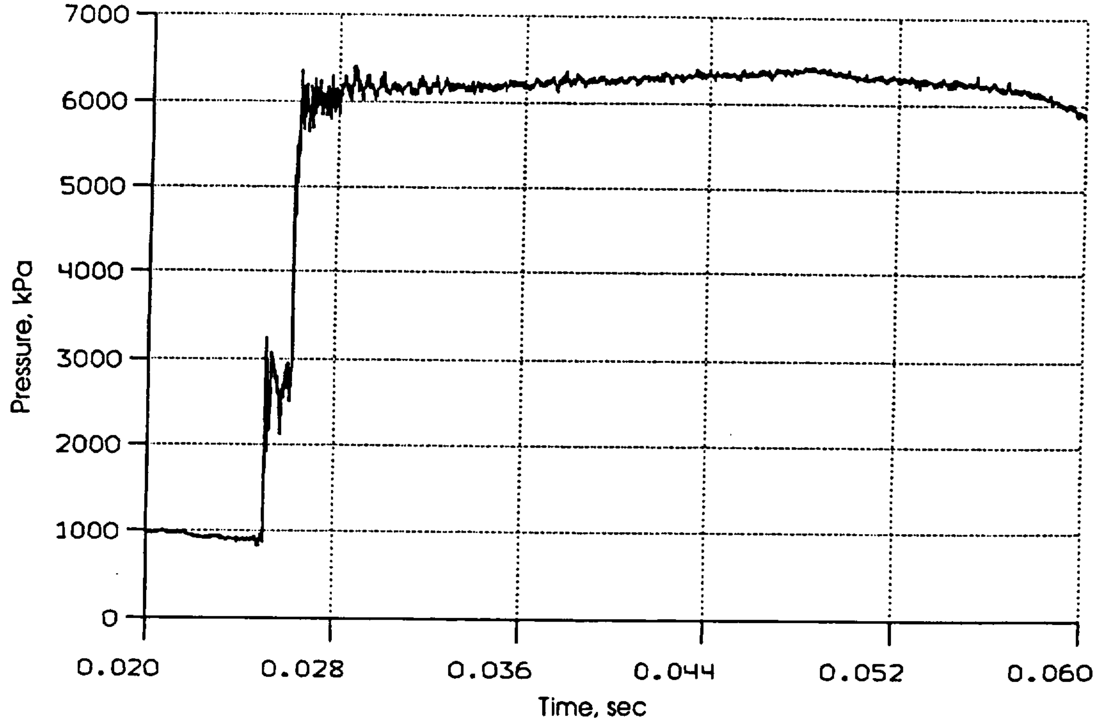


**Fig.8(a) Reflected–shock pressure history**

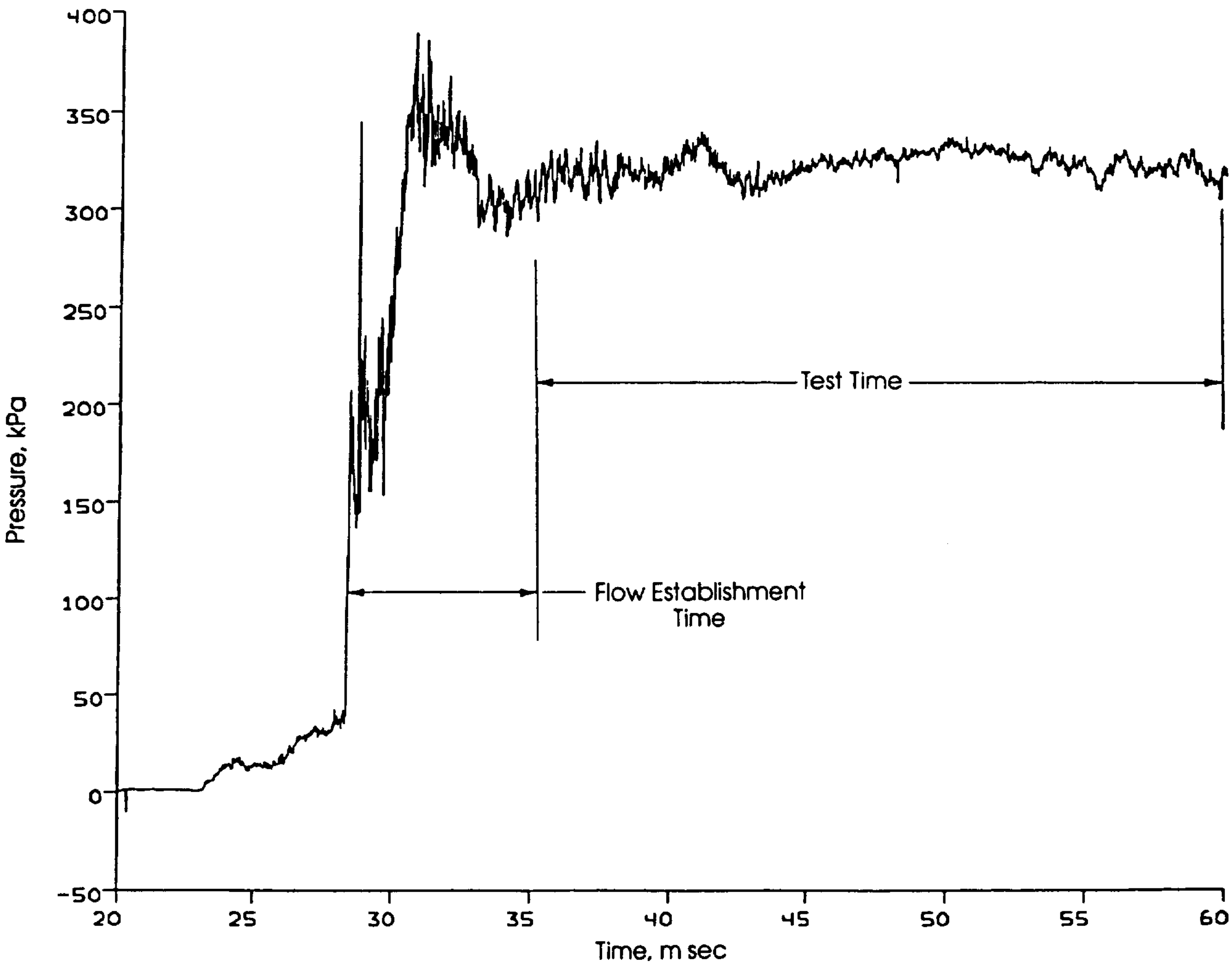


**Fig. 8(b) Static pressure at outer wall just upstream of first vane**

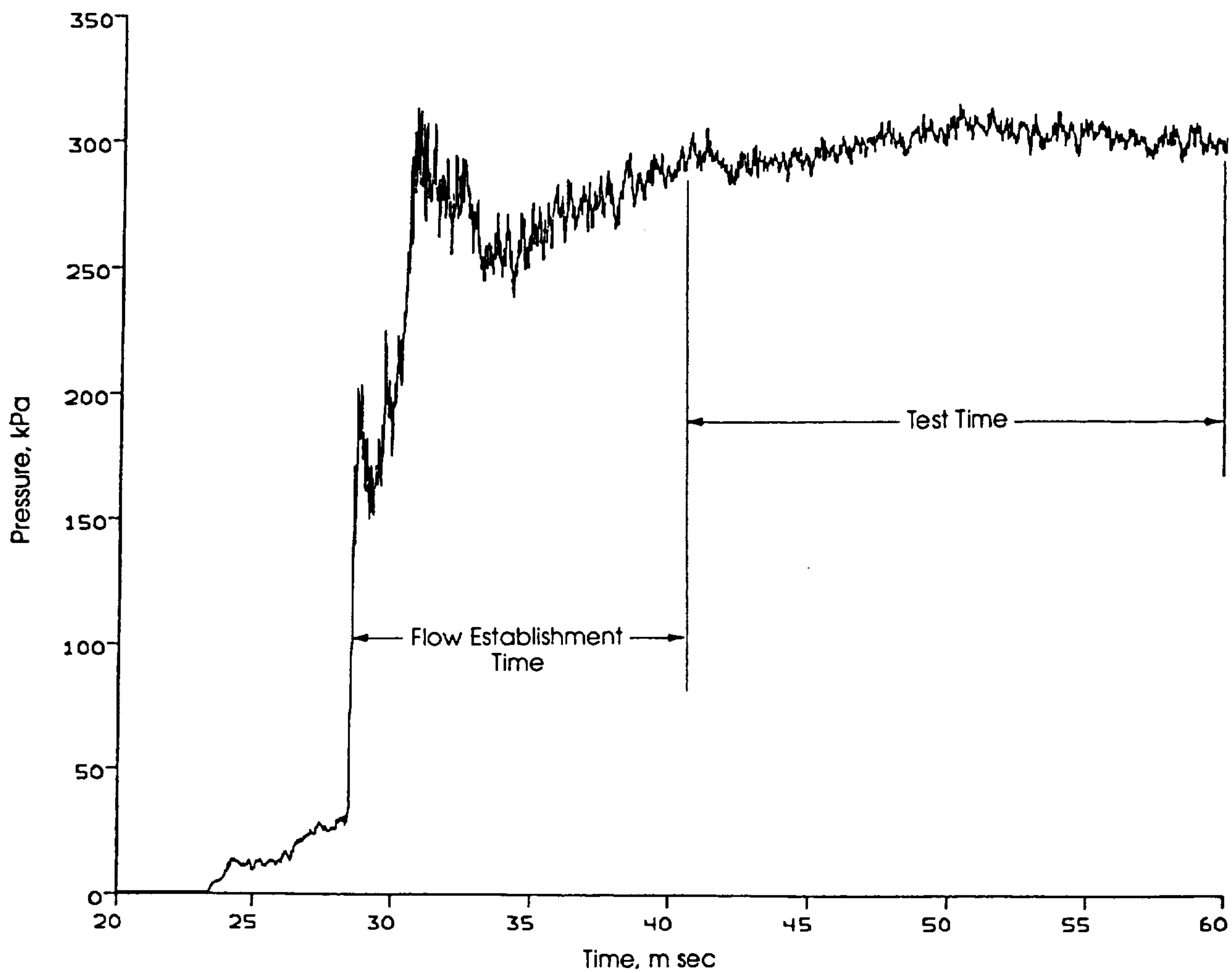


**Fig. 8(c) Static pressure at outer wall between first vane and first blade**

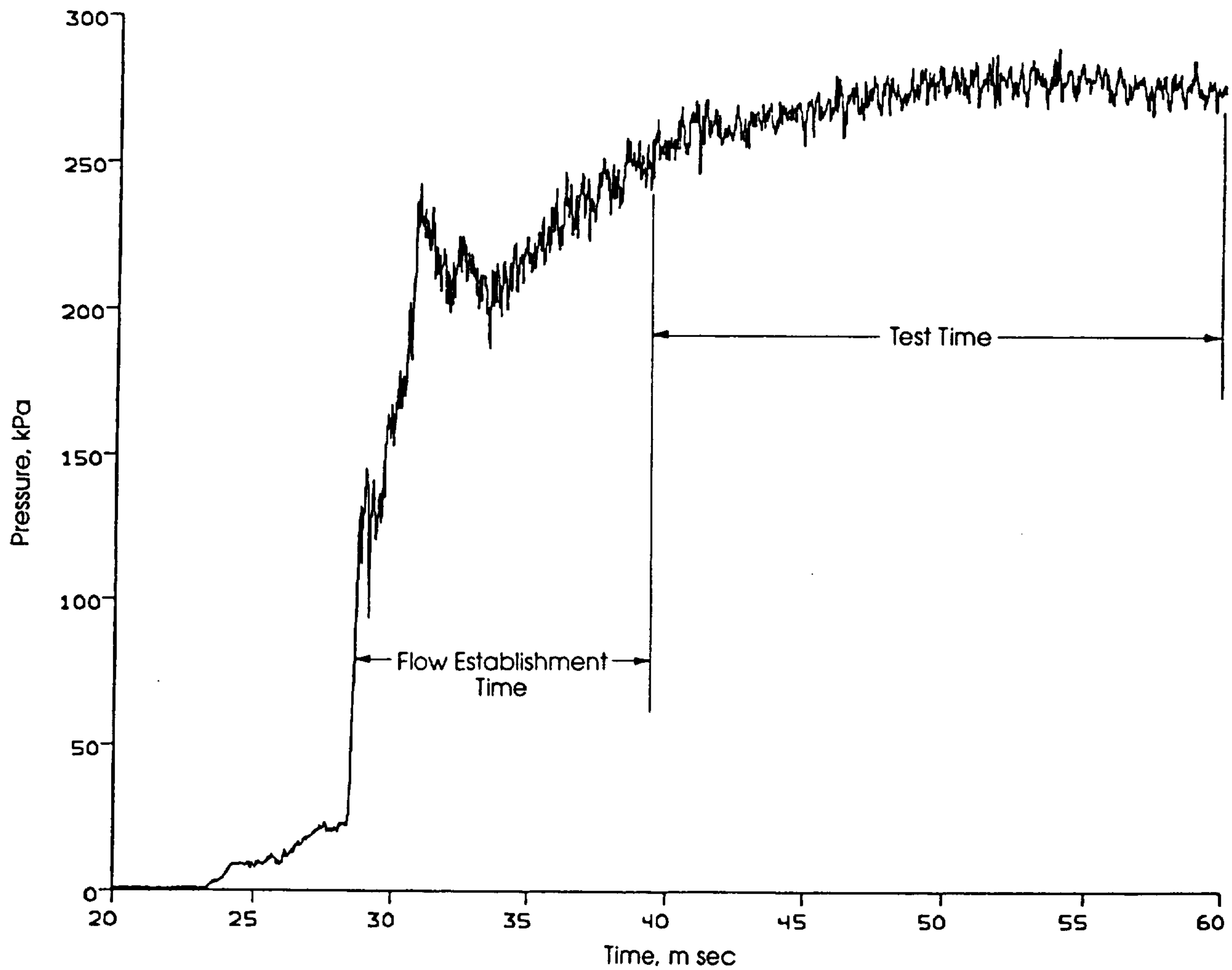


**Fig. 8(d) Static pressure at outer wall between first blade and second vane**

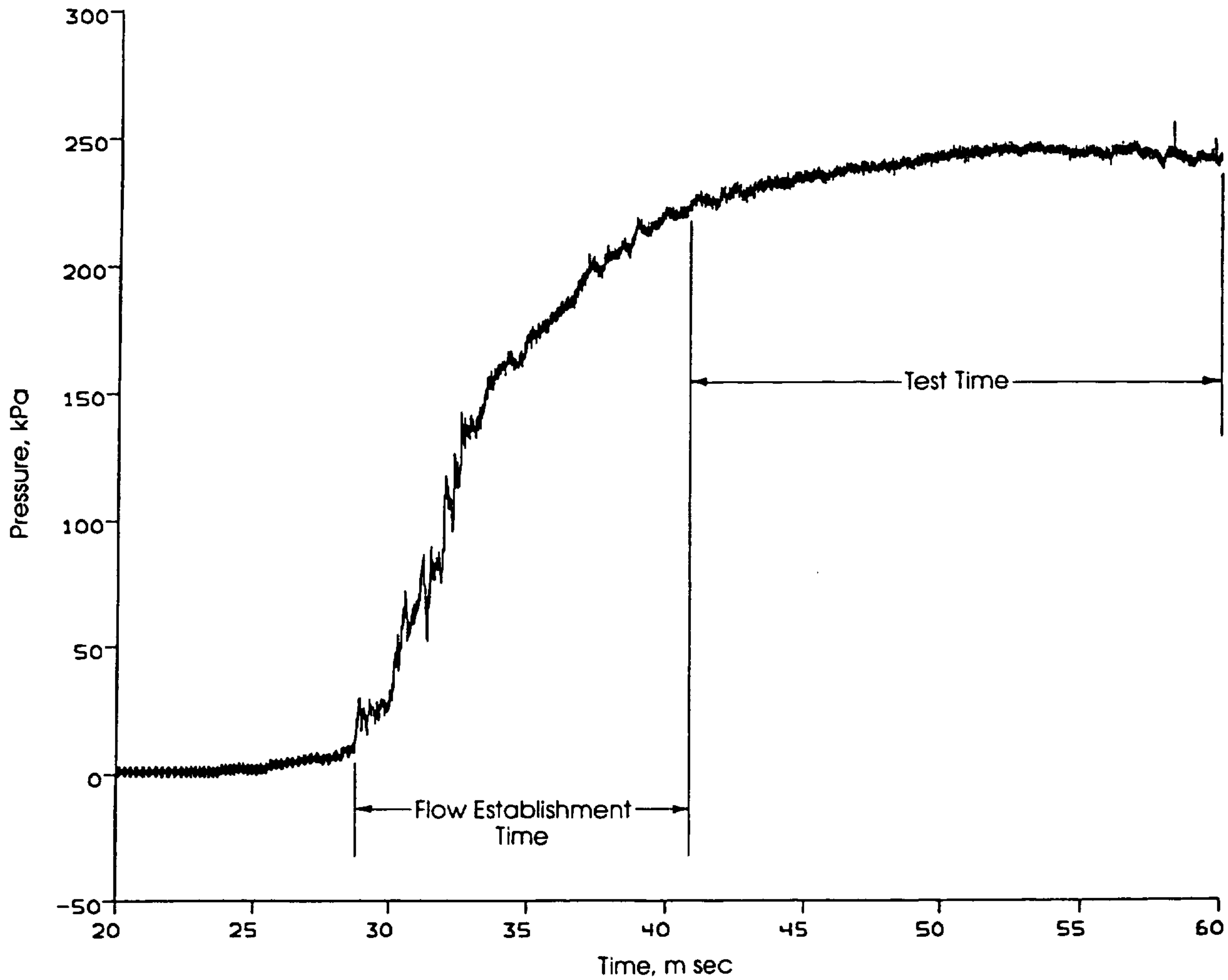


**Fig. 8(e) Static pressure at outer wall downstream of second vane**

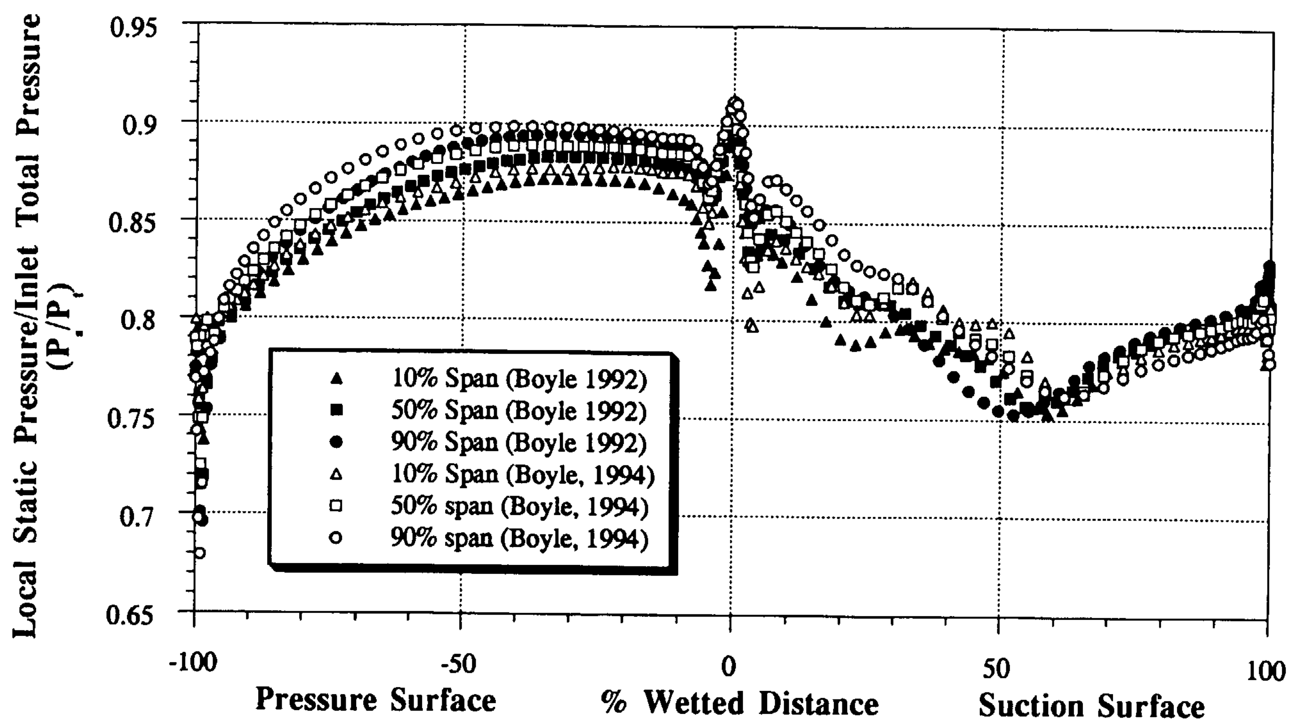


**Fig. 9 Comparison of predictions for 10, 50, and 90% spans for SSME first-stage blade**

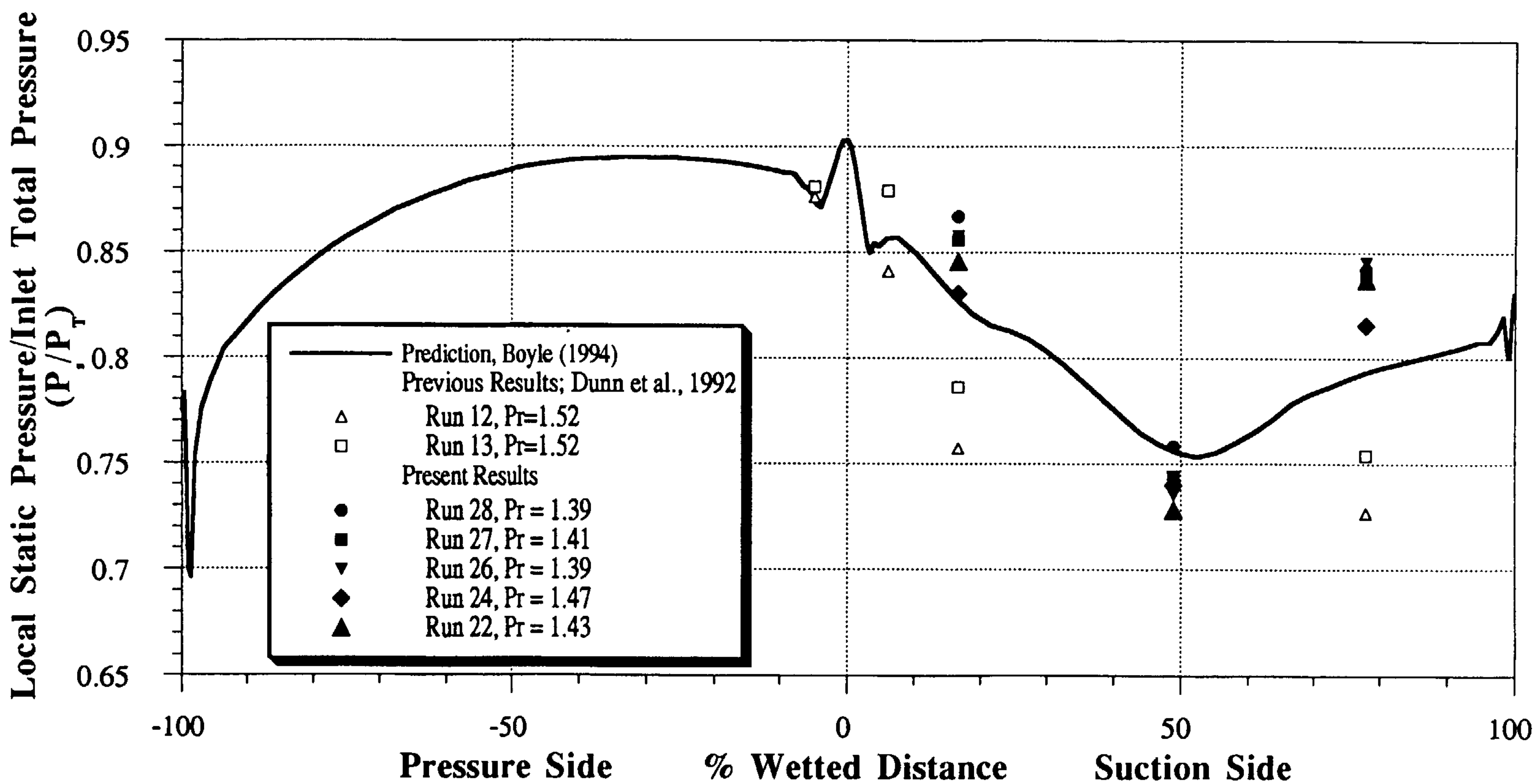


**Fig. 10 SSME first-stage blade surface pressure vs. wetted distance at 90% span**

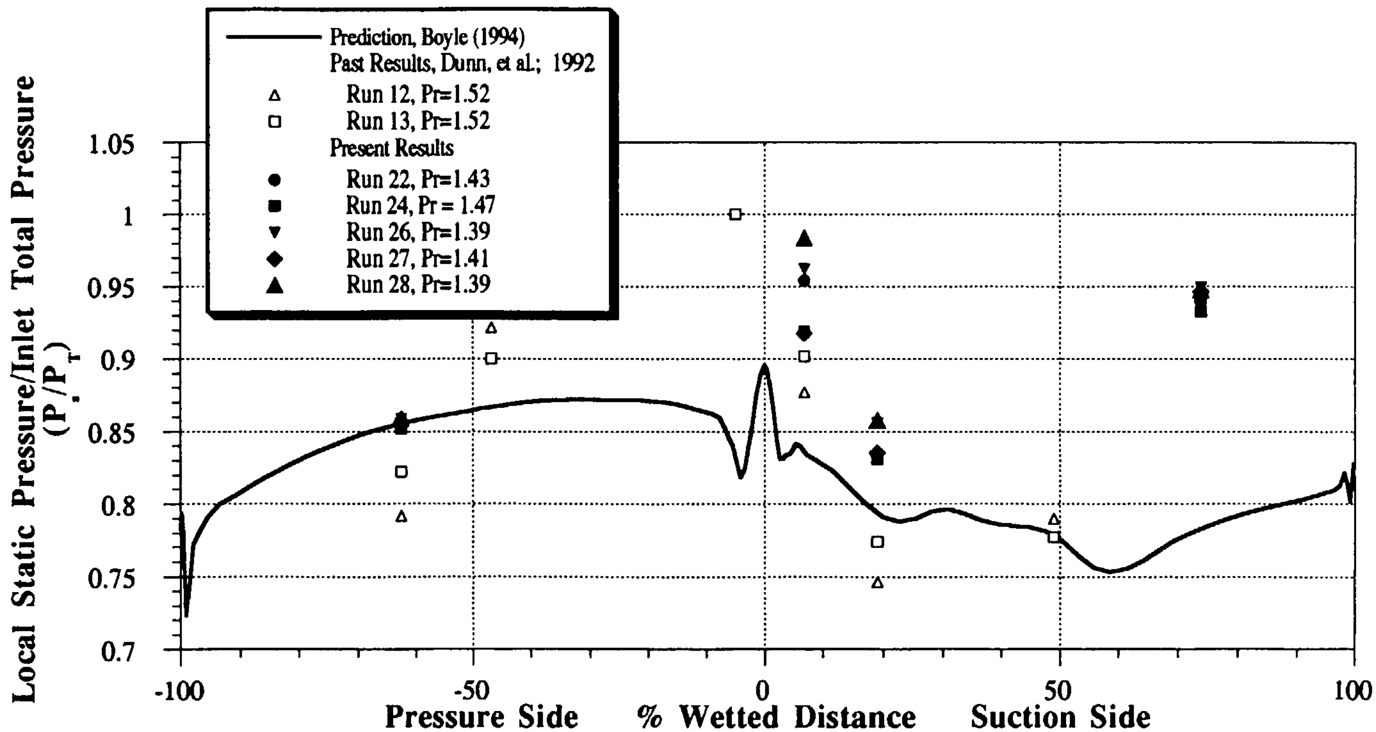


Fig. 11 SSME first-stage blade surface pressure vs. wetted distance at 10% span

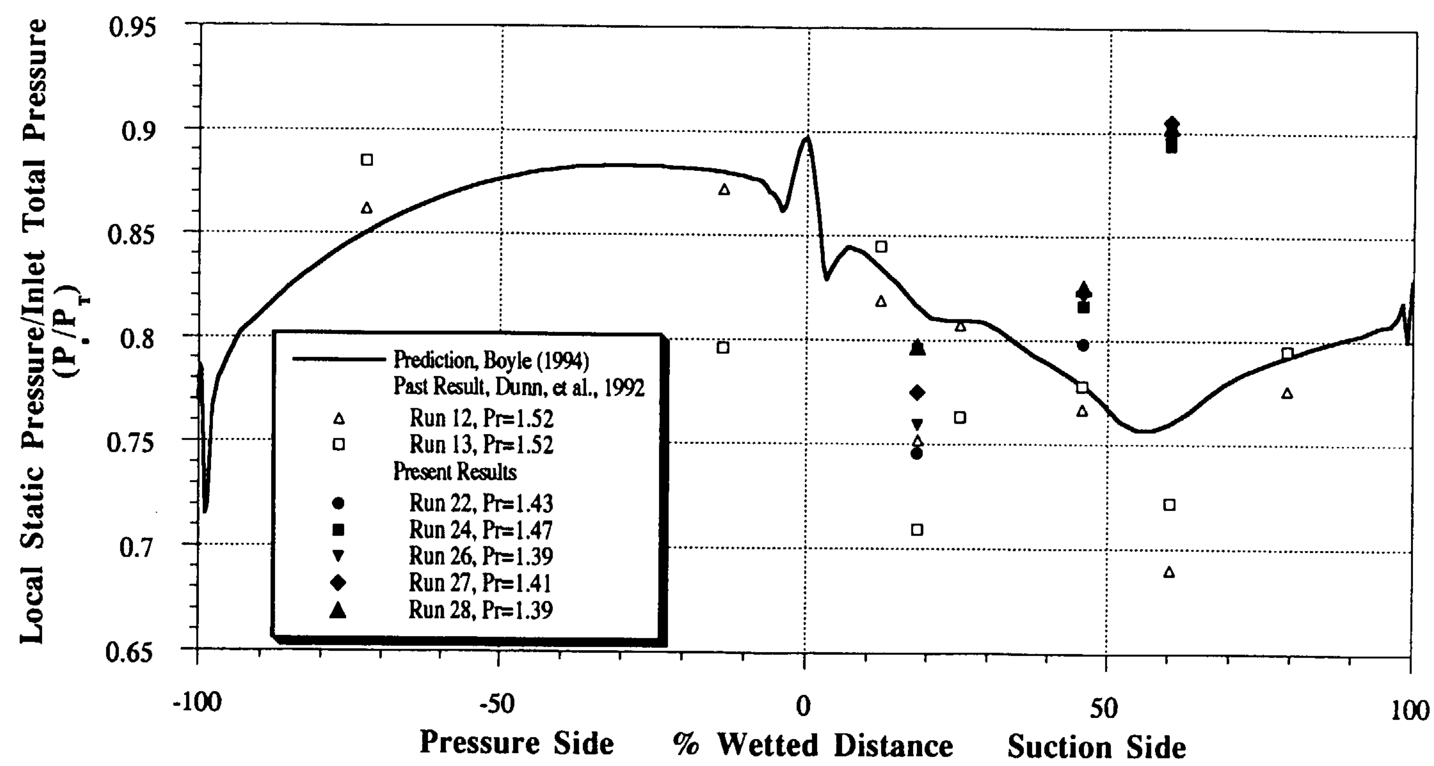


**Fig. 12** SSME first-stage blade surface pressure vs. wetted distance at 50% span

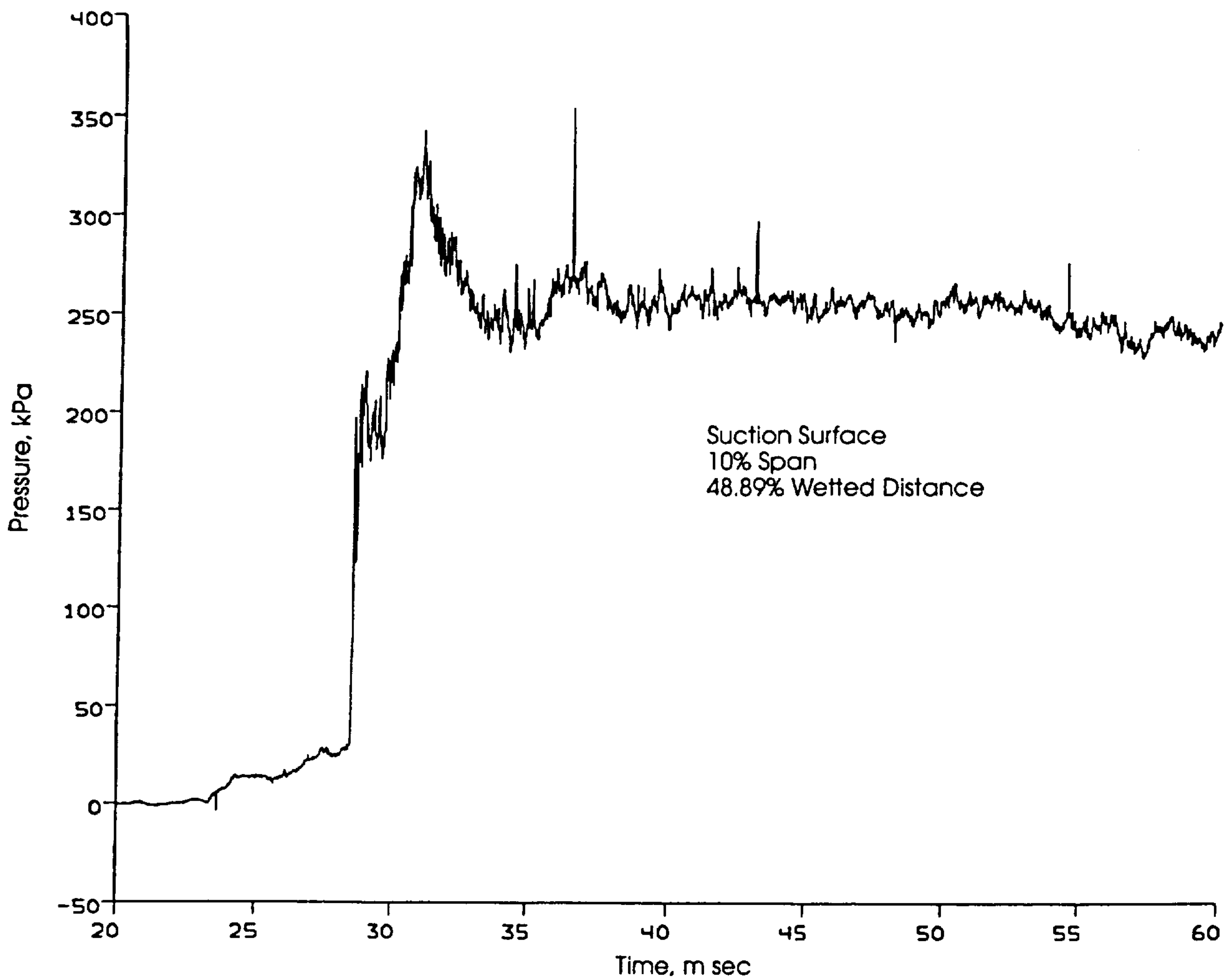


**Fig.13 Pressure history on first blade at 10% span**

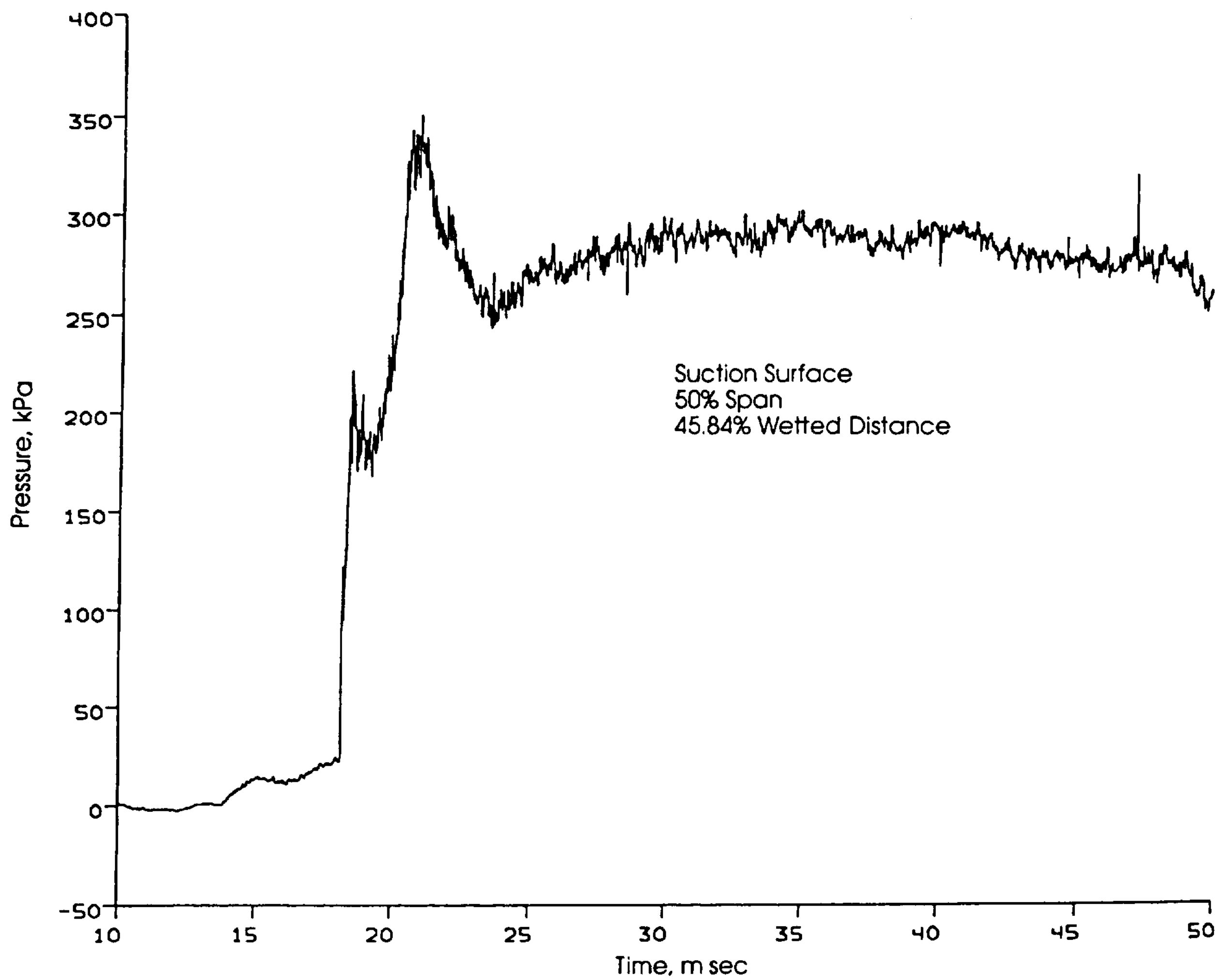


**Fig. 14 Pressure history on first blade at 50% span**

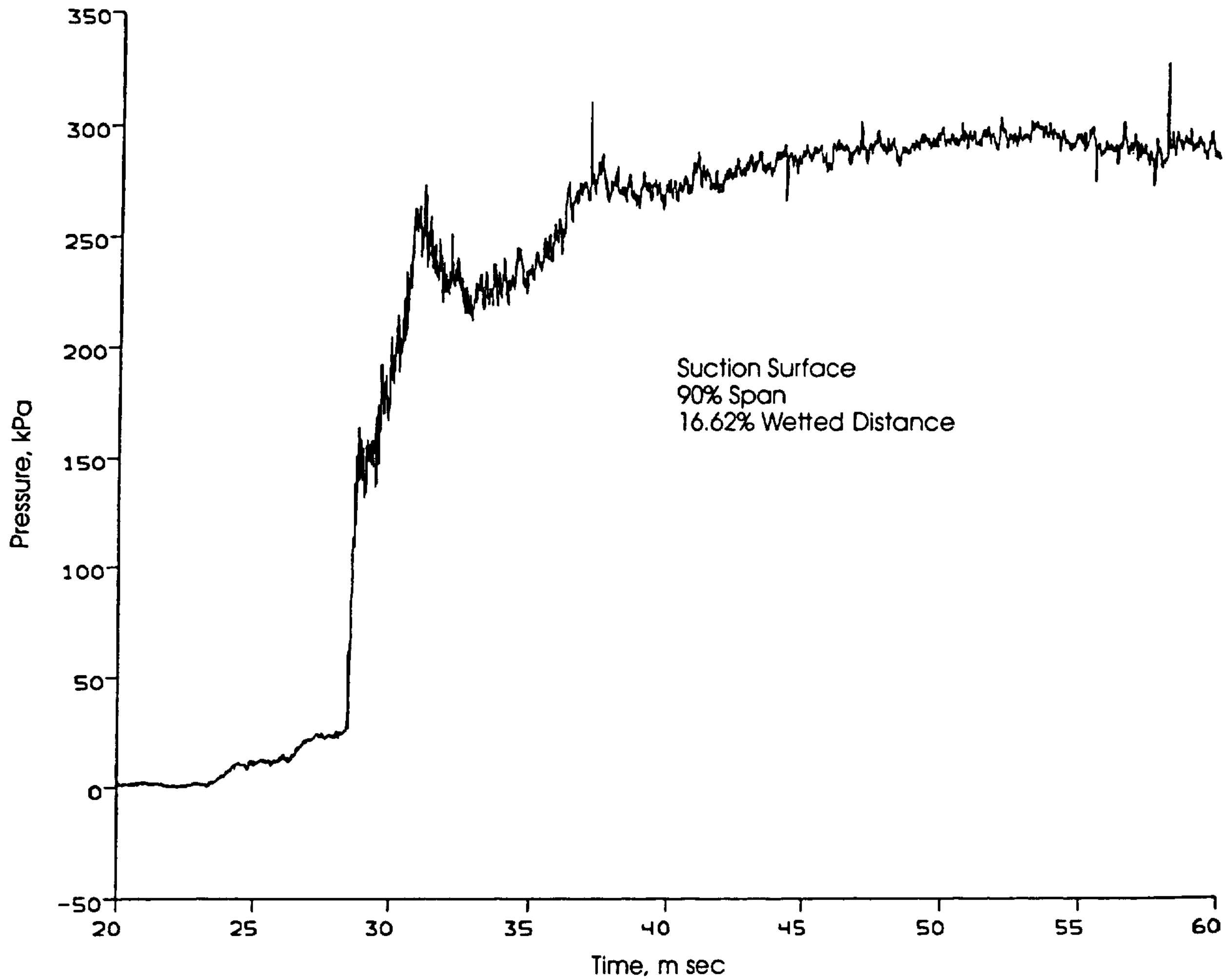


**Fig. 15 Pressure history on first blade at 90% span**

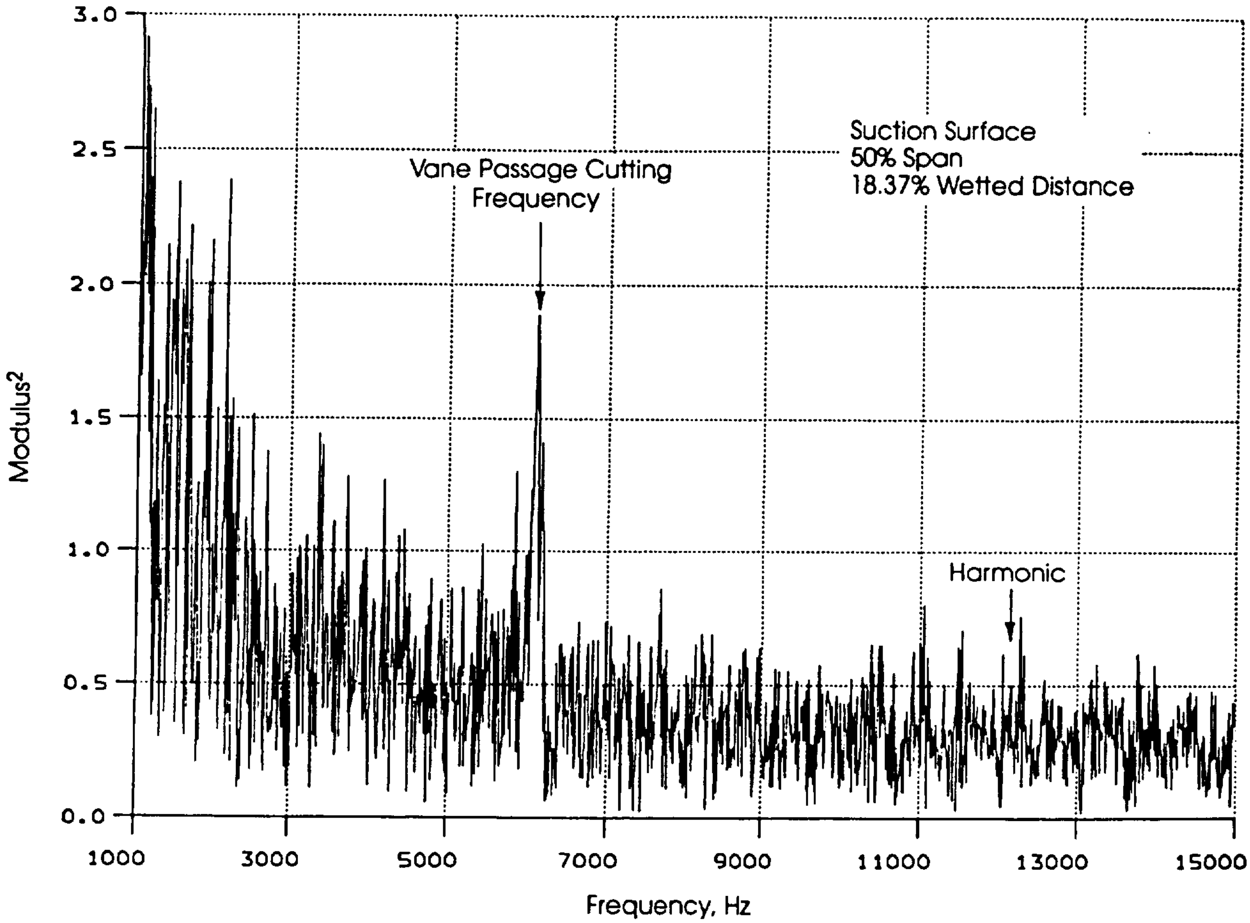


**Fig. 16 FFT of blade pressure data**

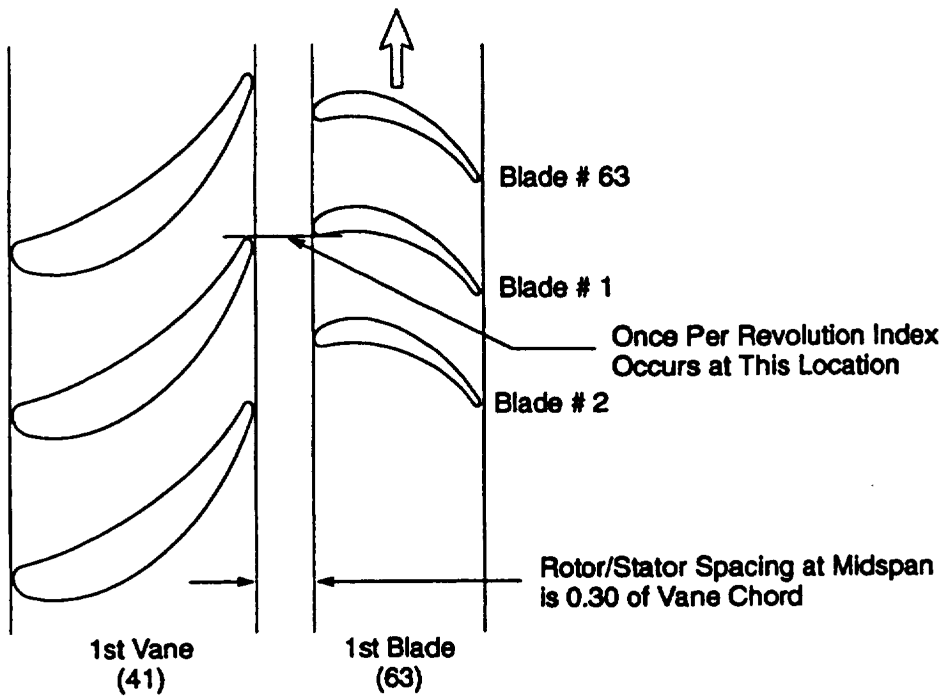


| | Blade # |
|---|---|
| Leading edge heat–flux gauges insert is on blade | 1 |
| Button gauges on pressure surface 50% span are on blade | 13 |
| Button gauges on suction surface 50% span are on blade | 14 |
| Pressure transducers on pressure surface 50% span are on blade | 28 |
| Pressure transducers on suction surface 50% span are on blade | 29 |
| Pressure transducers on pressure surface 10% span are on blade | 39 |
| Pressure transducers on suction surface 10% span are on blade | 40 |
| Pressure transducers on pressure surface 90% span are on blade | 44 |
| Pressure transducers on suction surface 90% span are on blade | 45 |

Fig. 17 Location of instrumentation relative to index pulse

Fig_13/1

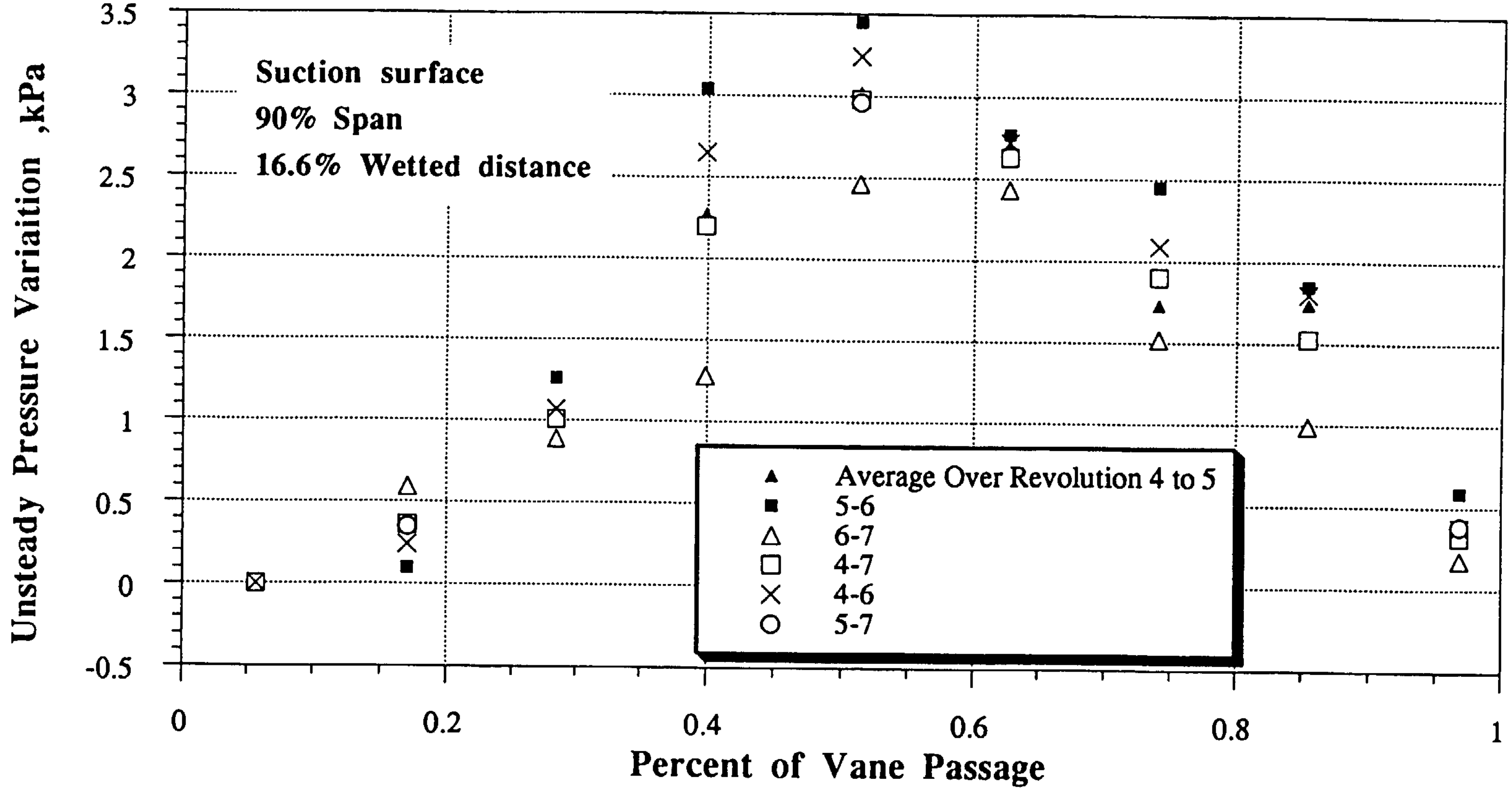


Fig. 18 Ensemble average of pressure over various number of revolutions

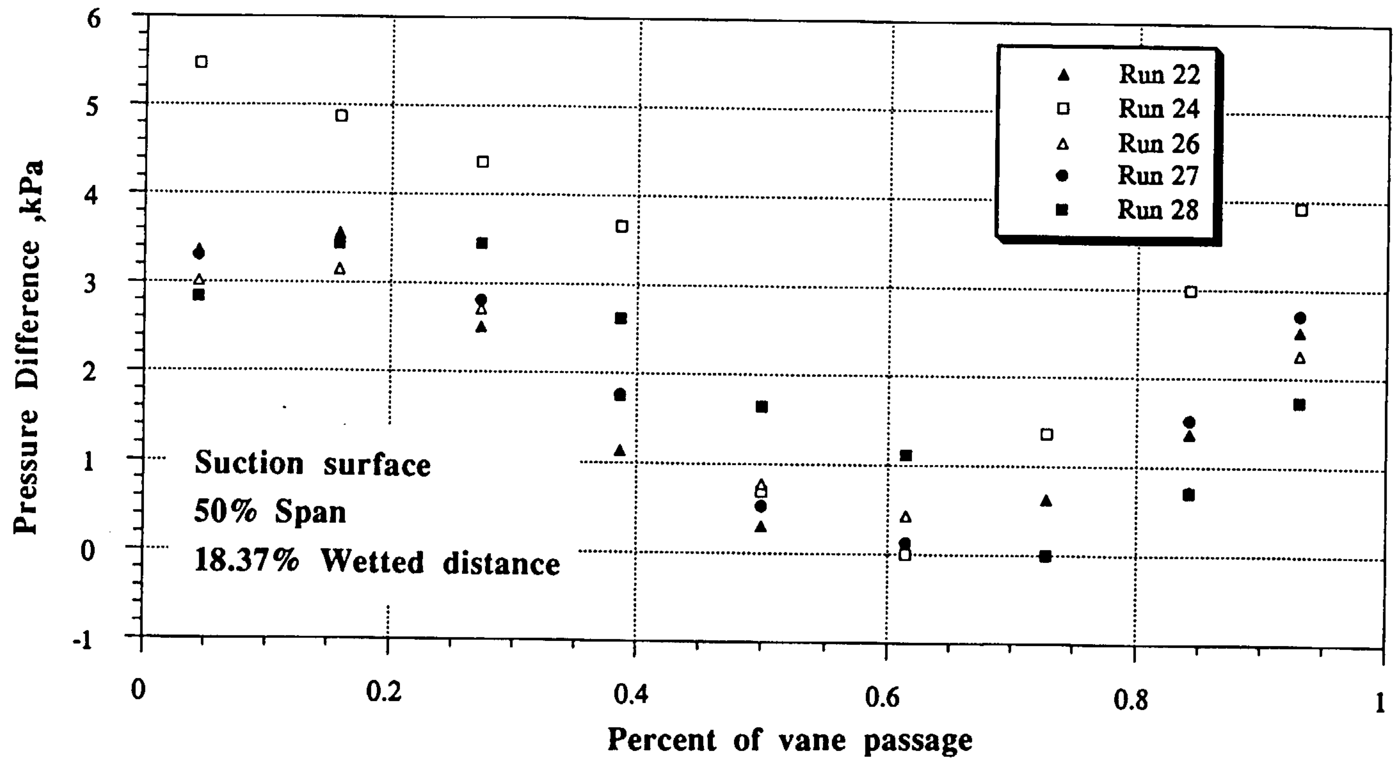


Fig. 19 Ensemble average of pressure at 18.37% on suction surface

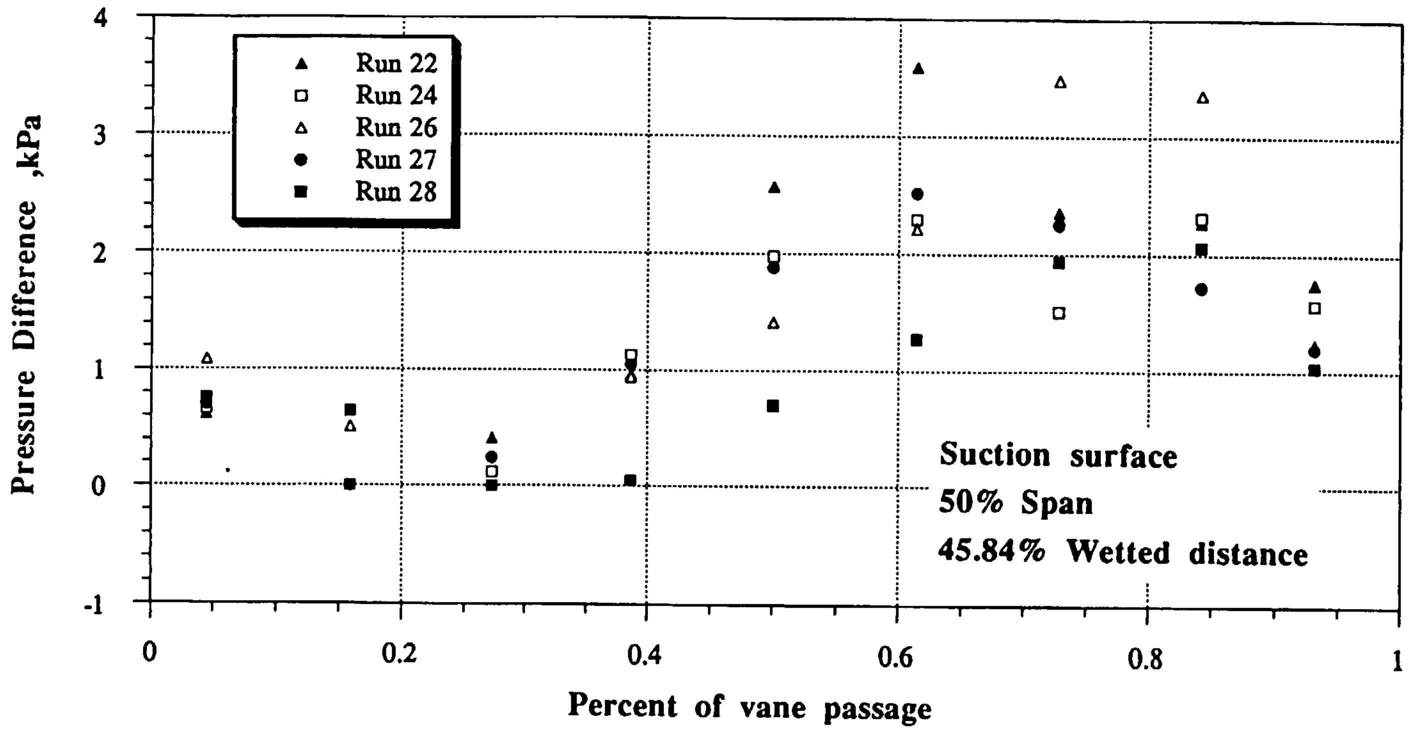


Fig. 20 Ensemble average of pressure at 45.84% on suction surface

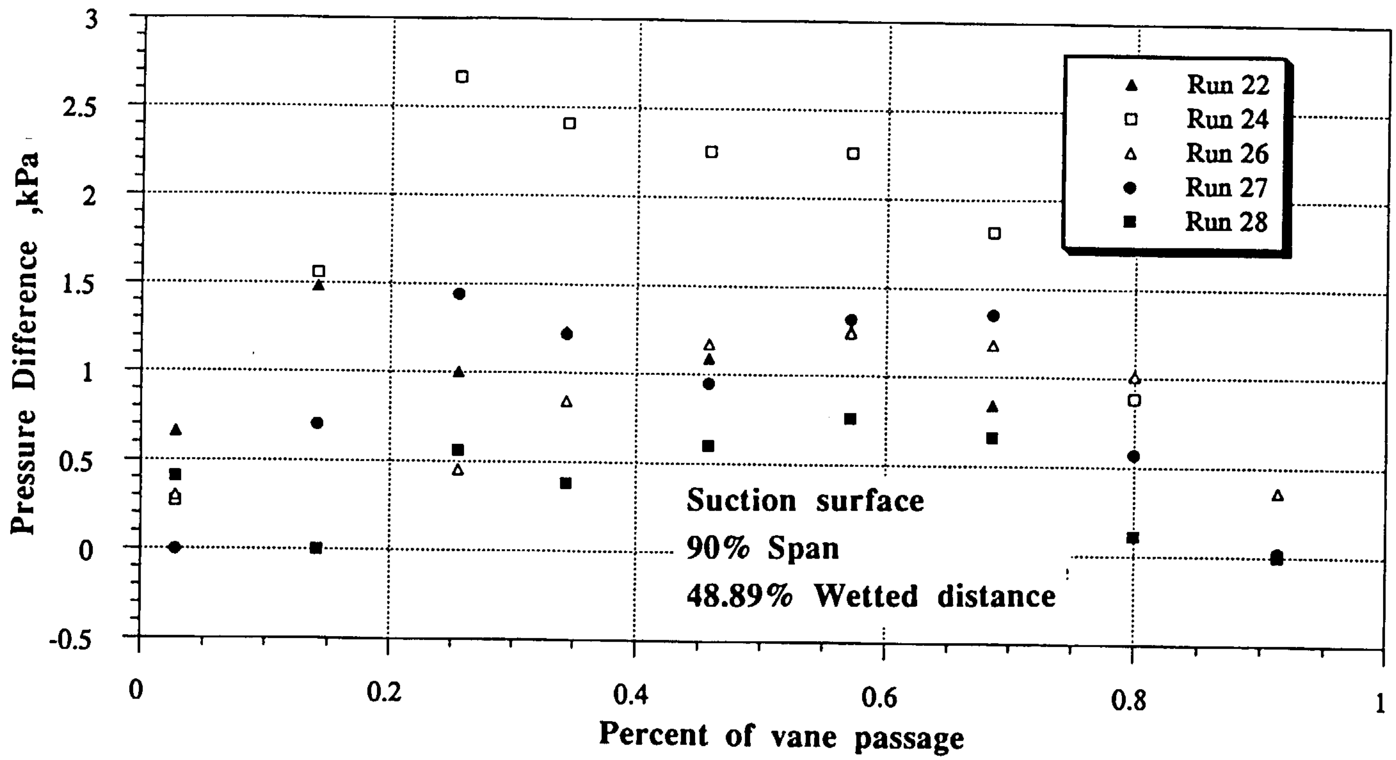


Fig. 21 Ensemble average of pressure data at 48.89% and 90% span on suction surface

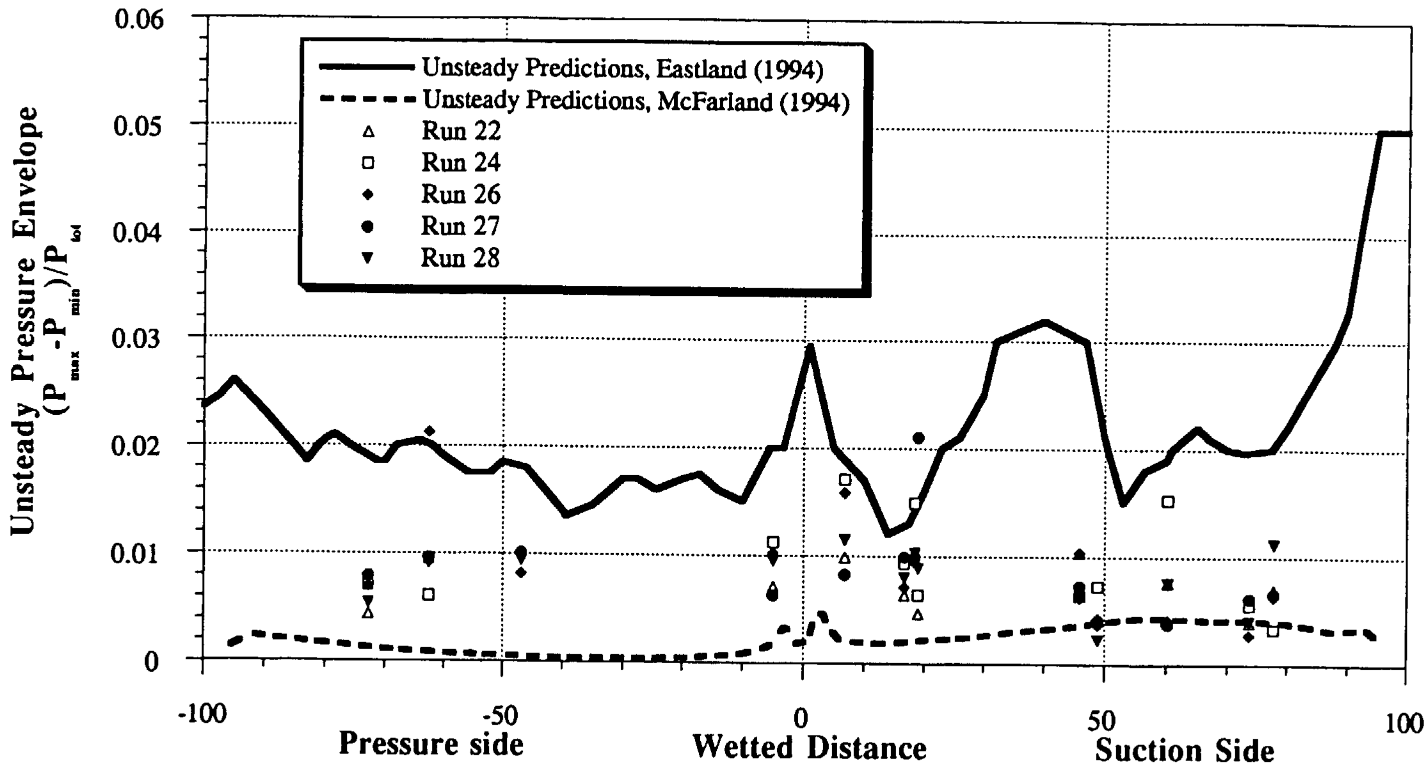


**Fig. 22 Comparison of measured and predicted unsteady pressure envelope for first-stage blade**

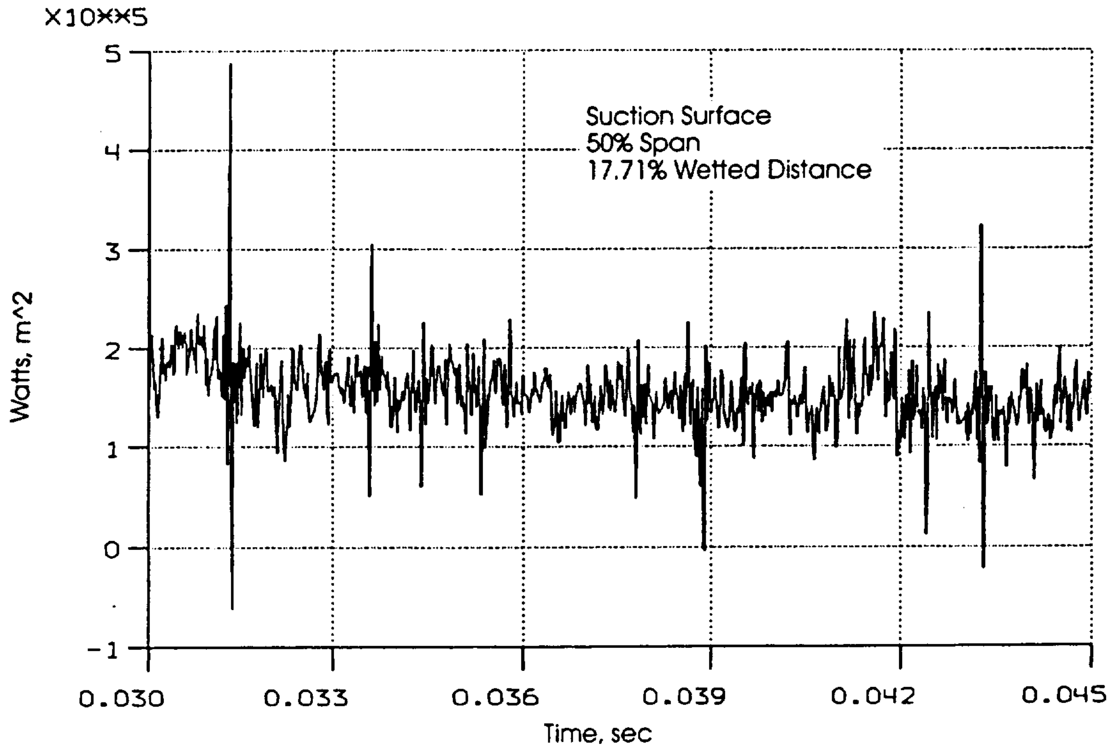


**Fig. 23 Heat-flux history during test time**

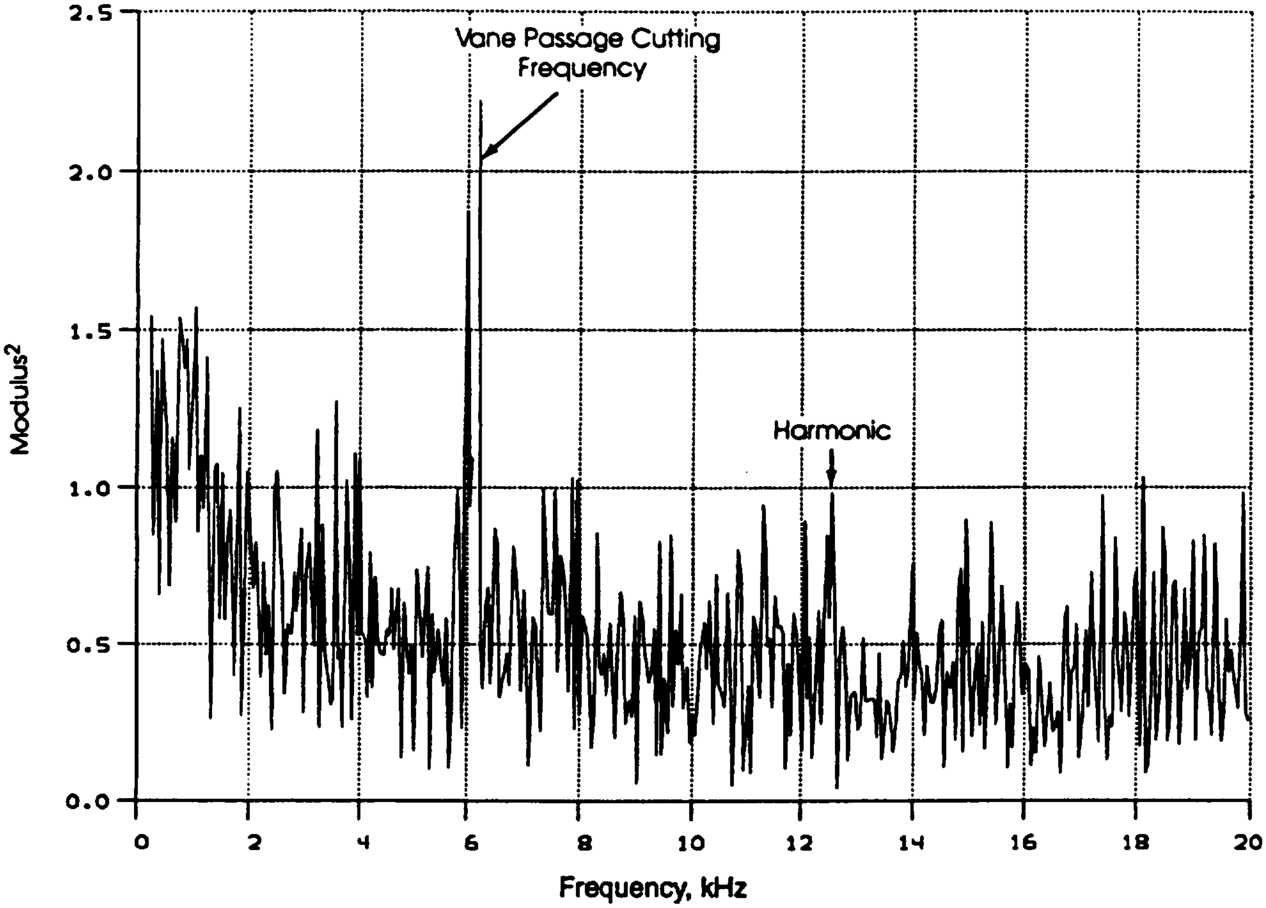


Fig. 24 FFT of blade heat-flux data

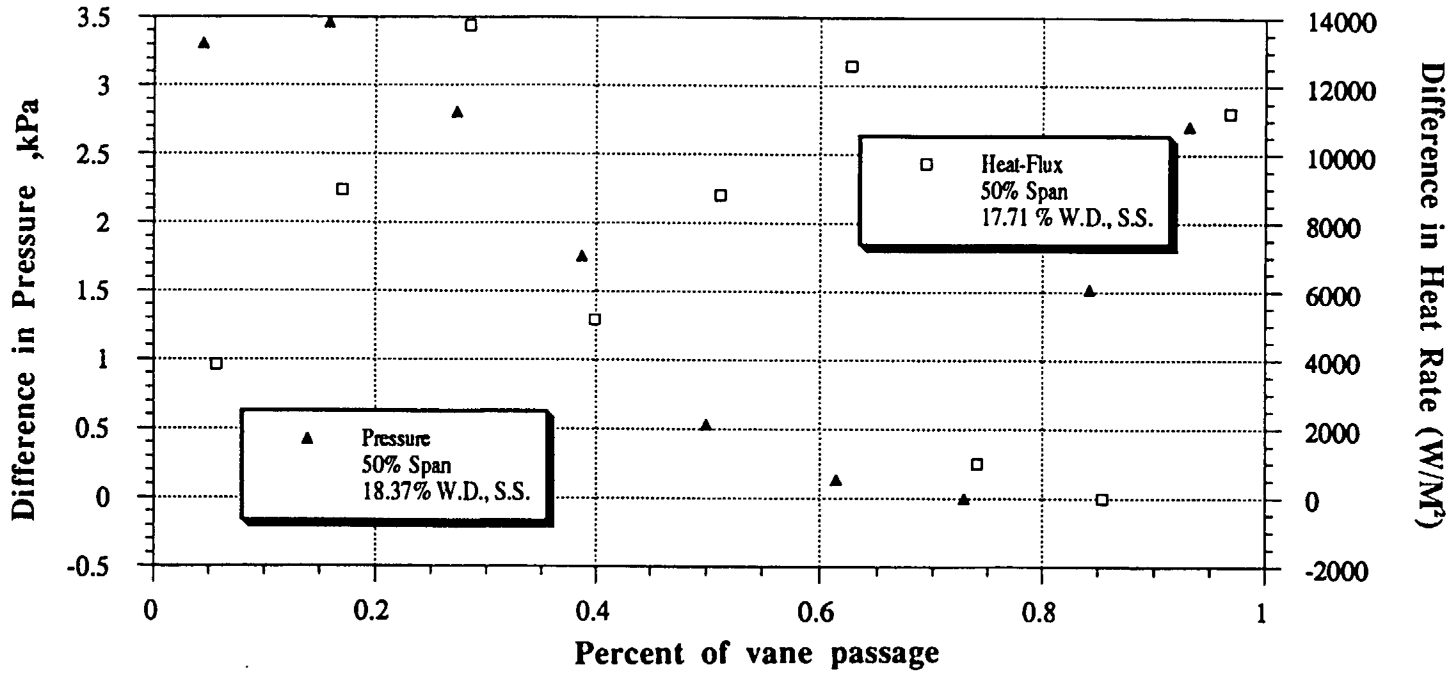


**Fig. 25 Comparison of phase-resolved heat flux and surface pressure on the blade at a wetted distance of approximately 18%**

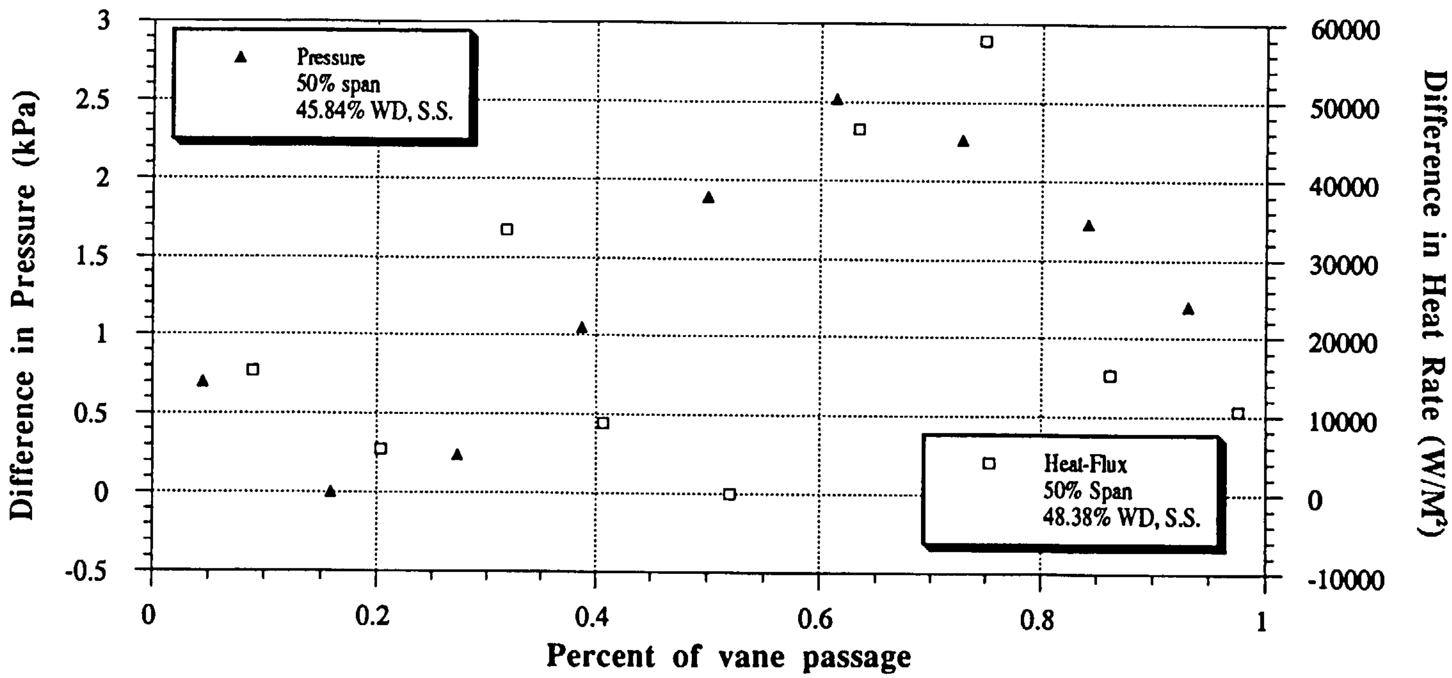


**Fig. 26 Comparison of phase-resolved heat flux and surface pressure on the blade at wetted distance of approximately 47%**